REPORT DOCUMENTATION PAGE

AD-A202 459

ECTE

1 8 1988

D

1b. RESTRICTIVE MARKINGS	
2b. DECLASSIFICATION / DOWNGRADING SCHEDULE	3. DISTRIBUTION / AVAILABILITY OF REPORT Approved for public release; distribution unlimited.
4. PERFORMING ORGANIZATION REPORT NUMBER(S)	5. MONITORING ORGANIZATION REPORT NUMBER(S) ARO 22533.12-CH
6a. NAME OF PERFORMING ORGANIZATION Clark University	6b. OFFICE SYMBOL (If applicable)
6c. ADDRESS (City, State, and ZIP Code) Worchester, Mass. 01620	7a. NAME OF MONITORING ORGANIZATION U. S. Army Research Office
8a. NAME OF FUNDING / SPONSORING ORGANIZATION U. S. Army Research Office	8b. OFFICE SYMBOL (If applicable)
8c. ADDRESS (City, State, and ZIP Code) P. O. Box 12211 Research Triangle Park, NC 27709-2211	7b. ADDRESS (City, State, and ZIP Code) P. O. Box 12211 Research Triangle Park, NC 27709-2211
	9. PROCUREMENT INSTRUMENT IDENTIFICATION NUMBER DAAG29-85-K-0126
	10. SOURCE OF FUNDING NUMBERS PROGRAM ELEMENT NO. / PROJECT NO. / TASK NO. / WORK UNIT ACCESSION NO.

11. TITLE (Include Security Classification)
A NMR Study of the Molecular Interactions and Dynamic Behavior in Polymer-Diluent Blends in the Solid State

12. PERSONAL AUTHOR(S)
Paul T. Inglefield and Alan A. Jones

13a. TYPE OF REPORT	13b. TIME COVERED	14. DATE OF REPORT (Year, Month, Day)	15. PAGE COUNT
Final	FROM 6/1/85 TO 6/30/88	July 25, 1988	

16. SUPPLEMENTARY NOTATION
The view, opinions and/or findings contained in this report are those of the author(s) and should not be construed as an official Department of the Army position, policy, or decision, unless so designated by other documentation.

17. COSATI CODES		
FIELD	GROUP	SUB-GROUP

18. SUBJECT TERMS (Continue on reverse if necessary and identify by block number)
Nuclear Magnetic Resonance, Molecular Interactions, Polymers, Polymer Blends, Poly Blends, Polystyrene, Plasticization, Antiplasticization, Polycarbonates

19. ABSTRACT (Continue on reverse if necessary and identify by block number)

A study of the molecules details of the interactions between small molecule diluents and polymers was carried out using a variety of Nuclear Magnetic Resonance methods. The focus of the study was to allow a molecular level comparison with macroscopic properties (thermal and mechanical) in multicomponent polymer blends. The details of plasticization, antiplasticization diluent sorption and blend compatibility were addressed. The polymer systems studied were high impact strength engineering plastics: Polycarbonates and poly (2,6-dimethylphenyl oxide) blends with polystyrene and structural analogues of these two fundamental systems. A three fold approach was used, with experiments which probe (a) the host polymer and changes in its dynamics as a consequence of diluent addition, (b) the dynamics of the diluent itself modified by the host and (c) experiments which probe directly the intermolecular intimacy in a multicomponent glassy blend.

20. DISTRIBUTION / AVAILABILITY OF ABSTRACT ☐ UNCLASSIFIED/UNLIMITED ☐ SAME AS RPT. ☐ DTIC USERS	21. ABSTRACT SECURITY CLASSIFICATION Unclassified
22a. NAME OF RESPONSIBLE INDIVIDUAL	22b TELEPHONE (Include Area Code) / 22c. OFFICE SYMBOL

DD FORM 1473, 84 MAR 83 APR edition may be used until exhausted. All other editions are obsolete

SECURITY CLASSIFICATION OF THIS PAGE
UNCLASSIFIED

A NMR STUDY OF THE MOLECULAR INTERACTIONS AND DYNAMIC BEHAVIOR IN POLYMER-DILUENT BLENDS IN THE SOLID STATE

FINAL REPORT

Paul T. Inglefield and Alan A. Jones

July 25, 1988

U.S. ARMY RESEARCH OFFICE
GRANT NUMBER DAAG 29-85-K-0126

Clark University
Worcester, Mass. 01620

Table of Contents

(1) Statement of the Problem

A study of the molecules details of the interactions between small molecule diluents and polymers is carried out using a variety of Nuclear Magnetic Resonance methods. The focus of the study is to allow a molecular level comparison with macroscopic properties (thermal and mechanical) in multicomponent polymer blends. The details of plasticization, antiplasticization diluent sorption and blend compatibility are addressed. The polymer systems studied are high impact strength engineering plastics: Polycarbonates and poly (2,6-dimethylphenyl oxide) blends with polystyrene and structural analogues of these two fundamental systems. A three fold approach is used, with experiments which probe (a) the host polymer and changes in its dynamics as a consequence of diluent addition, (b) the dynamics of the diluent itself modified by the host and (c) experiments which probe directly the intermolecular intimacy in a multicomponent glassy blend.

A number of NMR experiments are employed. Solid state lineshape analysis using a variety of nuclei depending on the systems involved and isotopic enrichment when appropriate yields information on the structural and dynamic details of conformational reorientation. The primary lineshape types here are due to chemical shift anisotropy and the nuclei involved are ^{13}C and ^{31}P. We have extended our previous studies on single component systems and added to the methodology of this powerful approach. NMR relaxation measurements (T_1 and $T_{1\rho}$) are a dominately dynamical probe and enable quantification of the

dynamics over a wide range of motional frequencies. Lastly spin diffusion techniques allow us to examine structural interactions on an interatomic distance scale in these multicomponent systems. These experiments can be collectively considered as spin dynamics and we clearly show that using a multifrequency, multinuclear approach NMR offers a rather unique probe of the molecular level events in polymer blend systems and can critically test many of the ideas and models put forward from macroscopic investigations. Questions of both dynamic and structural heterogeneity at the microscopic level and the distinction between plasticization and antiplasticization from a molecular viewpoint are clearly addressed.

(2) Summary of Most Important Results

In addressing blend behavior we have paid particular attention to interpreting the microscopic behavior as determined by NMR in relation to the thermal, mechanical and other macroscopic characteristics in multicomponent polymer blends.

In the system Bisphenol A Polycarbonate (BPAPC) and Di-n-Butyl Phthalate (DBP), the diluent DBP acts as an antiplasticizer at low concentrations and a plasticizer at high concentrations. We have made measurements of carbon spin diffusion from the DBP to the BPAPC repeat unit using ^{13}C enriched DBP at a carbonyl site. This technique has been used to probe molecular level mixing in blends. This is however the first time that specificity at the level of chemical structure has been observed in an amorphous glass. We have also measured ^{1}H $T_1\rho$'s for the phenyl protons of BPAPC in the same system with all other protons deuterated. This experiment is designed to probe the phenylene ring flip which has been shown to be related to the sub T_g mechanical behavior. The results of these experiments clearly indicate the distinctions between plasticization and antiplasticization at the molecular level. Namely:

(a) At low DBP concentrations (10wt %) in the antiplasticization regime there is structural specificity with the carbonyl of DBP being preferentially located near the carbonate of BPAPC. At higher concentrations of DBP (25wt %) this specificity is absent and the system exhibits plasticization behaviour as indicated by the modulus. A quantitative treatment including a lattice model to count polymer-diluent contacts has

been attempted. This is molecular evidence for the existence of specific interactions as a key property of an antiplasticizer.

(b) The ^{1}H $T_{1\rho}$ measurements as a function of diluent concentration (as shown in the attached figure) demonstrate the subtle changes in polymer repeat unit dynamics in the plasticized and antiplasticized regimes. At low diluent concentrations the $T_{1\rho}$ minimum moves to higher temperatures indicative of a decrease in the sub-T_g repeat unit motion thus leading to slight embrittlement in the polymer; at high concentration this trend remains but with the observation of a new $T_{1\rho}$ minimum and corresponding motion at a much lower temperature thus leading to a softening as the DBP concentration increases. This corresponds to the observation of two relaxations occuring as plastization increases and can be interpreted as the original relaxation for the pure polymer being split into two as the diluent concentration is increased. These two experiments clearly address the role of intermolecular structure and host polymer dynamics in this type of blend.

To investigate the role of the inherent diluent dynamics we have made CSA lineshape measurements of ^{31}P for a series of organic phosphate plasticizers in the blend system polyphenylene oxide (PPO) and polystyrene (PS) and in the BPAPC single host polymer system. Mechanical and thermal measurements by us have shown that the presence of the phosphate can introduce a low temperature mechanical loss absent in the pure blend PPO/PS and an additional loss in the BPAPC system. Our NMR lineshape measurements indicate that isotropic brownian motion of the

phosphate itself is considerable well below Tg and is responsible for this loss. Also there is clear evidence that the efficiency of these plasticizers is directly related to their own Tg. Thus plasticizers with inherently low Tg's will undergo motion when blended in concentrations up to 25wt % in a host polymer leading to sub Tg mechanical loss and plasticizing characteristics in the material, clear evidence that the inherent mobility of the diluent molecule has a significant role in overall properties of the resulting blend. Quantification of the diluent dynamics shows a heterogeneity of motional rates which tends to be characteristic of the dynamics in the glassy polymer systems we have studied.

The other contrasting system we have investigated is that in which the diluent molecule is a gas and the questions of interest are the nature of the sorbed gas and the modification to the host polymer. The polymer chain dynamics is modified in a similar way to that shown in the DBP-BPAPC system with small concentrations of gas producing slight antiplasticization indications. An extensive study of the ^{13}C NMR relaxation in $^{13}CO_2$ in BPAPC has been made to characterized the nature of the sorbed species in the glass. To interpret our data a two site model is presented which parallels at the molecular level the model presented by Koros and Paul (J. Poly Sci, Polym Phys Ed 14 678 (1976) based on permeability data. Their "Dual Mode" model postulates two CO_2 environments in the glass: a Langmuir species and a Henry's Law species. Our analysis gives quantitative data on the mobility of these two environments. In

contrast measurements of $^{13}CO_2$ in Silicone rubber are indicative of a single site environment, again in agreement with the macroscopic work of Koros and Paul.

The full details of these remarks and our related studies are contained in the appendix which is a compilation of the publications resulting from the project.

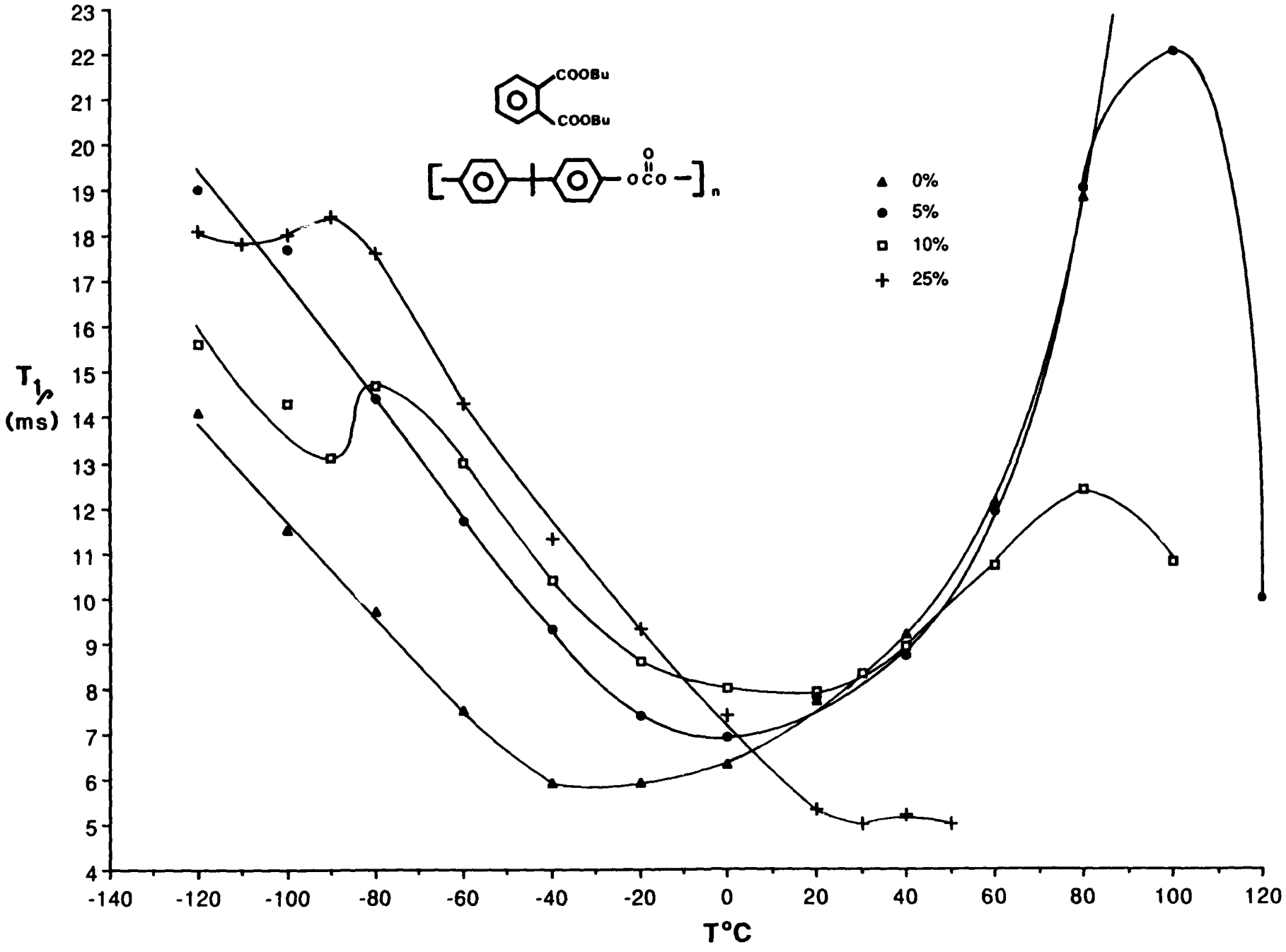
COOBu
COOBu
0%
5%
10%
25%
T1ρ (ms)
T°C
23
22
21
20
19
18
17
16
15
14
13
12
11
10
9
8
7
6
5
4
-140
-120
-100
-80
-60
-40
-20
0
20
40
60
80
100
120

(3) List of Publications:

1. "Phenylene Ring Dynamics in Solid Polycarbonate: An Extensive Probe by Carbon-13 Solid State NMR Line-Shape Studies at Two Field Strengths", A.K. Roy, A.A. Jones and P.T. Inglefield. Macromolecules 19, 1356 (1986).

2. "Solid State Lineshapes Calculated From a Fractional Exponential Correlation Function", A.K. Roy, A.A. Jones and P.T. Inglefield. Polymer Preprints 27, 1, 451 (1986).

3. Further Studies of Multiple Nuclear Spin Relaxation and Local Motions in Dissolved 1,1-Dichloro-2,2-Bis (4-Hydroxyphenyl) Ethylene Polyformal" C.-C. Hung, J.H. Shibata, M.F. Tarpey, A.A. Jones, J.A. Porco and P.T. Inglefield. Analytica Chemica Acta 189, 167 (1986).

4. "Molecular Motion in Glassy Polycarbonate" A.A. Jones, P.T. Inglefield, J.F. O'Gara and A.K. Roy. In Transport and Relaxation in Random Materials, World Scientific Press, M.F. Shlesinger, ed. 228, (1986).

5. "A Comparison of Spin Relaxation and Local Motion Between Symmetrically and Asymmetrically Ring-Substituted Bisphenol Units in Dissolved Polycarbonates." J.A. Ratto, P.T. Inglefield, R.A. Rutowski, K.-L. Li, A.A. Jones and A.K. Roy. J. Poly. Sci., Polymer Physics Ed. 25, 1419 (1987).

6. "Proton and Carbon-13 Relaxation and Molecular Motion in Glassy Bisphenol-A Polycarbonate". J.J. Connolly, P.T. Inglefield, and A.A. Jones. J. Chem. Phys. 86, 12 (1987).

7. Local Intermolecular Structure in an Antiplasticized Glass by Solid-State NMR. A.K. Roy, P.T. Inglefield, J.H. Shibata and A.A. Jones. Macromolecules 20, 1434 (1987).

8. "Dynamics of Sorbed $^{13}CO_2$ in Polycarbonate by NMR" W.Y. Wen, E.J. Cain, P.T. Inglefield, and A.A. Jones. Polymer Preprints 28 1, 225 (1987).

9. "Dynamics of Sorbed $^{13}CO_2$ in Polycarbonate Probed by Nuclear Magnetic Resonance" W.Y. Wen, E.J. Cain, P.T. Inglefield, and A.A. Jones. Z. Phys. Chem 155, 181 (1987).

10. "Motion of Trioctyl Phosphate in a PPO Polystyrene Blend by ^{31}P Line Shape", P.T. Inglefield, A.A. Jones, P.T. Inglefield, A.A. Jones, B.J. Cauley and R.P. Kambour. Polymer Reprints 29, 1. 82 (1988).

11. "Two-Site Model for the Relaxation of $^{13}CO_2$ Sorbed in Glassy Polycarbonate", E.J. Cain, A.A. Jones, P.T. Inglefield and W.Y. Wen. Polymer Preprints, 29, 1, 23 (1988).

12. "Spectroscopic Studies of Diluent Motion in Glassy Plasticized Blends", R.P. Kambour, J.M. Kelly, B.J. McKinley, B.J. Cauley, P.T. Inglefield, A.A. Jones. Macromolecules, to appear (1988)

13. "NMR Investigations of Structure and Dynamics of Polycarbonates and Polycarbonate Blends." A.K. Roy, PhD. Thesis, Clark University (1988)

(4) LIST OF SCIENTIFIC PERSONNEL

1. Dr. Paul T. Inglefield (Principal Investigator)
   Research Professor and Director, Worcester Consortium NMR Facility
   Department of Chemistry
   Clark University
   Worcester, MA 01610

2. Dr. Alan A. Jones (Co-Principal Investigator)
   Professor
   Department of Chemistry
   Clark University
   950 Main Street
   Worcester, MA 01610

3. Ajoy K. Roy (Research Assistant)
   Department of Chemistry, Graduate Student
   Clark University
   PhD Clark University 1988.

4. Michael F. Tarpey, (Research Assistant) Clark University.

5. The following participated to a lesser extent while supported from other sources.

Clark University	W.Y. Wen (Faculty)
	J.H. Shibata (Post-Doctoral Fellow)
	E.J. Cain (Graduate Student)
	C.-C. Hung (Graduate Student)
	J.J. Connelly (Graduate Student)
	K.-L. Li (Graduate Student)
	R.A. Rutowski (Undergraduate research assistant)
	B.J. Cauley (Undergraduate research assistant)
Holy Cross	J.A. Porco (Undergraduate research assistant)
	J.A. Ratto (Undergraduate researh assistant)

(5) APPENDIX: COMPILATION OF PUBLICATIONS

Phenylene Ring Dynamics in Solid Polycarbonate: An Extensive Probe by Carbon-13 Solid-State NMR Line-Shape Studies at Two Field Strengths

Ajoy K. Roy and Alan Anthony Jones

Department of Chemistry, Clark University, Worcester, Massachusetts 01610

Paul T. Inglefield*

Department of Chemistry, College of the Holy Cross, Worcester, Massachusetts 01610.
Received November 13, 1985

ABSTRACT: An analysis of carbon-13 chemical shift anisotropy (CSA) line shapes at two field strengths is carried out to probe the detailed nature of phenylene ring dynamics in the glassy polycarbonate of bisphenol A. The phenylene group in this polymer undergoes two types of motion simultaneously, both about the C_1C_4 axis. The primary motion is large-angle jumps between two sites whereas the secondary motion involves restricted rotational diffusion over limited angular amplitude. In the first category, the jumps from one minimum to the second occur over an angular range around each minimum associated with the range of restricted rotation. A simultaneous model with an inhomogeneous distribution of correlation times appears to be the best description for the composite motional process. The inhomogeneous distribution is described by a Williams–Watts fractional exponential correlation function and corresponds to a distribution of rates corresponding to different spatial positions in the polymer matrix. The correlation function is described by τ_p, the central correlation time, and α, the breadth parameter for the distribution. An apparent activation energy of 50 kJ/mol, found by an Arrhenius analysis of τ_p's, is in agreement with the values obtained from a relaxation map constructed from rates for proton relaxation minima, CSA line-shape collapse, dielectric loss maxima, and dynamic mechanical loss maxima. A value of 0.154 for the fractional exponent indicates a broad distribution of jump rates for polycarbonate and is consistent with defect diffusion past a distribution of barrier heights. Such diffusion has been proposed as the basic process behind the jumps in a motional model involving conformational interchange between a defect cis–trans conformation of the carbonate unit and neighboring trans–trans conformations.

Introduction

NMR line-shape experiments[1,2] have recently yielded new insights into the dynamics of the polycarbonates of bisphenol A (BPA-PC). To date, the solid-state NMR line-shape experiments[1,2] have defined the geometry of the dominant motions in this polymer, which supplemented the frequency information supplied by dielectric[3] and dynamic mechanical[4] experiments. The two major motional processes are (i) restricted rotational diffusion over limited angular amplitude around the C_1C_4 axis and (ii) π flips between two potential minima around the same axis, with the π flips constituting the primary motion. This geometric information has led to a new motional proposal[5] which attempts to reconcile NMR, dielectric, and dynamic mechanical data. To date, the analysis of the temporal aspects of the NMR line-shape data has been somewhat simplistic and incomplete. In this paper, new data are added and a more rigorous interpretation is pursued to improve the description of the time scale of motion as seen through NMR line shapes.

To review the situation at hand, first consider the chemical shift anisotropy (CSA) study,[1] which suffers from an interpretational inadequacy since the two important motions were treated sequentially. The secondary motion was treated first since it was always assumed to be in the rapid limit. A single-exponential correlation time with an Arrhenius form is then employed to account for the temperature dependence of the π flips.[1,6] The effects of the secondary motion were combined with the primary motion by using partially averaged parameters as the input basis for the primary motion. Problems were encountered with the simulation of the spectrum at 0 °C, the temperature at which both processes make comparable contributions to the line-shape narrowing. At this temperature, the maximum intensity of the theoretical line shape is displaced from the observed one.[1]

To avoid this difficulty, a new model[7] which allows for simultaneous treatment of both motions has been applied to the same set of CSA data. The problem in fitting the 0 °C data in the sequential treatment disappears in this simultaneous treatment. The interpretation for primary motion is also changed in the sense that in the simultaneous treatment jumps over a limited range around each minimum are allowed in addition to exact π flips. The simultaneous treatment also yields a more reasonable temperature dependence for the apparent simple harmonic nature of the secondary motion. However, one problem reported in the earlier CSA paper[1] still remains unaddressed.

The earlier CSA data at 22.6-MHz field strength were analyzed on the basis of a single-exponential correlation function. The Arrhenius analysis of the correlation times yielded an apparent activation energy of 11 kJ/mol. The simultaneous treatment activation energy is 26 kJ/mol. The earlier CSA report[1] also showed an activation energy of 48 kJ/mol, obtained from a linear least-squares analysis of a relaxation map which included spin–lattice relaxation data, dielectric data, and dynamic mechanical data. The phenylene proton T_1 and $T_{1\rho}$ data presented in the same earlier report could only be analyzed on the basis of a broad distribution of exponential correlation times, which corresponds to a fractional exponential correlation function with an exponent near 0.18. Thus there is a great deal of discrepancy between activation energies from two sets of analyses: 11 vs. 48 kJ/mol and the use of a single exponential vs. a broad distribution. The discrepancy points to the inadequacy of the kinetic treatment used for the line-shape data and is an indication of the existence of a distribution of correlation times in the dynamics. The simultaneous value of 26 kJ/mol is probably an improvement but hardly a total resolution. The earlier CSA data at 22.6 MHz represented a limited data set and as

0024-9297/86/2219-1356$01.50/0

such it did not warrant use of a correlation function based on a distribution of correlation times. It is, therefore, necessary that the CSA data base be expanded by acquiring line shapes at another field, preferably a higher one, and that a detailed analysis be carried out in order to reach a better agreement between different data sets.

The Ngai formalism[9,10] for the stretched exponential correlation function used in the earlier T_1 and $T_{1\rho}$ analyses[1] assumes a homogeneous distribution of correlation times where each phenylene group motion follows essentially the same nonexponential decaying process as opposed to an inhomogeneous distribution where spatially separated groups reorient with different time constants. In the case of proton T_1 and $T_{1\rho}$ data, the presence of an efficient spin-diffusion mechanism removes the difference between the two types of distributions. This is however not the case with carbon-13 T_1 and $T_{1\rho}$ data, where a T_1 dispersion can be observed because of weak spin diffusion. A dispersion of spin–lattice relaxation times, in general, indicates the presence of an inhomogeneous distribution, and phenylene carbon-13 $T_{1\rho}$ dispersions were observed by Schaefer et al.[11] for BPA-PC. Line-shape studies offer the possibility of confirming this characteristic of the correlation function.[12] Deuterium NMR[2] has already shown promise in this direction, although a detailed analysis is not yet available. In this context, it appears that if the existing CSA data base at 22.6 MHz is augmented by adding data at a higher field where changes in line-shape features are more pronounced, it might be possible to quantitatively distinguish between a single exponential and a distribution, and in the case of a distribution, between inhomogeneous and homogeneous.[12]

Experimental Section

The same BPA-PC sample with single-site carbon-13 enrichment (<90%) at one of the two phenylene carbons ortho to the carbonate is employed here as was used in an earlier study.[1] The FID's were acquired by using a single pulse with high-power decoupling on a Bruker WM-250 with the Doty solids accessory. A sufficient number of scans were taken at each temperature to ensure a good signal-to-noise ratio. The Fourier-transformed spectra are corrected for a contribution from the background, by using a subtraction scheme; i.e., spectra for the blank probe were obtained under the same conditions, using the same number of scans, and subtracted from the uncorrected spectra. The corrected line shapes at different temperatures were assigned a standard reference following the approach outlined before.[1] CSA line shapes at 62.9 MHz are shown in Figure 1 as a function of temperature. The CSA data on 22.6 MHz are reported in ref 1.

Interpretation

The principal axis system for the CSA tensor of aromatic carbons, as reported for benzene,[13] is oriented with the σ_{11} axis parallel to the C–H bond and the σ_{33} axis perpendicular to the ring plane. The σ_{22} axis is in the ring plane perpendicular to the C–H bond. Low-temperature (less than −140 °C) line shapes at both frequencies were then matched with theoretical spectra generated on the basis of the Bloembergen–Rowland equation.[14] The principal shielding tensor values used to obtain fits at both frequencies are $\sigma_{11} = -15$, $\sigma_{22} = 51$, and $\sigma_{33} = 171$ ppm on the CS_2 scale. These values are in good agreement with the ones reported earlier.[1] These principal values lead to an isotropic chemical shift of 69 ppm, which compares favorably with the observed chemical shift in solution of 72.5 ppm.

Simultaneous Model with a Single Correlation Time. This model[7] provided the best description of the CSA line-shape data at a single frequency and as such it can be considered first in the attempt to interpret the data at two field strengths. In this model, the multisite exchange formalism developed independently by Wemmer[6,15] and Mehring[13] is employed. It allows for all possible transitions with equal probability for a series of sites chosen to emulate large-angle jumps over a range around exact π flips, superimposed on low-amplitude libration both about the C_1C_4 axis of the phenylene ring. The line-shape equation for multisite exchange used for CSA line shapes has been described elsewhere.[1,7] Both two-site jump and simultaneous models make use of the multisite formalism. The two-site jump model includes only the primary motion. The simultaneous model, on the other hand, treats both motions. For BPA-PC, it is important to meet one restriction, i.e., using a correlation time that will treat the secondary motion, namely oscillation or libration in the rapid limit. With two rates, one for each process is conceivable though computationally difficult.

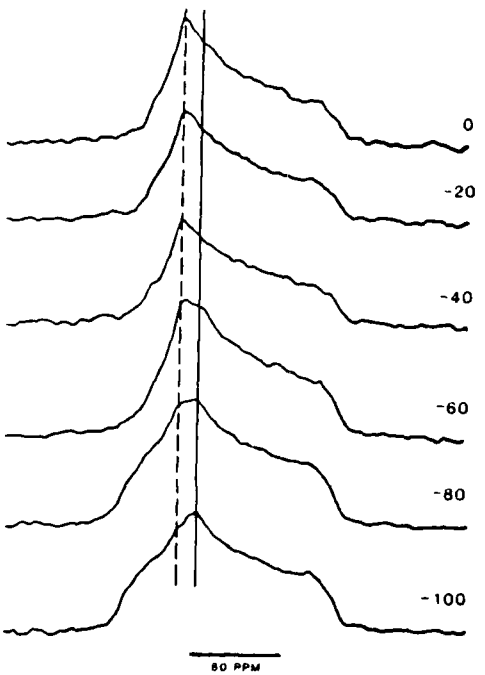

Figure 1. Variable-temperature carbon-13 CSA line shapes at 62.9 MHz. The solid vertical line indicates the position of the maximum in the rigid line shape corresponding to σ_{22}. The dashed vertical line indicates the position of the maximum in the high-temperature, motionally averaged spectra. At the intermediate temperatures of −60 and −80 °C, two maxima corresponding to the two lines are observed, which is indicative of an inhomogeneous distribution.

Whereas 22.6-MHz data were not difficult to simulate with this model, problems were encountered in fitting 62.9-MHz data, mainly the low-temperature ones as shown in parts a and d of Figure 2 for data at −80 and −60 °C. Here the line shapes in the slow-to-intermediate regime play the crucial role in determining the best description of the motion; and the inability to obtain a good match to both frequency sets points to the inadequacy of the treatment of the large-amplitude jumps by a single correlation time.

Inhomogeneous vs. Homogeneous Distribution. In view of the failure of the single correlation time model, a simulation of the data using both distributional models is attempted. The appearance of the spectra shown in Figure 1 is qualitatively indicative of an inhomogeneous distribution. For a simple two-line collapse, Garroway[12] showed the characteristic of a broad inhomogeneous correlation function is an intermediate three-line spectrum. Two of the three lines correspond to the position of the two lines in the absence of exchange. The third line

position corresponds to that of the rapid-exchange limit. Thus the intermediate three-line spectrum consists of two lines corresponding to the precollapse positions and a third line corresponding to the complete collapse position. In the spectra of Figure 1 a solid line is drawn through all spectra for the σ_{22} shift position of the rigid line shape. A dashed line is then drawn through all spectra corresponding to the high-temperature limit resulting from the motional averaging of σ_{11} and σ_{22}. This dashed line is based on the maximum of the high-temperature line shape. At the intermediate temperatures of −60 and −80 °C, maxima are present which correspond to both high-temperature and low-temperature limits, the solid and dashed lines. This feature is qualitatively indicative of an inhomogeneous distribution, and now a quantitative analysis centering on these intermediate temperatures is pursued.

Specifically the calculations will be restricted to the intermediate rate regime where correlation times for the primary motion are slow enough to cause distinctive changes in the maximum intensity area of the line shapes and where secondary motion is not as important. Since the distributions are concerned with the primary motion, a simple two-site jump model is used for preliminary calculation.

The distribution formalism, in general, makes use of a fractional exponential correlation function. The commonly used Williams–Watts expression[16] is

$$\phi(t) = \exp(-t/\tau_p)^\alpha \qquad (1)$$

where τ_p is the center correlation time, and α, the breadth parameter. Smaller α's are associated with broader distributions. As shown by Kaplan and Garroway[12] eq 1 can be recast in the form

$$\phi(t) = \int_0^\infty d\tau\, \rho_\alpha(\tau) \exp(-t/\tau) = \int_{-\infty}^{\infty} d(\log \tau) G(\log \tau) \exp(-t/\tau) \qquad (2)$$

Instead of the continuous distribution of eq 2, $\phi(t)$ can be represented as a discrete sum.

$$\phi(t) = \sum_j p_j \exp(-t/\tau_j) \qquad (3)$$

with a normalization condition given by $\phi(0) = 1 = \sum_j p_j$:

$$p_j = G(\log \tau_j)[\log (\tau_{j+1}/\tau_j)] \qquad (4)$$

where by the definition in eq 2

$$G(\log \tau) = \tau \rho_\alpha(\tau)/\log e \qquad (5)$$

Montroll and Bendler[17] reported a lognormal expansion of $\rho_\alpha(\tau)$. Later on, Bendler and Shlesinger[18] showed that this series expansion (eq 60b, ref 17) suffers from poor convergence and lack of normalization. They found eq 59 of ref 17 to be superior in both respects. The same series expansion of $\rho_\alpha(\tau)$ as recast by Bendler et al.[18] (eq 51, ref 18) and shown below, is used in our calculation.

$$\rho_\alpha(\tau) = \frac{\alpha}{\tau_p}(\tau/\tau_p)^{\alpha-1} \exp[-(\tau/\tau_p)^\alpha] \times [1 - \alpha F_2 + \alpha^2 F_3 - \alpha^3 F_4 + \alpha^4 F_5 - \ldots] \qquad (6)$$

where

$$F_2 = U_2(1 - \mu^{-\alpha})$$

$$F_3 = U_3(1 - 3\mu^{-\alpha} + \mu^{-2\alpha})$$

$$F_4 = U_4(1 - 7\mu^{-\alpha} + 6\mu^{-2\alpha} - \mu^{-3\alpha})$$

$$F_5 = U_5(1 - 15\mu^{-\alpha} + 25\mu^{-2\alpha} - 10\mu^{-3\alpha} + \mu^{-4\alpha})$$

and $U_2 = 0.577\,216\,65$, $U_3 = -0.655\,877\,5$, $U_4 = -0.042\,003\,28$, $U_5 = 0.166\,538\,57$, and $\mu = \tau_p/\tau$.

Using the correlation function expression of eq 3, Kaplan et al. developed the final line-shape expression for a homogeneous distribution for a two-site exchange process (eq 22, ref 12). In our calculation, the same expression is extended to a polycrystalline type line shape.

For the inhomogeneous distribution, the same Wemmer line-shape expression[6] for multisite exchange is employed with a distribution of correlation times instead of a single correlation time. Each correlation time makes its own contribution toward the total line-shape collapse and the contribution in each case is weighted according to the distribution embodied in eq 3. In essence, the mathematical difference between the homogeneous and inhomogeneous treatments is that in the inhomogeneous case we have a set of uncoupled equations corresponding to the magnetization sites evolving under exchange independently without regard to state of the magnetization at other sites and for the homogeneous case the exchange of each site is coupled with the overall magnetization from all sites.

To save computer time, the following scheme was adopted. At the longer correlation time end, some point is reached when the line shape approaches the rigid limit; i.e., τ_j becomes so long that the jump for such a long τ_j does not cause line-shape collapse and essentially the rigid-case line shape results. There can still be some τ_j's left which are longer than this τ_j and their weightings must be considered. It is not necessary to repeat the line-shape calculation for these long τ's since the rigid limit has already been reached. Instead, the weightings for these τ's are combined with the weighting for this τ_j. The same time-saving scheme can be adopted for τ's at the shorter τ end where at one point the line shape reaches the rapid limit and further decrease in the value of τ leads to no additional narrowing.

For our calculation, 57 τ's were used, 28 on each side of τ_p spanning 28 decades of time (eq 4 and 5). Two τ's thus cover one decade, in accordance with the approach adopted by Kaplan et al.[12] An α value of near 0.16 is suitable for comparing both types of distributions. Comparisons focused on the 62.9-MHz data, which are sensitive enough to force a choice between the two distributions.

Calculations were restricted to the spectra at −80, −60, and −40 °C, which show distinctive temperature-dependent changes in the maximum-intensity area. Figure 2b,e (homogeneous) and Figure 2c,f (inhomogeneous) show the theoretical simulations with appropriate τ_p's for the experimental data at −80 and −60 °C. The distinctive dual-peak nature of the top part of the spectra can only be simulated by using the inhomogeneous distribution, which is at once evident from the figures for data at −80 and −60 °C. A homogeneous distribution results in featureless broadening as can be seen from the figure. These findings are thus in agreement with similar observations based on deuterium spectra[2] and we therefore concentrate the remaining interpretational efforts on the inhomogeneous distribution.

Simultaneous Model with an Inhomogeneous Distribution. For an improved interpretation, the simultaneous model is combined with an inhomogeneous distribution so that both motional processes can be treated at the same time. Some precautions are necessary. For BPA-PC, the secondary motion is always to be treated in the rapid limit. This condition is not met with for some of the longer τ's at the long-τ end, especially when τ_p is long, i.e., when slow-rate-regime line shapes are encountered. Again the following reasonable approximation is pursued. In doing calculation for the entire distribution,

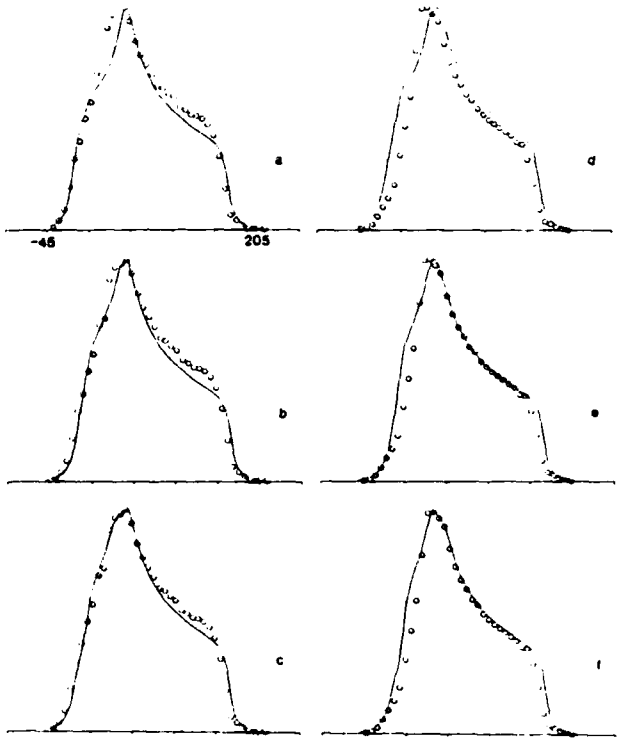

Figure 2. Comparison of simultaneous (a and d), two-site homogeneous (b and e), and two-site inhomogeneous (c and f) treatments for simulation of 62.9-MHz CSA data at −80 and −60 °C. In each case, the solid line represents the best simulation of the experimental data (O). (a) $\tau = 8.0 \times 10^{-4}$ s; (b) $\tau_p = 2.0 \times 10^{-7}$ s, $\alpha = 0.16$; (c) $\tau_p = 5.5 \times 10^{-3}$ s, $\alpha = 0.16$; (d) $\tau = 2.6 \times 10^{-4}$ s; (e) $\tau_p = 1.0 \times 10^{-8}$ s, $\alpha = 0.16$; (f) $\tau_p = 2.6 \times 10^{-4}$ s, $\alpha = 0.16$.

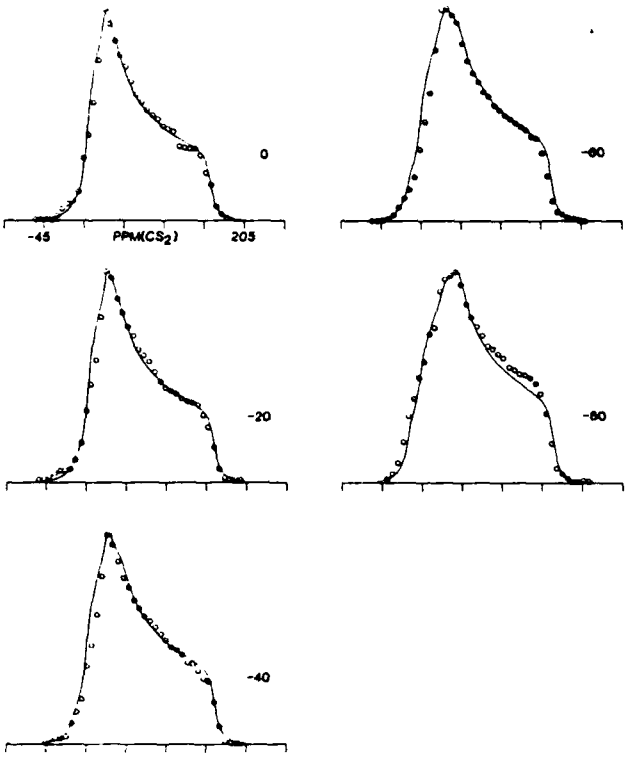

Figure 3. The solid lines are simulations of the 62.9-MHz CSA data (O) at several temperatures.

a point is reached when the τ_j no longer treat the secondary motion in the rapid limit. Again it is also possible that for that particular τ_j and all larger τ's, the rigid line shape is already achieved with respect to the large-amplitude jumps. This means simultaneous jump calculations are not necessary for the τ's in question; instead, line-shape intensities due to oscillation are calculated over an adequate number of frequency points to cover the entire spectrum by applying this motion alone to the rigid tensor principal values. The intensities are then multiplied by the sum of weightings for those long τ's, yielding a line-shape contribution for the long τ's part. For the remaining shorter τ's, the jump calculation is important. The simultaneous model is therefore applied for these remaining τ's, with the intensities obtained by summing up contributions for each τ according to the weighting factor given by the stretched exponential form. We then add up intensities for both the long and short correlation time parts to get the final line shape for the entire distribution. Again 57 τ's are employed.

Since the CSA line shape data do not seem critical enough to allow a precise estimation of α, the same simultaneous plus inhomogeneous consideration has been applied to the phenylene proton T_1 and $T_{1\rho}$ data reported earlier.[1] The proton data are not able to distinguish between homogeneous and inhomogeneous distributions since spin diffusion exchanges magnetization at different spatial sites. However, the overall breadth of either type of distribution is equivalently reflected in the breadth and shape of T_1 and $T_{1\rho}$ minima. The new interpretation of the proton data, including the contribution of restricted rotation, leads to an improved fit relative to the one obtained earlier with the Ngai formalism.[1] This improved analysis yields a value of 0.154 for α, and this same α is employed in the line-shape calculation. The amplitude of the restricted rotation is estimated from the high-temperature region where the flip contribution has already reached the rapid limit. We make use of the estimates reported earlier[7] based on the simultaneous model, which range in value from 64° at +120 °C to 23° at −80 °C. These estimates also prove to be effective for fitting the T_1 and $T_{1\rho}$ data where restricted rotation is included as a second motion in addition to π flips. A summary of line shape calculations at both fields is shown in Figures 3 and 4. The simulations are within the limit of experimental error. An Arrhenius analysis of τ_p's as shown in Figure 5 yields an apparent activation energy of 50 kJ/mol. Spectra at higher temperatures become rate independent for both primary and secondary processes. Simulations at temperatures beyond 0 °C are therefore not presented.

In the previous report,[1] the relaxation map log ν_c vs. T^{-1} was constructed with correlation frequencies and the corresponding temperatures for T_1 and $T_{1\rho}$ minima, average point of CSA line-shape coalescence, and maxima in dielectric and dynamic mechanical data. With the newer simultaneous-inhomogeneous description of phenylene motion, improved values of correlation frequencies for the π flips at T_1 and $T_{1\rho}$ minima and temperature for CSA collapse are obtained and used for reconstruction of the relaxation map as shown in Figure 6. The apparent activation energy (50 kJ/mol) and τ_∞ (4×10^{-17} s) obtained from linear least-squares analysis of the data are in good agreement with CSA line-shape analysis values (50 kJ/mol and 1×10^{-16} s).

The mechanical loss, $G_\gamma(\omega)^{loss}$, is given by the equation

$$G_\gamma(\omega)^{loss} = \frac{\langle \sigma_\gamma(0)^2 \rangle}{k_B T} \int_0^\infty \sin(\omega t) \phi'(t)\, dt \qquad (7)$$

where $\phi'(t)$ is the derivative of the correlation function as expressed in eq 3 and σ_γ is the stress arising from the

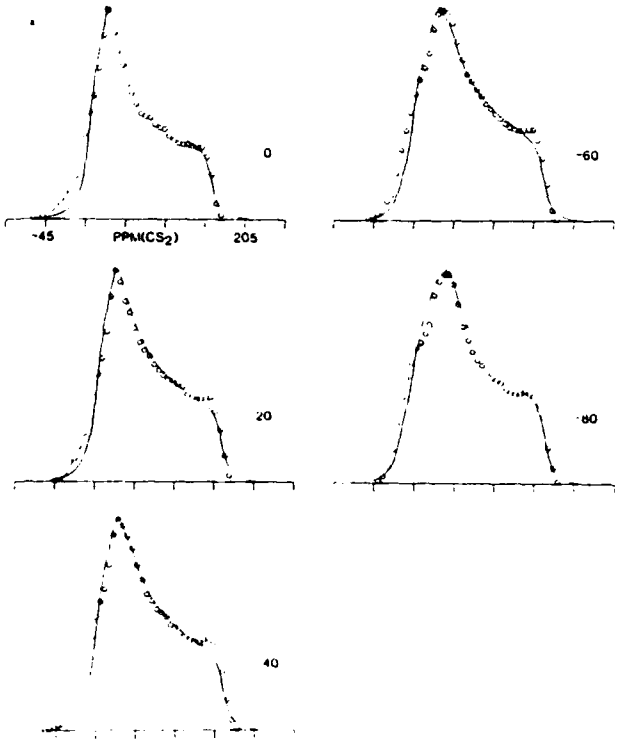

Figure 4. The solid lines are simulations of the 22.6-MHz CSA data (O) at several temperatures. The data are taken from ref 1.

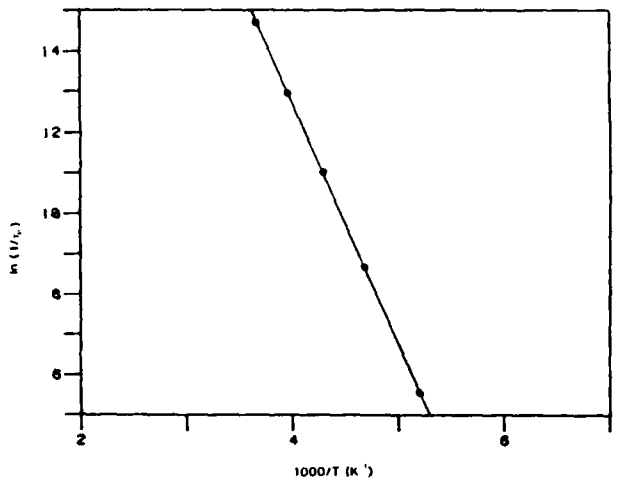

Figure 5. Logarithm of the inverse τ_ρ (as obtained from line-shape analysis) vs. inverse temperature.

molecular change. With this changed version of correlation function, the position and shape of the dynamic mechanical loss peaks as observed by Yee[4] were simulated by making use of eq 7, activation parameters as obtained from line-shape analysis, and an α value of 0.154. Figure 7 again shows rather good agreement between experiment and the prediction based on the interpretation of NMR data.

Discussion

In the present report, the carbon-13 CSA data base is expanded by collecting data at a higher field, i.e., 62.9 MHz, and we find the simultaneous-inhomogeneous description provides the best interpretation at both frequencies. This is a significant extension of the previous interpretation and demonstrates that NMR line-shape analysis in solids can yield a very detailed picture of the overall nature of the dynamics if a sufficiently wide data

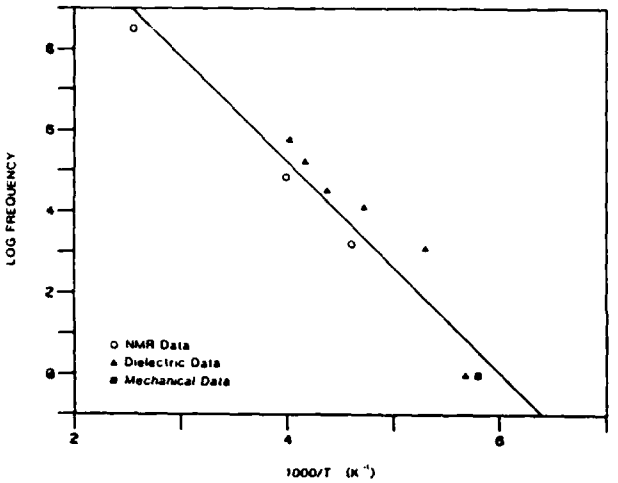

Figure 6. log (frequency) vs. inverse temperature or relaxation map. The highest frequency NMR point is the 90-MHz proton T_1 minimum, the next highest (43 kHz) is the $T_{1\rho}$ minimum, and the lowest is the average position of CSA line-shape coalescence. The filled triangles are maxima of dielectric loss curves taken at different temperatures. The positions of all points have an associated uncertainty of the order of 10 °C because of the broadness of loss peaks and relaxation minima.

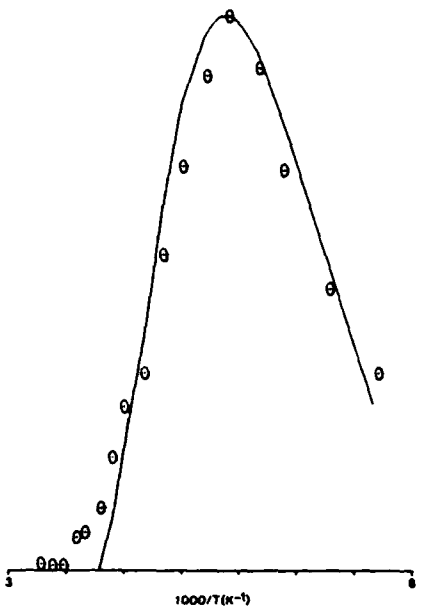

Figure 7. Dynamic mechanical spectrum. The solid line is the simulation employing the Williams–Watts inhomogeneous correlation function (eq 3) with the parameters set from the CSA line-shape analysis.

base is available. The previous estimates for the amplitude of restricted rotation or oscillation seem to be effective for fitting data at both frequencies. The primary motion includes jumps which extend over a range around exact π flips. The inhomogeneous nature of the motion indicated by the CSA spectra is plausible for a polymeric glass. Differences in packing lead to microscopic density fluctuation or a free volume distribution. Also differences in more specific interaction between chains, aside from packing effects, are also conceivable. Spatially separated groups therefore experience different barriers to motion.

The Williams–Watts formalism as expressed in eq 3 and its incorporation in multisite exchange line-shape expression represent this distribution. The breadth of the distribution may depend on the polymer structure and the nature of the motion. For BPA-PC, an α value of 0.154

indicates a broad distribution. A model[5] for motion in solid BPA-PC links the phenylene motion of the concerted cis–trans, trans–trans conformational interchange involving the carbonate unit. Since the whole process extends over more than one monomer unit, it is reasonable that the motion is more sensitive to steric hindrance and reacts to a greater degree to any density fluctuations or free volume distribution present in the system, thus yielding a broader distribution than in a case when the motion is simple and very localized.

The proposed motional model leads to the diffusion of a defect conformation along the polymer chain. The diffusing defect experiences a range of barrier heights resulting from various local packing and interaction effects and this leads to a distribution of waiting times. A diffusional process experiencing a distribution of barrier heights has been shown to lead to the stretched exponential form of correlation function.[20-22] This development from the theoretical side lends further credence to an analysis based on a Williams–Watts type correlation function.

Defect diffusion motion in combination with a distribution of barrier heights has been used to derive a stretched exponential correlation function.[20-22] However, if the distribution of barrier heights is different in the vicinity of spatially distinct relaxing groups, an inhomogeneous correlation function would result, i.e., relaxing groups at different spatial positions would have different relaxation rates. If the distribution of barriers were equivalent surrounding each spatial site, a homogeneous correlation would result. A derivation of the first case is not available, with the only derivations[20-22] corresponding to one set of barrier heights. These derivations start with a fundamentally inhomogeneous description but lead to a description of relaxation at only one site without considering the prospect of the barrier height inhomogeneity invoked, producing unequivalent relaxation at other sites.

From a general physical viewpoint, it seems unlikely that the correlation function itself is either purely inhomogeneous or purely homogeneous. The analysis considered here assumes complete inhomogeneity, and our earlier analysis,[1] complete homogeneity. The line-shape data are indicative of considerable inhomogeneity. Proton relaxation is sensitive to the presence of a distribution but cannot distinguish between homogeneous and inhomogeneous because of extensive averaging over spatial sites by spin diffusion. Carbon-13 T_1[19] and $T_{1\rho}$[11] data indicate inhomogeneous character, with spin dynamics playing a lesser role especially in the case of the T_1 data.[19] A decisive partitioning between the homogeneous and inhomogeneous aspects of relaxation in a glass which is consistent with spin–lattice relaxation and line-shape data warrants further consideration both theoretically and in the development of additional experimental data.

Temperature also affects the apparent homogeneous vs. inhomogeneous character in line-shape data. At low temperatures and intermediate exchange rates both deuterium[2] and CSA line shapes indicate an inhomogeneous distribution. However, at high temperatures, both sets of line-shape results indicate that all phenylene rings undergo large-angle flips in the fast limit. From the defect diffusion viewpoint, at lower temperature the defects can diffuse over a limited range past the lower barriers in the distribution of barrier heights. The associated rings will appear as mobile, each with its own rate. Phenylene groups experiencing high barriers will not undergo flips on the time scale of the experiment or only very slowly and will therefore appear as rigid. At high temperatures, all barriers can be surmounted in the time scale of the experiment so all rings are observed to undergo flips. If the temperature is sufficiently high, say 100 °C in BPA-PC, a distribution of flip rates still exists but all of the rates are in the fast limit, yielding the simple rapid-limit line shape, which can be simulated by any jump faster than the frequency separation of the exchanging line positions. The apparent activation energy of 50 kJ/mol, which is typical of polymeric glasses, seems quite reasonable and is in agreement with values from relaxation map analysis, mechanical data,[4] and T_1 and $T_{1\rho}$ simulations. Thus the phenomenological link in time among different NMR, dielectric, and dynamic mechanical measurements is further supported. In the same vein, the experimental data for dynamic mechanical measurements can be matched rather well, using activation parameters from line-shape analysis as input basis for eq 7, which is similarly reassuring.

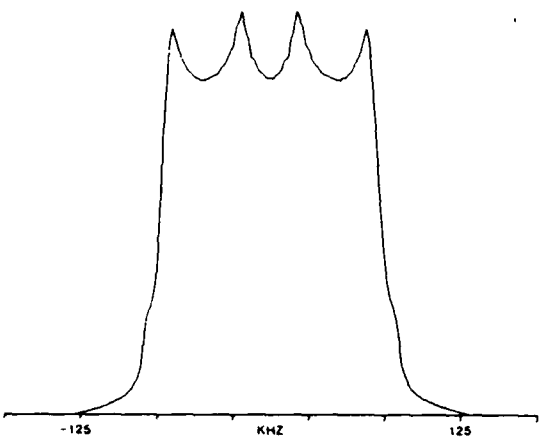

Figure 8. Theoretical deuterium spectrum, using the simultaneous–inhomogeneous description and parameters at −20 °C obtained from CSA line-shape analysis.

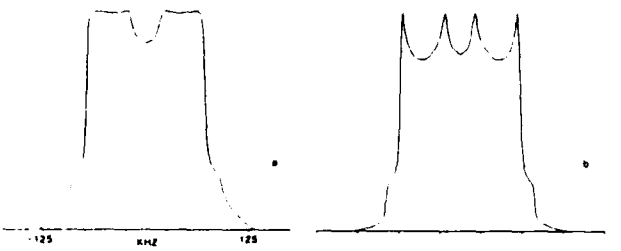

Figure 9. Comparison of homogeneous (a) and inhomogeneous (b) theoretical treatments of deuterium line shapes for phenylene group rotation for equivalent intermediate rates: (a) $\tau_p = 1.8 \times 10^{-10}$ s, $\alpha = 0.16$; (b) $\tau_p = 5.0 \times 10^{-6}$ s, $\alpha = 0.16$.

In view of the success of the simultaneous–inhomogeneous description in fitting different sets of experimental data, it seems worthwhile to generate a theoretical deuterium powder spectrum using the same motional picture and the correlation time at −20 °C. The generated spectrum should closely match the experimental deuterium spectrum at −20 °C, which has distinct features reflecting the inhomogeneous distribution.[2] Since the pulse widths and quadrupolar echo delays are not published, the corrections to the deuterium line shape cannot be affected. However, similar calculations showed that for the case of phenylene flipping, incorporating the corrections shifts the correlation times by a certain factor, but the basic line-shape features remain. Figure 8 shows the calculated line shape, which displays the same general features as the −20 °C expermental spectrum. This similarity in line shape obtained with the correlation time at −20 °C from CSA

line-shape analysis gives additional confidence in the phenylene dynamics picture as outlined here. It should be noted that due to the increased quadrupolar interaction, the features that distinguish homogeneous and inhomogeneous line shapes for intermediate rates, i.e., the differences at the absorption maxima, are enhanced over the CSA case as shown in Figure 9.

Acknowledgment. This research was carried out with the financial support of National Science Foundation Grant DMR-790677, of National Science Foundation Equipment Grant No. CHE 77-09059, of National Science Foundation Grant No. DMR-8018679, and of U.S. Army Research Office Grants DAAG 29-82-G-0001 and DAAG 29 85-K0126.

Registry No. BPA-PC (copolymer), 25037-45-0; BPA-PC (SRU), 24936-68-3.

References and Notes

(1) O'Gara, J. F.; Jones, A. A.; Hung, C.-C.; Inglefield, P. T. *Macromolecules* **1985**, *18*, 1117.
(2) Spiess, H. W. *Advances in Polymer Science*; Kausch, H. H., Zachmann, H. G., Eds.; Springer-Verlag: Berlin, 1984.
(3) (a) Illers, K.; Bruer, H. *Kolloid-Z.* **1961**, *176*, 110. (b) Krum, F.; Muller, F. H. *Kolloid-Z.* **1957**, *164*, 81. (c) Krum, F. *Kolloid-Z.* **1959**, *165*, 77.
(4) Yee, A. F.; Smith, S. A. *Macromolecules* **1981**, *14*, 54.
(5) Jones, A. A. *Macromolecules* **1985**, *18*, 902.
(6) Wemmer, D. E. Ph.D. Thesis, University of California, Berkeley, CA, 1979.
(7) Roy, A. K.; Jones, A. A.; Inglefield, P. T. *J. Magn. Reson.* **1985**, *64*, 441.
(8) Ngai, K. L. *Comments Solid State Phys.* **1979**, *9*, 127.
(9) Ngai, K. L.; White, C. T. *Phys. Rev. B* **1979**, *20*, 2476.
(10) Ngai, K. L. *Phys. Rev. B* **1980**, *22*, 2066.
(11) (a) Schaefer, J.; Stejskal, E. O.; Steger, T. R.; Sefcik, M. D.; McKay, R. A. *Macromolecules* **1980**, *13*, 1121. (b) Steger, T. R.; Schaefer, J.; Stejskal, E. O.; McKay, R. A. *Macromolecules* **1980**, *13*, 1127.
(12) Kaplan, J. I.; Garroway, A. N. *J. Magn. Reson.* **1982**, *49*, 464.
(13) Mehring, M. *High Resolution NMR in Solids*, 2nd ed.; Springer-Verlag: New York, 1983.
(14) Bloembergen, N.; Rowland, T. J. *Acta Metall.* **1955**, *1*, 731.
(15) Wemmer, D. E.; Ruben, D. J.; Pines, A. *J. Am. Chem. Soc.* **1981**, *103*, 28.
(16) Williams, G.; Watts, D. C. *Trans. Faraday Soc.* **1970**, *66*, 80.
(17) Montroll, E. W.; Bendler, J. T. *J. Stat. Phys.* **1984**, *34*, 129.
(18) Bendler, J. T.; Shlesinger, M. F. In *Studies in Statistical Mechanics*; Shlesinger, M. F., Weiss, G. H., Eds.; North-Holland: New York, 1985; Vol. 12.
(19) Connolly, J.; Jones, A. A.; Inglefield, P. T., to be published.
(20) Shlesinger, M. F.; Montroll, E. W. *Proc. Natl. Acad. Sci. U.S.A.* **1984**, *81*, 1280.
(21) Shlesinger, M. F. *J. Stat. Phys.* **1984**, *36*, 639.
(22) Blumen, A.; Zumofen, G.; Klafter, J. *Phys. Rev. B* **1984**, *30*, 5379.

SOLID STATE LINE SHAPES CALCULATED FROM A FRACTIONAL EXPONENTIAL CORRELATION FUNCTION

Ajoy K. Roy and Alan Anthony Jones
Department of Chemistry
Clark University

Paul T. Inglefield
Department of Chemistry
College of the Holy Cross

Introduction:

Local packing differences observed in polymeric glasses result in density fluctuations or a free volume distribution. This, coupled with a variety of intermolecular interactions, may cause motion in solid-state to be distributional in character. A fractional exponential correlation function of the form $e^{-(t/\tau_p)^\alpha}$ with $0<\alpha<1$, commonly referred to as the Williams-Watts function, has long been employed to describe such distributional effects. Williams and Watts have used this function to interpret dielectric relaxation in polymers. Recently Bendler et al.[2] have used this stretched exponential form to describe defect diffusion in a situation where a distribution of barrier heights exists. NMR line shapes for a simple two-site exchange based on this function display the obvious features of distribution.[3] However, the distribution may arise in two ways:[3] (i) a homogeneous distribution where the motional process is the same throughout the matrix, but is non-exponential in character, and (ii) an inhomogeneous distribution where there is a true spatial distribution of molecular processes, each of which is characterized with its own exponential time-constant. Powder NMR line shapes, both CSA and quadrupolar, are in general more informative than a simple single line exchange line shape particularly with respect to the geometry of the motion. Use of the Williams-Watts function for CSA line shapes has been successful in predicting the nature of distribution.[4] The large quadrupolar interaction often renders the deuterium line shapes even more sensitive than the CSA line shapes. In this report, the Williams-Watts non-exponential correlation function will be applied to calculate homogeneous and inhomogeneous solid deuterium line shapes for the case of phenylene π-flipping around C_1C_4 axis. The line shapes are compared with the ones obtained for a single correlation time. The applications are related to published experimental data on PBT[5] and our own CSA findings.[4]

Calculation:

Line shapes for single correlation times are calculated according to the two-site exchange formalism developed independently by Mehring[6] and Wemmer.[7] The distributional models make use of the Williams-Watts function:

$$\phi(t) = e^{-(t/\tau_p)^\alpha} \qquad (1)$$

where τ_p is the center correlation time, and α, the breadth parameter. Smaller α's are associated with broader distributions. Eq. (1) can be recast in the form:[3]

$$\phi(t) = \int_{-\infty}^{\infty} d(\log \tau)\, G(\log \tau)\, \exp(-t/\tau) \qquad (2)$$

The following discrete summation form is easy to use

$$\phi(t) = \sum_j P_j \exp(-t/\tau_j) \qquad (3)$$

with a normalization constant given by $\phi(0) = \sum_j P_j = 1$;

$$P_j = G(\log \tau_j)\,[\log(\tau_j/\tau_{j+1})]$$

where by the definition in Eq. (2)

$$G(\log \tau) = \tau\rho(\tau)/\log e$$

For $\rho(\tau)$, the series expansion form as reported by Bendler et al.[8] and shown below, is used in our calculation.

$$\rho(\tau) = \alpha/\tau_p(\tau/\tau_p)^{\alpha-1}\, e^{-(t/\tau_p)^\alpha}\,[1-\alpha F_2+\alpha^2F_3-\alpha^3F_4+\alpha^4F_5+\ldots.$$

The terms F_2, F_3, F_4 and F_5 which have α and τ_p dependence are defined in ref. 2.

For a homogeneous distribution, Kaplan et al. use the correlation function expression (3) and develop the final line shape expression for a two-site exchange process [Eq. (22), ref. 3]. For our case, the same expression is extended to a polycrystalline type line shape. For an inhomogeneous distribution, the same line shape expression as used for a single correlation time process, is employed but with a distribution of correlation times. Each correlation time makes its own contribution towards the total line shape collapse and the contribution in each case is weighted according to the distribution embodied in Eq. (3). A scheme adopted to save computer time is described elsewhere.[4] In all our calculations involving distribution, we use an α value of 0.30. The α values are usually estimated in conjunction with other sets of experiments such as carbon-13 or proton T_1 or $T_{1\rho}$ data.[4] It may also be possible to set an α value by matching both shapes and true intensities in quadrupole echo experiments. It needs to be emphasized here, however, that general shapes are determined primarily on the basis of the particular motional description, irrespective of intensities. Since our main objective is to test wider applicability of the Williams-Watts function for NMR line shapes and since the published data do not contain reduction factors showing loss in intensity relative to true FID's, we use an α value of 0.30, which is reasonable for glassy polymers. The calculated spectra are corrected for pulse power fall-off as a function of frequency[8] and for motions that occur during the quadrupole echo delay time.[9] Attempts were made to fit line shapes reported in ref. 5 (p. 2402) and results for simulation at 50°C are shown in Fig. 1. Calculated line shapes are indicated by solid lines and the experimental by dashed lines.

Discussion:

Results in Fig. 1 show that calculated line shapes for single correlation time (——, 1a) and homogeneous distribution (——, 1b) have quite similar features. A homogeneous distribution adds some extra broadening effects without altering the basic line shape features. With an inhomogeneous distribution, this is, however, not the case as can be seen from the calculated line shape (——) shown in Fig. 1c. The line shape has obvious features which allow one to easily distinguish the inhomogeneous case from the other two categories. This is to be expected, since in polymers, local density fluctuation coupled with interaction effects produce different local environs for the same motional process. The motional processes thus experience apparently different barrier heights, leading to the inhomogeneous distribution. These results are also in agreement with our CSA line shape analyses[4] and clearly demonstrate the utility of stretched exponential form as a basis for explaining distribution in polymers. The improved match of the experimental line shape with the inhomogeneous calculaton is easily noted in the figure. An Arrhenius analysis of τ_p's gives an activation energy of 45 kJ/mole which is typical for polymeric glasses but is much larger than the estimate based on a single exponential correlation function. A detailed analysis of a larger data base is desirable for a better estimate of α and activation energy.

The present report and numerous other quadrupole, CSA and spin-lattice relaxation studies[4,10-12] on glassy polymers clearly demonstrate that in general the dynamics is distributional in character and the distribution can be conveniently and accurately characterized by the stretched exponential or Williams-Watts function. A physical origin of this distribution has been a topic of recent discussion in the literature[2,13-15] and lends further credence to this

approach. Also from the experimental literature examined thus far there is a strong indication that the distribution is in general inhomogeneous in glassy polymers.

Acknowledgements:

This research was carried out with the financial support of the National Science Foundation Grant DMR-790677, of National Science Foundation Equipment Grant No. CHE 77-09059, of National Science Foundation Grant No. DMR-8108679, and of U.S. Army Research Office Grant DAAG 29-82-G-0001. DAAG29-85-K-0126

References:

1. William G., Watts, D.C., Trans. Faraday Soc. 1970, 66, 80.

2. Bendler, J.T., Shlesinger, M.F., The Wonderful World of Stochastics, Shlesinger, M.F. and Weiss, G.H., ed., Studies in Statistical Mechanics; North Holland: New York, 1985; Vol. 12.

3. Kaplan, J.I., Garroway, A.N., J. Mag. Res. 1982, 49, 464.

4. Roy, A.K., Jones, A.A., Inglefield, P.T., Submitted to Macromolecules.

5. Cholli, A.L., Dumais, J.J., Engel, A.K., Jelinski, L.W., Macromolecules 1984, 17, 2399.

6. Mehring, M., High Resolution NMR in Solids, 2nd. Ed.; Springer-Verlag: New York, 1983.

7. Wemmer, D.E., Ph.D. Thesis, University of California, Berkeley, CA, 1979.

8. Bloom, M., Davis, J.H., Valic, M.I., Can. J. Phys. 1980, 58, 1510.

9. Spiess, H.W., Sillescu, H.J., J. Mag. Res. 1981, 42, 381.

10. Garroway, A.N., Ritchey, W.M., Moniz, W.B., Macromolecules 1982, 15, 1051.

11. Fischer, E.W., Hellmann, G.P., Spiess, H.W., Makromol. Chem., Suppl. 1985, 12, 189.

12. Connolly, J., Jones, A.A., Inglefield, P.T., to be published.

13. Shlesinger, M.F., Montroll, E.W., Proc. Natl. Acad. Sci. (USA) 1984, 81.

14. Shlesinger, M.F., J. Stat. Phys. 1984, 36, 639.

15. Blumen, A., Zumofen, G., Klafter, J., Physical Review B 1984, 30, 5379.

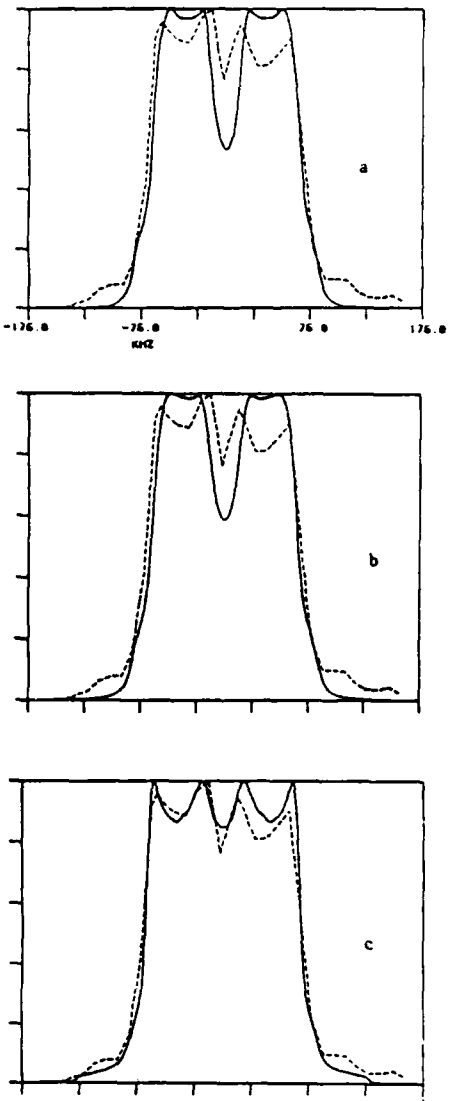

Fig. 1: Comparisons of single correlation time (a), homogeneous (b) and inhomogeneous (c) treatments for simulation of deuterium line shape on PBT at 50°C (ref. 5, p. 2402). In each case, the calculated line shape is represented by the solid (——) line and the experimental by the dashed (----) line. The correlation times for the calculated spectra are: a) 9.0×10^{-7}s (τ), b) 1.0×10^{-8}s (τ_p), and c) 1.2×10^{-5}s (τ_p).

Analytica Chimica Acta, 189 (1986) 167—181
Elsevier Science Publishers B.V., Amsterdam — Printed in The Netherlands

FURTHER STUDIES OF MULTIPLE NUCLEAR SPIN RELAXATION AND LOCAL MOTIONS IN DISSOLVED 1,1-DICHLORO-2,2-BIS(4-HYDROXYPHENYL)ETHYLENE POLYFORMAL

CHI-CHENG HUNG, JOHN H. SHIBATA, MICHAEL F. TARPEY and ALAN A. JONES*
Jeppson Laboratory, Department of Chemistry, Clark University, Worcester, MA 01610 (U.S.A.)
JOHN A. PORCO and PAUL T. INGLEFIELD
Department of Chemistry, College of the Holy Cross, Worcester, MA 01610 (U.S.A.)
(Received 6th March 1986)

SUMMARY

Deuterium, carbon-13 and proton spin-lattice relaxation times at two fields are reported for dilute solutions of 1,1-dichloro-2,2-bis(4-hydroxyphenyl)ethylene polyformal. The carbon-13 and proton relaxation measurements were made at a concentration of 10% (w/w) in deuterated s-tetrachloroethane and as a function of temperature. A partially deuterated analog with deuterated methylene groups was used in order to remove cross-relaxation effects from the phenylene proton relaxation. In addition, deuterium relaxation measurements were made on this sample at a concentration of 10% (w/w) in tetrachloroethane as a function of temperature. The data are interpreted in terms of segmental motion arising within the bisphenol units and anisotropic internal rotations of the other structural components. Motions of the phenylene groups in the backbone are described by the Hall-Helfand segmental correlation function plus the Woessner anisotropic internal-rotation correlation function. Motions of the formal linkage are described by the same segmental correlation function plus an internal correlation function based on restricted double rotation about the two carbon/oxygen bonds. The local motion of the formal group is discussed in terms of conformational transitions that are likely in a polyformal in view of the conformational energy surface. A Helfand Type II motion of the formal group corresponding to a transition from *gg'* to *tg* is identified as the most plausible rearrangement of this unit.

Spin relaxation in dilute solution has been used to characterize local chain motion in several polymers with aromatic backbone units [1–5]. One notable type is aromatic polycarbonates which are common high-impact-resistant engineering plastics. The polymer examined here, 1,1-dichloro-2,2-bis(4-hydroxyphenyl)ethylene polyformal, shown in Fig. 1 and abbreviated Chloral-PF, is a structural analog of a well studied polycarbonate, Chloral-PC [4, 5]. The only difference in the structure of Chloral-PF relative to Chloral-PC is the replacement of the carbonate units by formal units. The formal unit presents an opportunity to monitor chain motion at a site inaccessible in polycarbonates because the carbonate unit contains no protons and thus cannot be probed by the usual approach. Additional motivation for study

0003-2670/86/$03.50

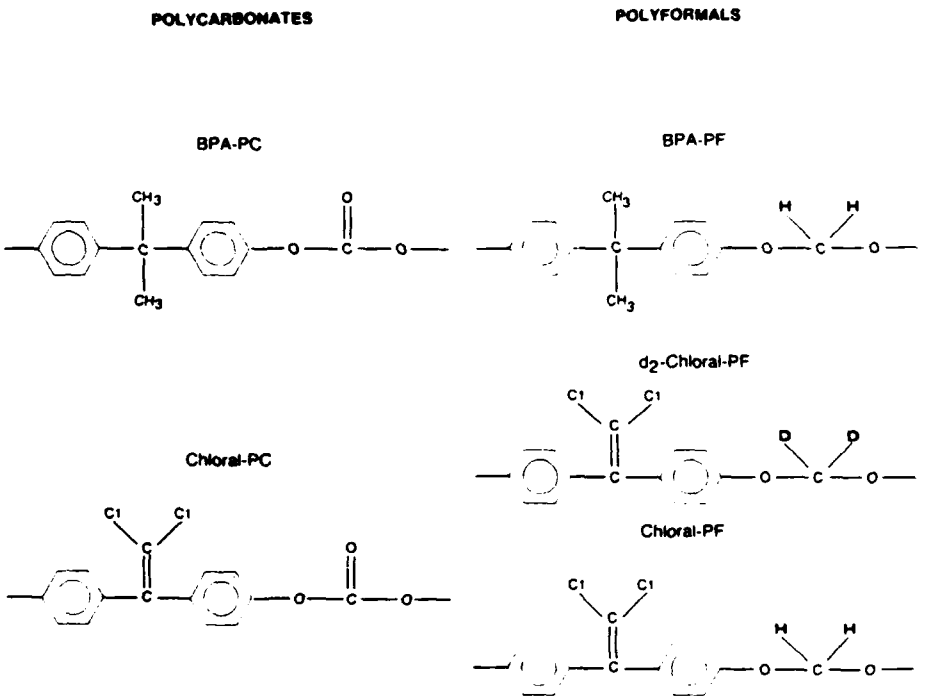

Fig. 1. Structure of the repeat units and the associated abbreviations.

arises because this polymer has a dynamic mechanical spectrum similar to the impact-resistant polycarbonates [6].

An early report of spin relaxation and local motion of dissolved Chloral-PF has already been presented [7]. In the present paper, an expanded data base is presented to verify and extend the previous interpretation. On the basis of the earlier data, the formal group was viewed as undergoing segmental motion originating in the bisphenol unit plus restricted rotational diffusion about an axis between the oxygens of the formal group. As discussed in the previous study, the choice of the O—O rotation axis is an approximation, leading to the conclusion that the formal group rotates freely about the O—O axis at high temperature. With an enlarged experimental data base, it is now possible to consider a more detailed and realistic model for the formal group motion. This model consists of simultaneous, restricted rotations about the C—O bonds in the formal linkage. The Szabo convention [8, 9] is adopted to describe simultaneous trans—gauche two-site jumps about the C—O bonds. This picture is consistent with solid-state deuterium n.m.r. studies on several polymers in which the methylene units in the backbone of the polymer chain undergo trans—gauche isomerization [10—12]. In the earlier study, it was also assumed that formal group rotation has no effect on the phenylene group motion. In the interpretation to be presented here, this assumption of

localized independent formal group motion continues to yield the best simulation of the data.

The deuterium magnetic resonance data reported here provide an independent probe of chain motion because the relaxation mechanism stems from the quadrupolar interaction. This mechanism is entirely different from the source of proton and carbon-13 relaxation which results from modulation of the dipole/dipole interaction. Also, certain complexities present in dipolar relaxation such as cross-relaxation and cross-correlation are absent from quadrupolar relaxation. The deuterium spin-relaxation times in this report are measured at two field strengths in the deuterated Chloral-PF analog shown in Fig. 1. The combination of deuterium, proton and carbon-13 relaxation measurements each at different field strengths provides an unusually extensive frequency probe (13.8—250 MHz) yielding a critical data base for quantifying the dynamics.

EXPERIMENTAL

High-molecular-weight samples of the polyformal were kindly supplied by General Electric. The structure of the repeat unit is shown in Fig. 1 as well as the structure of a partially deuterated form which was synthesized here [13]. Based on instrinsic viscosity, the weight-average molecular weight of the polyformal is 3.7×10^4 Daltons and that of the deuterated analogue is 2.9×10^4 Daltons. A 10% (w/w) solution of the polyformal in $C_2D_2Cl_4$ was prepared for proton and carbon-13 spin relaxation measurements. Another 10% (w/w) solution of the partially deuterated polymer in tetrachloroethane was also prepared for deuterium spin-relaxation measurements. These two samples were subjected to five freeze/pump/thaw cycles before sealing.

Two spectrometers were used. The 30- and 90-MHz proton measurements, the 22.6-MHz carbon-13 measurement and 13.815-MHz deuterium measurement were obtained on a Bruker SXP 20-100. The 250-MHz proton, 62.9-MHz carbon-13 and 38.397-MHz deuterium measurements were obtained on a Bruker WM-250. Temperature control was maintained to ±2 K with a Bruker B-ST 100/700 variable-temperature accessory calibrated against a thermocouple placed in a sample tube. All T_1 measurements were made with a standard $180°—\tau—90°$ sequence and are reported with an experimental uncertainty of 10%. Typical $\pi/2$ pulse widths for all nuclei are in the range 10—25 μs. The 10% error reported for T_1 includes errors arising from sample preparation, temperature control, pulse sequence and the fitting of the recovery of magnetization to equilibrium.

RESULTS

The recovery of magnetization to equilibrium monitored in the $180°—\tau—90°$ sequence follows a simple exponential dependence on delay time, τ. The data were fitted both with the standard linear least-squares form and non-

linear least-squares form. The two treatments yielded relaxation times (T_1) within 10% of each other and average values are reported. No evidence of cross-relaxation or cross-correlation were observed in the decay curve of the recovery of magnetization. The presence of cross-relaxation in the proton data was further checked by comparing the phenylene T_1 value in the fully protonated polymer to the phenylene T_1 value in the deuterated polymer. The phenylene proton T_1 is about 10% longer in the deuterated polymer indicating a small amount of cross-relaxation though the 10% change is essentially the same as the experimental uncertainty. Table 1 contains proton, carbon-13 and deuterium T_1 values as a function of temperature and Larmor frequency.

Interpretation

The standard relationships between T_1 values and spectral densities, J, are used for carbon-13, the expressions are:

$$1/T_1 = W_0 + 2W_{1c} + W_2$$

$$W_0 = \sum_j \gamma_C^2 \gamma_H^2 \hbar^2 J_1(\omega_0)/20 r_j^6$$

TABLE 1

Spin-lattice relaxation times of Chloral-PF

Temp. (°C)	Relaxation time (ms)			
	Phenylene proton		Phenylene carbon	
	90 MHz	30 MHz	62.9 MHz	22.6 MHz
0	548	153	137	72
20	499	189	174	106
40	522	274	243	156
60	628	412	377	349
80	794	553	543	448
100	1168	763	798	679
120	1411	939	1113	936

Temp. (°C)	Relaxation time (ms)					
	Formal proton		Formal carbon		Formal deuterium	
	250 MHz	90 MHz	62.9 MHz	22.6 MHz	38.4 MHz	13.8 MHz
−20					3.15	1.09
0	335	129	81	36	3.09	1.55
20	282	114	91	52	3.97	2.70
40	268	133	115	82	6.21	5.44
60	295	198	158	123	11.92	10.65
80	350	258	229	193	17.95	17.00
100	467	320	339	275	28.86	27.40
120	628	433	403	377	41.08	40.57

$$W_{1c} = \sum_j 3\gamma_C^2\gamma_H^2\hbar^2 J_1(\omega_C)/40r_j^6 \tag{1a}$$

$$W_2 = \sum_j 3\gamma_C^2\gamma_H^2\hbar^2 J_2(\omega_2)/10r_j^6$$

$$\omega_0 = \omega_H - \omega_C \quad \omega_2 = \omega_H + \omega_C$$

and for protons the relationship is

$$1/T_1 = \sum_j (9/8)\gamma^4\hbar^2 r_j^{-6}[(2/15)J_1(\omega_H) + (8/15)J_2(2\omega_H)] \tag{1b}$$

For deuterium quadrupole relaxation in liquids, the expression [14] is

$$1/T_1 = (3/80)(1 + \eta^2/3)(e^2qQ/\hbar)^2[J(\omega_D) + 4J(2\omega_D)] \tag{1c}$$

where $e^2qQ/\hbar$ is the quadrupole coupling constant. The asymmetry parameter, η, is negligibly small for deuterium [11, 14].

The internuclear distances used are 1.09 Å for the phenylene C–H distance, 1.135 Å for the formal C–H distance, 2.36 Å for the 2–3 phenylene proton distance, and 1.79 Å for the formal proton–proton distance. The internuclear distance between the 2 and 3 phenylene protons is small but it is consistent with x-ray results on a similar low-molecular-weight molecule, dimethyl terephthalate [15]. The quadrupolar relaxation expression requires knowledge of the quadrupole coupling constant. For polymethylene oxide, the methylene quadrupole coupling constant is 154 ± 2 kHz [11]. For the polymethylene chains, the coupling constant is 167 kHz [12]. The coupling constant used here, 160 kHz, is in reasonable agreement with these values.

The expressions for the spectral densities can be developed from models for local motion in randomly coiled chains. The local motions to be considered here are segmental rearrangements, phenylene group rotation and formal group rotation. Segmental motion is described by a model developed by Helfand and coworkers [16, 17], based on computer simulations of chain dynamics. The correlation function for segmental motion involves two motional processes and is given by

$$\phi(t) = \exp(-t/\tau_0)\exp(-t/\tau_1)I_0(t/\tau_1) \tag{2}$$

where τ_1 is the correlation time for cooperative conformational transitions involving several bonds, τ_0 is the correlation time for single-bond conformational transitions, and I_0 is a modified Bessel function of order zero. This correlation function has been successfully applied to the solution study of polycarbonates [5]. Single bond and cooperative transitions occur in the bisphenol units of the backbone. Segmental motions about the bonds of this unit, depicted in Fig. 2, affect the dynamics of both the phenylene and formal groups. The correlation function can be Fourier-transformed to yield the following spectral density required for calculation of spin relaxation.

$$J(\omega) = 2\{[(\tau_0^{-1})(\tau_0^{-1} + 2\tau_1^{-1}) - \omega^2]^2 + [2(\tau_0^{-1} + \tau_1^{-1})\omega]^2\}^{-1/4}$$
$$\cos\{1/2 \arctan 2(\tau_0^{-1} + \tau_1^{-1})\omega/[\tau_0^{-1}(\tau_0^{-1} + 2\tau_1^{-1}) - \omega^2]\} \tag{3}$$

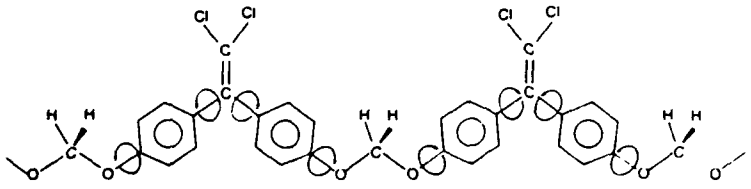

Fig. 2. The physical picture of segmental motion within the bisphenol unit. The arrows indicate those bonds in the bisphenol unit, the reorientation of which is included in the description of segmental motion.

Local phenylene and formal group rotation can be described by anisotropic internal rotation [18]. The correlation function for a trans–gauche two-site jump in the formal group can be calculated by using the Jones two-site jump model [19]. For two rotational equilibrium positions, the time-dependent probabilities can be calculated:

$$P(\phi_i, 0) = 1/2$$

$$P(\phi_j, t|\phi_i 0) = 1/2\ [1 + \exp(-t/\tau)]\ (\text{for } i = j) \tag{4}$$

$$P(\phi_j, t|\phi_i, 0) = 1/2\ [1 - \exp(-t/\tau)]\ (\text{for } i \neq j)$$

where $P(\phi_i, 0)$ is the probability of finding the internuclear vector at angle ϕ_i, $P(\phi_j, t|\phi_i, 0)$ is the time-dependent probability of finding the internuclear vector at angle ϕ_j given ϕ_i at time $t = 0$. The correlation function can thus be calculated by using those probabilities:

$$g_{mp}(t) = \exp[im\phi_i(0)]\ \exp[-ip\phi_j(t)]$$

$$= \sum_i P(\phi_i, 0)\ \exp(im\phi_i)\ [\sum_j \exp(-ip\phi_j)\ P(\phi_j, t|\phi_i, 0)] \tag{5}$$

Assuming that the correlation function is independent of the initial position, $\phi_i(0)$, which is dependent on the choice of the coordinate system, then

$$g_{mm}(t) = 1/2[1 + \exp(-t/\tau_{irf})] + 1/2[1 - \exp(-t/\tau_{irf})]\ (\cos m\phi) \tag{6}$$

When $m \neq p$, $g_{mp}(t) = 0$. Here, ϕ is the jump angle, and τ_{irf} is the jump relaxation time. For the trans–gauche conformational change, $\phi = 120°$, and thus

$$g_{00}(t) = 1;\ g_{\pm1\,\pm1}(t) = g_{\pm2\pm2}(t) = 1/4 + 3/4\ \exp(-t/\tau_{irf}) \tag{7a}$$

For $\phi = 180°$, referred to as a π flip,

$$g_{00}(t) = 1;\ g_{\pm1\pm1}(t) = \exp(-t/\tau_{irf});\ g_{\pm2\pm2}(t) = 1 \tag{7b}$$

The Szabo formula is used next to express the internal correlation function for double rotations as

$$G(t) = \sum_{mn} \sum_p d^2_{mo}[\Delta]\ d^2_{no}[\Delta]^*\ d^2_{pn}(\beta_{21})\ d^2_{pm}(\beta_{21})\ g^{(1)}_{mn}(t) g^{(2)}_{pp}(t) \tag{8}$$

where $d^2_{mo}[\Delta]$, $d^2_{no}[\Delta]$, $d^2_{pn}[\beta_{21}]$ and $d^2_{pm}[\beta_{21}]$ are reduced Wigner rotation matrices. A frame 1 is defined such that the rotation axis, Z_1, is along the Z axis of frame 1. The internuclear vector I rotates about the Z_1 axis, as shown in Fig. 3. Similarly, the Z_1 axis rotates about the Z axis of frame 2. Here, Δ is the angle between the internuclear vector and the rotation axis Z_1; β_{21} is the Euler angle between the two rotation axes Z_1 and Z_2; and $g^{(1)}_{mn}(t)$ and $g^{(2)}_{pp}(t)$ are the correlation functions describing rotation of the internuclear vector about the Z_1 axis, and the rotation of frame 1 about the Z axis of frame 2, respectively. Equation 8 can be simplified when the correlation function is independent of initial states. For this case, $m = n$, and $G(t)$ becomes,

$$G(t) = \sum_{mp} [d^2_{mo}(\Delta)]^2 [d^2_{pm}(\beta_{21})]^2 g^{(1)}_{mm}(t) g^{(2)}_{pp}(t) \tag{9}$$

By using this equation, several types of anisotropic motion can be introduced including jumps between two minima, jumps between three minima or stochastic diffusion.

In the case of one internal rotation axis, the correlation function in Eqn. 8 reduces to

$$G(t) = \sum_{mn} d^2_{mo}[\Delta] d^2_{no}[\Delta] * g_{mn}(t) = \sum_{m} \{d^2_{mo}[\Delta]\}^2 g_m(t) \tag{10}$$

where $g_m(t)$ is the correlation function described by Woessner [18]. For stochastic diffusion of phenylene group rotation about the C_1—C_4 axis, the correlation function is

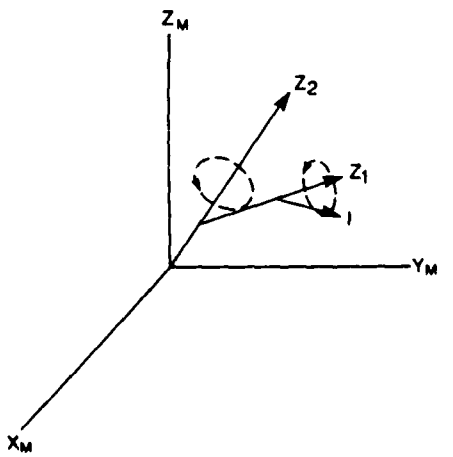

Fig. 3. The coordinate systems for double internal rotations of the formal group. The internuclear vector, I, rotates about the Z_1 axis. Z_1 rotates about the Z_2 axis which is the Z axis of frame 2. The axes of the molecular frame (Z_m, Y_m, X_m) are arbitrarily chosen to coincide with those of frame 2 (cf. [20]).

$$G(t) = A + B\exp(-t/\tau_{irp}) + C\exp(-4t/\tau_{irp}) \tag{11}$$

where $A = (3\cos^2\Delta - 1)^2/4$, $B = 3(\sin^2 2\Delta)/4$, and $C = 3(\sin^4\Delta)/4$.

The correlation function for segmental motion can be combined with formal group rotation and phenylene group rotation to yield a composite correlation function when each of the three local motions is considered to be independent. By using Eqns. 2 and 9, this composite correlation function can be Fourier-transformed to yield the following spectra density:

$$\begin{aligned} J(\omega) &= 2\,Re\int_0^\infty \phi(t)\,G(t)\exp(i\omega t)dt \\ &= 2\,Re\int_0^\infty \sum_{mp} [d^2_{mo}(\Delta)]^2\,[d^2_{pm}(\beta_{21})]^2\exp(-t/\tau_0)\exp(-t/\tau_1)\,I_0(t/\tau_1) \\ &\quad g^{(1)}_{mm}(t)g^{(2)}_{pp}(t)\exp(i\omega t)dt \end{aligned} \tag{12}$$

By inserting the internal correlation function for formal group motion described by Eqn. 7(a) and integrating, the spectra density becomes

$$\begin{aligned} J(\omega) &= J_a(\tau_0,\tau_1,\omega)\,[d^2_{00}(\Delta)]^2\,[d^2_{00}(\beta_{21})]^2 \\ &\quad + [1/16\,J_a(\tau_0,\tau_1,\omega) + 3/8\,J_b(\tau_{b0},\tau_1,\omega) + 9/16\,J_c(\tau_{c0},\tau_1,\omega)] \\ &\quad < 2[d^2_{20}(\Delta)]^2\ \{[d^2_{22}(\beta_{21})]^2 + [d^2_{22}(\beta_{21})]^2\} \\ &\quad + 2[d^2_{10}(\Delta)]^2\ \{[d^2_{11}(\beta_{21})]^2 + [d^2_{1\text{-}1}(\beta_{21})]^2\} \\ &\quad + 2\{[d^2_{10}(\Delta)]^2 + [d^2_{20}(\Delta)]^2\}\ \{[d^2_{21}(\beta_{21})]^2 + [d^2_{2\text{-}1}(\beta_{21})]^2\} > \\ &\quad + [1/4\,J_a(\tau_0,\tau_1,\omega) + 3/4\,J_b(\tau_{b0},\tau_1,\omega)] \\ &\quad < 2\{[d^2_{00}(\Delta)]^2 + [d^2_{20}(\Delta)]^2\}\ [d^2_{20}(\beta_{21})]^2 \\ &\quad + 2\{[d^2_{00}(\Delta)]^2 + [d^2_{10}(\Delta)]^2\}\ [d^2_{10}(\beta_{21})]^2 > \end{aligned} \tag{13}$$

with $\tau^{-1}_{b0} = \tau^{-1}_0 + \tau^{-1}_{irf}$ and $\tau^{-1}_{c0} = \tau^{-1}_0 + (\tau_{irf}/2)^{-1}$

Here, $J_a(\tau_0, \tau_1, \omega)$, $J_b(\tau_{b0}, \tau_1, \omega)$ and $J_c(\tau_{c0}, \tau_1, \omega)$ have the same form as Eqn. 3 with τ_0 replaced by τ_0, τ_{b0} and τ_{c0}, respectively. A correlation time, τ_{irf}, is set for the time scale of formal rotation about the C—O axes.

For phenylene group motion, two approaches were considered. The first approach allows no effect from formal group rotation and the second approach allows for the effect of rotation of formal group. In the first case, simply substituting Eqn. 11 for $G(t)$ into Eqn. 12 yields the spectral density

$$J(\omega) = AJ_x(\tau_0,\tau_1,\omega) + BJ_y(\tau_{y0},\tau_1,\omega) + CJ_z(\tau_{z0},\tau_1,\omega) \tag{14}$$

For stochastic diffusion,

$$\tau^{-1}_{y0} = \tau^{-1}_0 + \tau^{-1}_{irp};\ \tau^{-1}_{z0} = \tau^{-1}_0 + (\tau_{irp}/4)^{-1} \tag{15}$$

The form of J_x, J_y and J_z is the same as in Eqn. 3 with τ_0 replaced by τ_0, τ_{y0} and τ_{z0}, respectively. A correlation time, τ_{irp}, is set for the time scale of phenylene rotation. In the second case, the correlation function for phenylene group motion is obtained by multiplying the correlation function for stochastic diffusion given by Eqn. 11 with a correlation function given by Eqn. 7(a). Following the same calculation as in the derivation of Eqn. 13, then yields a lengthy but very similar result to Eqn. 13.

Because of the simple form for segmental motion in the Hall-Helfand correlation function [16], Eqns. 13 and 14 can be used in a nonlinear least-squares program to fit the data as a function of temperature if an Arrhenius dependence is assumed for τ_0, τ_1 and τ_{irf}. Two frequencies of phenylene proton data and six more frequencies, two each for formal proton, carbon and deuterium data, are simulated by three parameters: τ_0, τ_1 and τ_{irf}. Because both the formal group and phenylene group are in the backbone, it is required that the same τ_0 and τ_1 parameters for segmental motion are used in fitting the formal and phenylene group motion. After the segmental and formal motion parameters have been measured, the correlation time, τ_{irp}, for phenylene group rotation is determined from the phenylene carbon data. All experimental relaxation times can be simulated to about 10%, which is within experimental error. Correlation times and Arrhenius parameters are compiled in Table 2.

Because the phenylene proton/proton dipole interaction is parallel to the C_1—C_4 axis of the ring, proton T_1 values of the phenylene group measured at two frequencies can conceivably be affected by both segmental motion and formal group motion. If the effect of formal group rotation is included in the simulation as discussed above, the phenylene group would rotate 120° about the C—O axis. This leads to deviations from the experimental phenylene T_1 values, producing high T_1 predictions for the entire temperature

TABLE 2

Simulation parameters for Chloral-PF using the Hall-Helfand model

Temp. (°C)	τ_1(ns)	τ_0(ns)	τ_{irp}(ns)	τ_{irf}(ns)
−20	3.40	25.0	—	15.0
0	2.38	11.0	2.15	4.5
20	1.14	6.5	1.19	2.5
40	0.60	4.14	0.81	0.99
60	0.34	2.77	0.37	0.57
80	0.21	1.94	0.26	0.34
100	0.13	1.41	0.18	0.21
120	0.088	1.06	0.126	0.149
E_a (kJ mol^{-1})	24.5	17.4	21.0	26.1
τ_∞ (fs)	48.9	5160.0	188.4	77.4
Correlation coefficient	0.99	0.99	0.99	0.99

range. Inclusion of the formal motion in the calculation of the phenylene group relaxation simply leads to too much motion. If the phenylene group rotation is considered over smaller angles, e.g., 60° or less, about the C—O axis, it is possible to simulate the proton and carbon data by re-adjusting the simulation parameters (τ_1, τ_0 and τ_{irf}). However, the deuterium data cannot be simulated well with this set of parameters. This difficulty indicates the utility of a large data base in discriminating between various motional possibilities. The only consistent interpretation found restricts formal group internal rotation to the formal group with no associated motion of the phenylene group. It is possible that very small amplitude motion of the phenylene group resulting from formal motion exists but major reorientation is unlikely to view of the present simulation results.

DISCUSSION

The results for formal group motion differ from the earlier study on this system. The current interpretation involves trans—gauche isomerization within the formal unit and this motion does not extend beyond the formal unit. By applying the double internal rotation concept to the formal group and including two deuterium frequency measurements, it is possible to obtain

TABLE 3

Comparisons of simulation parameters of polycarbonates and polyformal

Polymer	Segmental motion					Ref.
	Apparent activation energy (kJ mol^{-1})			Arrhenius prefactor τ_∞ (fs)		
		Cooperative segmental	Single backbone rotation	Cooperative segmental	Single backbone rotation	
	T_g(°C)	(τ_1)	(τ_0)	(τ_1)	(τ_0)	
BPA-PC	150	19	16	280	10030	4
Chloral-PC	164	17	18	940	4090	4
Chloral-PF	103	25	17	50	5160	This work

	Phenylene ring motion			
	T_γ(°C)[a]	Type	E_a (kJ mol^{-1})	τ_∞ (fs)	
BPA-PC	−100	Stochastic diffusion	22	60	4
Chloral-PC	−100	Stochastic diffusion	18	400	4
Chloral-PF	−100	Stochastic diffusion	21	190	This work

[a]The temperature of the main sub-glass transition loss peak measured at 1 Hz [6].

reasonable time scales and activation energies for segmental motion and internal rotation which can be compared to the corresponding values obtained for the polycarbonates [3–5]. Table 3 contains those comparisons. The similarity of the segmental motion is apparent and reasonable because the segmental description reflects motions within the bisphenol unit as shown in Fig. 2 and is not associated with the formal or carbonate groups. One interesting difference between the Hall-Helfand interpretation of Chloral-PF and the polycarbonates is the relative apparent activation energies for τ_1 and τ_0. For the polycarbonates, the activation energies for cooperative segmental motion and single backbone bond rotation are found to be similar. This can only occur if cooperative segmental motions occur sequentially as opposed to simultaneously [21–23]. For the Chloral-PF, the activation energy for the cooperative process is somewhat higher than for the single transitions which may be indicative of more nearly simultaneous cooperative transitions such as those produced by crankshaft motions. The same result was also found in another solution study of a related system, Bisphenol A polyformal (BPA-PF) [24]. The difference in activation energy for the above two processes in BPA-PF is smaller but still significant. The single transitions are minor processes in both the polycarbonates and polyformals, primarily because of the larger prefactor as opposed to a larger activation energy.

Phenylene group rotation in the Chloral-PF can also be compared to that of Chloral-PC. Phenylene group rotation in Chloral-PF is a factor of 1.5 to 2.0 slower at a given temperature relative to Chloral-PC but the activation energy for phenylene group rotation in both polymers are quite similar [5]. This suggests that phenylene group rotation is dominated by the local potential energy surface and is not greatly affected by the change from a formal link to a carbonate link. The phenylene group rotation in solution is best modeled by stochastic diffusion while it is modeled by π flips in glassy polycarbonates [20, 25, 26]. *Calculations by* Tonelli [27] suggest a low barrier to phenylene group reaction for an isolated polycarbonate chain. MNDO calculations on the dichloroethylene unit indicate a high barrier, 42 kJ mol^{-1}, to phenylene group rotation [28]. The discrepancy between these solution results and the calculation is not resolved but the similarity of the experimental data between the Chloral unit and the Bisphenol A unit is indicative of comparable mobility.

The best simulation for formal group rotation is obtained by applying double internal rotations about the C—O bonds while not allowing these motions to contribute to phenylene relaxation. This motion is described as a product form of two single exponential correlation functions. A physical representation of formal group motion that is consistent with the simulation results, particularly the lack of influence on the phenylene group, is a challenging task. The conformational states of the formal group are not known with certainty but can be inferred from similar small-molecule structures and for this purpose the conformational energy map of dimethoxymethane is important [29, 30]. The lowest conformational states of the formal group in dimethoxymethane are gg' and $g'g$. This unusual situation relative to poly-

ethylene chains is commonly called the anomeric effect [31, 32]. Corresponding to each of these conformations, there are two conformations which are only 4 kJ higher in energy. The tg' and gt conformations are energetically near the gg' conformation while the tg and $g't$ conformations are energetically near the $g'g$ conformation. The $g'g'$, gg and tt states are higher in energy. Because of the similarity of conformational changes for gg' and $g'g$ and for simplicity, only the gg' case is illustrated. The most facile conformational changes from the lowest states can be represented by

$$gg' \leftrightharpoons (tg') \leftrightharpoons tg \tag{16}$$

$$gg' \leftrightharpoons (gt) \leftrightharpoons g't \tag{17}$$

These conformational changes can be applied to the formal groups of polymer chain. Figure 4 illustrates local formal group motion resulting from conformational state changes in a repeat unit. The lowest conformational state is gg' as shown in Fig. 4(1). In Eqn. 16, gg' undergoes trans—gauche rotation to form tg' in Fig. 4(2). This simple trans—gauche isomerization leads to rotation of the chain end but this dislocation can be avoided by allowing a second reorientation, tg' to tg. Here the chain end is translated but not reorientated which corresponds to a Helfand Type II motion [21].

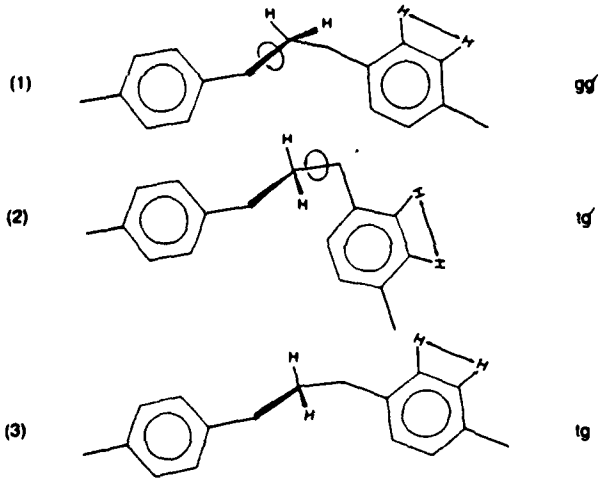

Fig. 4. Likely conformational transitions of the formal group. The motional process associated with Eqn. 16 is shown (see text) with arrows indicating the rotations of the conformational changes from (1) to (3). The overall conformational process is gg' to tg with the intermediate state of tg' shown only to indicate the two conformational changes involved in the overall process. The intermediate state, tg', is an unlikely transition state because it involves a large rotation of the chain end and some other pathway avoiding the tg' intermediate is likely. Nevertheless, the conformations of two bonds change, which is the point made by the inclusion of the tg' state. The proton/proton dipolar interaction of the phenylene group is only translated and not reoriented. This is a Helfand Type II motion thought to be a generally plausible form of segmental motion [21].

Thus the net conformational change is gg' to tg but for calculational purposes, it can be produced in two steps: gg' to tg' and then tg' to tg. However, the state tg' is not proposed as a real intermediate but rather as calculational intermediate. The process, gg' to tg, is not observed in the computer simulations of Helfand which were used to verify the importance of Type II processes. This gg' conformation is rare in an alkane backbone but important in polyethers such as polymethylene oxide where the dynamic process gg' to tg could be quite significant.

Returning to the aromatic polyformal of this study, the motion proposed in Fig. 4 does not reorientate the proton/proton interaction in the phenylene group and thus this formal motion will not cause phenylene group relaxation, which is consistent with experimental results. An exactly analogous process involving the other C—O bond can occur as noted in Eqn. 17. In this case, gg' undergoes two 120° bond rotations to form $g't$. If one combines both processes in Eqns. 16 and 17, there are two possible isomerization mechanisms to cause reorientation in a formal group. This picture is consistent with the mathematical interpretation of double trans—gauche rotations on the formal group developed in the context of the Szabo formulae.

Because the formal group motion may be coupled with other formal groups across the bisphenol group and undergo cooperative transitions, the orientation correlation function describing these cooperative transitions was examined. In general, these correlation functions are not exponential [33]. Helfand derived the orientation correlation function given in Eqn. 2, which includes a Bessel function to describe cooperative transitions. This correlation function has been applied in the present treatment of formal group motion in place of a single-exponential function. However, this correlation function does not simulate the data throughout the entire temperature and frequency range, which is not surprising because a distribution of correlation times would increase the breadth of the T_1 minimum whereas the experimental T_1 curves are quite narrow. Other types of correlation functions corresponding to crankshaft and the three-bond-jump motion also involve a distribution of correlation times and would similarly increase the breadth of the T_1 minimum. Skinner and Budimir [34] have presented a treatment of cooperative sequential motions which leads to a single exponential form but no simple identification was found between the Skinner treatment and the polyformal conformational transitions.

The interpretation described here has been successfully tested by another solution T_1 study of BPA-PF which includes data as a function of field, temperature and concentration [24].

The trans—gauche isomerization in Chloral-PF is also under study in the glassy state by solid-state deuterium n.m.r. experiments; the simulation of these experimental results are still in progress. It would be interesting to know whether the local chain dynamics model proposed here for formal and phenylene group internal rotation still persists in the glassy state. Recently, Jones [35] proposed a model for the chain dynamics of polycarbonates which

involves trans—cis conformational changes of the carbonate unit. The polycarbonate chain is mainly composed of trans—trans carbonate units with occasional cis—trans or trans—cis carbonate units. The phenylene rings undergo flips in association with the C—O bond rotations. The neighboring carbonate would undergo counter-rotation from the trans—cis state to the trans—trans state. The C_1—C_4 axes of the phenylene rings between these two rotating carbonate units only reorient by 11° or less. Over a period of time, all phenylene rings would be flipped as the cis—trans and trans—cis conformations diffuse along the chain. This dynamic model is somewhat different than the formal group model discussed above though they are related. In the formal motional description, there is no cooperative reorientation of a neighboring formal unit which could compensate the translational motion whereas such a compensatory process is proposed in glassy polycarbonates. The results of relaxation studies on glassy polyformal will help sharpen the similarities and differences between the two systems.

The ability of multinuclear, multifrequency n.m.r. to distinguish complex dynamic possibilities existing in high-molecular-weight polymer solutions is encouraging and suggests that n.m.r. with its ability to probe different atomic sites in the repeat unit and differing motional timescales offers real potential for testing the various chain dynamic models based on repeat unit structure and conformation.

This research was done with the financial support of the National Science Foundation Grant DMR-790677, of National Science Foundation Equipment Grant No. CHE 77-09059, of National Science Foundation Grant No. DMR-8108679, and of U.S. Army Research Office Grants DAAG 29-82-G-0001, and DAAG 29 85-K0126. We thank the Worcester Consortium NMR Facility for use of the SXP90 and WM250 spectrometers, and Mr. Frank Shea for his assistance.

REFERENCES

1 A. A. Jones and R. P. Lubianez, Macromolecules, 11 (1978) 126.
2 R. P. Lubianez, A. A. Jones and M. Bisceglia, Macromolecules, 12 (1980) 1141.
3 A. A. Jones and M. Bisceglia, Macromolecules, 12 (1979) 1136.
4 J. F. O'Gara, S. G. Dejardins and A. A. Jones, Macromolecules, 14 (1981) 64.
5 J. J. Connolly, E. Gordon and A. A. Jones, Macromolecules, 17 (1984) 722.
6 A. F. Yee and S. A. Smith, Macromolecules, 14 (1981) 54.
7 M. F. Tarpey, Y.-Y. Lin, A. A. Jones and P. T. Inglefield, in J. C. Randall (Ed.), NMR and Macromolecules, American Chemical Society, Washington, DC, 1984; Am. Chem. Soc. Symp. Ser., No. 247, 1984, p. 67.
8 A. Szabo, J. Chem. Phys., 81 (1984) 1.
9 R. J. Wittebort and A. Szabo, J. Chem. Phys., 69 (1978) 1722.
10 L. W. Jelinski, J. J. Dumais and A. K. Engel, Macromolecules, 16 (1983) 492.
11 D. Hentschel, H. Sillescu, H. Spiess, H. Voelkel and R. Willenberg, XIX Congress Ampere, Heidelberg 1976, p. 381.
12 T. H. Huang, R. P. Skarjune, R. J. Wittebort, R. G. Griffin and E. J. Oldfield, J. Am. Chem. Soc., 102 (1980) 7377.

13 A. S. Hay, F. J. Williams, G. M. Loucks, H. M. Relles, B. M. Boulette, P. E. Donabue and D. S. Johnson, Polym. Prepr. Am. Chem. Soc. Div. Polym. Chem., 23(2) (1982) 117.
14 A. Abragam, The Principles of Nuclear Magnetism, Oxford University Press, Clarendon, 1961, p. 347.
15 P. F. Brisse and S. Perez, Acta Crystallogr., 1332 (1976) 2110.
16 C. K. Hall and E. Helfand, J. Chem. Phys., 77 (1982) 3275.
17 T. A. Weber and E. Helfand, J. Phys. Chem., 87 (1983) 2881.
18 D. E. Woessner, J. Chem. Phys., 36 (1962) 1.
19 A. A. Jones, J. Polym. Sci., Polym. Phys. Ed., 15 (1977) 863.
20 H. W. Spiess, Colloid Polym. Sci., 261 (1983) 193.
21 E. Helfand, J. Chem. Phys., 54 (1971) 4651.
22 E. Helfand, Z. R. Wasserman and T. A. Weber, Macromolecules, 13 (1980) 526.
23 J. Skolnik and E. Helfand, J. Chem. Phys., 72 (1980) 5489.
24 C.-C. Hung, J. H. Shibata, A. A. Jones and P. T. Inglefield, Polymer, in press.
25 P. T. Inglefield, R. M. Amici, J. F. O'Gara, C.-C. Hung and A. A. Jones, Macromolecules, 16 (1983) 1552.
26 J. F. O'Gara, A. A. Jones, C.-C. Hung and P. T. Inglefield, Macromolecules, 18 (1985) 1117.
27 A. E. Tonelli, Macromolecules, 5 (1972) 558; 6 (1973) 503.
28 A. A. Jones, J. F. O'Gara, P. T. Inglefield, J. T. Bendler, A. F. Yee and K. L. Ngai, Macromolecules, 16 (1983) 658.
29 I. Tvaroska and T. Bleha, J. Mol. Struct., 24 (1975) 249.
30 G. A. Jeffrey and R. Taylor, J. Comput. Chem., 1 (1980) 99.
31 S. Wolfe, Acc. Chem. Res., 5 (1972) 102.
32 E. L. Ehel, Angew. Chem., 84 (1972) 779.
33 J. L. Skinner, J. Chem. Phys., 79 (1983) 1955.
34 J. L. Skinner and J. Budimir, J. Chem. Phys., 82 (1985) 5232.
35 A. A. Jones, Macromolecules, 18 (1985) 902.

7

POLYMER MOTION IN THE SOLID STATE

Alan A. Jones

DEPARTMENT OF CHEMISTRY
CLARK UNIVERSITY
WORCESTER, MA 01610

Introduction

Nuclear magnetic resonance provides a new tool for characterizing chain dynamics in bulk polymers. It complements other experimental approaches, such as dielectric and dynamic mechanical response, with the advantage of greater structural specificity versus these more traditional approaches. Nuclear magnetic resonance can probe motion at several places in a repeat unit by utilizing either one or several experiments. Carbon-13 experiments often can probe several sites[1] simultaneously, whereas systems labeled with either carbon-13[2] or deuterium[3,4] (see Chapter 10) probe only one site per labeled polymer. Even proton spectroscopy can be used to probe specific sites under favorable circumstances.[2,5,6]

If the goal is to develop a repeat-unit-level characterization of local motion, certain aspects of the motion must be defined. Arbitrarily, one can start with the geometry of the motion. Is it isotropic? If not, is there an axis of anisotropic rotation? Does the motion take place by large-angle jumps between well-defined minima or does it take place by stochastic diffusion over a relatively flat potential surface? If the motion is anisotropic, is it restricted in angular amplitude at low temperatures, becoming a complete anisotropic rotation about a given axis at higher temperatures?

A second aspect of the motion to be characterized is time scale. In the time

Komoroski (ed): High-Resolution NMR Spectroscopy of Synthetic Polymers in Bulk

domain this is best summarized by a correlation function and in the frequency domain by a spectral density. In this regard, polymer motions are often complex, with two general factors contributing to this complexity. First, motions taking place in an isolated polymer backbone are complex relative to small molecules because of the nature of a chain system. Conformational changes, such as conformational exchange in a chain molecule, lead to Bessel function correlation functions[7-8] as opposed to an exponential correlation function for rotational diffusion in a small molecule. The second factor leading to complexity in solid polymers is intermolecular interactions. In bulk polymers, especially glasses,[9-11] these interactions can lead to correlation functions characterized in terms of very broad distributions of exponential correlation times.

Another aspect of the motion is the temperature dependence or energetics. As just mentioned, the amplitude of various motions can change with temperature, although more commonly one thinks of changes in the time scale.[12] The time scale of a given motion is often found to have an Arrhenius dependence on temperature; and therefore this dependence can be summarized conveniently by an apparent activation energy.

A last issue is often extremely important to the materials scientist studying chain dynamics. After motions are detected and characterized by NMR, a relationship to the results of other dynamics experiments is sought as well as a relationship to material properties. For instance, the glass transition is an important concept in the study of polymeric solids. This transition can be observed by NMR[13] and the influence of this transition on local motions can be observed also (see Chapter 4). In the end, an improved understanding of local motion above and below the glass transition can serve to better define the nature of the glass transition itself.

Experimental Techniques for Characterizing Local Motions

Spin–Lattice Relaxation

Spin–lattice relaxation measurements have been used widely to characterize chain dynamics in solution[14] and the same general approach can be extended to bulk polymers,[1] although some more difficulties are encountered. Several points should be considered in designing a spin–lattice relaxation study.

First, each spin–lattice relaxation time samples motion at one frequency or one combination of frequencies. In a pure spin–lattice measurement, the frequencies are related to the Larmor frequencies of the nuclei involved.[13] If spin–lattice relaxation in the rotating frame is measured, the relevant frequency is given by the magnitude of the spin-lock field[13] (see Chapter 2).

To vary the circumstances of the experiment, temperature commonly is swept, which changes the nature of the motion sampled by the spin–lattice relaxation experiment. Whereas temperature variation is a valuable experimental control, it is even more useful to vary the frequency of the measurement.[15,16] Here a drawback to the NMR approach is encountered. To vary frequency in a spin–lattice relaxation measurement, the magnetic field must be varied. With common commercial instrumentation, magnetic fields are fixed so an individual spectrometer is required for each frequency. Another possible approach to varying frequency is to study different nuclei such as protons and carbon in the same polymer[17] because they have different gyromagnetic ratios and therefore different Larmor frequencies at the same field strength. For spin–lattice relaxation in the rotating frame the spin-lock field can be varied, but frequently the range of useful variation only extends over a factor of two or three.[18] However, relaxation in the rotating frame nicely complements normal spin–lattice relaxation because the former is in the kilohertz region and the latter is in the megahertz region.

The particular experimental approach used to observe spin–lattice relaxation in bulk polymers depends on the state of the polymer. The easiest experimental situation to study is a rubber at a temperature somewhat above the glass transition[19] (see Chapter 4). Here ^{13}C spectra can be obtained with low-power or scalar proton decoupling, allowing for relaxation studies almost entirely analogous to solution studies. The presence of nearly isotropic segmental motion[12] removes dipolar couplings and chemical-shift anisotropy, leaving a spectrum comparable to a dissolved macromolecule. A standard measurement of spin–lattice relaxation time, T_1, by a 180-τ-90 pulse sequence as a function of temperature and Larmor frequency should be sufficient to characterize local motion in a rubber.

In a glassy polymer at least two general types of experimental approaches may be employed. The first is wide-line relaxation studies. Here the best system is one where only one nucleus contributes to the spectrum because the presence of several nuclei leads to signal overlap. One therefore must first select a polymer system where only one chemical position contributes to the spectrum, and this is usually achieved through labeling, although occasionally a judicious choice provides an appropriate case.[6] In typical wide-line relaxation studies, the lineshape is governed by the orientation of the molecule relative to the externally applied field. The sources of this orientation dependence may be dipolar coupling, quadrupole coupling, or chemical-shift anisotropy. In proton dipolar studies, relaxation of all points in a lineshape are equal because of spin diffusion (homogeneous broadening).[6] However for deuterium quadrupolar and ^{13}C chemical shift anisotropy cases, relaxation of the lineshape changes across the lineshape and can depend on the orientation of the molecule relative to the externally applied field (heterogeneous broadening). Exploitation of this latter situation has just begun.

High-resolution ^{13}C spectra can be obtained in glassy polymers through a combination of cross-polarization, high-power dipolar decoupling and magic

angle spinning[1] (see Chapters 2 and 3). The resulting spectra are almost comparable to liquid spectra in resolution, so studies of unlabeled systems in natural abundance are straightforward. Both spin–lattice relaxation and spin–lattice relaxation in the rotating frame can be observed. However several complicating factors are often present. The return of the magnetization to equilibrium is often nonexponential. Several possible sources of the nonexponential behavior have been proposed, including a distribution of correlation times[1] and spin–spin relaxation contributions.[18,20] In any case, ^{13}C relaxation times in glassy solids have not been susceptible to quantitative interpretation with a correlation function comparable to the interpretations developed for relaxation of dissolved polymers. Qualitative interpretations and comparisons of mobility between polymers is possible and has proved most useful in a number of cases.[1]

In any application of the spin–lattice relaxation approach, the information generated primarily reflects the time scale of the motion. Some information about the geometry of the motion can be determined by performing spin–lattice relaxation experiments at several positions in the repeat unit.[17] Some information about the amplitude of anisotropic restricted rotation can be ascertained also.[21] However, in solid polymers the best information about the geometry of local motions comes from the study of lineshape.

Lineshape

Examination of lineshape and linewidth also provides insight into chain dynamics. Following the analogy to solution studies, one might consider employing the spin–spin relaxation time, T_2, as a source of information. In the rubbery state, T_2 can be determined from the linewidth but careful examination by several authors shows this relaxation effect to be dominated by long-range motions and not by local motion.[12,22,23] This situation is also true for concentrated solutions and interpretations based on motions, such as the Rouse-Zimm modes and reptation, have been proposed.[24] The validity of these interpretations has been challenged[12] but it is clear that linewidths or other measures of spin–spin relaxation are not sources of information about local chain dynamics. This view is presented here in spite of early work by this author[25] and others[19] attempting to use spin–spin relaxation as a source of information on local chain dynamics in rubbers.

In glassy polymers under conditions of magic angle spinning and dipolar decoupling, ^{13}C linewidths are also not a function of local motions. Here the linewidth results from isotropic chemical-shift heterogeneity, which reflects the heterogeneity of the glass itself.[1] In cases where chemical exchange occurs, local chain dynamics can be studied in a manner comparable to chemical exchange in small, dissolved molecules.[26] The major difference between the glassy polymer and the small molecule in solution is again in the complexity of the correlation function reflecting the strong intermolecular interactions in the

glass. High-resolution lineshape studies on phenomena loosely categorized as chemical exchange yield primarily information about the time scale of the chain dynamics, although some inferences about geometry can be drawn by considering the observed lineshape changes.

The best information about the geometry of motions below the glass transition comes from wide-line NMR. Until recently the only wide-line spectra commonly obtained were those of proton and fluorine nuclei. Proton spectra of glassy solids are always dominated by dipolar interactions. The presence of this strong coupling in addition to a very limited chemical-shift range yields spectra with extensive overlap of resonances from chemically distinct points in the repeat unit. Under such circumstances, very little geometric information is available. In certain cases only one type of proton is present in a repeat unit and then geometric information can be extracted.[2,5] Fluorine spectra also are dominated by dipolar interactions in the solid state, but the chemical-shift anisotropy is large and can be observed more easily under coherent averaging conditions[27].

Major advances in solid-state ^{13}C[2,28] and deuterium[3,4] spectroscopy have made detailed geometric information available. Depending on the experimental approach, the lineshape reflects either chemical-shift anisotropy,[2] quadrupole,[3,4] or dipolar interactions.[2,5] Whatever the interaction, the observed lineshape depends on the orientation of the repeat unit with the externally applied field. If molecular motion is present, orientations are exchanged and the lineshape becomes partially averaged when the motion becomes rapid with respect to the frequency separation between the points in the lineshape under exchange.[29] Lineshape changes are very distinctive and provide a fairly decisive test of various motional possibilities.

The time scale of the motion also can be examined when the rate of the motion is comparable to the frequency of the lineshape.[30] The analysis of the lineshape is quite comparable to the analysis of chemical exchange in high-resolution spectra of dissolved molecules. The major differences are the summation over all orientations present in the glassy state and the possible complexity of the correlation function from strong intermolecular interactions. Only a restricted range of frequency is accessible in a lineshape experiment, which limits the ability of this approach to characterize a complex correlation function. The lineshape studies can be performed in conjunction with spin-lattice relaxation measurements to extend the sampling in the frequency domain.[31]

Another method for extending the range in time or frequency of lineshape studies is to employ the Jeener-Brockaert pulse sequence.[3] This method has yet to be applied fully to a polymer glass because the analysis of the raw data requires a knowledge of the correlation function. Currently, correlation functions for motions in glassy polymers are not readily available or even known to be of a particular form. This general approach will no doubt be more useful as the understanding of local chain dynamics in bulk polymers grows.

Polycarbonates as an Example

The chain dynamics of the polycarbonate of bisphenol A (BPA) has been studied widely by solid-state NMR.[1-3,5,6] The polymer itself is a commercially successful engineering plastic, highly touted for impact resistance. This polymer is also known to be very mobile below the glass transition and this mobility often is associated with the property of impact resistance.[32,33] Many traditional dynamic studies have been performed on BPA, but until the recent NMR work a repeat-unit-level understanding of the motions was not agreed upon. Even now some aspects of the motion are under review, although a reasonable consensus exists about other aspects.

Isolated Chain Studies

It is easier to consider local chain motion for a single polymer backbone, both experimentally and theoretically. In the isolated chain, intermolecular effects are absent and these effects can dominate some aspects of motional properties in the glass. On the other hand, a characterization of the motions in an isolated chain is still helpful in understanding motion in the bulk polymer. If a specific local conformational process is not possible in a chain in the absence of intermolecular interactions, it is not likely to occur in the presence of such additional contributions, which increase the barriers restricting motion. It seems more reasonable to find which motions are possible in the absence of large intermolecular interactions and then see how these motions are altered when the interactions are present.

Following this line of thought, dilute solution spin–lattice relaxation studies can be employed effectively to characterize local chain motion in a situation where intermolecular contributions are relatively small. High-resolution proton and ^{13}C relaxation studies have been performed on dissolved BPA polycarbonate and a number of related polymers.[17,21,34,35] Figure 7-1 shows the repeat units of the polycarbonates studied to date.

In the most recent solution studies,[21,35] proton-relaxation measurements are conducted at at least two field strengths and frequently partially deuterated forms are employed to reduce dipole–dipole interactions among protons in different chemical environments in the repeat unit. Two partially deuterated repeat units employed are shown in Figure 7-2. The proton spin–lattice relaxation time can be written in terms of the spectral density, J, the internuclear distance, r, and constants γ_H and $\hbar$ as follows:

$$1/T_1 = \sum_j (9/8)\gamma_H^4 \hbar^2 r^{-6}[(2/15)J_1(\omega_H) + (8/15)J_2(2\omega_H)] \qquad (7\text{-}1)$$

Here ω_H is the proton Larmor frequency. If partially deuterated forms are employed, the relevant distances in this equation usually are known to within a few hundredths of an Ångstrom.

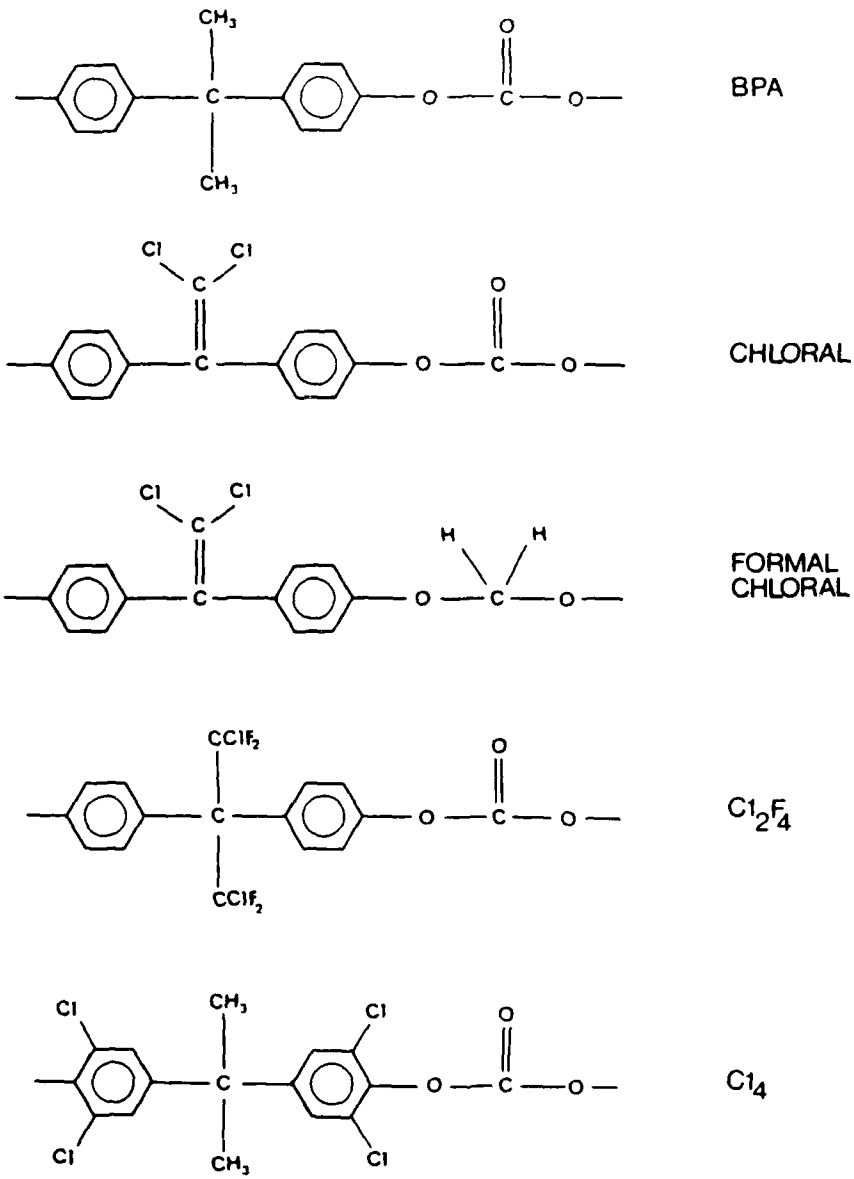

Figure 7-1. Structures of the repeat units and abbreviations for the polycarbonates and polycarbonate analogs.

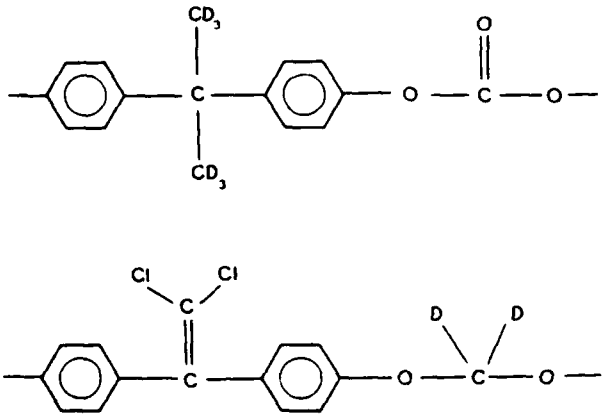

Figure 7-2. Structures of the repeat units of partially deuterated polymers used in proton relaxation studies.

To obtain data at other frequencies and with different geometric orientations in the repeat unit, ^{13}C spin–lattice relaxation times usually are measured as well. Only carbons with directly bonded protons are measured because the relaxation mechanism is usually dipole–dipole relaxation and known carbon-proton internuclear distances are required (see Chapter 4). Again, measurements are performed at several frequencies to obtain a data base capable of supporting an informative analysis. The equation relating the spin–lattice relaxation time to the spectral density for ^{13}C is:

$$1/T_1 = W_0 + 2W_{1C} + W_2 \tag{7-2}$$

where

$$W_0 = \sum_j \gamma_C^2 \gamma_H^2 \hbar^2 J_0(\omega_0)/20r_j^6$$

$$W_{1C} = \sum_j 3\gamma_C^2 \gamma_H^2 \hbar^2 J_1(\omega_C)/40r_j^6$$

$$W_2 = \sum_j 3\gamma_C^2 \gamma_H^2 \hbar^2 J_2(\omega_2)/10r_j^6$$

$$\omega_0 = \omega_H - \omega_C, \qquad \omega_2 = \omega_H + \omega_C$$

The dynamic information is contained in the spectral densities and differences among the spectral densities at different points in the repeat unit. In dilute solution, local chain motions have been divided generally between segmental motions and anisotropic rotation of functional groups.[25] Segmental motions correspond to changes of direction of backbone bonds. These motions are thought to involve one or several backbone units but not long portions of the chain. Hall and Helfand[7] have developed a correlation function for segmental motion based on observations made during computer simulations of segmental motion in polyethylene. Two subclasses of segmental

motion are observed. First, there are conformational changes produced by rotation about a single backbone bond. This process is described by a single exponential correlation time, τ_0. The second process is correlated motions where a second rotation about a backbone bond is observed to follow a first rotation closely in time. The second rotation compensates for distortion of the backbone produced by the first conformational event. Relaxation caused by this correlated motion is characterized by a Bessel function of order zero (I_o) with a time constant τ_1. The Bessel function is a standard solution for one-dimensional diffusion problems.[36] The complete Hall-Helfand correlation function is written:

$$\phi(t) = \exp(-t/\tau_0) \exp(-t/\tau_1) I_o(t/\tau_1) \tag{7-3}$$

which may be Fourier transformed to yield the spectral density:

$$J(\omega) = 2\{[(\tau_0^{-1})(\tau_0^{-1} + 2\tau_1^{-1}) - \omega^2]^2 + [2(\tau_0^{-1} + \tau_1^{-1})\omega]^2\}^{-1/4} \times \cos\{1/2 \arctan 2(\tau_0^{-1} + \tau_1^{-1})\omega/[\tau_0^{-1}(\tau_0^{-1} + 2\tau_1^{-1}) - \omega^2]\} \tag{7-4}$$

For consideration of substituent groups attached to the backbone, the Hall-Helfand correlation function may be combined with anisotropic internal rotation, as originally described by Woessner[37] under the assumption of independence of the two motions. The correlation time for internal rotation of the substituent group is τ_{ir} and the geometry of the motion is characterized by the angle Δ between the axis of internal rotation and the internuclear interaction. The complete spectral density for segmental motion and internal rotation of functional groups is:

$$J(\omega) = AJ_a(\tau_0, \tau_1, \omega) + BJ_b(\tau_{b0}, \tau_1, \omega) + CJ_c(\tau_{c0}, \tau_1, \omega) \tag{7-5}$$

where

$$A = (3\cos^2\Delta - 1)^2/4$$

$$B = 3(\sin^2 2\Delta)/4$$

$$C = 3(\sin^4\Delta)/4$$

For stochastic diffusion:

$$\tau_{b0}^{-1} = \tau_0^{-1} + \tau_{ir}^{-1}$$

$$\tau_{c0}^{-1} = \tau_0^{-1} + (\tau_{ir}/4)^{-1}$$

For a threefold jump:

$$\tau_{b0}^{-1} = \tau_{c0}^{-1} = \tau_0^{-1} + \tau_{ir}^{-1}$$

The form of J_a, J_b, and J_c is the same as in Eq. (7-4) with τ_0 replaced by τ_0, τ_{b0}, τ_{c0}, respectively.

The results of proton and ^{13}C spin–lattice relaxation studies on polycarbonates can be summarized in terms of correlation times for segmental motion, methyl group rotation, and phenylene group rotation.[17,21,34,35] The

time scale of each motion can be separated from the others based on repeat unit structure and the orientation of the dipole–dipole interactions in the repeat unit. A complete discussion of the analysis is presented in the original work.[17] Because measurements are made as a function of temperature, the temperature dependence of the correlation times is usually expressed in terms of the Arrhenius equation. Table 7-1 lists the activation energies and prefactors for the polycarbonates shown in Figure 7-1.

The uncertainty in the activation energies is usually about 5 kJ/mol, although the measurements made in the solvent $C_2D_2Cl_4$ are more accurate than the measurements made in $CDCl_3$. A larger frequency base was employed in the $C_2D_2Cl_4$ study, as well as partially deuterated forms to reduce cross relaxation. Also, the $CDCl_3$ studies were interpreted with an earlier segmental motion model and the outcome of that analysis has been approximately converted to the Hall-Helfand approach using a published conversion factor.[36]

In solution, BPA is found to be a rather mobile chain, especially considering the complexity of the repeat unit. Segmental motion is dominated by cooperative backbone motions as opposed to single backbone bond reorientations.[35] Phenylene group rotation is rapid and rather similar to the cooperative backbone motions in time scale. This similarity persists as concentration is raised from 5 to 30%. Methyl group rotation is also facile, although it is not coincident with the time scale of cooperative segmental motion or phenylene group motion as concentration is raised from 5 to 30%.

The chloral polycarbonate is very similar to BPA polycarbonate in all regards[35] except that it contains no methyl group. The polyformal, structurally analogous to the chloral polycarbonate, has similar phenylene group rotation, although segmental motions are different.[21] In polyformal, the cooperative segmental motions dominate at high temperatures and the single backbone reorientations dominate at low temperatures.

The last two polycarbonates listed, Cl_2F_4 and Cl_4, are rather different. Segmental motion is somewhat slower in these two polymers but phenylene group rotation is reduced greatly. Because of the limited data base, the phenylene group rotation was modeled as slow, complete anisotropic rotation, which yields low apparent activation energies and large Arrhenius prefactors. A more complete study and simulation might well have shown the motion to be restricted anisotropic diffusion or, in other words, an incomplete anistropic rotation. In any case phenylene group motion is either reduced in amplitude or slower than in the other three polymers because rather little additional motion beyond segmental motion is indicated by the ^{13}C T_1s.

This change in phenylene group motion was linked empirically to the low-temperature or γ dynamic mechanical loss peak. The first three polymers all have similar dynamic mechanical spectra below the glass transition, dominated by the presence of a substantial loss peak near 173 K. All three of these polymers also have comparable phenylene group rotation in solution. In the last two polymers, the γ relaxation peak is shifted to much higher tem-

TABLE 7-1. APPARENT ACTIVATION ENERGIES AND ARRHENIUS PREFACTORS

		Apparent activation energies (kJ/mol)				Arrhenius prefactor ($\tau_\infty \times 10^{14}$ s)			
Polymer[a]	Solvent[b]	Correlated segmental τ_1	Single backbone rotation	Phenylene rotation	Methyl rotation	Correlated segmental τ_1	Single backbone rotation	Phenylene rotation	Methyl rotation
BPA	$C_2D_2Cl_4$	19	16	22	24	28	1603	6	1
	$CDCl_3$	~19	—	13	22	—	—	—	—
Chloral	$C_2D_2Cl_4$	17	18	18	—	94	409	40	—
	$CDCl_3$	~13	—	15	—	—	—	—	—
Formal chloral	$C_2D_2Cl_4$	30	9	21	—	1	9700	30	—
Cl_2F_4	$CDCl_3$[c]	~16	—	13	14	—	—	—	—
Cl_4	$CDCl_3$[c]	~18	—	15	19	—	—	—	—

[a] See Figure 7-1 for repeat-unit structures corresponding to abbreviations.
[b] 10 wt% solutions.
[c] The studies performed in $CDCl_3$ are less accurate because they are based on a poorer data set.

peratures and the phenylene group rotation in solution is reduced or restricted greatly. These empirical correlations were noted and phenylene group rotation was linked phenomenologically to the low-temperature loss peak.

These dilute solution studies on BPA show the intramolecular barriers to motion to be quite low: 15–25 kJ. Theoretical calculations on an isolated BPA chain also indicate very low barriers for local chain motions.[32,33,38] For instance, rotation about the backbone CO bonds is found to be 10 kJ by one investigator[38] and 12 kJ by another.[32,33] Somewhat higher values would be found in solution because the effects of solvent viscosity are added to the intramolecular barrier.

Bulk Relaxation Measurements

Solution studies and theoretical calculations show conformational changes to be easy in isolated polycarbonate chains. Also, some correlation between phenylene group motion and the low-temperature loss peak is indicated. However, direct measurement of relaxation in the bulk polymer is the best way to delineate further the nature of the motions below the glass transition.

Spin–lattice relaxation times can be used to set the time scale of the motion in the bulk polymer. McCall determined the proton T_1 and $T_{1\rho}$ on BPA polycarbonate, but the observed relaxation behavior is dominated by the methyl protons and methyl group rotation.[13] To determine motion at the phenylene group, proton relaxation times were measured on the chloral polycarbonate[6] shown in Figure 7-1. The dynamic mechanical spectrum[39] and the solution relaxation results show this polymer to be quite similar to BPA polycarbonate.[35] Because it contains only phenylene protons, the proton relaxation times will reflect phenylene group motion. Either phenylene group rotation or translation modulates intermolecular dipole–dipole interactions to produce relaxation. Figure 7-3 shows the proton T_1 at 20 and 90 MHz as well as the $T_{1\rho}$ at 43 kHz.

The relaxation measurements at all three frequencies show the presence of one broad, asymmetrical minimum. The $T_{1\rho}$ data as a function of temperature show the shape of the minimum best and all these data can be fitted with a correlation function in a fashion similar to the solution data. The proton T_1s have the same functional form as shown in Eq. (7-1); in solids, however, it is traditional to write the equation in terms of the second moment, S:

$$1/T_1 = (2/3)\gamma^2 S[J_1(\omega_H) + 4J_2(2\omega_H)] \tag{7-6}$$

The proton $T_{1\rho}$ can be written in a similar fashion, but here the relaxation depends on the spectral density at the frequency corresponding to the strength of the radiofrequency field, ω_e, as well as the Larmor frequency, ω_H:

$$1/T_{1\rho} = (2/3)\gamma^2 S[1.5J_e(2\omega_e) + 2.5J_1(\omega_H) + J_2(2\omega_H)] \tag{7-7}$$

As before, the spectral density is the Fourier transform of the correlation function, which should reflect the nature of the local motion in the bulk

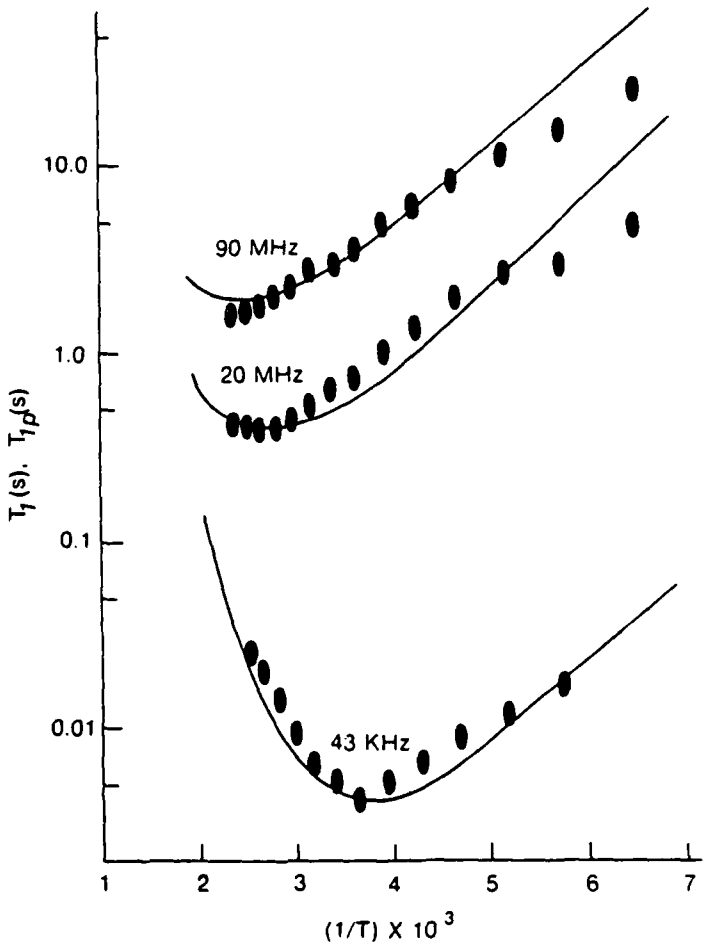

Figure 7-3. Proton spin–lattice relaxation time and spin–lattice relaxation time in the rotating frame versus inverse temperature for chloral polycarbonate. The solid line corresponds to a fit of the relaxation data with a Williams-Watts-Ngai fractional exponential correlation function. Abscissa is in K^{-1}. (Reprinted with permission from Jones, A. A.; O'Gara, J. F.; Inglefield, P. T.; Bendler, J. T.; Yee, A. F.; Ngai, K. L. *Macromolecules* **1983**, *16*, 658. Copyright 1983, American Chemical Society.)

polymer. Correlation functions of the type used in solution based on segmental motion and anisotropic rotation of functional groups do not account for the data in Figure 7-3.[6] A variety of correlation functions was tested, but the only successful one was the Williams-Watts fractional exponential,[11] commonly written:

$$\phi_{ww}(t) = \phi(0) \exp\left[-(t/\tau_{ww})^{\beta}\right] \tag{7-8}$$

Ngai[9,10] has proposed an explanation of the occurrence of this function in glassy materials and writes the correlation function in the form:

$$\phi(t)_{CSM} = \phi(0) \exp\left[-(t/\tau_p)^{1-n}\right] \tag{7-9}$$

where $0 < n < 1$ and the loss peak frequency is located at $\omega_p \propto \tau_p^{-1}$, where

$$\tau_p = [(1-n)e^{nu}E_c^n\tau_0]^{1/(1-n)}$$

The model yielding this correlation function is based on a correlated states model; hence the subscript CSM. The symbol u designates Euler's constant (0.5722). The two key parameters used to fit the data are τ_p and n. As just shown, τ_p is a function of n, the cutoff energy, E_c, and the microscopic correlation time, τ_0. This correlation cannot be determined from a fit of the data but the activation energy for the microscopic process, E_A, can be determined for the apparent activation energy, E_A^*, according to the equation:

$$E_A^* = E_A/(1-n) \tag{7-10}$$

In practice one writes the correlation time τ_p in an Arrhenius form:

$$\tau_p = \tau_\infty^* \exp(E_A^*/RT) \tag{7-11}$$

where

$$\tau_\infty^* = [(1-n)\exp(nu)E_c^n\tau_\infty]^{1/(1-n)}$$

The parameters E_A^*, τ_∞^*, and n are varied to fit the data as a function of temperature. Figure 7-3 shows the fit of the CSM model to the T_1 and $T_{1\rho}$ data using the parameters $E_A = 10$ kJ, $n = 0.8$, and $\tau_\infty^* = 2.29 \times 10^{-16}$ s. The activation energy, E_A, corresponds to the barrier encountered in the isolated chain and is comparable to the barriers calculated for simple rotations.[32,33,38] The apparent activation energy E_A^* is much higher and reflects the contribution to the barrier height from intermolecular interactions encountered in the glass. The parameter n controls the effective width of the relaxation process and accounts for the breadth and asymmetry of the T_1 and $T_{1\rho}$ minima. The parameter n also relates E_A and E_A^* as written in Eq. (7-10) above.

The fit of the data argues for the utility of the fractional exponential correlation function but it is also worth noting the realistic value obtained for E_A. Also, the correlated states model rationalizes the physically unrealistic value obtained for τ_∞^* because it is not simply an Arrhenius prefactor but a combination of several parameters.

Recently a comparable proton-relaxation study has been completed on a partially deuterated form of BPA where the methyl protons have been replaced with deuterons.[40] This system will reflect phenylene group motion just as chloral did, and, indeed, rather similar T_1 and $T_{1\rho}$ data were obtained. With a summary of the time scale of the motion contained in the Williams-Watts-Ngai correlation function it becomes quite interesting to consider the geometry of the motion.

First it is important to consider the ^{13}C $T_{1\rho}$ reported for BPA polycarbonate.[1] Although these relaxation times can be written in terms of the spectral density just as the proton times, the $T_{1\rho}$ decay curves cannot be characterized by a single time constant. The decay curves reflect the presence of at least two time constants and possibly more. In addition, there may be some spin–spin contributions to the decay curves as well.[18,20] The net effect of these complications is enough to discourage quantitative data fitting comparable to the proton interpretation. The ^{13}C $T_{1\rho}$s indicate the presence of considerable local chain motion in agreement with the proton interpretation and with approximately the same time scale. However, the ^{13}C data may reflect an inhomogeneous distribution of correlation times,[26] yielding the observed $T_{1\rho}$ dispersions, whereas spin diffusion equalizes the proton relaxation data, yielding a single relaxation time. Another source of the dispersion may be anisotropic motion leading to relaxation dependent on orientation in a glass. In any case, an analysis of the ^{13}C relaxation data in terms of a correlation function is not yet in hand.

Solid-State Lineshape Studies

Proton lineshape measurements provided the first direct information on the geometry of the motion of the phenylene group. To obtain significant information, the chloral polycarbonate was selected for the first proton lineshape study because it contains only one type of proton, phenylene protons.[5] Therefore this system contains geometrically significant information, whereas most proton spectra of polymers consist of overlapping resonances of several chemical types of protons with little chance of extracting information.

Figure 7-4 shows several proton spectra observed as a function of temperature for the chloral polycarbonate as well as a frozen solution of the chloral polycarbonate. At low temperatures, the spectra are featureless bell-shaped curves with no obvious information content. At about 193 K, the line narrows and at a temperature of 273 K the lineshape becomes that of a Pake doublet with substantial broadening. The splitting of the Pake doublet is 2.5 G which corresponds to a proton–proton internuclear distance of 2.6 Å. The only intramolecular interaction comparable to this is between the 2 and 3 protons on the phenylene ring.

As temperature is raised from 273 K up to the glass transition, the line continues to narrow gradually but the Pake doublet persists with an undiminished splitting. These observations have significant implications for the motions of the phenylene group in polycarbonates. The substantial line narrowing shown in Figure 7-5 in terms of the decrease of the second moment of the proton lineshape as the temperature is raised is indicative of the presence of considerable motion in the glassy polymer. This point has been generally recognized. However, the observation of the Pake doublet and the persistence of the doublet up to the glass transition greatly restricts the motions that may be proposed for the phenylene group. The interaction

between the 2,3 protons of the phenylene group is parallel to the C_1C_4 axis of the phenylene group. This axis must not be reoriented substantially if the Pake doublet persists as temperature is raised. Considerable motion of the phenylene group must be present because intermolecular dipole-dipole interactions between phenylene groups are averaged. The only intramolecular motion consistent with averaging of intermolecular interactions while preserving the Pake doublet is rotation or rotational oscillation about the C_1C_4 axis of the phenylene group. While proton NMR is most effective at locating the axis about which motion must be occurring, it cannot identify the exact nature of the

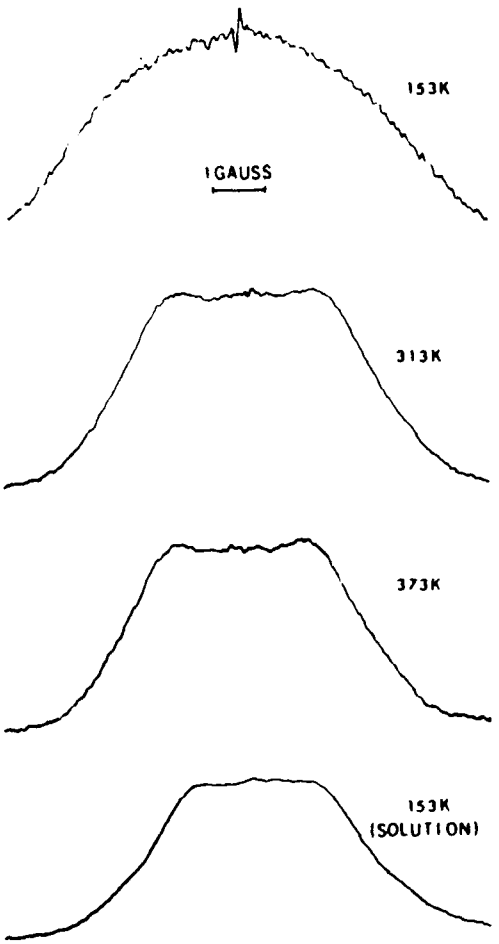

Figure 7-4. Solid-state proton lineshapes as a function of temperature for chloral polycarbonate. The bottom spectrum is for a 15 wt% frozen solution of the polymer in $C_2D_2Cl_4$. (Reprinted with permission from Inglefield, P. T.; Jones, A. A.; Lubianez, R. P.; O'Gara, J. F. *Macromolecules* **1981**, *14*, 288. Copyright 1981, American Chemical Society.)

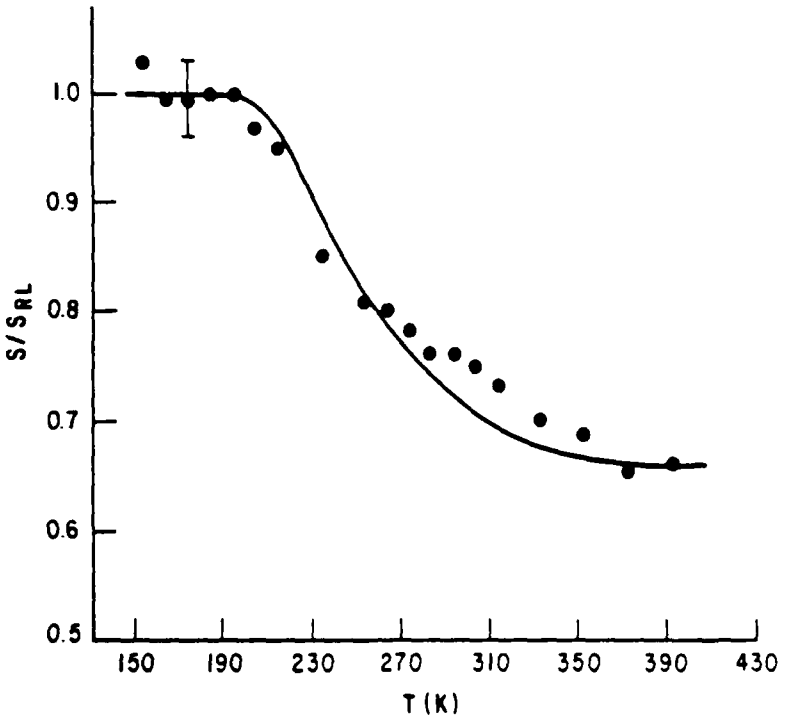

Figure 7-5. Proton second moment versus temperature for the chloral polycarbonate. The solid line is a fit of the second moment data using the same parameters used to account for spin–lattice relaxation shown in Figure 7-3. (Reprinted with permission from Jones, A. A.; O'Gara, J. F.; Inglefield, P. T.; Bendler, J. T.; Yee, A. F.; Ngai, K. L. *Macromolecules* **1983**, *16*, 658. Copyright 1983, American Chemical Society.)

motion about the axis because the motion does not affect the predominant intramolecular interaction contributing to the proton lineshape.

The change in proton second moment, S, from the rigid lattice value, S_{RL}, can be written in terms of the spectral density just as the spin–lattice relaxation time was earlier [Eq. (7-6)].[6]

$$S/S_{RL} = a + m \int_{-\delta\nu}^{+\delta\nu} J_0(\nu)\, d\nu \tag{7-12}$$

Here, a and m are constants and the integration is carried out over the frequency range of the absorption line. Because a correlation function has already been developed to characterize the time scale of motions contributing to T_1 and $T_{1\rho}$, this same correlation function can be employed to predict the change in proton second moment. Figure 7-5 shows this prediction, which leads to an adequate interpretation of the second moment without further adjustment of the parameters used in the Williams-Watts-Ngai correlation function.

Although the axis of motion is clear from the proton lineshape, the nature of the motion about this axis is not apparent. Possibilities include free rotation, restricted rotation, or jumps between distinct minima. To distinguish between these possibilities additional lineshape studies were performed. The first report came from Spiess[3] and employed deuterium spectroscopy. Phenylene protons were replaced with deuterons in BPA and deuterium wide-line spectra were reported at room temperature and at 380 K. The spectra were simulated by the combination of two motions: jumps between two minima separated by 180° and restricted rotation over an rms angular amplitude of $\pm 15^{\circ}$ at room temperature. The jumps between two minima separated by 180 are referred to as π flips and the presence of this motion initially was disputed. Because the deuterium quadrupolar interaction is axially symmetrical, the high-temperature spectra given by Spiess could be simulated fairly well by large-amplitude restricted rotation.

A second lineshape approach confirmed the motion as π flips and removed the possibility of large-amplitude oscillation as the only motion.[2,31] A ^{13}C labeled BPA polycarbonate was prepared as shown in Figure 7-6 with 90% of

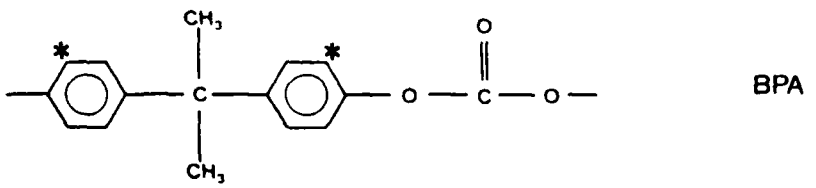

Figure 7-6. Structure of the ^{13}C-labeled repeat unit for BPA polycarbonate. The asterisks indicate the position labeled to a level of more than 90%.

the carbons in the aromatic ring at the position ortho to the carbonate replaced with ^{13}C. Carbon-13 spectra were then taken under conditions of cross polarization and dipolar decoupling. The resulting spectra are shown in the low- and high-temperature limit in Figure 7-7. There is a pronounced change in the lineshape as temperature is raised from 113 to 393 K. Also the low-temperature lineshape shows the classical asymmetric chemical shift anisotropy pattern (see Figure 2-2C). This pattern can be fit with the Bloembergen and Rowland[41] equation:

$$I(\sigma; \sigma_{11}, \sigma_{22}, \sigma_{33}, \Delta\sigma) = \int_{-\infty}^{+\infty} I^0(\sigma - \xi; \sigma_{11}, \sigma_{22}, \sigma_{33}) F \, d\xi \qquad (7\text{-}13)$$

For $\sigma_{33} \leq \sigma < \sigma_{22}$:

$$I^0(\sigma; \sigma_{11}, \sigma_{22}, \sigma_{33}) = \pi^{-1} K(x)(\sigma_{11} - \sigma)^{-0.5}(\sigma_{22} - \sigma_{33})^{-0.5}$$

and

$$x = (\sigma_{11} - \sigma_{22})(\sigma - \sigma_{33})/[(\sigma_{22} - \sigma_{33})(\sigma_{11} - \sigma)]$$

For $\sigma_{22} < \sigma \leq \sigma_{11}$

$$I^0(\sigma; \sigma_{11}, \sigma_{22}, \sigma_{33}) = \pi^{-1} K(x)(\sigma - \sigma_{33})^{-0.5}(\sigma_{11} - \sigma_{22})^{-0.5}$$

and

$$x = (\sigma_{11} - \sigma)(\sigma_{22} - \sigma_{33})/[(\sigma - \sigma_{33})(\sigma_{11} - \sigma_{22})]$$

For $\sigma < \sigma_{11}$, and $\sigma \geq \sigma_{33}$

$$I^0(\sigma; \sigma_{11}, \sigma_{22}, \sigma_{33}) = 0$$

to yield the three values of the shielding tensor in the principal axis system.

In all cases

$$K(x) = \int_0^{\pi/2} (1 - x^2 \sin^2 \Psi)^{-1/2} \, d\Psi$$

$$F = f(\sigma; \Delta\sigma) = 1/[1 + (2\sigma/\Delta\sigma)^2]$$

where F describes the Lorentzian line broadening of the chemical-shift dispersion, I^0.

The principal shielding values are $\sigma_{11} = 17 \pm 1$, $\sigma_{22} = 52 \pm 1$, and $\sigma_{33} = 175 \pm 1$ ppm relative to liquid CS_2 scale. Positive values are upfield in the direction of increasing shielding. In the principal axis system, the shielding interaction usually is written as a diagonal tensor.

$$\boldsymbol{\sigma}_{123} = \begin{bmatrix} \sigma_{11} & 0 & 0 \\ & \sigma_{22} & 0 \\ 0 & 0 & \sigma_{33} \end{bmatrix} \tag{7-14}$$

To consider the effects of motion, it is necessary to transform the shielding tensor in the principal axis system to the axis system of the molecular motion. For the case at hand, the shielding tensor can be transformed to the new coordinate system by a rotation matrix $\tilde{\mathbf{R}}$ defined by a set of Euler angles α, β, and γ using the convention of Rose.[42] The angle α is a rotation about the original z axis, β is about the new y axis, and γ is about the final z axis.

$$\mathbf{R}(\alpha\beta\gamma) = \begin{bmatrix} \cos\alpha\cos\beta\cos\gamma - \sin\alpha\sin\gamma & \sin\alpha\cos\beta\cos\gamma + \cos\alpha\sin\gamma & -\sin\beta\cos\gamma \\ -\cos\alpha\cos\beta\sin\gamma - \sin\alpha\cos\gamma & -\sin\alpha\cos\beta\sin\gamma + \cos\alpha\cos\gamma & \sin\beta\sin\gamma \\ \cos\alpha\sin\beta & \sin\alpha\sin\beta & \cos\beta \end{bmatrix} \tag{7-15}$$

The effects of motion on the shielding tensor in the motional axis system are analogous to chemical exchange. Because the chemical shift experienced by a

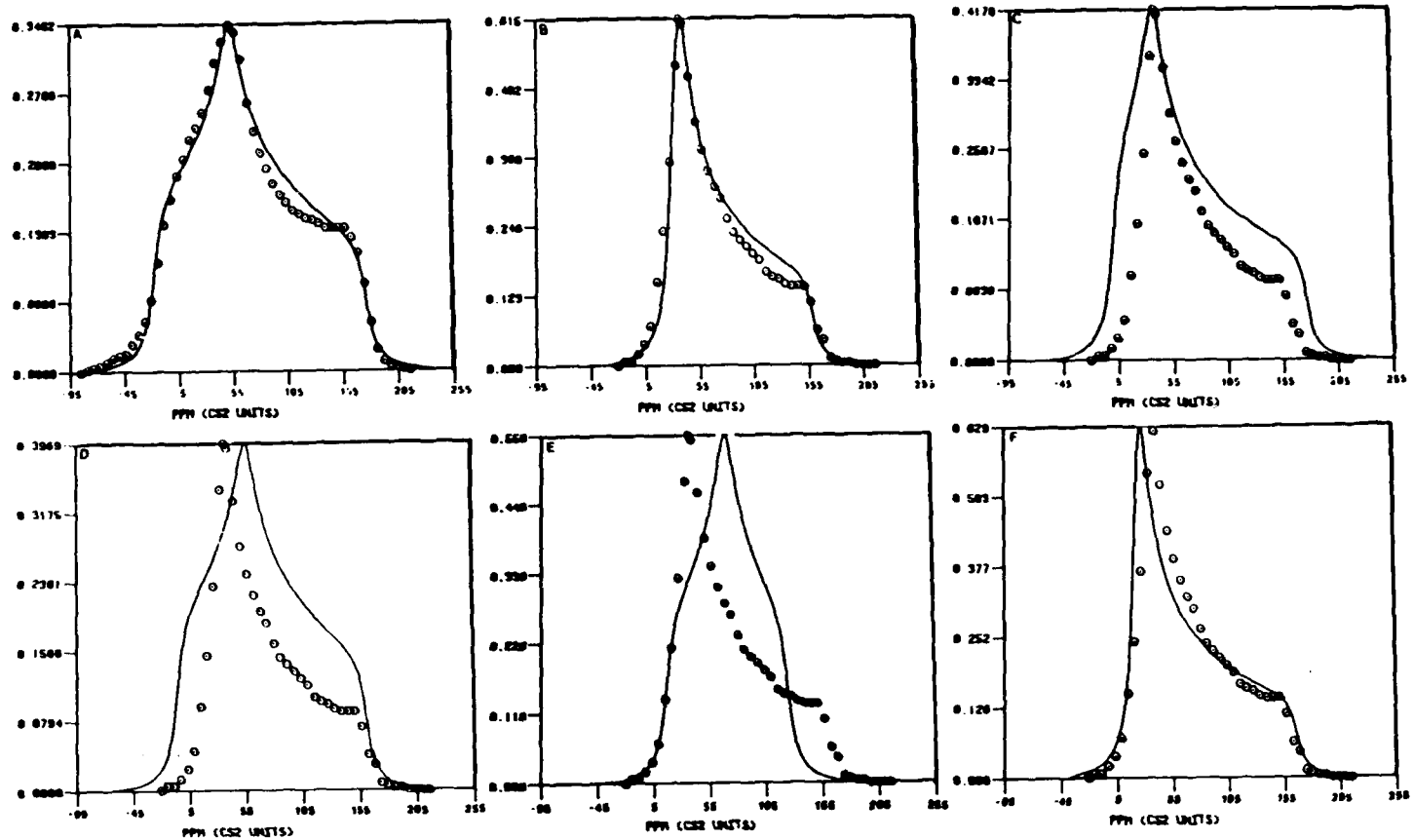
A
B
C
D
E
F
PPM (CS2 UNITS)

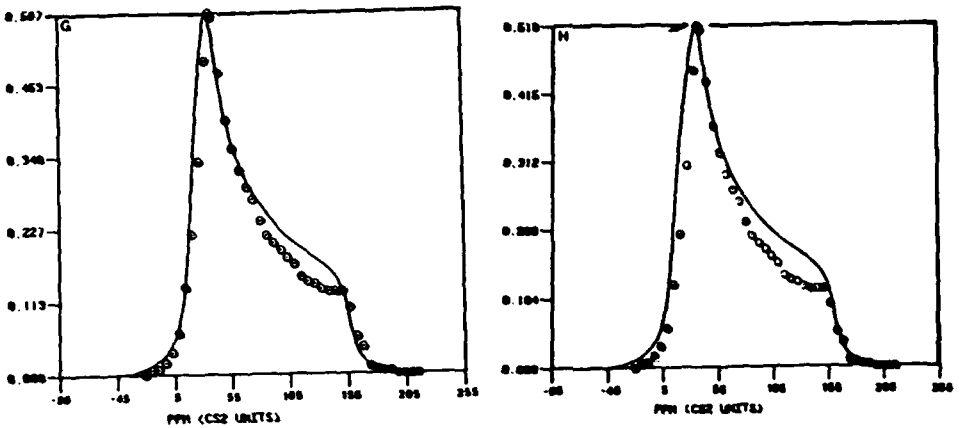

Figure 7-7. Carbon-13 chemical-shift anisotropy (CSA) lineshapes: (A) low-temperature data and simulation based on powder pattern function; (B) high-temperature data and simulation based on powder function; (C) high-temperature data and simulation based on π flips about the C_1C_4 axis; (D) high-temperature data and simulation based on restricted rotation about the C_1C_4 axis over a 60° range; (E) high-temperature data and simulation based on restricted rotation about the C_1C_4 axis over a 120° range; (F) high-temperature data and simulation based on restricted rotation over a 180° range about an axis inclined at 70° to C_1C_4 (parallel to the O—CO bond axis); (G) high-temperature data and simulation based on flips between 0 and 140° about the C_1C_4 axis; (H) high-temperature data and simulation based on C_1C_4 axis π flips plus restricted rotation over a 60° range. The points represent experimental data and the line the theoretical simulation. (Reprinted with permission from Inglefield, P. T.; Amici, R. M.; O'Gara, J. F.; Hung, C.-C.; Jones, A. A. *Macromolecules* **1983**, *16*, 1552. Copyright 1983, American Chemical Society.)

^{13}C nucleus depends on the orientation of the phenylene group relative to the field, as the orientation is exchanged by molecular motion so is the chemical shift. The main complicating factor is the superposition of all chemical shifts for all orientations corresponding to a powder lineshape.

The simplest case to deal with is rapid chemical exchange, which is achieved at high temperatures. For the data taken on labeled BPA at 22.6 MHz, the high-temperature limit for π flips is achieved at about room temperature. The chemical-shift anisotropy (CSA) pattern observed at these temperatures can be simulated by an approach outlined by Slotfeldt-Ellingsen and Resing.[29] Here the x axis of the molecular motion is chosen to be coincident with the C_1C_4 axis of the phenylene group and the shielding tensor is transformed to this axis system by using a rotation matrix $\mathbf{R}(\delta)$ as follows:

$$\boldsymbol{\sigma}_{xyz} = \mathbf{R}(\delta) \cdot \boldsymbol{\sigma}_{123} \cdot \mathbf{R}(\delta)^{-1} \tag{7-16}$$

where

$$\mathbf{R}(\delta) = \begin{bmatrix} \cos\delta & -\sin\delta & 0 \\ \sin\delta & \cos\delta & 0 \\ 0 & 0 & 1 \end{bmatrix}$$

and δ is the angle between x and y axes of the motion system and the x and y axes of the principal shielding system. With the shielding tensor in the molecular motional axis system, various possible motions about the C_1C_4 axis can be modeled. Rotating the molecule about the x axis by an angle α can be defined as follows:

$$\boldsymbol{\sigma}_{xyz}(\alpha) = \mathbf{R}(\alpha) \cdot \boldsymbol{\sigma}_{xyz} \cdot \mathbf{R}(\alpha)^{-1} \tag{7-17}$$

where

$$\mathbf{R}(\alpha) = \begin{bmatrix} 1 & 0 & 0 \\ 0 & \cos\alpha & -\sin\alpha \\ 0 & \sin\alpha & \cos\alpha \end{bmatrix}$$

Using this approach, jumps between various minima can be modeled by averaging the shift experienced in each of the minima. For π flips, the shielding is averaged over two values separated by a 180° rotation about the x axis ($\alpha = 180°$).

$$\boldsymbol{\sigma}_{flip} = (1/2)[\boldsymbol{\sigma}_{xyz} + \boldsymbol{\sigma}_{xyz}(\alpha)] \tag{7-18}$$

Another possible type of motion about the x axis is rapid rotation through all angular positions in a specified angular range. This can be modeled by averaging over α in the equation:

$$\langle \boldsymbol{\sigma}_{xyz} \rangle_\alpha = \langle \mathbf{R}(\alpha) \cdot \boldsymbol{\sigma}_{xyz} \cdot \mathbf{R}(\alpha)^{-1} \rangle_\alpha \tag{7-19}$$

The preceding average depends on the potential function and if one assumes a square well with walls at $+\alpha/2$ and $-\alpha/2$, then the average shift is:

$$\langle \sigma_{xyz} \rangle_\alpha = \int_{-\alpha/2}^{+\alpha/2} \mathbf{R}(\alpha) \cdot \sigma_{xyz} \cdot \mathbf{R}(\alpha)^{-1} \, d\alpha \Big/ \int_{-\alpha/2}^{+\alpha/2} d\alpha \qquad (7\text{-}20)$$

These examples are only a few of the possibilities. Calculated chemical-shift anisotropy lineshapes are compared with the observed high-temperature limit in Figure 7-7. Neither the π-flip lineshape nor restricted rotation can simulate the shape individually. The π-flip lineshape has the correct general shape but is too broad. The restricted rotation lineshape does not even approximately match the observed shape when the angular amplitude is made large, so this possibility may be ruled out. Another arbitrary axis inclined at 70° to the C_1C_4 yields a lineshape close to the observed but this choice of axis is inconsistent with the solid-state proton spectrum of BPA-d_6 shown in Figure 7-8. A reasonably good simulation of the observed lineshape at high temperatures can be obtained by combining π flips with restricted rotation over a modest

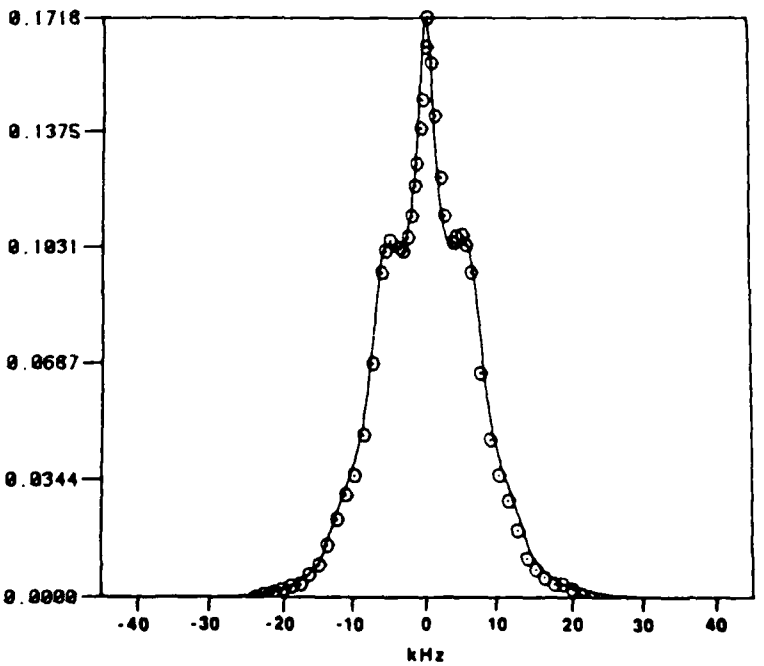

Figure 7-8. Proton dipolar lineshapes of BPA-d_6 in perdeutero-BPA. The points represent experimental data and the line the theoretical simulations in the high-temperature limit simulation. The lineshape consists of a Pake doublet plus a sharp line from a small percentage of protons remaining in deuterated sites. (Reprinted with permission from Inglefield, P. T.; Amici, R. M.; O'Gara, J. F.; Hung, C.-C.; Jones, A. A. *Macromolecules* **1983**, *16*, 1552. Copyright 1983, American Chemical Society.)

angular amplitude. The simulated spectrum for a restricted rotation over a range of $\pm 36°$ in addition to π flips yields a lineshape comparable to the observed lineshape at 393 K.

The proton and ^{13}C lineshape data in conjunction with the deuterium lineshape results specify the nature of the geometry of the motion of the phenylene group. Carbon–proton dipolar rotational spin-echo lineshape experiments (a technique discussed in Chapters 2 and 3) are also consistent with the π flips and limited restricted rotation.[43] With the geometry of the motion determined by comparing the spectra in low-temperature and high-temperature limits, the rates and amplitudes of the motions can then be considered.

If the rate of motion is comparable to the frequency width of the lineshape, a more elaborate simulation procedure must be undertaken. Equations are available for multiple site exchange, leading to the collapse of CSA lineshape.[30] The general lineshape equation for N sites is:

$$g(\omega) = (1/N)(L/(1 - KL)) \tag{7-21}$$

where

$$L = \sum_{j=1}^{N} [i(\omega - \omega_j) - (1/T_{2j}) + NK]^{-1}$$

T_{2j} = the spin–spin relaxation time, $K = \tau^{-1}$ = exchange or flipping rate, N = number of sites, and ω_j = frequency of site j:

$$\begin{aligned}\omega_j = \sigma_{iso} &+ (\sigma_{33} - \sigma_{iso})[P_2(\cos\beta)P_2(\cos\theta) \\ &+ (3/4)\sin^2\theta\sin^2\beta\cos^2(\phi+\gamma) - 3\sin\theta\cos\theta\sin\beta\cos\beta\cos(\phi+\gamma)] \\ &+ [(\sigma_{11} - \sigma_{22})/2][\sin^2\theta\cos^4\beta\cos[2(\phi+\gamma+\alpha)] \\ &+ \sin^2\theta\sin^4\beta\cos[2(\phi+\gamma-\alpha)] + \sin\theta\cos\theta\sin\beta \\ &\times \{(\cos\beta^{+1})\cos(\phi+\gamma+2\alpha) + (\cos\beta^{-1})\cos(\phi+\gamma+2\alpha)\} \\ &+ P_2(\cos\theta)\sin^2\beta\cos(2\alpha)]\end{aligned}$$

Other terms in the equation are the Legendre polynomial, P_2; the Euler angles of the flip axis with respect to the principal axis system of the shift tensor, (α, β, γ); and the Euler angles of the magnetic field with respect to the flip axis, (θ, ϕ). For an NMR lineshape, $I(\omega)$, the real part of $g(\omega)$ is required. The preceding formulation is for a single orientation with respect to the magnetic field and an average over all orientations must be taken:

$$I(\Omega) = \int d\Omega P(\Omega) I(\omega, \Omega) \tag{7-22}$$

where $P(\Omega) = (1/4\pi)$ and $d\Omega = \sin\theta\, d\theta\, d\phi$. Very suitable computer programs for these lineshape simulations as a function of rate are given in the Ph.D. thesis of Wemmer.[44]

While the π-flip process is simulated as a specific example of the general N-site exchange, the restricted rotation is simulated not with a temperature-dependent rate but with a temperature-dependent amplitude. At temperatures above 293 K, the π-flip process is in the rapid limit and all further narrowing is attributed to an increase in an amplitude of the restricted rotation. The root mean square of the amplitude of the restricted rotation is found to be linear versus the square root of temperature above 293 K. This linear dependence is assumed for lower temperatures as well, which allows for a complete simulation of the spectra at all temperatures as a result of both motions. The amplitudes of the restricted rotation as a function of temperature are summarized in Figure 7-9 and the comparable π flip rate information in Figure 7-10. The experimental spectra are shown in Figure 7-11 and comparisons between the simulations and the experimental spectra are shown in Figure 7-12.

An apparent activation energy can be calculated from the temperature

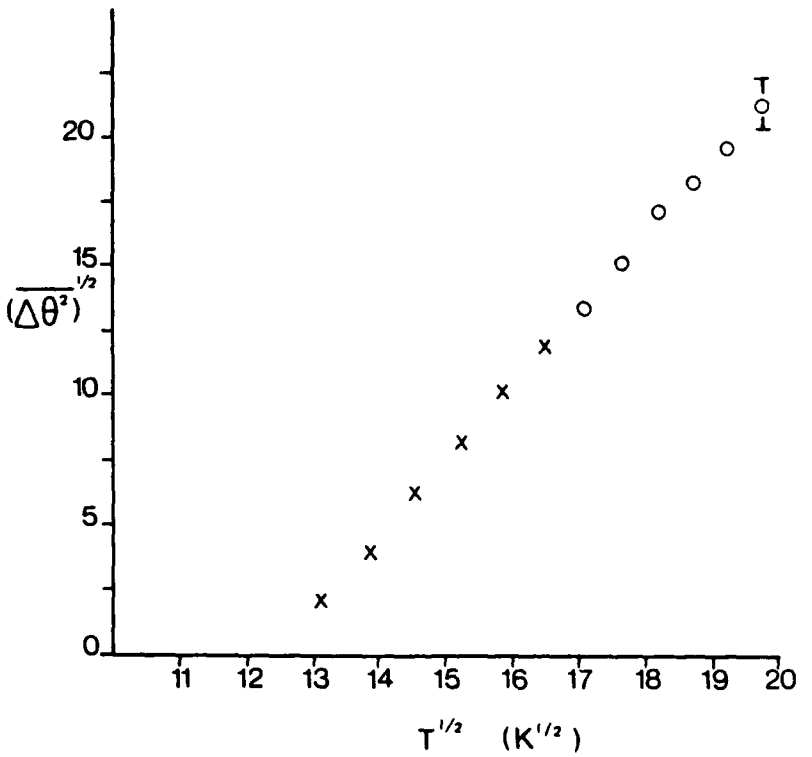

Figure 7-9. Root-mean-square amplitude of restricted phenylene group rotation about the C_1C_4 axis versus temperature to the one half power. The rms amplitude is determined from simulating the ^{13}C CSA lineshape. (Reprinted with permission from O'Gara, J. F.; Jones, A. A.; Hung, C.-C.; Inglefield, P. T. *Macromolecules* **1985**, *18*, 1117. Copyright 1985, American Chemical Society.)

dependence of the π-flip rate. The rather low value of 11 ± 5 kJ is found that is not consistent with the apparent activation energy of 50 kJ determined from proton spin–lattice relaxation data. The discrepancy reflects the use of an exponential correlation function for the simulation of the CSA spectra, whereas a highly nonexponential correlation function was used in the simulation of the T_1 and $T_{1\rho}$ data. The lineshape data can be simulated fairly well with a single exponential correlation function because only a limited range of frequencies near 1 kHz is sampled and the temperature dependence of π flips can be observed only from 183 to 273 K. On the other hand, the T_1 and $T_{1\rho}$ data extended from 90 MHz to 43 kHz and the temperature dependence could be determined from 153 to 393 K.

One other set of relevant lineshape data is available on the BPA unit in an epoxy resin.[26] The spectroscopic technique employed was variable-temperature ^{13}C magic angle sample spinning. At low temperatures, the protonated phenylene carbon lines become doublets reflecting two slightly different chemical environments. As temperature is raised the high-resolution lines obtained under these experimental conditions collapse to the single sharp line usually observed near room temperature. The two lines for a single type of carbon present at low temperature are attributed to two rotational conformations of the phenylene ring although at the time of the report it was not clear that the process involved was π flips. A correlation function was used to interpret the spectral collapse. In this case, as for the proton-relaxation data, a Williams-Watts-Ngai fractional exponential correlation function was employed with a correlation time, apparent activation energy, and fractional exponent comparable to the values used in the chloral polycarbonate interpretation. (See Chapter 3.)

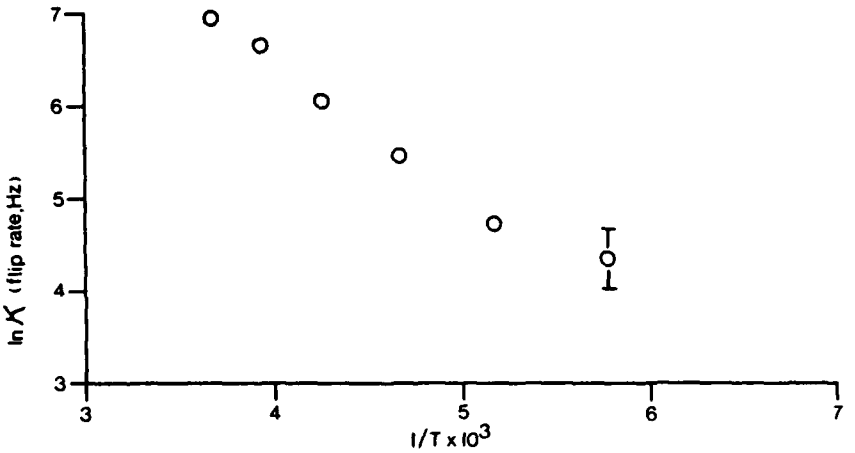

Figure 7-10. The natural logarithm of the π-flip rate versus inverse temperature. The π-flip rate is determined from simulation of the ^{13}C CSA lineshape. Abscissa is in K^{-1}. (Reprinted with permission from O'Gara, J. F.; Jones, A. A.; Hung, C.-C.; Inglefield, P. T. *Macromolecules* **1985**, *18*, 1117. Copyright 1985, American Chemical Society.)

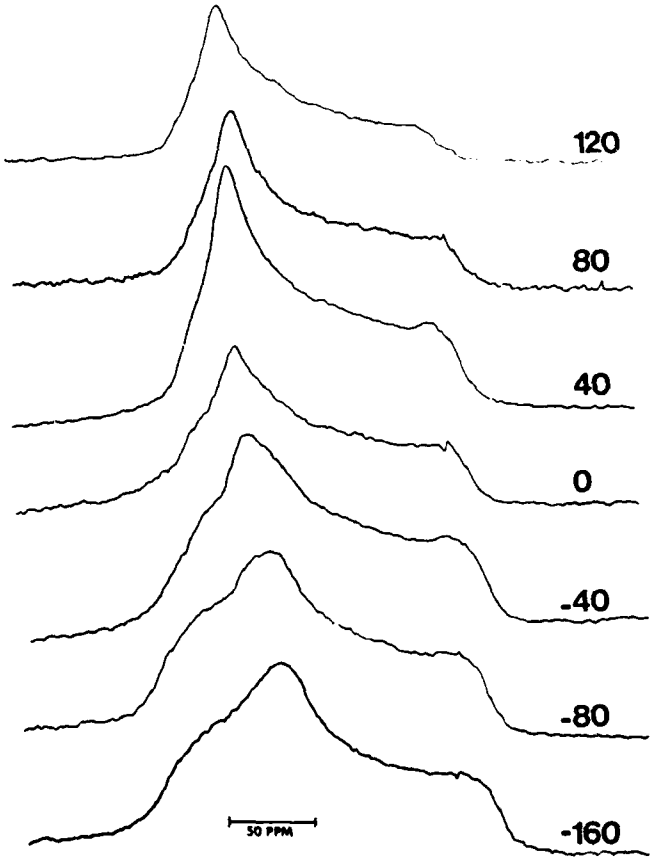

Figure 7-11. Carbon-13 CSA lineshapes at several temperatures. (Reprinted with permission from O'Gara, J. F.; Jones, A. A.; Hung, C.-C.; Inglefield, P. T. *Macromolecules* **1985**, *18*, 1117. Copyright 1985, American Chemical Society.)

Carbon-13 chemical-shift anisotropy lineshape spectra are also available on the carbonate unit in BPA polycarbonate.[28] These spectra were obtained by Henrichs on a labeled sample under conditions comparable to the phenylene labeled system. The carbonate carbon CSA lineshape is quite broad, about 150 ppm, but shows rather little change with temperature. This result is surprising because a large dielectric loss is present in BPA polycarbonate, which can only reflect motion of the carbonate unit. Henrichs interprets the small change in the CSA tensor to be oscillation of the carbonate unit with an angular amplitude of about 40° at room temperature. The interpretation is not decisive because the principal axis system of the shielding tensor is not entirely clear in the carbonate unit and the lineshape change is rather small. However this information cannot be ignored as a complete dynamic picture of polycarbonate is developed.

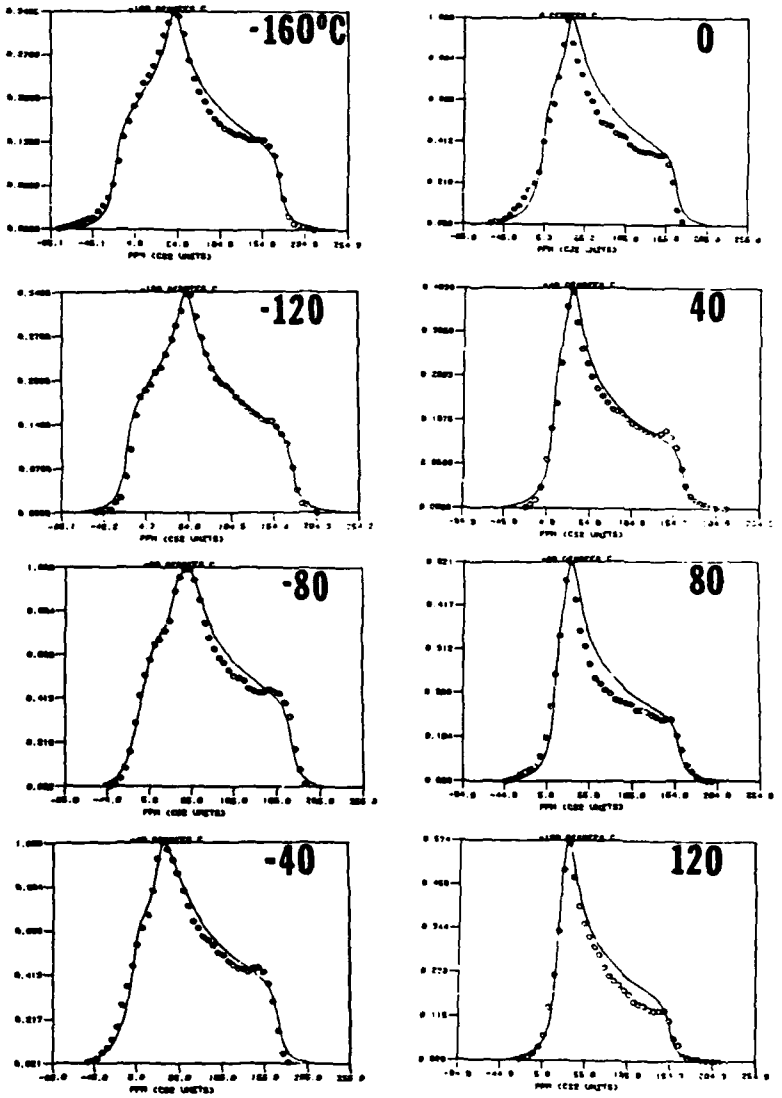

Figure 7-12. The lines are simulations of the ^{13}C CSA lineshapes at several temperatures, and the points are taken from the spectra in Figure 7-11. (Reprinted with permission from O'Gara, J. F.; Jones, A. A.; Hung, C.-C.; Inglefield, P. T. *Macromolecules* **1985**, *18*, 1117. Copyright 1985, American Chemical Society.)

Summary of Polycarbonate Dynamics from NMR

Polycarbonate is intrinsically a very mobile polymer chain in spite of a rather complex repeat unit. In dilute solution, segmental motion, phenylene group rotation and methyl group rotation are all rapid and have rather low apparent barriers to surmount. However, even in dilute solution, segmental motion cannot be characterized by a single correlation time, although phenylene group rotation and methyl group rotation can still be treated in the simplest manner. Presently, the best model for segmental motion appears to be the approach by Hall and Helfand[7] based on computer simulations of chain dynamics in polyethylene.

In the bulk, segmental motion of the type that creates new backbone directions is present above the glass transition. Below the glass transition, the backbone bonds represented by the BPA unit are not reorientated significantly, as evidenced by the proton spectra. Carbon-13 and deuterium spectroscopy show phenylene group rotation persists in the glass in the form of π flips and restricted rotation. Carbon-13 spectroscopy is less definitive with respect to the motion of the carbonate unit.

Proton-relaxation experiments show the correlation function describing the motion to be complex. In the frequency domain, there is significant spectral density over five decades. The lineshape, time-scale analysis does not require as complex a correlation function, although it is not inconsistent with the presence of it either. The only correlation function found that is capable of summarizing the relaxation data is the fractional exponential form commonly referred to as the Williams-Watts function. Justifications of this form have been offered by Ngai[9,10] and by Schlesinger and Montroll.[45]

Relationship Between NMR and Other Dynamical Methods

Nuclear magnetic resonance has clearly established the geometry of the phenylene motion in BPA polycarbonate and proton relaxation yields the correlation function. It is fair to ask whether the motions seen by proton and ^{13}C spectroscopy are the same and then whether these motions are related to dynamic mechanical response and dielectric relaxation.

First a relaxation map can be constructed by plotting the logarithm of the frequencies versus temperature for the T_1 minima, the $T_{1\rho}$ minima, the average coalescence point of ^{13}C lineshape collapse, and maximum point of dynamic mechanical loss. In Figures 7-13 and 7-14, this plot is seen to be linear for chloral polycarbonate and BPA polycarbonate. The line on these plots is derived from the Williams-Watts-Ngai fit of the proton-relaxation data shown in Figures 7-3 and 7-5. The conclusion to be drawn is that the NMR data are linked in time and they are linked to the time scale of the mechanical loss.

Furthermore, the breadth as well as the position of the mechanical loss peak is fairly well represented by the correlation function developed from proton-relaxation data as shown in Figure 7-15.

The frequency–temperature superposition of the NMR data and the dynamic mechanical loss data raises questions. It is difficult to see how jumps of a symmetrical group between two equivalent minima can produce a large mechanical loss. Also motion of the phenylene group certainly cannot produce a large dielectric loss nor does it seem likely that the large dielectric loss can be attributed entirely to carbonate group oscillation. The dynamic mechanical and dielectric loss peaks are rather large for such sub-glass transition peaks and a mechanism reflecting this fact is required.

A motion can be proposed that is consistent with the NMR data and the presence of large low-temperature loss peaks.[46] This proposal is offered in the

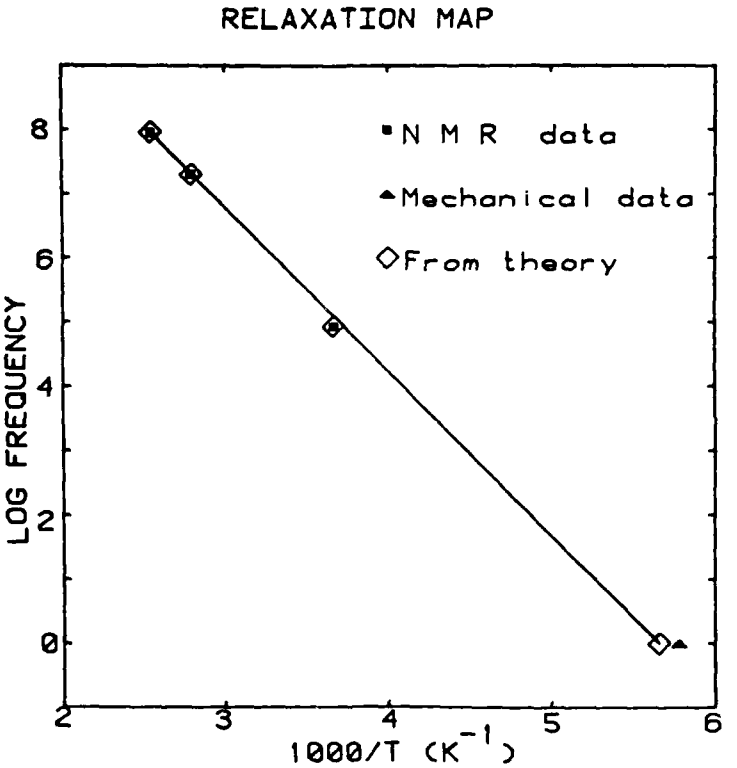

Figure 7-13. Relaxation map for chloral polycarbonate. The three NMR points are spin–lattice relaxation minima at 90 MHz, 50 MHz, and 43 kHz corresponding to the data in Figure 7-3. The mechanical datum is the maximum of a dynamic mechanical loss peak at 1 Hz. The line is a Williams-Watts-Ngai fit based on parameters determined from the proton-relaxation data in Figure 7-3. (Reprinted with permission from Jones, A. A.; O'Gara, J. F.; Inglefield, P. T.; Bendler, J. T.; Yee, A. F.; Ngai, K. L. *Macromolecules* **1983**, *16*, 658. Copyright 1983, American Chemical Society.)

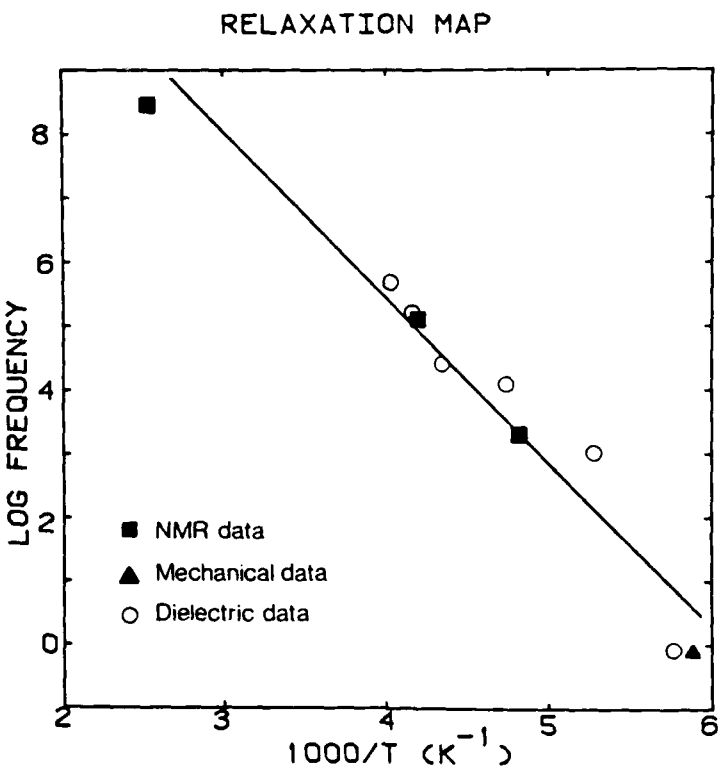

Figure 7-14. Relaxation map for BPA polycarbonate. The highest frequency NMR point is the 90 MHz proton T_1 minimum. The next highest frequency NMR point is the 43 kHz $T_{1\rho}$ minimum. The lowest frequency NMR point is the ^{13}C chemical-shift anisotropy lineshape. The open circles are maxima of various dielectric loss curves taken at different frequencies. The positions of all points have an uncertainty of the order of 10° because of the breadth of the loss peaks and relaxation minima. (Reprinted with permission from O'Gara, J. F.; Jones, A. A.; Hung, C.-C.; Inglefield, P. T. *Macromolecules* **1985**, *18*, 1117. Copyright 1985, American Chemical Society.)

spirit of stimulating further investigation because, although it is consistent with the data in hand, it is not proved by it. No doubt further experimental and theoretical tests can be developed to evaluate the proposal.

The basic motion is shown in Figure 7-16 and consists of an interchange of a cis–trans carbonate conformation with a neighboring trans–trans carbonate conformation. This is not a simultaneous interchange but a correlated conformational change of the type observed by Helfand[7] in computer simulations of polyethylene chains. The carbonate groups are reoriented by this process but the BPA groups are not reoriented significantly, although they are translated. The carbonate groups are thought to be mostly in the trans–trans conformation, with a smaller number of cis–trans units present. The conformational interchange diffuses the cis–trans conformation down the chain of largely

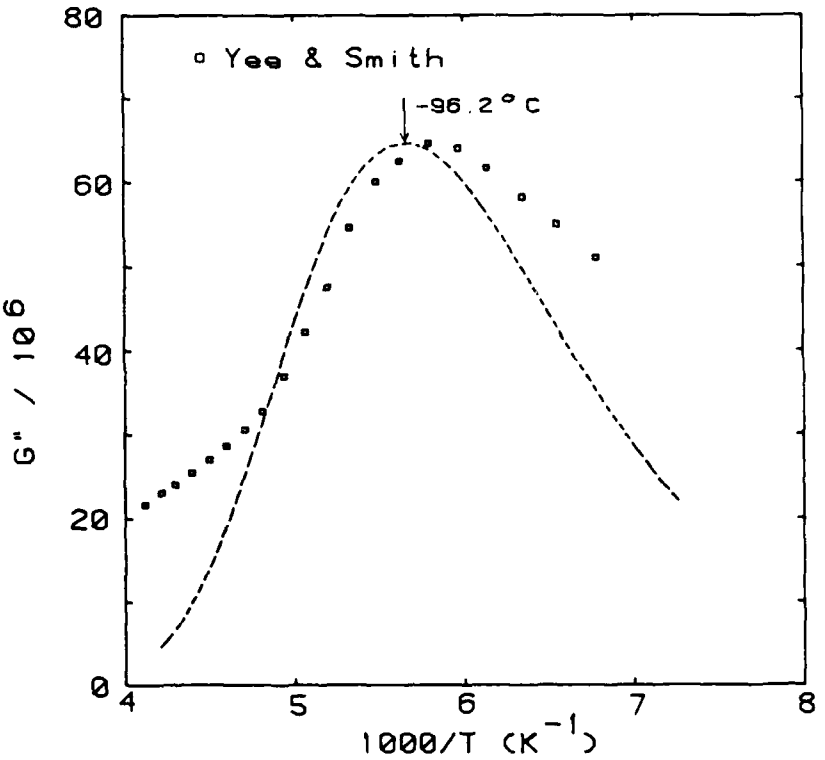

Figure 7-15. Dynamic mechanical spectrum for chloral polycarbonate. The dashed line is the simulation employing the Williams-Watts-Ngai fractional exponential with the parameters set from the proton relaxation data and fit shown in Figure 7-3. (Reprinted with permission from Jones, A. A.; O'Gara, J. F.; Inglefield, P. T.; Bendler, J. T.; Yee, A. F.; Ngai, K. L. *Macromolecules* **1983**, *16*, 658. Copyright 1983, American Chemical Society.)

trans–trans units. As this diffusional process occurs, BPA units are translated. The occurrence of π flips is coupled to this motion through intramolecular or intermolecular interactions. The presence of mobile phenylene groups may make the barrier to conformational interchange smaller by providing some fluctuations in the surrounding glassy matrix and vice versa.

The proposed motion is in agreement with NMR data because the BPA unit is not reoriented significantly although the phenylene groups undergo π flips and oscillation about the C_1C_4 axis, which corresponds to a virtual backbone bond direction. The proton lineshape data show these virtual backbone bonds do not change direction whereas the ^{13}C and deuterium results show π flips and oscillation about the C_1C_4 axis. The ^{13}C carbonate lineshape may not show significant changes because of coincidental geometric relationships or because most of the carbonate units are trans–trans and a minority are cis–trans, so interchange produces an average shape not greatly different from

the trans–trans case. In the proposed model, the shear dynamic mechanical loss and the dielectric loss result from the reorientation of the carbonate group. A larger bulk mechanical loss results from the translation of the larger BPA unit during the conformational interchange. The translation produces volume fluctuations between chains. The bulk loss, shear loss, and dielectric loss are all coincident in time because the same cooperative motion is involved. The π flips are linked in time because they are controlled by the fluctuations in the glassy environment. The correlation function describing this motion is complex because the motion is a segmental rearrangement and also because of the strong intermolecular interactions in the glass. A complex correlation function would lead to broad loss peaks and relaxation minima. This segmental motion is different from the segmental motions of the glass transition because it creates no new backbone bond directions but merely interchanges carbonate group conformations. Because the proposed motion is a segmental motion, albeit not as general as those of the glass transition, large dielectric and mechanical loss peaks may result. The phenylene group and the rest of the chain undergo oscillations reflecting the general flexibility of this polymer but these oscillations do not produce the large loss peaks. The

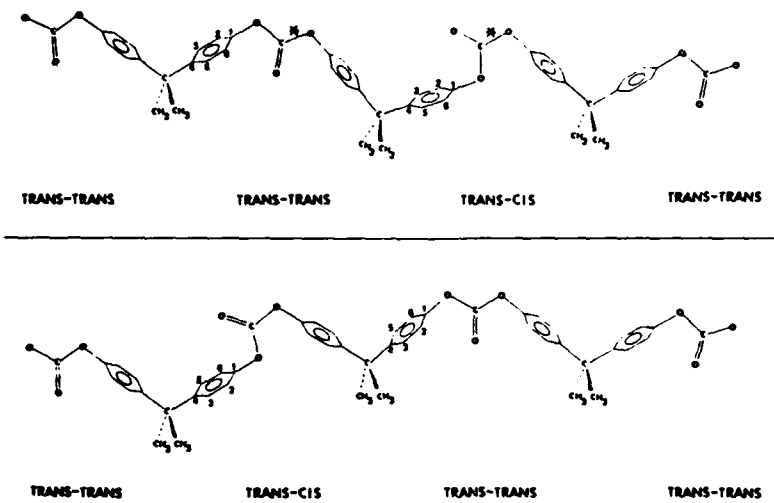

Figure 7-16. BPA polycarbonate chains and the local motion corresponding to the loss maxima and relaxation minima in the glass. The carbonate CO bonds with asterisks indicate points of bond rotation. The phenylene rings undergoing flips in association with the CO bond rotations are numbered. The correlated conformational change from the top chain to the lower chain involves two neighboring carbonate groups and is produced by the CO bond rotations which interchange the trans–trans and cis–trans conformations. Conventional bond angles of 109° are used for all backbone bonds except the carbonate bonds, which are set at 120°. These choices lead to an 11° change in the C_1C_4 axis of the phenylene groups in the BPA unit between the carbonate unit undergoing conformational change. (Reprinted with permission from Jones, A. A. *Macromolecules* **1985**, *18*, 902. Copyright 1985, American Chemical Society.)

general flexibility of polycarbonate may lower the transition state during the conformational interchange, thus playing an important secondary role.

This dynamic model came out of the new information provided by NMR and the picture of segmental motion developed by Hall and Helfand.[7] The model agrees quantitatively with the phenylene group NMR data and is at least consistent with other dynamic information on polycarbonate. Quantitative estimates of the magnitude of the dielectric and mechanical loss peaks based on this proposal would be helpful in evaluating it but represent substantial projects in themselves. In any case, NMR spectroscopy has interjected new ideas into the discussion of motion in polycarbonate.

Acknowledgment

This research was carried out with the financial support of National Science Foundation Grant DMR-790677, of National Science Foundation Equipment Grant No. CHE 77-09059, of National Science Foundation Grant No. DMR-8108679, and of U.S. Army Research Office Grant DAAG 29-82-G-0001.

References

1. Schaefer, J.; Stejskal, E. O.; Buchdahl, R. *Macromolecules* **1977**, *10*, 384.
2. Inglefield, P. T.; Amici, R. M.; O'Gara, J. F.; Hung, C.-C.; Jones, A. A. *Macromolecules* **1983**, *16*, 1552.
3. Spiess, H. W. *Colloid Polym. Sci.* **1983**, *261*, 193.
4. Jelinski, L. W.; Dumais, J. J.; Engel, A. K. *Macromolecules* **1983**, *16*, 492.
5. Inglefield, P. T.; Jones, A. A.; Lubianez, R. P.; O'Gara, J. F. *Macromolecules* **1981**, *14*, 288.
6. Jones, A. A.; O'Gara, J. F.; Inglefield, P. T.; Bendler, J. T.; Yee, A. F.; Ngai, K. L. *Macromolecules* **1983**, *16*, 658.
7. Hall, C. K.; Helfand, E. *J. Chem. Phys.* **1982**, *77*, 3275.
8. Weber, T. A.; Helfand, E. *J. Phys. Chem.* **1983**, *87*, 2881.
9. Ngai, K. L.; White, C. T. *Phys. Rev. B* **1979**, *20*, 2475.
10. Ngai, K. L. *Phys. Rev. B* **1980**, *22*, 2066.
11. Williams, G.; Watts, D.C. *Trans. Faraday Soc.* **1970**, *66*, 80.
12. English, A. D.; Dybowski, C. R. *Macromolecules* **1984**, *17*, 446.
13. McCall, D. W. *Acc. Chem. Res.* **1971**, *4*, 223.
14. Heatley, F. "Progress in NMR Spectroscopy", Vol. 13; Pergamon Press, Ltd.: Oxford, 1979, p. 47.
15. Jones, A. A.; Robinson, G. L.; Gerr, F. E.; Bisceglia, M.; Shostak, S. L.; Lubianez, R. P. *Macromolecules* **1980**, *13*, 95.
16. Levy, G. C.; Axelson, D. E.; Schwartz, R.; Hochmann, J. *J. Am. Chem. Soc.* **1978**, *100*, 410.
17. Jones, A. A.; Bisceglia, M. *Macromolecules* **1979**, *12*, 136.
18. Garroway, A. N.; VanderHart, D. L. *J. Chem. Phys.* **1979**, *71*, 2772.
19. Schaefer, J. *Macromolecules* **1973**, *6*, 882.
20. Fleming, W. W.; Lyerla, J. R.; Yannoni, C. S. *ACS Symp. Ser.* **1984**, *247*, 83.
21. Tarpey, M. F.; Lin, Y.-Y.; Jones, A. A.; Inglefield, P. T. *ACS Symp. Ser.* **1984**, *247*, 67.
22. Cohen-Addad, J. P. *J. Chem. Phys.* **1974**, *60*, 2440.
23. Cohen-Addad, J. P.; Faure, J. P. *J. Chem. Phys.* **1974**, *61*, 1571.
24. Cohen-Addad, J. P.; Guillermo, A. *J. Polym. Sci., Polym. Phys. Ed.* **1984**, *22*, 931.

25. Jones, A. A.; Robinson, G. L.; Gerr, F. E. *ACS Symp. Ser.* **1974**, *103*, 271.
26. Garroway, A. N.; Ritchey, W. M.; Moniz, W. B. *Macromolecules* **1982**, *15*, 1051.
27. Vega, A. J.; English, A. D. *Macromolecules* **1980**, *13*, 1635.
28. Henrichs, P. M.; Linder, M.; Hewitt, J. M.; Massa, D.; Isaacson, H. V. *Macromolecules* **1984**, *17*, 2412.
29. Slotfeldt-Ellingsen, D.; Resing, H. A. *J. Phys. Chem.* **1980**, *84*, 2204.
30. Mehring, M. "Principles of High Resolution NMR in Solids"; Springer Verlag: Berlin, 1983.
31. O'Gara, J. F. Ph.D. Thesis, Clark University, Worcester, MA, 1984.
32. Tonelli, A. E. *Macromolecules* **1972**, *5*, 558.
33. Tonelli, A. E. *Macromolecules* **1973**, *6*, 503.
34. O'Gara, J. F.; Desjardins, S. G.; Jones, A. A. *Macromolecules* **1981**, *14*, 64.
35. Connolly, J. J.; Gordon, E.; Jones, A. A. *Macromolecules* **1984**, *17*, 722.
36. Lin, Y.-Y.; Jones, A. A.; Stockmayer, W. H. *J. Polym. Sci., Polym. Phys. Ed.* **1984**, *22*, 2195.
37. Woessner, D. E. *J. Chem. Phys.* **1962**, *36*, 1.
38. Bendler, J. T. *Ann. N.Y. Acad. Sci.* **1981**, *371*, 299.
39. Yee, A. F.; Smith, S. A. *Macromolecules* **1981**, *14*, 54.
40. O'Gara, J. F.; Jones, A. A.; Hung, C.-C.; Inglefield, P. T. *Macromolecules* **1985**, *18*, 1117.
41. Bloembergen, N.; Rowland, T. J. *Acta Metall.* **1955**, *1*, 731.
42. Rose, M. "Elementary Theory of Angular Momentum"; John Wiley and Sons: New York, 1957.
43. Schaefer, J.; Stejskal, E. O.; McKay, R. A. *Macromolecules* **1984**, *17*, 1479.
44. Wemmer, D. E. Ph.D. Thesis, University of California, Berkeley, CA, 1979.
45. Schlesinger, M. F.; Montroll, E. W. *Proc. Nat. Acad. Sci. (USA)* **1984**, *81*, 1280.
46. Jones, A. A. *Macromolecules* **1985**, *18*, 902.

"Transport and Relaxation in Random Materials", World Scientific Press, M. F. Shlesinger, ed., 1986, page 228.

MOLECULAR MOTION IN GLASSY POLYCARBONATE

Alan Anthony Jones, Paul T. Inglefield, J.F. O'Gara and A.K. Roy
Jeppson Laboratory, Department of Chemistry
Clark University, Worcester, MA 10610

Motion in polymeric glasses is greatly reduced both in amplitude and rate relative to either the rubbery or dissolved state.[1] In rubbers and solutions of random coil macromolecules, the backbone bonds sample nearly all directions in space over relatively short times, certainly less than microseconds. In the glass or near the glass transition, backbone bonds do not reorient isotropically even on the time scale of seconds but the presence of considerable local motions is still evident in mechanical and dielectric relaxation studies.[1]

The polycarbonate of bisphenol A (BPA-PC) pictured in Figure 1 displays especially large dielectric and mechanical loss peaks well below the glass transition. Mobility in this glass exceeds the norm for polymeric materials and this fact has attracted many investigators. One would like to characterize the time scale, energetics and geometry of the motion. Dielectric and dynamic mechanical relaxation measurements yield broad loss peaks with an apparent activation energy of about 50 kJ/mole.[2-3] Considerable speculation concerning the geometry of the motions responsible for the loss peaks accompanied the dielectric and mechanical studies.[2] However these techniques are not capable of determining this aspect of motion relative to the structure of the repeat unit of the polymer.

Geometry of Motion from Solid State NMR

In the past five years, solid state NMR has been able to determine the geometry of motion relative to the chemical structure of the macromolecule.[4-10] Large magnetic interactions such as dipolar, shielding and quadrupolar lead to distinctive line shapes when the motion is restricted or anisotropic. Since these magnetic interactions can be precisely related to the local structure, the presence of motion can be be set into the context of the repeat unit geometry.

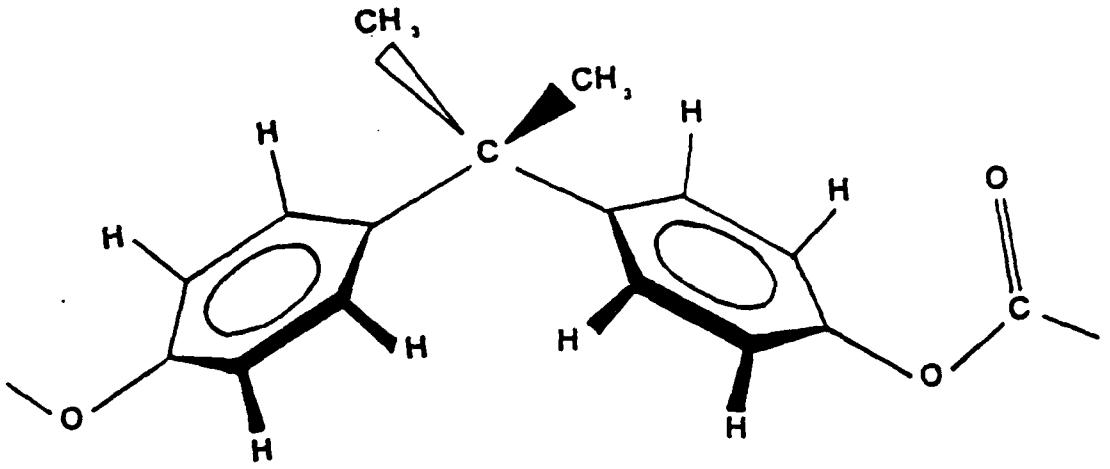

Figure 1. The repeat unit of the polycarbonate of bisphenol A (BPA-PC).

This advance has provided detailed information on local motion in glasses but in the end raises new questions as it answers the old.

The first indication of the geometry of local motion in BPA-PC came from a proton line shape study of a closely related structural analogue.[4] Here the proton-proton dipolar interaction between the neighboring protons on the phenylene groups is monitored by the presence of a Pake doublet. This distinctive line shape feature would collapse if a vector drawn between the two neighboring protons is reoriented by the onset of local motion. The Pake doublet persists in an undiminished form until the glass transition indicating no reorientation of the proton-proton internuclear direction. This direction is parallel to the effective backbone bond consisting of the phenylene group indicating that this virtual bond is not reoriented.

Proton spin-lattice relaxation in the same polymer shows the presence of considerable rapid, large amplitude motion.[11] If the phenylene protons are moving yet the corresponding backbone bond is not reorienting, the motion must be a rotation about that backbone bond. In chemists' parlance, the rotation would be about the C_1C_4 axis where C_1 is the phenylene carbon attached to the oxygen and C_4 is the phenylene carbon furthest from C_1.

This defines one aspect of the motion but the rotation needs further specification. Is it free rotation about the C_1C_4 axis or rotation by jumps between minima or a restricted rotation-libration? The first answer came from deuterium quadrupole line shape NMR[5] which indicated it was jumps between two minima separated by 180° plus restricted rotation in the bottom of each of the two minima. This result was substantiated by carbon-13 chemical shift anisotropy line shape results which can definitely distinguish between the three possibilities mentioned.[6] Carbon-13 proton dipolar line shapes are also consistent with the 180° jump or π flips plus restricted rotation.[9] These NMR experiments provide a description of the geometry of phenylene group motion not available from any other technique.

Both deuterium and carbon-13 proton dipolar[9] line shape studies on the methyl group of BPA show this entity to be rotating about the three fold symmetry axis. The motion is independent of phenylene group flips. Also the methyl group line shapes show the presence of at best only a little wiggling besides the rotation about the symmetry axis. Thus the bisphenol-A unit including the two phenylene groups, the two methyl carbons and the bridge carbon is not moving as a whole. The phenylene groups move in a two fold potential about their symmetry axis and the methyl groups move in a three fold potential about their symmetry axis.

The motion of the carbonate unit, $-O-\overset{O}{\overset{\|}{C}}-O-$ remains to be defined. Here an apparent inconsistency between NMR line shape data and dielectric data arises. Clearly the carbonate unit must be reorienting to account for the presence of the appreciable dielectric loss. However carbon-13 chemical shift anisotropy line shape data[12] on the carbonate carbon shows the presence of very little motion. This point must be addressed later in an overall motional model.[13]

Time Scale of Local Motion

Motions in polymers are known to have complex character in time which is quite apparent in the broad, skewed loss peaks usually observed in macromolecular glasses.[1] Such broad loss peaks could arise in at least two different manners.[14] First the motion of a given

polar group at a certain spatial position in the glass could be highly non-exponential. The motion of other polar groups of the same chemical type but at different spatial locations could be moving with a comparable non-exponential correlation function. This situation is referred to a homogeneous by NMR spectroscopists.[14]

An alternative source of broad loss peaks or relaxation minima can be imagined. Suppose an individual polar group at a particular location in a glass reorients in a Debye like fashion characterized by a simple exponential correlation function. However other polar groups at other locations also relay with simple exponential time constants but the time constants are different.[14] The various time constants at various locations in the glass arise from the inhomogeneous nature of the glass at a microscopic level. In particular different polar groups at different locations experience different packings or intermolecular environments leading to different time scales for reorientation. This situation is referred to as inhomogeneous and leads to broad loss peaks just as the earlier homogeneous description.

Mechanical loss, dielectric loss and proton spin-lattice relaxation cannot distinguish between the origin of the distribution. However carbon-13 spin-lattice relaxation and the solid state line shape experiments can distinguish between the two possibilities[7,14,15] and now definitively point to a predominately inhomogeneous distribution in polycarbonate.

To quantitatively summarize the inhomogeneous distribution of relaxation times in polycarbonates, two forms of correlation functions have been used. Spiess[16] has employed a log normal distribution which extends over about three decades in time to account for a variety of deuterium line shape experiments. An apparent activation energy of about 40 kJ describes the temperature dependence and some change in breadth accompanies change in temperature.

Jones[11,15] et al. has employed the fractional exponential correlation function to summarize proton spin-lattice relaxation, carbon-13 spin-lattice relaxation and carbon-13 chemical shift anisotropy line shape data. A fractional exponent (β) of 0.15 is required to fit the

proton data[15,17] and is consistent with the carbon data. The fractional exponent is determined from the temperature dependence of spin-lattice relaxation data since insufficient data was available to fix the exponent at different temperatures. This fixed β was capable of matching the published deuterium data[7,15] though more detailed results from this technique are forthcoming.

The Jones group has also presented a quantitative analysis of the temperature dependence of the amplitude and time scale of the restricted rotation based on a correlation function developed by Gronski.[15,18] The amplitude of the restricted rotation is found to increase with the square root of temperature which is plausible. However the amplitude extrapolated to absolute zero is large which is difficult to interpret. The time scale of the restricted rotation is contained in a rotational diffusion constant which varies linearly with temperature and falls in the range of 10^{-8}s.[17] This time scale is characteristic of phenylene group libration and is much longer than infrared vibrational oscillation.

A More Complete Motional Model

An NMR spectroscopist might be tempted to stop with the motional interpretation developed thus far. This would include methyl group rotation, phenylene group π flips plus libration and little motion of the carbonate or the bisphenol unit as a whole. While this view satisfies the NMR data it is not easily reconciled with the mechanical and dielectric data. A relaxation map[6,11,15] constructed from spin-lattice relaxation minima, line shape coalescence, dielectric and mechanical maxima shows these phenomena to be linked phenomenologically in time. Such a map is shown in Figure 2 but the motions identified by NMR will not lead to large mechanical or dielectric loss.

The discrepancy between an apparently static carbonate carbon based on line shape data and the virtual necessity of carbonate reorientation for dielectric loss has been mentioned. Similarly, the only large amplitude motions noted are anisotropic rotations of symmetric groups, methyl and phenylene; and such motions do not lead to significant shear loss as is observed.

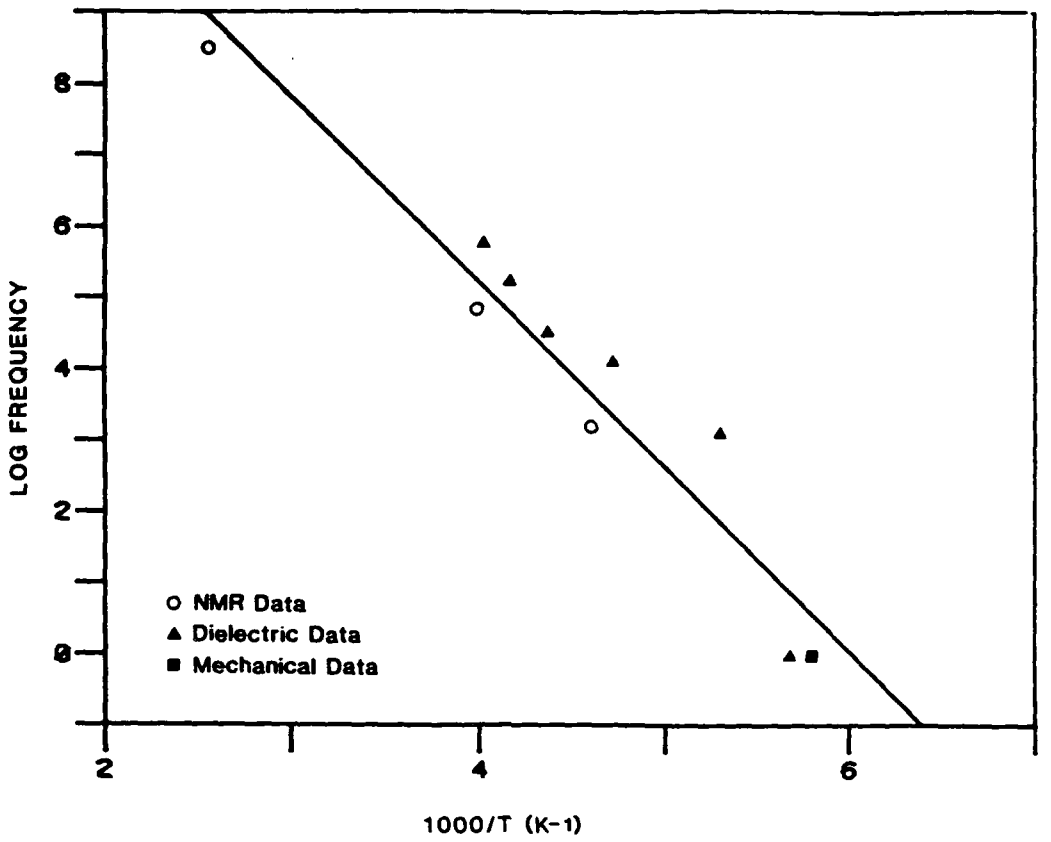

Figure 2. Log frequency versus inverse temperature or relaxation map. The highest frequency NMR point is the 90 MHz proton T_1 minimum, the next highest, 43 KHz $T_{1\rho}$ minimum and the lowest, the average position of CSA line shape coalescence. The open circles are maxima of dielectric loss curves taken at different frequencies and the square of the dynamic mechanical loss peak. The positions of all points have an associated uncertainty of the order of 10 degrees because of the broadness of loss peaks and relaxation minima.

Given the phenomenological linkage of the various relaxation experiments, the geometry of motion given by NMR, and the need to account for dielectric and mechanical loss, a motional model is proposed.[13] The model is constructed to be consistent with observations but unfortunately the data in hand do not "prove" the validity of the model.

The proposed local motion focuses on the conformation of the carbonate group. This unit is believed to reside predominantly in the

trans-trans conformation.[19] As part of the motional model, the existence of a few defect conformations of either cis-trans or trans-cis forms are proposed. A cis-trans or trans-cis conformation with respect to the carbonate unit is found to be only somewhat higher in energy from quantum mechanical calculations on diphenyl carbonate.[20] Also the barrier for conformational change from cis-trans or trans-cis is found to be the lowest rotational backbone barrier in polycarbonate from the same calculations.

The motion proposed is a conformational exchange between a cis-trans or trans-cis and a neighboring trans-trans unit. This process is displayed in Figure 3. the pathway of the conformational exchange is a sequential set of rotation of the cooperative type suggested by Helfand.[21-24] The carbonate bonds which rotate are indicated by asterisks in Figure 3 and the backbone phenylene groups undergoing rotations are labelled with numbers.

The phenylene groups effectively execute π flips which is consistent with NMR line shape data. However in this motional picture, the π flips are part of a more complex limited segmental motion. The carbonate group changes shape in changing from trans-trans to cis-trans or trans-cis and the dipole moment should change in magnitude as well as orientation. These characteristics should lead to mechanical and dielectric loss linked in time to the π flips.

The carbonate carbon chemical shift anisotropy line shape does not collapse in the presence of this motion because a large population of trans-trans conformations is interchanged with a small population of cis-trans or trans-cis conformations. Even at high temperature, the average line shape in the rapid exchange limit will be close to the trans-trans line shape thereby displaying little indication of the motion. However since defect diffusion is involved, many carbonates can be reoriented by one defect leading to significant dielectric relaxation.

The BPA unit as a whole is not appreciably reoriented during the conformational interchange save for π flips which is again consistent with NMR line shape data. The BPA unit is translated which could lead

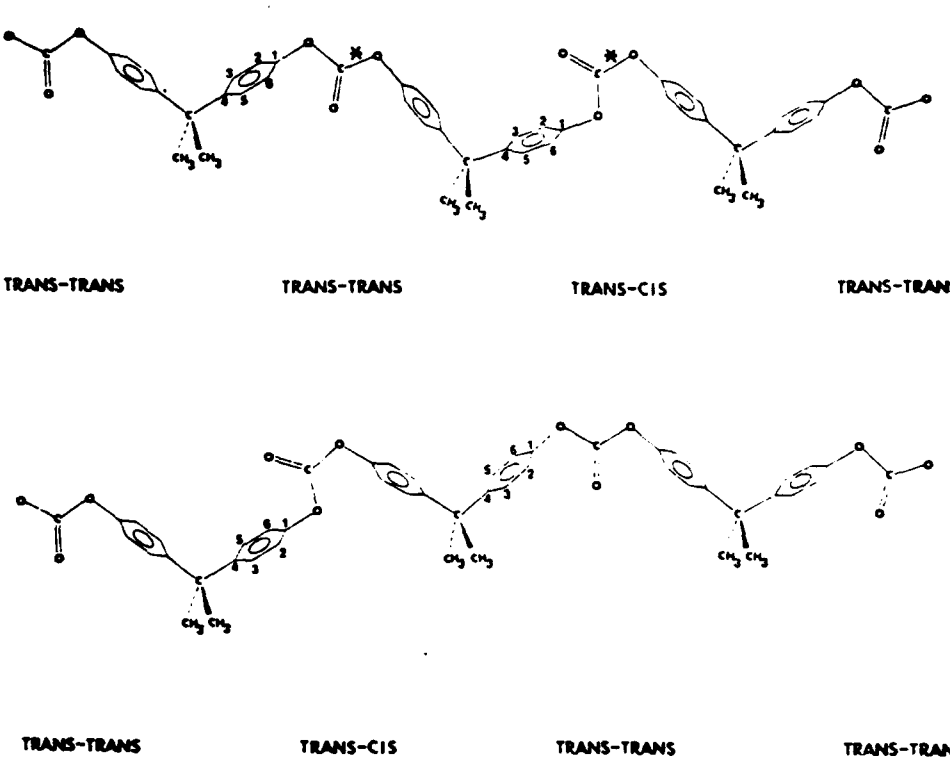

Figure 3. BPA polycarbonate chains. The top chain fragment is the initial state and the lower chain fragment is the final state. The carbonate CO bonds with asterisks indicate points of bond rotation. The phenylene rings undergoing flips in association with the CO bond rotations are numbered. The correlated conformational change from the top chain to the lower chain involves two neighboring carbonate groups and is produced by the CO rotations which interchange the trans-trans and trans-cis conformations. Note that the choice of a trans-cis unit in the figure is arbitrary. If a cis-trans unit were used, the other phenylene rings would be flipped so over a period of time all rings could be flipped as the cis-trans and trans-cis conformations diffuse along the chain.

to a bulk mechanical loss which has been observed in BPA-PC.

The interchange of a few cis-trans or trans-cis conformations with neighboring trans-trans conformation diffuses the cis-trans or trans-cis units along the predominantly trans-trans backbone. This defect diffusion character is related to several experimental observations.

to a bulk mechanical loss which has been observed in BPA-PC.

First at high temperatures, all phenylene groups undergo π flips. If defect diffusion is sufficiently rapid on the line shape experiment time scale, all phenylene groups will appear to flip by either a cis-trans to trans-trans interchange or a trans-cis to trans-trans interchange. However as temperature is lowered in the glass, some carbonate units will no longer be able to participate in the interchange process because some local environments present too high a barrier. The phenylene groups near these units will appear rigid while other phenylene groups near carbonates with lower intermolecular barrier to conformational interchange will still appear as mobile. This would lead to the observed inhomogeneous character of the line shape collapse at intermediate temperatures. At quite low temperatures, little conformational interchange at any carbonate unit would result in the rigid line shape limit observed below -100°C.

Intermolecular interactions must contribute significantly to barrier heights since the observed activation energy in the glass is 50 kJ/mole. In solutions involving low viscosity solvents, the barriers to rotation or segmental motion is in the range of 10 to 15 kJ/mole in agreement with isolated chain calculations.[25-26] Thus the 35 to 40 kJ increase in apparent activation energy must be ascribed to intermolecular interactions allowing for the rationalization of the inhomogeneous character of line shape collapse just presented.

The defect diffusion character of the conformational interchange process involving a distribution of barrier heights can be identified with one of the derivations of fractional exponential correlation functions.[27-29] If the proposed motional model is correct, then the use of the fractional exponential correlation function is more than a convenient mathematical form but is also a physically sensible form.

In this motional model, phenylene group libration and methyl group rotation while present are not key aspects of the dynamics. Similarly, the presence of some low amplitude chain oscillation or w'ggling is also a secondary aspect.

Remaining Questions

The defect conformations have not been directly observed so they remain as only postulated entities. The defect diffusion character of the motion may not be the source of the inhomogeneous distribution of relaxation times. Rather, the distribution of relaxation times may result from packing differences at individual motional sites. In this picture there is no diffusion from site to site but each site reorients with its own time scale. If this were the case, the fractional exponential function is just a convenient mathematical form and not connected with a physical derivation.

The defect diffusion conformational interchange process is shown in Figure 3 for an extended chain conformation. This extended chain conformation is not likely with other rotational angles placing one phenylene group out of the plane of the paper with respect to the other. These rotations will lead to the random coil character appropriate for polycarbonate. However whatever the relative disposition of the phenylene rings in one BPA unit, the interchange of carbonate conformations can still take place leaving the BPA unit motionless. Thus the particular conformational sequence shown in Figure 3 is convenient to draw but not a requirement of the motional model. A detailed analysis of the action of conformational interchange for other conformations associated with relative rotations of the phenylene groups in a BPA unit will be pursued with computer graphics.

The analysis of phenylene group libration in the data treatment and its role in the motional model is simplistic.[18] All phenylene groups are treated as thought they undergo the same librational amplitude. However the librational amplitude is governed by intermolecular interactions since rotation is found to be four fold or higher from calculations[10,26] and dilute solution spin-lattice relaxation.[25] If intermolecular effects dominate, a glassy matrix should lend to a distribution of libration amplitudes as well as a distribution of barrier heights. The failure of the line shape simulation to produce a reasonable intercept for the amplitude of libration at absolute zero may reflect the single amplitude approximation.

Further experimental work and analysis of the consequences of the motional model are required. At this stage it can be regarded as an interesting proposal or conjecture which may prompt particular lines of inquiry.

Acknowledgement

This research was carried out with the financial support of the National Science Foundation Grant DMR-790677, of National Science Foundation equipment Grant No. CHE 77-09059, of National Science Foundation Grant No. DMR-8108679, and of U.S. Army Research Office Grant DAAG 29-82-G-0001.

References

1. N.G. McCrum, B.E. Read and G. Williams, Anelastic and Dielectric Effects in Polymeric Solids, Wiley, New York (1967).

2. A.F. Yee and S.A. Smith, Macromolecules (1981) 14, 54.

3. S. Matsuoka and Y. Ishida, J. Polym. Sci., Part C (1966) 14, 247.

4. P.T. Inglefield, A.A. Jones, R.P. Lubianez and J.F. O'Gara, Macromolecules (1981) 14, 288.

5. H.W. Spiess, Colloid. Polym. Sci. (1983) 261, 193.

6. P.T. Inglefield, R.M. Amici, J.F. O'Gara, C.-C. Hung and A.A. Jones, Macromolecules (1983) 16, 1552.

7. H.W. Spiess, in Advances in Polymer Science, Vol. 66, H.H. Kausch and H.G. Zachmann, eds., Springer Verlag, Berlin (1985).

8. J.F. O'Gara, A.A. Jones, C.-C. Hung and P.T. Inglefield, Macromolecules (1985) 18, 1117.

9. J. Schaefer, E.O. Stejskal, R.A. McKay, W.T. Dixon, Macromolecules (1984) 17, 1479.

10. J. Schaefer, E.O. Stajskal, D. Perchak, J. Skolnik and R. Yaris, Macromolecules (1985) 18, 368.

11. A.A. Jones, J.F. O'Gara, P.T. Inglefield, J.T. Bendler, A.F. Yee and K.L. Ngai, Macromolecules (1983) 16, 658.

12. P.M. Kenricks, M. Linder, J.M. Hewitt, D. Massa and H.V. Isaacson, Macromolecules (1984) 17, 2412.

13. A.A. Jones, Macromolecules (1985) 18, 902.

14. J.I. Kaplan and A.N. Garroway, J. Mag. Res. (1982) 49, 464.

15. A.K. Roy, A.A. Jones and P.T. Inglefield, submitted to Macromolecules.

16. E.W. Fischer, L.P. Hellman, H.W. Spiess, F.J. Horth, A. Ecarius and M. Wherle, Mackro. Mol. Chem. Suppl. (1985) 12, 189.

17. J.J. Connolly, A.A. Jones and P.T. Inglefield, to be submitted to Macromolecules.

18. A.K. Roy, A.A. Jones, P.T. Inglefield, J. Mag. Res. (1985) 64, 441.

19. D.D. Williams and P.J. Flory, J. Polym. Sci. A-2 (1968); 6 (1945).

20. J.T. Bendler, Ann. N.Y. Acad. Sci. (1981) 371, 229.

21. E. Helfand, J. Chem. Phys. (1971) 54, 4651.

22. E. Helfand, Z.R. Wasserman and T.A. Weber, Macromolecules (1980) 13, 526.

23. C.K. Hall and E. Helfand, J. Chem. Phys. (1982) 77, 3275.

24. T.A. Weber and E. Helfand, J. Phys. chem. (1983) 87, 2881.

25. J.F. O'Gara, S.G. Desjardins and A.A. Jones, Macromolecules (1981) 14, 64.

26. A.E. Tonelli, Macromolecules (1972) 5, 558.

27. M.F. Shlesinger, E.W. Montroll, Proc. Natl. Acad. Sci. (USA) 1984, 81.

28. M.F. Shlesinger, J. Stat. Phys. (1984) 36, 639.

29. A. Blumen, G. Zumufen, J. Klafter, Phys. Rev. B (1984) 30, 5379.

A Comparison of Spin Relaxation and Local Motion Between Symmetrically and Asymmetrically Ring-substituted Bisphenol Units in Dissolved Polycarbonates

J. A. RATTO and PAUL T. INGLEFIELD, *Department of Chemistry, College of the Holy Cross, Worcester, Massachusetts* and R. A. RUTOWSKI, K.-L. LI, ALAN ANTHONY JONES, and AJOY K. ROY, *Department of Chemistry, Clark University, Worcester, Massachusetts*

Synopsis

Carbon-13 and proton spin-lattice relaxation times were measured at two field strengths on solutions 10% by weight of two polycarbonates in $C_2D_2Cl_4$ from -20 to $+120$°C. The first polycarbonate is an asymmetrically substituted form with one chlorine on one of the two phenylene aromatic rings of the bisphenol unit, whereas the second polycarbonate is symmetrically substituted with two chlorines on each of the two rings. The nuclear spin relaxation data are interpreted in terms of several local motions likely in these polymers. Segmental motion was described by the Hall–Helfand correlation function. Segmental motion in the monosubstituted polycarbonate is somewhat slower than in unsubstituted polycarbonate, whereas segmental motion in the tetrasubstituted polycarbonate is considerably slower. Phenylene ring rotation is observed in unsubstituted polycarbonate and in the monosubstituted polycarbonate above 40°C. Below 40°C in the monosubstituted species, and at all temperatures in the tetrasubstituted species, ring rotation is replaced by ring libration as the predominant motion contributing to spin lattice relaxation. In addition, the rotational motion of the two types of rings in the asymmetric monosubstituted form are very similar although not identical. The substituted ring is slightly less mobile than the unsubstituted, and both rings are substantially less mobile than the rings of unsubstituted polycarbonate. This indicates a strong coupling of ring motion, although the coupling leads to less than synchronous motion. Methyl group rotation is present in both polymers and is little affected by the various structural modifications.

INTRODUCTION

Both solution[1-7] and solid-state[8-13] spin relaxation studies on structurally related polycarbonates have shown the influence of modifications of the repeat unit on local chain dynamics. In the unsubstituted polycarbonate, BPA-PC, shown in Figure 1, several local motions occur on a rapid time scale in solution, including segmental rearrangements of the backbone, phenylene group rotation, and methyl group rotation.[5] In the glass, general segmental motion ceases, phenylene group rotation changes to π flips, and methyl group rotation continues as jumps between three symmetrically disposed minima.[8-15] The π flip process is linked in time scale to the low temperature dynamic mechanical loss peak.[11,13]

In the dimethyl ring-substituted polycarbonate,[6] TMBPA-PC, also shown in Figure 1, segmental motion is slowed in solution, and rapid phenylene group rotation essentially ceases. Phenylene group libration continues on a time

Journal of Polymer Science: Part B: Polymer Physics, Vol. 25, 1419–1430 (1987)

CCC 0098-1273/87/071419-12$04.00

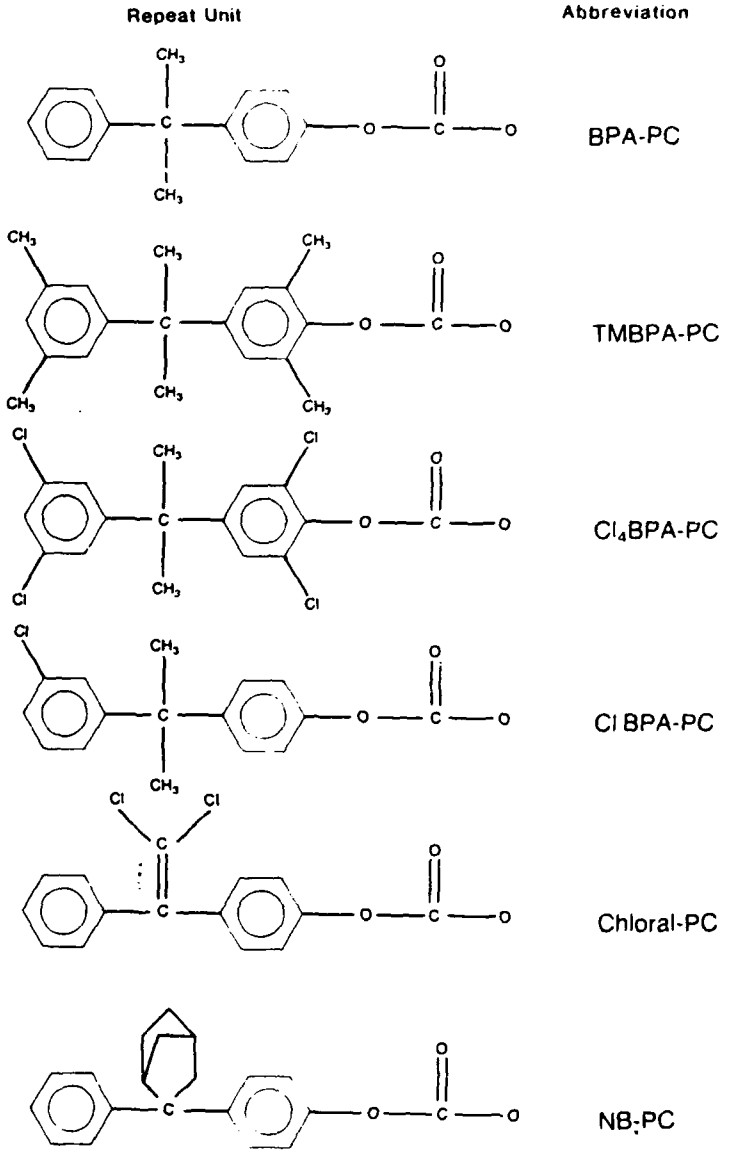

Fig. 1. Repeat unit structure for bisphenol-A polycarbonate (BPA-PC) and various analogues.

scale sufficiently fast to contribute to spin relaxation, but the motion of the phenylene group is significantly altered by this structural modification. Methyl group rotation is little influenced by the introduction of ring substituents, indicating the lack of coupling of this motion to other local processes.

In this report the dynamics of the two chloronated derivatives displayed in Figure 1 are considered. One of the polymers is a dichloro ring-substituted system, Cl_4BPA-PC, which is structurally similar to TMBPA-PC; thus a similarity in dynamics might be expected between these two closely related repeat units. The second chlorinated polycarbonate is a monochloro ring-substituted system with substitution on only one of the two rings in the bisphenol

unit. This is the first report of the local motion in an asymmetrically substituted polycarbonate.

Several important questions can be raised in the context of the asymmetrically substituted repeat unit. The primary question is the independence versus interdependence of the rotational motion of the two phenylene rings in a bisphenol unit. Since only one of the rings is substituted, the motion of that ring could be quite different from the unsubstituted ring. On the other hand if there is sufficient steric interaction across either the isopropylidine group or the carbonate group, the motion of the unsubstituted phenylene group could be coupled to the motion of the substituted phenylene group.

The dynamic mechanical spectrum of the asymmetrically substituted ClBPA-PC shows only one loss peak at 105° above the position of the loss peak in unsubstituted polycarbonate.[16] This result indicates coupling of the motion of the two phenylene groups, since from the most naive viewpoint the motion of the two structurally distinct phenylene groups could lead to two distinct loss peaks. However, the motion contributing to the mechanical loss could involve either the substituted or the unsubstituted ring alone. If cooperative character is present, then both rings could be contributing. High-resolution NMR is a structurally specific technique, and the motion of each ring can be individually monitored. Thus a clear determination of the relative intramolecular mobility of the two rings can be directly ascertained in this solution NMR study.

In Cl_4BPA-PC the two rings are expected to have equivalent mobility. The dynamic mechanical spectrum[16] shows the low-temperature loss peak associated with phenylene group rotation to be raised by almost 200° relative to BPA-PC. Thus a comparison between BPA-PC, ClBPA-PC, and Cl_4BPA-PC in solution might be expected to indicate a parallel reduction in phenylene group mobility unless the asymmetry of ClBPA-PC fundamentally alters local dynamics relative to the two other symmetric forms.

EXPERIMENTAL

High molecular weight samples of Cl_4BPA-PC and ClBPA-PC were supplied by General Electric. The structures of the repeat units are shown in Figure 1 along with the structures for BPA-PC and TMBPA-PC. Solutions of ClBPA-PC and Cl_4BPA-PC in $C_2D_2Cl_4$ (10 Wt. %) were degassed and sealed in NMR tubes.

The T_1 measurements were made using the standard 180°-τ-90° inversion recovery method and are reported with an experimental uncertainty of 10%. The 22.6 MHz carbon-13 and 90 MHz proton measurements were made on a Bruker SXP 20/100, and the 62.9 MHz carbon-13 and 250 MHz proton were made on a Bruker WM-250. For the Bruker SXP 20/100 the temperature was regulated to ± 1 K with a Bruker B-ST 100/700 that was calibrated against a thermocouple placed in a sample tube. In the case of the WM-250 calibration, the standard chemical shift technique was employed using ethylene glycol for high temperatures and methanol for low temperatures.

RESULTS

In general the decay of both proton and carbon-13 magnetizations followed a simple exponential dependence on delay time τ. The data were fitted with

TABLE I
Backbone Methyl Spin-lattice Relaxation Times of Cl_4BPA-PC and ClBPA-PC (in ms)

	^{1}H T_1 Cl_4BPA-PC		^{1}H T_1 ClBPA-PC		^{13}C T_1 Cl_4BPA-PC		^{13}C T_1 ClBPA-PC	
T (°C)	250 MHz	90 MHz	250 MHz	90 MHz	62.9 MHz	22.6 MHz	62.9 MHz	27.6 MHz
− 20	239	55	146	38	44	22	46.6	25.8
0	144	46	118	48	58	32	65.5	43.7
20	121	53	120	64	63	43	90	63
40	126	74	144	97	91	78	117	95
60	144	92	185	137	128	118	174	141
80	187	132	238	172.5	179	155	263	225
100	212	178	310	232.6	255	230	365	290
120	265	227	388	291.7	335	317	490	389.4

standard linear regression and nonlinear two-parameter and three-parameter fits. In some cases a slight upward curvature in the plots of $\ln(A_\infty - A_\tau)$ versus τ was noted, and in those cases only the initial portion of the decay curve was considered.

Spin-lattice relaxation times are presented in Tables I and II.

INTERPRETATION

The standard relations between T_1 and spectral densities J are employed. For carbon-13, the expressions are

$$\frac{1}{T_1} = W_0 + 2W_{1C} + W_2$$

$$W_0 = \sum_j \gamma_C^2 \gamma_H^2 \hbar^2 \frac{J_1(\omega_0)}{20 r_j^6}$$

$$W_{1C} = \sum_j 3\gamma_C^2 \gamma_H^2 \hbar^2 \frac{J_1(\omega_C)}{40 r_j^6}$$

$$W_2 = \sum_j 3\gamma_C^2 \gamma_H^2 \hbar^2 \frac{J_2(\omega_2)}{10 r_j^6}$$

$$\omega_0 = \omega_H - \omega_C, \qquad \omega_2 = \omega_H + \omega_C \tag{1a}$$

and for protons it is

$$\frac{1}{T_1} = \sum_j \frac{9}{8} \gamma^4 \hbar^2 r_j^{-6} \left[\frac{2}{15} J_1(\omega_H) + \frac{8}{15} J_2(2\omega_H) \right] \tag{1b}$$

The internuclear distances are similar to the standard distances used in earlier studies, i.e., 1.08 Å for the phenyl C—H distance, 1.12 Å for the methyl

TABLE II
Phenylene Ring Carbon-13 Spin-lattice Relaxation Times of Cl_4BPA-PC and ClBPA-PC (in ms; protonated carbons only)

	Cl_4BPA-PC		ClBPA-PC Unsubst. ring		ClBPA-PC Cl subst. ring	
T (°C)	62.9 MHz	22.6 MHz	62.9 MHz	22.6 MHz	62.9 MHz	22.6 MHz
− 20	193	50	140.4	61.7	143	55
0	159	55	160	94.8	159	68
20	140	66	235	146	205	109
40	147	82	276	215	240	173
60	166	122	418	359	358	302
80	210	147	594	538	503	459
100	277	183	920	817	721	580
120	325	291	1196	936	994	838

C—H distance, and 1.77 Å for the backbone methyl proton–proton distance.

Expressions for the spectral density can be derived from the action of particular local motions on intramolecular internuclear interactions. The local motions to be expected are segmental rearrangements of backbone bonds and anisotropic rotation of methyl and phenylene groups. The segmental motion description of Hall and Helfand[17] will be employed, and for this segmental description the time scale is set by two parameters; τ_0, the correlation time for single conformational transitions, and τ_1, the correlation time for cooperative or correlated transitions. This model for segmental motion[5] is then combined with anisotropic internal rotation to give the following composite spectral density function:

$$J(\omega) = AJ_a(\tau_0, \tau_1, \omega) + BJ_b(\tau_{b0}, \tau_1, \omega) + CJ_c(\tau_{c0}, \tau_1, \omega) \qquad (2)$$

where

$$A = \tfrac{1}{4}(3\cos^2\Delta - 1)^2, \qquad B = \tfrac{3}{4}(\sin^2 2\Delta), \quad \text{and} \quad C = \tfrac{3}{4}(\sin^4\Delta)$$

For stochastic diffusion:

$$\tau_{b0}^{-1} = \tau_0^{-1} + \tau_{ir}^{-1}$$

$$\tau_{c0}^{-1} = \tau_0^{-1} + \left(\tfrac{1}{4}\tau_{ir}\right)^{-1}$$

For a twofold jump:

$$\tau_{b0}^{-1} = \tau_0^{-1} + \tau_{ir}^{-1}$$

$$\tau_{c0}^{-1} = \tau_0^{-1}$$

For a threefold jump:

$$\tau_{b0}^{-1} = \tau_{c0}^{-1} = \tau_0^{-1} + \tau_{ir}^{-1}$$

The angle Δ is between the internuclear vector and the axis of rotation.

The form of J_a, J_b, and J_c is the same as J given below with τ_0 replaced by τ_0, τ_{b0}, and τ_{c0}, respectively.

$$J(\omega) = 2\left\{\left[\left(\tau_0^{-1}\right)\left(\tau_0^{-1} + 2\tau_1^{-1}\right) - \omega^2\right]^2 + \left[2\left(\tau_0^{-1} + \tau_1^{-1}\right)\omega\right]^2\right\}^{-1/4} \times \cos\left\{\frac{1}{2}\arctan\left[\frac{2\left(\tau_0^{-1} + \tau_1^{-1}\right)\omega}{\tau_0^{-1}\left(\tau_0^{-1} + 2\tau_1^{-1}\right) - \omega^2}\right]\right\}$$

The segmental motion description can also be combined with anisotropic restricted rotational diffusion in place of complete anisotropic rotation.[3,18] For this case, we have:

$$J_i(\omega_i) = AJ_i^{01}(\omega_i) + \frac{B}{l^2}\left\{\left[(1 - \cos l)^2 + \sin^2 l\right] J_i^{01}(\omega_i) + \frac{1}{2}\sum_{n=1}^{\infty}\left[\left(\frac{1 - \cos(l - n\pi)}{1 - n\pi/l} + \frac{1 - \cos(l + n\pi)}{1 + n\pi/l}\right)^2 + \left(\frac{\sin(l - n\pi)}{1 - n\pi/l} + \frac{\sin(l + n\pi)}{1 + n\pi/l}\right)^2\right] J_i^{\lambda n}(\omega_i)\right\}$$

$$+ \frac{C}{2l^2}\left\{\frac{1}{2}\left[(1 - \cos 2l)^2 + \sin^2 2l\right] J_i^{01}(\omega_i) + \sum_{n=1}^{\infty}\left[\left(\frac{1 - \cos(2l - n\pi)}{2 - n\pi/l} + \frac{1 - \cos(2l + n\pi)}{2 + n\pi/l}\right)^2 + \left(\frac{\sin(2l - n\pi)}{2 - n\pi/l} + \frac{\sin(2l + n\pi)}{2 + n\pi/l}\right)^2\right] J_i^{\lambda n}(\omega_i)\right\}$$

where

$$J_i^{01}(\omega_i) = \left\{\left[\tau_0^{-1}\left(\tau_{01}^{-1} + \tau_1^{-1}\right) - \omega_i^2\right]^2 + \left(2\tau_{01}^{-1}\omega_i\right)^2\right\}^{-1/4} \times \cos\left\{\frac{1}{2}\arctan\frac{2\tau_{01}^{-1}\omega_i}{\tau_0^{-1}\left(\tau_{01}^{-1} + \tau_1^{-1}\right) - \omega_i^2}\right\}$$

$$J_i^{\lambda n}(\omega_i) = \left\{\left[\tau_0^{-1}\left(\tau_{01}^{-1} + \lambda_n\right)\left(\tau_{01}^{-1} + \tau_1^{-1} + \lambda_n\right) - \omega_i^2\right]^2\right\}^{-1/4} \times \cos\left\{\frac{1}{2}\arctan\frac{2\left(\tau_{01}^{-1} + \lambda_n\right)\omega_i}{\left(\tau_0^{-1} + \lambda_n\right)\left(\tau_{01}^{-1} + \lambda_n\right) - \omega_i^2}\right\}$$

where

$$\tau_{01}^{-1} = \tau_0^{-1} + \tau_1^{-1} \quad \text{and} \quad \lambda_n = \left(\frac{n\pi}{l}\right)^2 D_{ir}.$$

The new parameters for restricted anisotropic rotational diffusion are the angular amplitude l over which rotational diffusion occurs and the rotational diffusion constant D_{ir}.

The starting point for the interpretation for either Cl_4BPA-PC or ClBPA-PC is the phenylene carbon data. In some earlier interpretations,[2-4] phenylene proton data were the starting point since these are influenced only by segmental motion. In the polymers reported here and in other substituted polycarbonates,[5-6] the phenylene proton data are complex and cannot be easily interpreted. Hence our use of phenylene carbon data, which are influenced by both segmental motion and phenylene group rotation. To compensate for the lack of simple phenylene proton data, extensive field dependent data were taken to provide a sufficiently large data base.[5-6] In the study of a closely related structure (TMBPA-PC), a combination of phenylene carbon and ring methyl (both proton and carbon) data at two field strengths were used to develop a description of segmental motion and phenylene group rotation. The segmental motion description in that study employed the Hall–Helfand[17] correlation function and was verified by the use of the same segmental motion parameters in the description of the backbone methyl proton and carbon relaxation data. This same verification procedure is used in the systems of interest here.

In addition to following an established interpretational approach, both the carbon and proton relaxation data in Cl_4BPA-PC are almost the same as is observed in TMBPA-PC. Since the substitution pattern of the phenylene groups is so similar, we felt confident by beginning the interpretation with the TMBPA-PC motional description and then making minor adjustments. The phenylene carbon data at two field strengths are the starting point that quickly led to values of τ_0, τ_1, D_{ir}, and l. Here the Gronski[18] picture for restricted anisotropic rotation in combination with the Hall–Helfand[17] description for motion nicely accounted for the phenylene carbon relaxation data. The same approach was used on the backbone methyl proton and carbon data to yield the time scale for methyl group rotation, τ_{irm}, plus a check on the segmental motion parameters τ_0 and τ_1. The methyl group rotation was found to be complete anisotropic rotation by jumps between minima separated by 120°.

The ClBPA-PC data were an intermediate case between Cl_4BPA-PC and BPA-PC. Again we started with phenylene carbon data, but this was a truly different situation with no exact parallel in our previous experience. Since the relaxation data did fall between two familiar systems, likely estimates for segmental motion and phenylene rotation could be made and adjusted to reproduce the phenylene carbon relaxation data at two field strengths. Since the repeat unit is asymmetric in this polymer, different phenylene rotation parameters were used for the two types of phenylene groups. The same segmental description was applied to both phenylene groups since this motion is assumed to involve several virtual backbone bonds. The segmental description was checked by the methyl proton and carbon relaxation data as before; this data also provided the basis for determining the time constant τ_{irm} for methyl group rotation.

In the description of ring motion in ClBPA-PC, the Woessner[19] description for complete anisotropic rotation by stochastic diffusion is successful at higher

TABLE III
Simulation Parameters for Segmental Motion, Phenylene Rotation, and Methyl Motion in Cl_4BPA-PC and ClBPA-PC

	Cl_4PBA-PC					ClBPA-PC								
									Unsubstituted ring			Cl substituted ring		
T (°C)	τ_1 (ns)	τ_0 (ns)	τ_{irm} (ns)	l (deg.)	D_{ir} ($s^{-1} \times 10^8$)	τ_1 (ns)	τ_0 (ns)	τ_{irm} (ns)	τ_{irp} (ns)	l (deg.)	D_{ir} ($s^{-1} \times 10^8$)	τ_{irp} (ns)	l (deg.)	D_{ir} ($s^{-1} \times 10^8$)
− 20	5.80	295	2.01	73.0	10.0	2.86	94	1.21	—	100	10.0	—	70	7.0
0	3.80	111	0.80	77.0	13.0	1.35	41.8	0.56	—	120	17.0	—	85	13.0
20	1.39	22.0	0.43	80.5	14.2	0.70	20.8	0.35	—	145	26.0	—	100	19.0
40	0.94	13.9	0.23	83.5	15.2	0.42	11.5	0.212	0.52	—	—	0.75	—	—
60	0.44	5.20	0.182	86.5	16.4	0.24	6.3	0.14	0.31	—	—	0.42	—	—
80	0.27	3.40	0.120	88.5	17.2	0.175	3.1	0.082	0.195	—	—	0.26	—	—
100	0.17	1.80	0.094	90.5	18.0	0.12	2.67	0.055	0.115	—	—	0.195	—	—
120	0.14	1.00	0.062	92.5	19.2	0.084	2.04	0.038	0.103	—	—	0.130	—	—
E_a (kJ/m)	23	33	20	—	—	20	23	20	22	—	—	22	—	—
τ_∞ ($s \times 10^{14}$)	20	3	15	—	—	10	130	8.7	12	—	—	10	—	—

temperatures (> 40°C) but is not appropriate for either ring below 20°C. The Gronski[18] formulation is successful over the temperature range 20° to −20°C, and the unsubstituted ring experiences slightly greater librational freedom relative to the chlorinated ring.

The simulation parameters for Cl_4BPA-PC and ClBPA-PC are contained in Table III, and all observed T_1's were matched within the experimental uncertainty of 10% by the simulations just discussed. These simulations, especially ClBPA-PC, would have been quite difficult were it not for our experience with closely related polycarbonates and may have required a more extensive data base if the related systems had not already been completed.

DISCUSSION

Since dilute solution studies have been performed on a number of structurally related polycarbonates, comparisons between the descriptions of local dynamics can be made. Such a comparison is made for segmental motion in Table IV, where it can be noted that as the apparent activation energy for τ_0 increases, T_g increases. However the trend is not followed for ClBPA-PC relative to BPA-PC probably because intermolecular contributions to T_g are reduced in the asymmetric ClBPA-PC, since it most likely packs less efficiently relative to the symmetric species. However, T_g and E_a for τ_0 of Cl_4BPA-PC is much higher than either BPA-PC or ClBPA-PC, which is typical of the phenomenological link noted before.[6]

Dynamic mechanical studies[16] suggest that the degree of substitution rather than the type of substituent is important to the dynamics. That conclusion is reinforced by the solution data that show TMBPA-PC to be very similar to Cl_4BPA-PC. The shifts in E_a or τ_0 generally track the shifts in T_g, with both rising on increased substitution. The changeover in phenylene ring mobility from anisotropic free rotation in BPA-PC to restricted libration in the tetrasubstituted species with the asymmetric ClBPA-PC exhibiting a combination of these motions depending on temperature range is paralleled by the

TABLE IV
Segmental Motion in Polycarbonates

Polymer	T_g[a] (C°)	Apparent activation energy (kJ/mole)		Arrhenius prefactor ($\tau_\infty \times 10^{14}$ s)		Ref.
		Cooperative segmental (τ_1)	Single backbone rotation (τ_0)	Cooperative segmental (τ_1)	Single backbone rotation (τ_0)	
BPA-PC	150	19	16	28	1003	4
Chloral-PC	164	17	18	94	409	4
ClBPA-PC	146	23	20	10	130	Current work
TMBPA-PC	203	23	34	11	3	6
Cl_4BPA-PC	225	23	34	20	3	Current work
NB-PC	232	24	30	6	17	5

[a] From Ref. 16.

TABLE V
Phenylene Group Motion in Polycarbonates

Polymer	T_γ[a] (C°)	Form of solution motion	E_a (kJ/mole)	$\tau_\infty \times 10^{14}$ s	Ref.
BPA-PC	−100	Stochastic diffusion	22	6	4
Chloral-PC	−100	Stochastic diffusion	18	40	4
ClBPA-PC	+5	Stochastic diffusion for $T > 40$°C	22	~ 14	Current work
		Restricted rotation for $T < 40$°C	—	—	—
TMBPA-PC	+50	Restricted rotation	—	—	6
Cl_4BPA-PC	+49	Restricted rotation	—	—	Current work
NB-PC	−108	Restricted rotation	—	—	5

[a]The temperature of the main subglass transition loss peak measured at 1 Hz (Ref. 16).

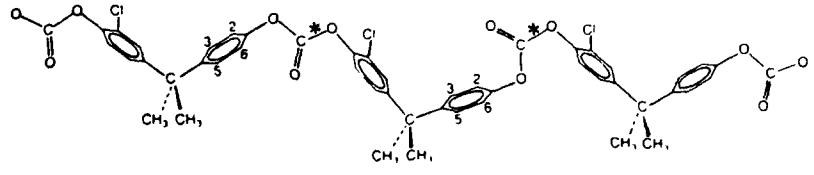

TRANS-TRANS TRANS-TRANS TRANS-CIS TRANS-TRANS

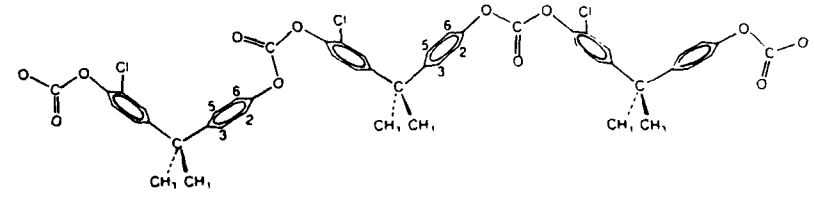

TRANS-TRANS TRANS-CIS TRANS-TRANS TRANS-TRANS

Fig. 2. Proposed motion responsible for low-temperature loss in ClBPA-PC. (a) *Trans-cis* to *trans-trans* conformational interchanges with corresponding ring flips occurring on the unsubstituted phenylenes. (b) *Trans-cis* to *trans-trans* conformational interchanges with corresponding ring flips occurring on the Cl substituted phenylenes. In all cases the asterisk indicates the isomerizing carbonate bond.

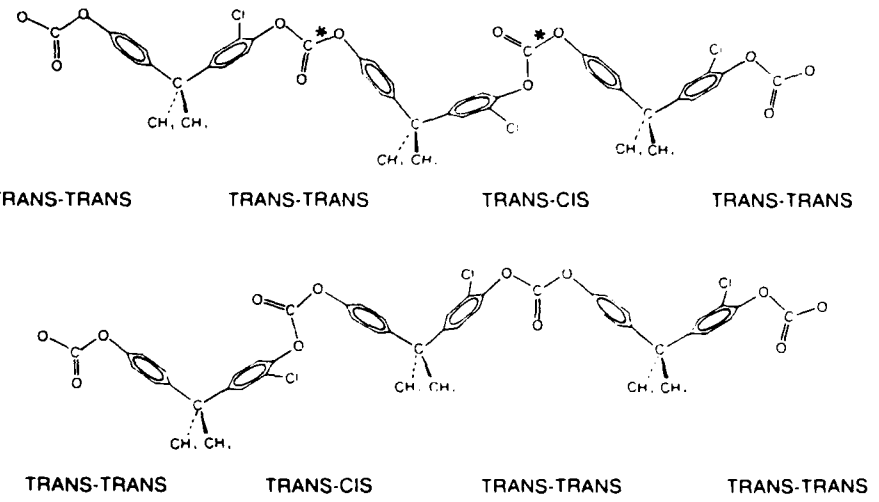

Fig. 2. (*Continued from the previous page.*)

overall trends in the temperature of the subglass transition loss peak T_γ, as shown in Table V.

In ClBPA-PC, the raw T_1 data and the analysis in terms of correlation times or rotational diffusion constants show the two phenylene rings to have comparable mobility, although the unsubstituted phenylene ring exhibits somewhat greater librational amplitude.

The nature of this apparent cooperativity between the phenylene rings remains as a point for discussion. Phenylene ring rotation could be linked by intramolecular steric interactions across the isopropylidene unit, across the carbonate unit, or both. Bendler[20] has performed quantum mechanical calculations on diphenyl propane that indicate that rotating one phenylene ring causes partial but incomplete rotation of the other ring. This is less than synchronous motion, and this level of cooperativity is roughly indicated by the solution NMR data. Both the T_1 data and the motional analysis show motion of the rings to be similar but certainly not identical.

The similarity in motion could also be reinforced by a coupling across the carbonate unit in addition to the isopropylidene unit. In a recent proposal[21] for the motion causing the low-temperature loss peak in BPA-PC, bond rotation within the carbonate unit was combined with ring rotation. The proposal consists of an interchange of *trans-cis* and *trans-trans* conformations with associated phenylene ring flips. Figure 2 displays the dynamic process as applied to the asymmetric ClBPA-PC, and two subsets of the motion are conceivable in this asymmetric system with the isomerizing carbonate bond either adjacent to a chlorinated ring with a corresponding unsubstituted ring flip (Fig. 2a) or with the isomerizing bond adjacent to an unsubstituted ring with a corresponding chlorinated ring flip (Fig. 2b). In these figures and discussions, regioregularity of the asymmetric polycarbonate chain is assumed. In either subset the chlorine substituent would reduce mobility either by proximity to the isomerizing carbonate bond or by proximity to the flipping C_1C_4 axis. Thus it would appear that neither subset of

carbonate motions is unimpeded; and when this effect is combined with coupling across the isopropylidene unit, it is not surprising that a single shifted loss peak is observed in the solid rather than two peaks, one shifted the other unshifted.

In ClBPA-PC a similar coupling of segmental motion and phenylene rotation is generally reflected in the correlation times of Table III. At temperatures above 20°C where ring motion is primarily characterized by ring rotation, the correlation time for rotation of either ring is rather similar to the time scale of cooperative segmental motion. This general tracking of phenylene group motion and segmental motion has been noted before in dissolved polycarbonates and is consistent with the arguments presented in the solid for a single loss-peak involving motion of more than individual phenylene rings.

This research was carried out with the financial support of the National Science Foundation Grant DMR-790677, of National Science Foundation equipment Grant No. CHE 77-09059, of National Science Foundation Grant No. DMR-8108679, and of U.S. Army Research Office Grants DAAG 29-82-G-0001 and DAAG 29 85-K0126. We thank the Worcester Consortium NMR Facility for use of the SXP90 and WM250 spectrometers and Mr. Frank Shea for his assistance.

References

1. A. A. Jones and M. Bisceglia, *Macromolecules*, **12**, 1136 (1979).
2. J. F. O'Gara, S. G. Desjardins, and A. A. Jones, *Macromolecules*, **14**, 64 (1981).
3. M. F. Tarpey, Y.-Y. Lin, A. A. Jones, and P. T. Inglefield, in *NMR and Macromolecules*, J. C. Randall, Ed., American Chemical Society, Washington, D.C., 1984, ACS Symp. Ser. vol. 247, p. 67.
4. J. J. Connolly, E. Gordon, and A. A. Jones, *Macromolecules*, **17**, 722 (1984).
5. J. J. Connolly and A. A. Jones, *Macromolecules*, **18**, 910 (1985).
6. A. K. Roy and A. A. Jones, *J. Polym. Sci. Polym. Phys. Ed.*, **23**, 1793 (1985).
7. C. C. Hung, J. H. Shibata, M. F. Tarpey, A. A. Jones, J. A. Porco, and P. T. Inglefield, *Analitica Chimica Acta*, submitted.
8. J. Schaefer, E. O. Stejskal, and R. Buchdahl, *Macromolecules*, **10**, 384 (1977).
9. T. R. Steger, J. Schaefer, E. O. Stejskal, and R. A. McKay, *Macromolecules*, **13**, 1127 (1980).
10. J. Schaefer, E. O. Stejskal, R. A. McKay, and W. T. Dixion, *Macromolecules*, **17**, 1479 (1984).
11. A. A. Jones, J. F. O'Gara, P. T. Inglefield, J. T. Bendler, A. F. Yee, and K. L. Ngai, *Macromolecules*, **16**, 658 (1983).
12. P. T. Inglefield, R. M. Amici, J. F. O'Gara, C.-C. Hung, and A. A. Jones, *Macromolecules*, **16**, 1552 (1983).
13. J. F. O'Gara, A. A. Jones, C.-C. Hung, and P. T. Inglefield, *Macromolecules*, **18**, 1117 (1985).
14. H. W. Spiess, *Colloid. Polym. Sci.*, **261**, 193 (1983).
15. H. W. Spiess, in *Advances in Polymer Science*, H. H. Rausch and H. G. Zachmann, Eds., Springer-Verlag, Berlin, 1985, Vol. 66.
16. A. F. Yee and S. A. Smith, *Macromolecules*, **14**, 54 (1981).
17. C. K. Hall and E. Helfand, *J. Chem. Phys.*, **77**, 3275 (1982).
18. W. Gronski and N. Murayama, *Makromol. Chem.*, **179**, 1521 (1978).
19. D. E. Woessner, *J. Chem. Phys.*, **36**, 1 (1962).
20. J. T. Bendler, *Ann. N.Y. Acad. Sci.*, **371**, 229 (1981).
21. A. A. Jones, *Macromolecules*, **18**, 902 (1985).

Received June 13, 1986

Proton and carbon-13 relaxation and molecular motion in glassy bisphenol-A polycarbonate

John J. Connolly,[a] Paul T. Inglefield, and Alan Anthony Jones[b]
Jeppson Laboratory, Department of Chemistry, Clark University, Worcester, Massachusetts 01610

(Received 10 July 1986; accepted 6 March 1987)

An interpretation of proton and carbon-13 spin–lattice relaxation in glassy polycarbonate is developed which is consistent with the geometry, time scale, and amplitude determined from chemical shift anisotropy line shape collapse. The line shape data indicate π flips and libration about the same axis as the predominant motions. A correlation function incorporating these motions is developed to quantitatively interpret the proton spin–lattice relaxation data and the line shape collapse. The π flip process is described as an inhomogeneous distribution of correlation times using the Williams–Watts fractional exponential. An apparent activation energy of 46 kJ/mol is determined with the fractional exponent remaining constant at 0.15. The librational motion is described by the Gronski formalism where the amplitude increases with the square root of temperature; and the rotational diffusion constant, linearly with temperature. Rotational diffusion constants fall in the range of 10^8 to 10^9 s^{-1} which is comparable to those observed in solution in sterically hindered polycarbonates. The librational motion only contributes to spin–lattice relaxation at the higher temperatures so that only an order of magnitude estimate of the restricted rotational diffusion constant results. This correlation function is then applied to carbon-13 T_1 data taken at various positions across the chemical shift anisotropy line shape on an isotopically enriched system. Little change in spin–lattice relaxation with position is observed which is consistent with the broad distribution of π flip correlation times. The rate of carbon-13 spin–lattice relaxation is also fairly well predicted. Comparisons are made with magic angle sample spinning spin–lattice relaxation both in the laboratory and rotating frame. The former is fairly well approximated by the correlation function while the latter requires a significant spin–spin contribution to be reconciled with the rest of the interpretation.

INTRODUCTION

The geometry of phenylene ring motion in the glassy polycarbonate of bisphenol-A has been characterized by several solid state NMR line shape experiments.[1-7] Two motional processes are identified: π flips and librations, both occuring about the C_1C_4 axis. A detailed analysis of the carbon-13 chemical shift anisotropy (CSA) line shape was based on the presence of approximate π flips which occured over the librational range around each minimum.[7] The librational range increases with the square root of temperature in this interpretation from about 20° at -100 °C to about 60° at $+100$ °C.

In addition to the geometric information, the rate of π flips can be characterized from line shape collapse. However, motional processes in polymeric glasses are often complex, requiring data at a number of frequencies before a detailed interpretation can be attempted. In this report, a correlation function is developed which is consistent with both line shape and spin–lattice relaxation data. Geometric information from the carbon-13 CSA line shape data is combined with phenylene group proton relaxation data to develop this overall interpretation.

The proton relaxation data is taken from an earlier study[4] on the partially deuterated form of the polycarbonate, BPA-d_6-PC, shown in Fig. 1 along with other structures and abbreviations of the polymers mentioned in this paper. Proton T_1 data at 90 MHz on BPA-d_6-PC containing only phenylene protons is available, in addition to $T_{1\rho}$ data at 43.5 kHz. Magic angle spinning carbon-13 $T_{1\rho}$ data at 28 kHz on the fully protonated form is also available from the literature.[8] New carbon-13 T_1 data at 62.9 MHz on the carbon-13 enriched form, BPA-^{13}C-PC, are reported here. The T_1 measurements on the enriched form are taken at several positions across the CSA tensor line shape to rest the orientation dependence of the relaxation. Since the primary motions present in polycarbonate are anisotropic, carbon-13 relaxation might be expected to depend on the orientation of the motional axis with respect to the applied field.[9-13]

Earlier line shape and carbon-13 $T_{1\rho}$ data on polycarbonate indicated inhomogeneous relaxation mathematically corresponding to a distribution of correlation times for different spatial positions in the sample.[5,7,14] In view of this observation and the just-noted orientation dependence of carbon-13 relaxation, it is fair to ask whether the inhomogeneous character of the carbon-13 $T_{1\rho}$ data arises in part from the orientation dependence of anisotropic motion. In polymeric systems, other sources of inhomogeneity are also likely. Notably, a distribution of local interactions, such as the fluctuation of density at different spatial positions in the glass could also lead to different relaxation times independent of orientational effects. This aspect of the dynamics will be incorporated into the description of the π flip process through the use of a fractional or stretched exponential correlation function. Correlation functions of this form have been developed from physical pictures which may be appro-

[a] Present address: Ashland Chemical Co., P.O. Box 2219, Columbus, OH 43216.
[b] To whom correspondence should be addressed.

 0021-9606/87/126602-14$02.10

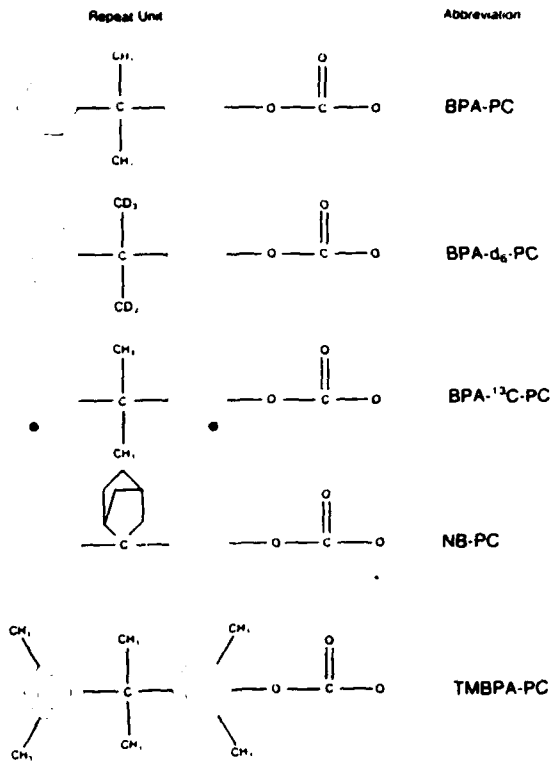

FIG. 1. Structures of the polycarbonate repeat units.

priate for polymeric glasses.[15,16] The inhomogeneous rate description for π flips will be combined with the proper geometric description for this anisotropic motion[9-13,17] so both sources of distribution effects can be considered. An earlier interpretation of proton relaxation did not consider the anisotropic character of the motion, but used an isotropic approximation.[4] To continue the improvement of the correlation function, the librational motion will be added to the π flip process using Gronski's description based on restricted diffusion.[18,19] In the earlier interpretation of proton T_1 and $T_{1\rho}$ data the librational motion was not considered. The amplitude of the restricted diffusion is determined from line shape data, but the rate will be determined from the proton spin–lattice relaxation data, and checked against the carbon-13 data.

Other aspects of the carbon-13 T_1 and $T_{1\rho}$ data will be considered as well. The T_1 measurements made on the carbon-13 CSA line shape of the enriched sample might be influenced by spin diffusion amongst the labeled spins. In this case the average relaxation rate would remain the same, but some of the inhomogeneous character would be lost. The $T_{1\rho}$ measurements made on a natural abundance sample under MASS conditions could be influenced by spin diffusion between the carbon-13 and proton dipolar reservoirs.[20,21] In this case, not only would some of the inhomogeneity be lost but an increase of relaxation rate would result from the new relaxation pathway.[6,8,14,20,22,23]

EXPERIMENTAL

From proton T_1 and $T_{1\rho}$ measurements a bisphenol-A polycarbonate sample with deuterated methyl groups was prepared to minimize cross relaxation between phenylene and methyl protons.[4] In an earlier report the phenylene proton T_1's were measured at 90 MHz, while proton $T_{1\rho}$'s were determined at an effective field at 43.5 kHz from a temperature of -120 to $+120$ °C. A polycarbonate sample with single site carbon-13 enrichment on one of the two phenylene rings ortho to the carbonate group was used in the chemical shielding anisotropy line shape relaxation experiment with data taken at 40 °C. Details on synthesis of the methyl-deuterated and carbon-13 enriched polycarbonates, and on proton T_1 and $T_{1\rho}$ measurements are previously given.[4]

The phenylene carbon-13 relaxation data was measured on a Bruker WM250 employing a Doty solids accessory with cross polarization at proton and carbon-13 Larmor frequencies of 250 and 62.9 MHz, respectively, at various frequencies across the chemical shielding anisotropy line shape using a nonselective π–τ–$\pi/2$ pulse sequence. Typical resulting decay curves are illustrated in Figs. 2 and 3. A radio frequency field of 1.0 mT was employed. Spin–lattice relaxation, T_1, was also observed at 62.9 MHz on a natural abundance sample under conditions of MASS spinning using the Torchia T_1 sequence,[10] and the associated data is in Fig. 4. Both the proton and carbon-13 T_1 measurements discussed here were performed on degassed, sealed samples. Comparisons are made with carbon-13 $T_{1\rho}$ data from the literature measured under magic angle spinning conditions at proton and carbon-13 Larmor frequencies of 60 and 15 MHz, and a carbon-13 radio frequency field of 28 kHz.[8]

RELAXATION EQUATIONS

The proton data has been interpreted before utilizing equations for isotropic motion.[4] The spectral density was

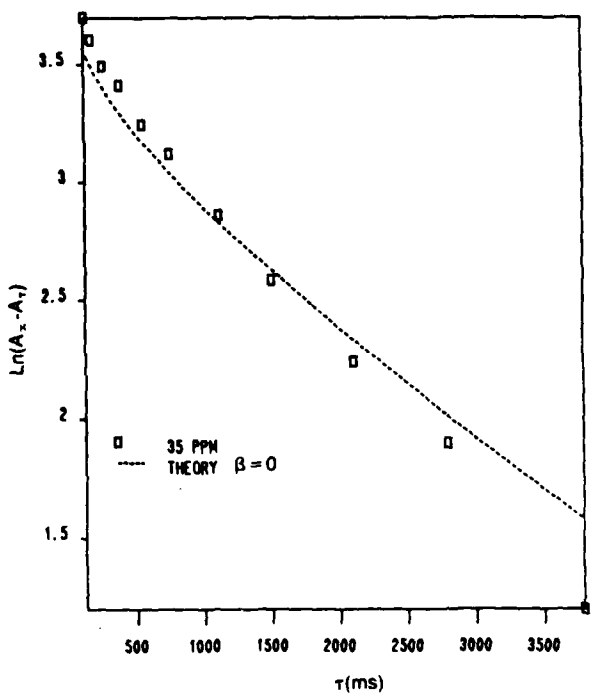

FIG. 2. The logarithm of the amplitude at delay time τ minus the amplitude at infinite τ vs delay time for carbon-13 relaxation taken at the orientation $\beta = 0$. The dashed curve is the prediction based on the correlation function.

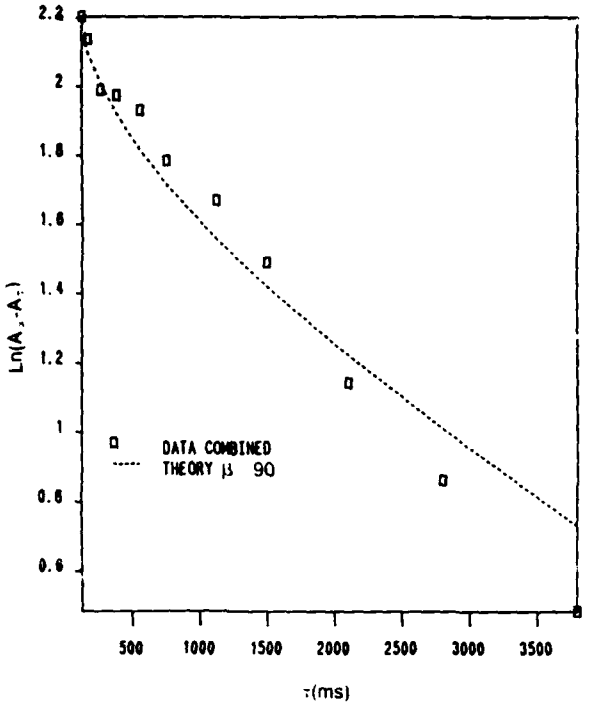

FIG. 3. The logarithm of the amplitude at delay time τ minus the amplitude at infinite τ vs delay time for carbon-13 relaxation taken at the orientation $\beta = 90$. Data at 10 and 164 ppm at which orientations $\beta = 90$ were combined. The dashed curve is the prediction based on the correlation function.

characterized in terms of a Kohlrausch or Williams–Watts[24] fractional exponential correlation function which yielded the apparent activation energy of 48 kJ/mol and an Arrhenius prefactor of 1.0×10^{-16} s. The fractional exponent α controlling the breadth of the distribution of correlation times was found to be 0.18. In the interpretation to be pursued here the knowledge of the geometry of the motion will be incorporated. A specific geometric description can be applied for both libration and flips allowing for a distinct estimate for the time scales of each motion.

Carbon-13 spin–lattice relaxation is primarily determined by intramolecular dipolar coupling to the adjacent proton. The strong r^{-6} dependence of dipolar relaxation on internuclear distance precludes large contributions to this quantity from other protons of the sample.[25]

In quite the opposite fashion protons on adjacent polycarbonate chains are primarily responsible for proton relaxation as depicted in Fig. 5. For the 2,3 phenylene protons, the axis of rotation is parallel to the intramolecular internuclear vector and relaxation for such protons will arise from dipolar interactions with protons on other chains. Further, an exact 180° flip interchanges the sites of the four protons on a phenylene ring, leaving the intramolecular dipole–dipole Hamiltonian invariant.[26]

To incorporate these ideas we begin by writing the intermolecular dipolar Hamiltonian:

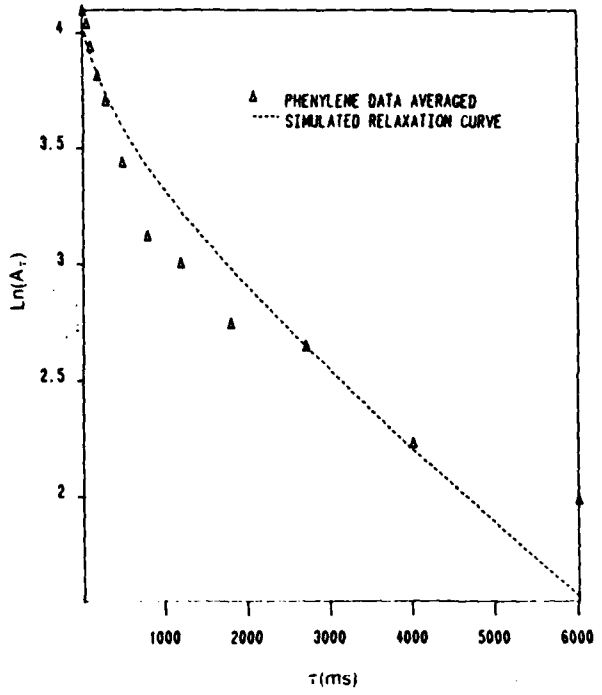

FIG. 4. The logarithm of the amplitude at delay time τ vs τ for the protonated phenylene carbons of unlabeled BPA-PC taken under MASS conditions. The dashed curve is the prediction based on the correlation function.

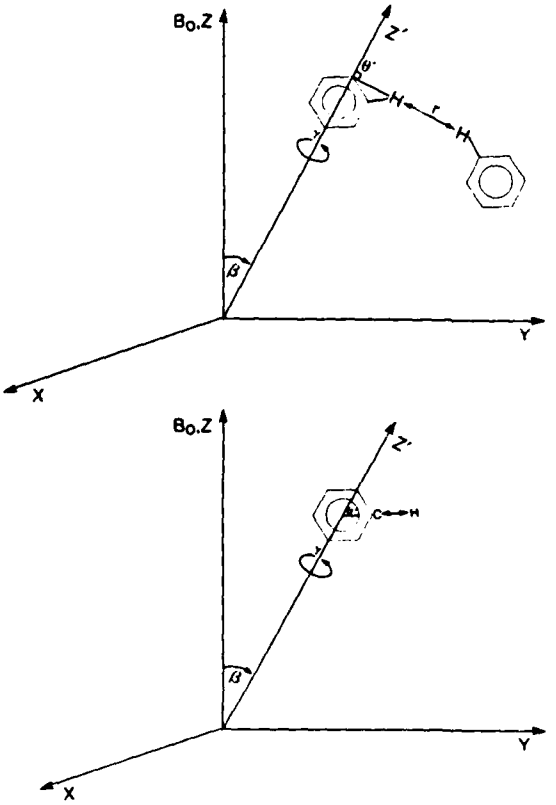

FIG. 5. Coordinate systems for BPA-d_6-PC and BPA-^{13}C-PC correlation function calculations.

$$H_d^{IS} = -(24\pi/5)^{1/2}\hbar\gamma_I\gamma_S r(t)^{-3}\sum_m^{+2}{}_2 Y^*_{2m}(t)T_{2m}\,. \tag{1}$$

This is the appropriate Hamiltonian for proton relaxation since both internuclear distance and orientation are allowed to be time dependent. The corresponding Hamiltonian for the carbon-13 dipolar interactions has only a time-dependent orientation factor:

$$H_d^{IS} = -(24\pi/5)^{1/2}\hbar\gamma_I\gamma_S r^{-3}\sum_{m=-2}^{+2} Y^*_{2m}(t)T_{2m}\,. \tag{2}$$

The Y_{2m} are normalized spherical harmonics, and the T_{2m} are tensor operators following the formalism given by Mehring.[27] The starting point for relaxation rate calculations is the equation of motion of the density matrix[28]:

$$\frac{d\rho}{dt} = -\int_0^\infty \langle[H_d(t),[H_d(t-\tau),\rho]]\rangle d\tau\,. \tag{3}$$

The result of the proton (I) T_1 and $T_{1\rho}$ calculation is[26–33]

$$1/T_1 = 6\pi/5\,\gamma_I^4\hbar^2\{J_1(\omega_I) + 4J_2(2\omega_I)\}\,, \tag{4}$$

$$1/T_{1\rho} = 6\pi/5\,\gamma_I^4\hbar^2\{1.5\,J_0(\omega_e) + 2.5\,J_1(\omega_I) + J_2(2\omega_I)\}\,. \tag{5}$$

For carbon-13 (S) the expressions are[27,30,34]

$$1/T_1 = 2\pi/5\,\gamma_I^2\gamma_S^2\hbar^2\{J_0(\omega_S-\omega_I) + 3J_1(\omega_S) + 6J_2(\omega_S+\omega_I)\}\,, \tag{6}$$

$$1/T_{1\rho} = \pi/5\,\gamma_I^2\gamma_S^2\hbar^2\{4J_0(\omega_e) + 6J_1(\omega_I) + J_0(\omega_S-\omega_I) + 3J_1(\omega_S) + 6J_2(\omega_S+\omega_I)\}\,. \tag{7}$$

The spectral density is defined as

$$J_m(\omega) \equiv (-1)^m\int_0^\infty \langle r(t)^{-3}r(t-\tau)^{-3}\rangle \times\langle Y_{2m}(t)Y_{2,-m}(t-\tau)\rangle\exp(i\omega\tau)d\tau\,. \tag{8}$$

For proton and carbon-13 calculations it is convenient to write the spherical harmonics with coordinates referred to the molecular rotation axis. For proton relaxation, interchain interactions will have a proton dipole–dipole interaction vector inclined at an angle θ' to the 1,4-phenylene axis as shown in Fig. 5. For carbon-13, molecular geometry indicates a 60° tilt between the dipole–dipole vector and the twofold axis of the phenylene group. In this formalism the azimuthal angle ϕ' is time independent. We also wish to express the spherical harmonics with the azimuthal and polar angles taken with respect to this symmetry axis.[9,17] Treating the combined effect of flips and librations as a double internal rotation we write

$$Y_{2m}(t) = \sum_n^{+2}{}_2\sum_k^{+2}{}_{-2} d^2_{mk}(\beta)d^2_{kn}(\beta_2) \times\exp[-ik\gamma_F(t)]\exp[-in\gamma_L(t)]Y_{2n}(\theta',\phi')\,. \tag{9}$$

The subscripts F and L refer to flips and librations, respectively. The d^2_{mn} are elements of the reduced Wigner rotation matrix, and are real. The angle between the static magnetic field and the symmetry axis is β while the angle between the symmetry axis and that about which libration takes place is β_2. As already noted, the flipping and librating motions are coaxial so $\beta_2 = 0$. For $k = n$ nonzero contributions occur, and we write

$$Y_{2m}(t) = \sum_{n=-2}^{+2} d^2_{mn}(\beta)\exp[-in\gamma_F(t)] \times\exp[-in\gamma_L(t)]Y_{2n}(\theta',\phi')\,. \tag{10}$$

Retaining secular terms only, the correlation function becomes

$$\langle Y_{2m}(t)Y_{2,-m}(t-\tau)\rangle = \sum_n^{+2}{}_{-2} d^2_{mn}(\beta)d^2_{-m,-n}(\beta)Y_{2n}(\theta',\phi')Y_{2,-n}(\theta',\phi')\langle\exp[\pm in\gamma_F(t)]\exp[\mp in\gamma_F(t-\tau)]\rangle \times\langle\exp[\pm in\gamma_L(t)]\exp[\mp in\gamma_L(t-\tau)]\rangle\,. \tag{11}$$

Evaluating these expressions yields

$$\langle Y_{20}(t)Y_{2,0}(t-\tau)\rangle = (45/128\pi)\{2/9[3\cos^2(\theta')-1]^2[3\cos^2(\beta)-1]^2 + \sin^4(\theta')\sin^4(\beta)\langle\exp[\pm 2i\gamma_F(t)] \times\exp[\mp 2i\gamma_F(t-\tau)]\rangle\langle\exp[\pm 2i\gamma_L(t)]\exp[\mp 2i\gamma_L(t-\tau)]\rangle + \sin^2(2\theta')\sin^2(2\beta) \times\langle\exp[\pm i\gamma_F(t)]\exp[\mp i\gamma_F(t-\tau)]\rangle\langle\exp[\pm i\gamma_L(t)]\exp[\mp i\gamma_L(t-\tau)]\rangle\}\,, \tag{12}$$

$$\langle Y_{21}(t)Y_{2,-1}(t-\tau)\rangle = -(15/64\pi)\{\tfrac{1}{2}[3\cos^2(\theta')-1]^2\sin^2(2\beta) + \sin^4(\theta')[1-\cos^4(\beta)]\langle\exp[\pm 2i\gamma_F(t)] \times\exp[\mp 2i\gamma_F(t-\tau)]\rangle\langle\exp[\pm 2i\gamma_L(t)] \times\exp[\mp 2i\gamma_L(t-\tau)]\rangle + \sin^2(2\theta')[\cos^2(2\beta)+\cos^2(\beta)] \times\langle\exp[\pm i\gamma_F(t)]\exp[\mp i\gamma_F(t-\tau)]\rangle\langle\exp[\pm i\gamma_L(t)]\exp[\mp i\gamma_L(t-\tau)]\rangle\}\,, \tag{13}$$

$$\langle Y_{22}(t)Y_{2,-2}(t-\tau)\rangle = (15/256\pi)\{2[3\cos^2(\theta')-1]^2\sin^4(\beta) + \sin^4(\theta')[1+6\cos^2(\beta)+\cos^4(\beta)] \times\langle\exp[\pm 2i\gamma_F(t)]\exp[\mp 2i\gamma_F(t-\tau)]\rangle\langle\exp[\pm 2i\gamma_L(t)]\exp[\mp 2i\gamma_L(t-\tau)]\rangle + 4\sin^2(2\theta')[1-\cos^4(\beta)]\langle\exp[\pm i\gamma_F(t)]\exp[\mp i\gamma_F(t-\tau)]\rangle \times\langle\exp[\pm i\gamma_L(t)]\exp[\mp i\gamma_L(t-\tau)]\rangle\}\,. \tag{14}$$

With proton spin–lattice relaxation times long with respect to the time for spin diffusion, the latter mechanism exchanges magnetization between different sites effectively averaging over all orientations with respect to the applied field. Thus only a T_1 averaged over all sites is observed. For this reason the spherical harmonic expansions are averaged over the polar angle β, which leads to the result

$$\langle Y_{2m}(t)Y_{2\,-m}(t-\tau)\rangle = (-1)^m(1/16\pi)\{[3\cos^2(\theta')-1]^2 + 3\sin^2(2\theta')\langle\exp[\pm i\gamma_F(t)]\exp[\mp i\gamma_F(t-\tau)]\rangle \times\langle\exp[\pm i\gamma_L(t)]\exp[\mp i\gamma_L(t-\tau)]\rangle + 3\sin^4(\theta')\langle\exp[\pm 2i\gamma_F(t)] \times\exp[\mp 2i\gamma_F(t-\tau)]\rangle\langle\exp[\pm 2i\gamma_L(t)]\exp[\mp 2i\gamma_L(t-\tau)]\}. \quad (15)$$

For carbon-13 relaxation, spin diffusion is less prevalent so we retain the dependence on β. According to molecular geometry $\theta' = \pi/3$, and we obtain

$$\langle Y_{20}(t)Y_{2\,-0}(t-\tau)\rangle = (135/512\pi)\{1/54[3\cos^2(\beta)-1]^2 + 3/4\sin^4(\beta)\langle\exp[\pm 2i\gamma_F(t)]\exp[\mp 2i\gamma_F(t-\tau)]\rangle \times\langle\exp[\pm 2i\gamma_L(t)]\exp[\mp 2i\gamma_L(t-\tau)]\rangle + \sin^2(2\beta)\langle\exp[\pm i\gamma_F(t)] \times\exp[\mp i\gamma_F(t-\tau)]\rangle\langle\exp[\pm i\gamma_L(t)]\exp[\mp i\gamma_L(t-\tau)]\rangle\}, \quad (16)$$

$$\langle Y_{21}(t)Y_{2\,-1}(t-\tau)\rangle = -(45/256\pi)\{1/6\sin^2(\beta)\cos^2(\beta) + 3/4[1-\cos^4(\beta)]\langle\exp[\pm 2i\gamma_F(t)] \times\exp[\mp 2i\gamma_F(t-\tau)]\rangle\langle\exp[\pm 2i\gamma_L(t)]\exp[\mp 2i\gamma_L(t-\tau)]\rangle + [\cos^2(2\beta)+\cos^2(\beta)] \times\langle\exp[\pm i\gamma_F(t)]\exp[\mp i\gamma_F(t-\tau)]\rangle\langle\exp[\pm i\gamma_L(t)]\exp[\mp i\gamma_L(t-\tau)]\rangle\}, \quad (17)$$

$$\langle Y_{22}(t)Y_{2\,-2}(t-\tau)\rangle = (45/1024\pi)\{1/8\sin^4(\beta) + 3/4[1+6\cos^2(\beta)+\cos^4(\beta)]\langle\exp[\pm 2i\gamma_F(t)] \times\exp[\mp 2i\gamma_F(t-\tau)]\rangle\langle\exp[\pm 2i\gamma_L(t)]\exp[\mp 2i\gamma_L(t-\tau)]\rangle + 4[1-\cos^4(\beta)] \times\langle\exp[\pm i\gamma_F(t)]\exp[\mp i\gamma_F(t-\tau)]\rangle\langle\exp[\pm i\gamma_L(t)]\exp[\mp i\gamma_L(t-\tau)]\rangle\}. \quad (18)$$

RELATIONSHIP OF SHIELDING AND MOTIONAL AXES

To interpret the relaxation at various points across the chemical shift anisotropy line shape, it is necessary to relate shielding to the orientation of the molecular motion axis. Shielding itself is described in a molecular fixed axis system determined by the electronic environment. To transform from the principal axis system to the motional axis system to consider the effects of the motion and to consider the orientation of the motional axes with respect to the applied field three similarity transformations are employed as follows:

	About axis	Angle	Degrees
(1)	z	δ	$\pi/3$
(2)	x'	α	variable
(3)	y''	θ	variable

The x, y, and z axes are the principal axes of the shielding tensor and are fixed as shown in Fig. 6.[35] The corresponding principal components of the chemical shielding tensor are σ_{11}, σ_{22}, and σ_{33}, with rigid lattice chemical shifts relative to CS_2 of [3]

$$\sigma_{11} = -17 \text{ ppm}, \quad (19a)$$

$$\sigma_{22} = 52 \text{ ppm}, \quad (19b)$$

$$\sigma_{33} = 175 \text{ ppm}. \quad (19c)$$

To develop the equations relating the observed chemical shift to these principal shielding components we begin in the principal axis system of the chemical shift tensor

$$\sigma^* = \begin{bmatrix} \sigma_{11} & 0 & 0 \\ 0 & \sigma_{22} & 0 \\ 0 & 0 & \sigma_{33} \end{bmatrix}. \quad (20)$$

We wish to transform the principal axis system to a motional axis system, the twofold axis. We rotate about the z axis through the angle δ using the rotation matrix:

$$R_\delta = \begin{bmatrix} \cos(\delta) & -\sin(\delta) & 0 \\ \sin(\delta) & \cos(\delta) & 0 \\ 0 & 0 & 1 \end{bmatrix}, \quad (21)$$

$$\sigma_1 = R_\delta \sigma^* R_\delta^{-1}, \quad (22)$$

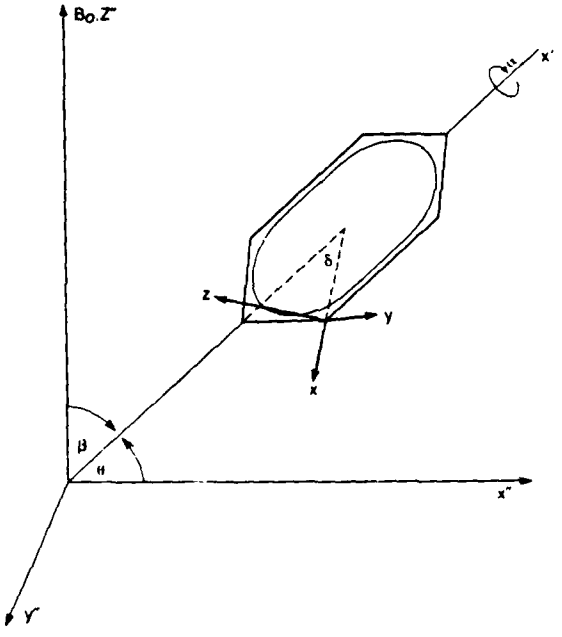

FIG. 6. Coordinate system for BPA-^{13}C-PC chemical shielding calculations.

$$\sigma_1 = \begin{bmatrix} \sigma_{11}\cos^2(\delta) + \sigma_{22}\sin^2(\delta) & (\sigma_{22} - \sigma_{11})\tfrac{1}{2}\sin(2\delta) & 0 \\ (\sigma_{22} - \sigma_{11})\tfrac{1}{2}\sin(2\delta) & \sigma_{11}\sin^2(\delta) + \sigma_{22}\cos^2(\delta) & 0 \\ 0 & 0 & \sigma_{33} \end{bmatrix}. \tag{23}$$

With $\delta = \pi/3$, $\cos^2(\delta) = 1/4$, $\sin^2(\delta) = 3/4$, and $\sin(2\delta) = \frac{1}{2}\sqrt{3}$ which reduces the tensor to

$$\sigma_1 = \begin{bmatrix} \tfrac{1}{4}(\sigma_{11} + 3\sigma_{22}) & \tfrac{1}{4}\sqrt{3}(\sigma_{22} - \sigma_{11}) & 0 \\ \tfrac{1}{4}\sqrt{3}(\sigma_{22} - \sigma_{11}) & \tfrac{1}{4}(3\sigma_{11} + \sigma_{22}) & 0 \\ 0 & 0 & \sigma_{33} \end{bmatrix}. \tag{24}$$

The second unitary transformation involves rotation about the x' axis through the angle α which is used to introduce the two motions (flips and librations) as well as describe the orientation of the phenylene ring:

$$\sigma_2(\alpha) = R_\alpha \sigma_1 R_\alpha^{-1}, \tag{25}$$

$$R_\alpha = \begin{bmatrix} 1 & 0 & 0 \\ 0 & \cos(\alpha) & -\sin(\alpha) \\ 0 & \sin(\alpha) & \cos(\alpha) \end{bmatrix}, \tag{26}$$

$$\sigma_2 = \begin{bmatrix} \tfrac{1}{4}(\sigma_{11} + 3\sigma_{22}) & \cos(\alpha)\tfrac{1}{4}\sqrt{3}(\sigma_{22} - \sigma_{11}) & \sin(\alpha)\tfrac{1}{4}\sqrt{3}(\sigma_{22} - \sigma_{11}) \\ \cos(\alpha)\tfrac{1}{4}\sqrt{3}(\sigma_{22} - \sigma_{11}) & \cos^2(\alpha)\tfrac{1}{4}(3\sigma_{11} + \sigma_{22}) + \sin^2(\alpha)\sigma_{33} & \tfrac{1}{2}\sin(2\alpha)[\tfrac{1}{4}(3\sigma_{11} + \sigma_{22}) - \sigma_{33}] \\ \sin(\alpha)\tfrac{1}{4}\sqrt{3}(\sigma_{22} - \sigma_{11}) & \tfrac{1}{2}\sin(2\alpha)[\tfrac{1}{4}(3\sigma_{11} + \sigma_{22}) - \sigma_{33}] & \sin^2(\alpha)\tfrac{1}{4}(3\sigma_{11} + \sigma_{22}) + \cos^2(\alpha)\sigma_{33} \end{bmatrix}. \tag{27}$$

We shall consider the effect on $\sigma_2(\alpha)$ of π flips and librations about the C_1C_4 axis. The π-flip averaged value of $\sigma_2(\alpha)$ is

$$\sigma_{\text{flip}} = \tfrac{1}{2}\{\sigma_2(\alpha) + \sigma_2(\alpha \pm \pi)\} \tag{28}$$

$$= \begin{bmatrix} \tfrac{1}{4}(\sigma_{11} + 3\sigma_{22}) & 0 & 0 \\ 0 & \cos^2(\alpha)\tfrac{1}{4}(3\sigma_{11} + \sigma_{22}) + \sin^2(\alpha)\sigma_{33} & \tfrac{1}{2}\sin(2\alpha)[\tfrac{1}{4}(3\sigma_{11} + \sigma_{22}) - \sigma_{33}] \\ 0 & \tfrac{1}{2}\sin(2\alpha)[\tfrac{1}{4}(3\sigma_{11} + \sigma_{22}) - \sigma_{33}] & \sin^2(\alpha)\tfrac{1}{4}(3\sigma_{11} + \sigma_{22}) + \cos^2(\alpha)\sigma_{33} \end{bmatrix}. \tag{29}$$

We next consider the effect of libration on this matrix. The libration-averaged value of σ_{flip} is $\langle\sigma_2(\alpha)\rangle$:

$$\langle\sigma_2(\alpha)\rangle = \int_{\alpha - \frac{1}{2}L}^{\alpha + \frac{1}{2}L} \sigma_{\text{flip}}\, d\alpha \Big/ \int_{\alpha - \frac{1}{2}L}^{\alpha + \frac{1}{2}L} d\alpha, \tag{30}$$

where L is the amplitude of angular libration. Utilizing this yields

$$\langle\cos^2(\alpha)\rangle = \tfrac{1}{2}\{1 + \cos(2\alpha)\sin(L)/L\}, \tag{31}$$

$$\langle\sin^2(\alpha)\rangle = \tfrac{1}{2}\{1 - \cos(2\alpha)\sin(L)/L\}, \tag{32}$$

and

$$\langle\sin(2\alpha)\rangle = \sin(2\alpha)\sin(L)/L, \tag{33}$$

and

$$\langle\sigma_2\rangle = \begin{bmatrix} \tfrac{1}{4}(\sigma_{11} + 3\sigma_{22}) & 0 & 0 \\ 0 & \tfrac{1}{2}[\{1 + \cos(2\alpha)\sin(L)/L\}\tfrac{1}{4}(3\sigma_{11} + \sigma_{22}) + \{1 - \cos(2\alpha)\sin(L)/L\}\sigma_{33}] & \{\tfrac{1}{2}\sin(2\alpha)\sin(L)/L\}[\tfrac{1}{4}(3\sigma_{11} + \sigma_{22}) - \sigma_{33}] \\ 0 & \{\tfrac{1}{2}\sin(2\alpha)\sin(L)/L\}[\tfrac{1}{4}(3\sigma_{11} + \sigma_{22}) - \sigma_{33}] & \tfrac{1}{2}[\{1 - \cos(2\alpha)\sin(L)/L\}\tfrac{1}{4}(3\sigma_{11} + \sigma_{22}) + \{1 + \cos(2\alpha)\sin(L)/L\}\sigma_{33}] \end{bmatrix}. \tag{34}$$

To allow the possibility that the symmetry axis is inclined at an arbitrary angle to the static field, we introduce a third unitary transformation permitting rotation about the y'' axis through an angle θ,

$$\sigma_3 = R_\theta \langle\sigma_2\rangle R_\theta^{-1}, \tag{35}$$

$$R_\theta = \begin{bmatrix} \cos(\theta) & 0 & -\sin(\theta) \\ 0 & 1 & 0 \\ \sin(\theta) & 0 & \cos(\theta) \end{bmatrix}. \tag{36}$$

The matrix resulting from the third transformation is

$$\sigma_3 = \begin{bmatrix} \sigma_{xx} & \sigma_{xy} & \sigma_{xz} \\ \sigma_{yx} & \sigma_{yy} & \sigma_{yz} \\ \sigma_{zx} & \sigma_{zy} & \sigma_{zz} \end{bmatrix} \tag{37}$$

with

$$\sigma_{xx} = \cos^2(\theta)\tfrac{1}{4}(\sigma_{11} + 3\sigma_{22}) + \sin^2(\theta)\tfrac{1}{2}[\{1 - \cos(2\alpha)\sin(L)/L\}\tfrac{1}{4}(3\sigma_{11} + \sigma_{22}) + \{1 + \cos(2\alpha)\sin(L)/L\}\sigma_{33}], \quad (37a)$$

$$\sigma_{yy} = \tfrac{1}{2}[\{1 + \cos(2\alpha)\sin(L)/L\}\tfrac{1}{4}(3\sigma_{11} + \sigma_{22}) + \{1 - \cos(2\alpha)\sin(L)/L\}\sigma_{33}], \quad (37b)$$

$$\sigma_{zz} = \sin^2(\theta)\tfrac{1}{4}(\sigma_{11} + 3\sigma_{22}) + \cos^2(\theta)\tfrac{1}{2}[\{1 - \cos(2\alpha)\sin(L)/L\}\tfrac{1}{4}(3\sigma_{11} + \sigma_{22}) + \{1 + \cos(2\alpha)\sin(L)/L\}\sigma_{33}], \quad (37c)$$

$$\sigma_{xy} = \sigma_{yx} = -\sin(\theta)\{\tfrac{1}{2}\sin(2\alpha)\sin(L)/L\}[\tfrac{1}{4}(3\sigma_{11} + \sigma_{22}) - \sigma_{33}], \quad (37d)$$

$$\sigma_{yz} = \sigma_{zy} = \cos(\theta)\{\tfrac{1}{2}\sin(2\alpha)\sin(L)/L\}[\tfrac{1}{4}(3\sigma_{11} + \sigma_{22}) - \sigma_{33}], \quad (37e)$$

$$\sigma_{xz} = \sigma_{zx} = \tfrac{1}{2}\sin(2\theta)\{\tfrac{1}{4}(\sigma_{11} + 3\sigma_{22}) - \tfrac{1}{2}[\{1 - \cos(2\alpha)\sin(L)/L\}\tfrac{1}{4}(3\sigma_{11} + \sigma_{22}) + \{1 + \cos(2\alpha)\sin(L)/L\}\sigma_{33}]\}. \quad (37f)$$

The angle θ lies between the symmetry axis and the x'' axis. Since the angle between the x'' axis and the z'' axis is $\pi/2$, $\theta = \pi/2 - \beta$, and we may write σ_{zz} as

$$\sigma_{zz}(\alpha,\beta) = \cos^2(\beta)\tfrac{1}{4}(\sigma_{11} + 3\sigma_{22}) + \sin^2(\beta)\tfrac{1}{2}[\{1 - \cos(2\alpha)\sin(L)/L\}\tfrac{1}{4}(3\sigma_{11} + \sigma_{22}) + \{1 + \cos(2\alpha)\sin(L)/L\}\sigma_{33}]. \quad (38)$$

Thus the chemical shielding is a function of $\sigma_{11}, \sigma_{22}, \sigma_{33}$, L, α, and β. Line shape studies[1-5] have set the first four parameters, and through α and β we may specify any orientation of the phenylene ring with respect to the static magnetic field and the corresponding chemical shift. We find three instances where choices of α and β result in unique values of the shielding relative to the CSA line shape as indicated in Fig. 7. For $\beta = \pi/2$ and $\alpha = 0$ we obtain maximum shielding, $\sigma_{zz} = 164$ ppm. By a rotation of $\pi/2$ degrees through α while keeping $\beta = \pi/2$ we move to the most deshielded position, $\sigma_{zz} = 10$ ppm. Thus the calculated linewidth of 154 ppm at 40 °C is in excellent agreement with the observed linewidth.[7] Finally, phenylene rings with their symmetry axes in the direction of the field ($\beta = 0$) overwhelmingly but not completely account for the chemical shift $\sigma_{zz} = 34$ ppm. In the fully relaxed spectrum, this is the position of maximum intensity.

CORRELATION FUNCTIONS

For proton relaxation, correlation functions for orientation variation and internuclear distance variation must be developed. Only the former aspect is required in carbon-13 calculations.

The approximate twofold flipping motion of the phenylene group can be described by Gibby's formalism[25] producing the internuclear distance correlation function:

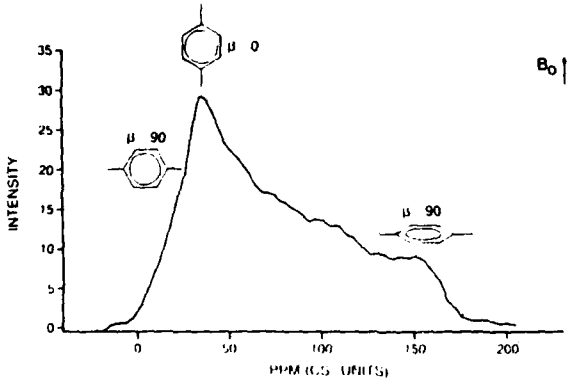

FIG. 7. Chemical shielding anisotropy spectrum at 40 °C including unique orientations of the phenylene ring

$$\langle r(t)^{-3} r(t-\tau)^{-3}\rangle = \sum_{i,j} p(r_i) r_i^{-3} p(r_i, t \,|\, r_j, t-\tau) r_j^{-3}, \quad (39)$$

where $p(r_i)$ is the probability that a phenylene group is in the r_i orientation and $p(r_i,t\,|r_j,t-\tau)$ is the conditional probability that the ring was at orientation r_j at time $t-\tau$, given that it is in the r_i position at time t.

The correlation function for phenylene group twofold anisotropic internal rotation has been presented by Jones.[36] The time-dependent probabilities for occupation of two rotational equilibrium positions are

$$p(r_i) = \tfrac{1}{2}, \quad (40a)$$

$$p(r_i,t\,|r_j,t-\tau) = \tfrac{1}{2}[1 + \exp(-|\tau|/\tau_k)], \quad i = j, \quad (40b)$$

$$p(r_i,t\,|r_j,t-\tau) = \tfrac{1}{2}[1 - \exp(-|\tau|/\tau_k)], \quad i \neq j. \quad (40c)$$

The parameter τ_k is the mean time between jumps. Illustrating the computation:

$$\begin{aligned}\langle r(t)^{-3} r(t-\tau)^{-3}\rangle = {} & \tfrac{1}{2} r_1^{-3} \tfrac{1}{2}[1 + \exp(-|\tau|/\tau_k)] r_1^{-3} \\ & + \tfrac{1}{2} r_1^{-3} \tfrac{1}{2}[1 - \exp(-|\tau|/\tau_k)] r_2^{-3} \\ & + \tfrac{1}{2} r_2^{-3} \tfrac{1}{2}[1 - \exp(-|\tau|/\tau_k)] r_1^{-3} \\ & + \tfrac{1}{2} r_2^{-3} \tfrac{1}{2}[1 - \exp(-|\tau|/\tau_k)] r_2^{-3}. \end{aligned} \quad (41)$$

The distances r_1 and r_2 correspond to minimum and maximum proton separations, respectively. Since the minimum position will be most efficient in inducing relaxation, we neglect the last three terms. The contribution of π flips to the spectral density from modulation of the internuclear distance yields:

$$\langle r(t)^{-3} r(t-\tau)^{-3}\rangle \approx \tfrac{1}{4}[1 + \exp(-|\tau/\tau_k)] r_1^{-6}. \quad (42)$$

The correlation function associated with flips of the azimuthal angle, γ_F can be calculated based on the twofold flipping motion. Again following Gibby's formalism[25]:

$$\langle \exp[\pm im\gamma(t)]\exp[\mp im\gamma(t-\tau)]\rangle = \sum_{i,j} p(\gamma_i)\exp(\pm im\gamma_i)p(\gamma_i,t\,|\gamma_j,t-\tau)\times\exp(\mp im\gamma_j)\,. \tag{43}$$

The same time-dependent probabilities for occupation of two rotational equilibrium positions[36] are employed yielding

$$p(\gamma_i) = \tfrac{1}{2}\,, \tag{44a}$$

$$p(\gamma_i,t\,|\gamma_j,t-\tau) = \tfrac{1}{2}[1+\exp(-|\tau|/\tau_k)]\,,\quad i=j\,, \tag{44b}$$

$$p(\gamma_i,t\,|\gamma_j,t-\tau) = \tfrac{1}{2}[1-\exp(-|\tau|/\tau_k)]\,,\quad i\neq j\,. \tag{44c}$$

Illustrating the computation:

$$\begin{aligned}\langle \exp[\pm im\gamma(t)]\exp[\mp im\gamma(t-\tau)]\rangle &= \tfrac{1}{2}\exp(\pm im\gamma_1)\tfrac{1}{2}[1+\exp(-|\tau|/\tau_k)]\exp(\mp im\gamma_1)+\tfrac{1}{2}\exp(\pm im\gamma_1)\tfrac{1}{2}[1-\exp(-|\tau|/\tau_k)]\exp(\mp im\gamma_2)\\ &+\tfrac{1}{2}\exp(\pm im\gamma_2)\tfrac{1}{2}[1-\exp(-|\tau|/\tau_k)]\exp(\mp im\gamma_1)+\tfrac{1}{2}\exp(\pm im\gamma_2)\tfrac{1}{2}[1+\exp(-|\tau|/\tau_k)]\exp(\mp \mathrm{i}m\gamma_2)\,,\end{aligned} \tag{45}$$

$$\langle \exp[\pm im\gamma(t)]\exp[\mp im\gamma(t-\tau)]\rangle = \tfrac{1}{2}[1+\exp(-|\tau|/\tau_k)]+\tfrac{1}{2}[1-\exp(-|\tau|/\tau_k)]C_m\,, \tag{46a}$$

where

$$C_m = \exp(\pm im\gamma_1)\exp(\mp im\gamma_2)\,. \tag{46b}$$

For exact π flips $\gamma_1 = \gamma_2 \pm \pi$ and $C_m = (-1)^m$. However, line shape data[3-5] indicates a range of positions reached by librational motions with an amplitude for phenylene group libration at each temperature given by

$$L = 6.67T^{1/2} - 68.4\,, \tag{47}$$

where L is the angular amplitude in degrees and T is the temperature (K). Through this equation C_m acquires temperature dependence.

When a ring flips, it is assumed to pass from any position within the librational range around the first minimum to any position within the same range around the second minimum. Thus there will be jumps of 175°, 185°, etc., as well as 180° though on the average the motion corresponds to π flips. Since a distribution of flip angles results, a composite value of $C_m(T)$ is sought.

We arrive at this composite by allowing jumps of equal probability from each site in the first minimum to each site in the second minimum and vice versa. The interval between sites in both minima is arbitrarily set at one degree, which is sufficiently fine to avoid graining effects. Finally we write the generalized flip correlation function for the azimuthal angle γ_F:

$$\langle \exp[\pm im\gamma_F(t)]\exp[\mp im\gamma_F(t-\tau)]\rangle = \tfrac{1}{2}[1+C_m(T)]+\tfrac{1}{2}[1-C_m(T)]\exp(-|\tau|/\tau_k)\,. \tag{48}$$

In practice, replacing $C_m = (-1)^m$ with the composite form results in virtually no change in the correlation function. However, since the composite is consistent with the overall form of the model it is retained.

The correlation function associated with libration will be calculated using a model for restricted rotational diffusion of a dipole pair about an internal rotation axis.[18,19] Model parameters are: D_{ir}, the diffusion constant for restricted diffusion, and L, the angular amplitude of the restricted diffusion. As mentioned, the temperature dependence of L is known from line shape studies and thus only D_{ir} remains as a variable.

We have for $m = 1$ or 2:

$$\begin{aligned}\langle \exp[\pm im\gamma_L(t)]\exp[\mp im\gamma_L(t-\tau)]\rangle &= 2(mL)^{-2}[1-\cos(mL)]+\frac{1}{2}\sum_{n=1}^{\infty}\{A_n^2[\cos(m\gamma)]\\ &+A_n^2[\sin(m\gamma)]\}\exp(-\lambda_n\tau)\end{aligned} \tag{49a}$$

with

$$\begin{aligned}A_n^2[\cos(m\gamma)]+A_n^2[\sin(m\gamma)] &= \left[\frac{\sin(mL-n\pi)}{(mL-n\pi)}+\frac{\sin(mL+n\pi)}{(mL+n\pi)}\right]^2\\ &+\left[\frac{1-\cos(mL-n\pi)}{(mL-n\pi)}+\frac{1-\cos(mL+n\pi)}{(mL+n\pi)}\right]^2\end{aligned} \tag{49b}$$

and

$$\lambda_n = (n\pi/L)^2 D_{ir}\,. \tag{49c}$$

The dimension of L is radians, D_{ir} is expressed in s^{-1}, and the sum over the index n typically includes eight terms.

DISTRIBUTION OF CORRELATION TIMES

In bulk polymers inhomogeneous packing of chains or groups of chains causes a distribution of spatial sites and correlation times for dynamic molecular processes. To quantify such a distribution the Williams–Watts fractional exponential correlation function is frequently employed[15,24,37]:

$$\Phi(\tau) = \exp(-(|\tau|/\tau_p)^{\alpha})\,. \tag{50}$$

The parameter α controls the breadth of the distribution of correlation times and τ_p^{-1} would be identified with the π flip rate at the center of the distribution. Kaplan and Garroway[38] showed that the above equation could be recast as a discrete sum:

$$\Phi(\tau) = \sum_{k=1}^{K}\exp(-\tau/\tau_k)P_k \tag{51}$$

with

$$\dot{\Phi}(0) = \sum_{k=1}^{K} P_k = 1 . \tag{52}$$

In practice 81 τ_k's were used ($K = 81$), 40 on either side of τ_p. This follows the approach of Kaplan and Garroway wherein two τ_k's cover one decade of time.

Bendler *et al.*[47] developed an expansion of the correlation function appropriate for α values between about 0.09 and 0.36. The expansion satisfies the normalization condition for the P_k's:

$$P_k = \tfrac{1}{2}\log_e(10)\tau_k\rho_\alpha(\tau_k) \tag{53a}$$

and

$$\rho_\alpha(\tau_k) = \alpha/\tau_p(\tau_k/\tau_p)^{\alpha-1}\exp(-\tau_k/\tau_p)^\alpha \times[1-\alpha F_2+\alpha^2F_3-\alpha^3F_4+\alpha^4F_5-\cdots], \tag{53b}$$

where

$$F_2 = U_2(1-\mu^{-\alpha}), \tag{53c}$$

$$F_3 = U_3(1-3\mu^{-\alpha}+\mu^{-2\alpha}), \tag{53d}$$

$$F_4 = U_4(1-7\mu^{-\alpha}+6\mu^{-2\alpha}-\mu^{-3\alpha}), \tag{53e}$$

$$F_5 = U_5(1-15\mu^{-\alpha}+25\mu^{-2\alpha}-10\mu^{-3\alpha}+\mu^{-4\alpha}), \tag{53f}$$

and

$$U_2 = 0.577\,216\,65, \tag{53g}$$

$$U_3 = -0.655\,877\,5, \tag{53h}$$

$$U_4 = -0.042\,003\,28, \tag{53i}$$

$$U_5 = 0.166\,538\,57, \tag{53j}$$

with

$$\mu = (\tau_p/\tau_k). \tag{53k}$$

The spin diffusion present in proton relaxation averages over the spatially homogeneous sites so an essentially homogeneous form of the correlation function can be employed:

$$\langle\exp[\pm im\gamma_F(t)]\exp[\mp im\gamma_F(t-\tau)]\rangle = \tfrac{1}{2}[1+C_m(T)]+\tfrac{1}{2}[1-C_m(T)]\exp(-(|\tau|/\tau_p)^\alpha). \tag{54}$$

For carbon-13 relaxation spin diffusion is less influential, and the inhomogeneous form is retained:

$$\langle\exp[\pm im\gamma_F(t)]\exp[\mp im\gamma_F(t-\tau)]\rangle = \tfrac{1}{2}[1+C_m(T)]+\tfrac{1}{2}[1-C_m(T)]\exp(-|\tau|/\tau_k). \tag{48}$$

PROTON SPECTRAL DENSITIES

With the requisite correlation functions now developed, we turn to calculation of spectral densities. Let us begin with consideration of the proton case for which we already have

$$\langle r(t)^{-3}r(t-\tau)^{-3}\rangle \approx \tfrac{1}{4}r_1^{-6}[1+\exp(-|\tau|/\tau_p)^\alpha] \tag{42}$$

and

$$\langle Y_{2m}(t)Y_{2-m}(t-\tau)\rangle = (-1)^m(1/16\pi)\{[3\cos^2(\theta')-1]^2+3\sin^2(2\theta')\langle\exp[\pm i\gamma_F(t)]\exp[\mp i\gamma_F(t-\tau)]\rangle \times\langle\exp[\pm i\gamma_L(t)]\exp[\mp i\gamma_L(t-\tau)]\rangle+3\sin^4(\theta')\langle\exp[\pm 2i\gamma_F(t)] \times\exp[\mp 2i\gamma_F(t-\tau)]\rangle\langle\exp[\pm 2i\gamma_L(t)]\exp[\mp 2i\gamma_L(t-\tau)]\rangle\}. \tag{15}$$

Equations (4), (5), and (8) have identified proton T_1, $T_{1\rho}$, and the spectral density. In light of Eqs. (42) and (15), it is convenient to define a correlation function specifically for proton relaxation:

$$\Phi_m(\tau)\equiv\{1+\exp(-|\tau|/\tau_p)^\alpha\}\{\langle\exp[\pm im\gamma_F(t)]\exp[\mp im\gamma_F(t-\tau)]\rangle\langle\exp[\pm im\gamma_L(t)]\exp[\mp im\gamma_L(t-\tau)]\rangle\}. \tag{55}$$

The half-Fourier transform of this correlation function, $j_m(\omega)$, can be related to the earlier spectral density $J_m(\omega)$ [Eq. (8)]:

$$j_m(\omega)\equiv\int_0^\infty\Phi_m(\tau)\exp(i\omega\tau)d\tau \tag{56}$$

and

$$J_m(\omega) = (r_1^{-6}/64\pi)\{[3\cos^2(\theta')-1]^2j_0(\omega)+3\sin^2(2\theta')j_1(\omega)+3\sin^4(\theta')j_2(\omega)\}. \tag{57}$$

Thus, Eqs. (4) and (5) become

$$1/T_1 = 3/160\,\gamma_I^4\hbar^2r_1^{-6}\{[3\cos^2(\theta')-1]^2[j_0(\omega_I)+4j_0(2\omega_I)]+3\sin^2(2\theta')[j_1(\omega_I)+4j_1(2\omega_I)] +3\sin^4(\theta')[j_2(\omega_I)+4j_2(2\omega_I)]\}, \tag{58}$$

$$1/T_{1\rho} = 3/160\,\gamma_I^4\hbar^2r_1^{-6}\{[3\cos^2(\theta')-1]^2[1.5j_0(\omega_e)+2.5j_0(\omega_I)+j_0(2\omega_I)]+3\sin^2(2\theta')[1.5j_1(\omega_e) +2.5j_1(\omega_I)+j_1(2\omega_I)]+3\sin^4(\theta')[1.5j_2(\omega_e)+2.5j_2(\omega_I)+j_2(2\omega_I)]\}. \tag{59}$$

Let us evaluate the spectral densities $j_m(\omega)$ for $m = 0,1,2$. For $m = 0$ we consider the half-Fourier transform of the fractional exponential correlation function:

$$j_0(\omega) = \int_0^\infty \Phi_0(\tau)\exp(i\omega\tau)d\tau$$
$$= \sum_{k=1}^{K} \int_0^\infty \exp(-|\tau|/\tau_k)\exp(i\omega\tau)d\tau P_k$$
$$= \sum_{k=1}^{K} \{\tau_k/[1+(\omega\tau_k)^2]\}P_k \tag{60}$$

and we obtain for $m = 1$ or 2:

$$j_m(\omega) = 1/4[1+C_m(T)] \sum_{n=1}^{\infty} \{A_n^2[\cos(m\gamma)] + A_n^2[\sin(m\gamma)]\}\{\lambda_n^{-1}/[1+(\omega/\lambda_n)^2] + 2(mL)^{-2}[1-\cos(mL)]$$
$$\times \sum_{k}^{K} \{\tau_k/[1+(\omega\tau_k)^2]\}P_k + 1/2 \sum_{k}^{K}\sum_{1\,n=1}^{\infty} \{A_n^2[\cos(m\gamma)] + A_n^2[\sin(m\gamma)]\}\{\tau_{kn}/[1+(\omega\tau_{kn})^2]\}P_k$$
$$+ 1/2[1-C_m(T)]\Big(2(mL)^{-2}[1-\cos(mL)] \sum_{k=1}^{K} \{\tau_k'/[1+(\omega\tau_k')^2]\}P_k$$
$$+ 1/2 \sum_{k}^{K}\sum_{1\,n}^{\infty} \{A_n^2[\cos(m\gamma)] + A_n^2[\sin(m\gamma)]\}\{\tau_{kn}'/[1+(\omega\tau_{kn}')^2]\}P_k\Big), \tag{61a}$$

where

$$(\tau_{kn})^{-1} = (\tau_k)^{-1} + \lambda_n, \tag{61b}$$
$$\tau_k' = \tau_k/2^{(1/\alpha)}, \tag{61c}$$

and

$$(\tau_{kn}')^{-1} = (\tau_k')^{-1} + \lambda_n, \tag{61d}$$
$$\lambda_n = (n\pi/L)^2 D_{ir}. \tag{61e}$$

Again, the dimension of L is radians, and D_{ir} is expressed in s^{-1}. A logarithmic plot of the spectral density vs Larmor frequency with and without the librational contribution is shown in Fig. 8 for the parameters

$\tau_\rho = 0.36\times 10^{-8}$ s,
$\alpha = 0.15$,
$D_{ir} = 0.438\times 10^{9}\ s^{-1}$,
$L = 50°$.

These T_1 and $T_{1\rho}$ equations were fitted to the proton data set by a nonlinear least-squares program. The program adjusts parameters to minimize the sum of squares of the percent deviations between calculated and experimental T_1 and $T_{1\rho}$ values, yielding the following fitting parameters:

$\tau_\infty = (7\pm 4)\times 10^{-17}$ s,
$E_a = 46\pm 5$ kJ/mol,
$\alpha = 0.15\pm 0.03$,
$\theta' = \pi/2 \pm \pi/18$,
$r_1 = 1.94\pm 0.10$ Å,
$D_{ir} = [(1.47\pm 0.40)\times 10^6 T - (2.22\pm 0.50)\times 10^7]\ s^{-1}$,

where T is in K. A semilogarithmic plot of the result of fitting the proton data is shown as Fig. 9.

Interchain interactions were expected to have a proton

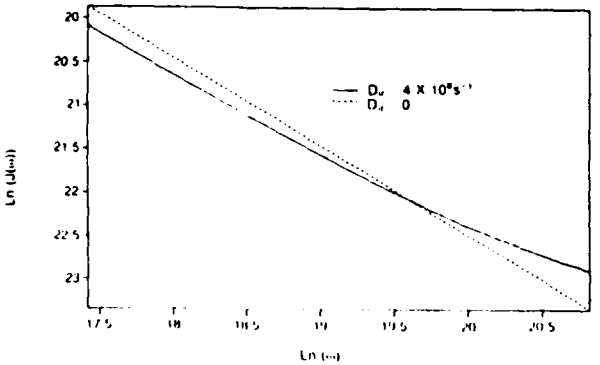

FIG. 8. Logarithm of the proton spectral density vs the logarithm of frequency with and without the librational contribution.

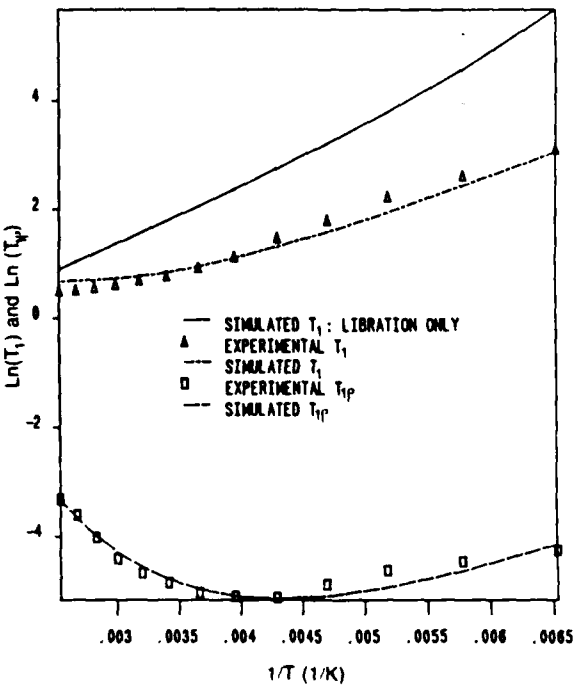

FIG. 9. Logarithm of BPA-d_6-PC proton T_1 and $T_{1\rho}$ vs $1/T$: data and model predictions.

dipole–dipole interaction vector inclined at approximately 90° to the 1,4-phenylene axis,[39] since this would correspond to the position of the nearest protons. Allowing this parameter to vary leads to the expected value. Note that the same values of E_a, τ_∞, and α also fit the carbon-13 CSA line shape collapse at two field strengths.[5,7]

CARBON-13 SPECTRAL DENSITIES

Carbon-13 calculations proceed on the basis of an inhomogeneous distribution of correlation times, giving rise to a distribution of spin–lattice relaxation times in the lab and rotating frames. Schaefer *et al.*[14] have shown that carbon-13 magnetization decays nonexponentially because of a distribution of relaxation times. Equations (6), (7), and (8) have identified carbon-13 T_1, $T_{1\rho}$, and the spectral density. Including contributions from phenylene ring libration [Eqs. (49a)–(49c)] and approximate π flips [Eq. (48)], we define the carbon-13 correlation function as

$$\Phi_m(\tau) \equiv \langle \exp[\pm im\gamma_F(t)] \times \exp[\mp im\gamma_F(t-\tau)] \rangle \langle \exp[\pm im\gamma_L(t)] \times \exp[\mp im\gamma_L(t-\tau)] \rangle . \tag{62}$$

The spectral density is the same as in Eq. (56), except that we have a unique j_{mk} for each correlation time τ_k. We calculate the carbon-13 correlation spectral distribution function as

$$j_{mk}(\omega) = \frac{1}{4}\Bigg([1 + C_m(T)] \sum_{n=1}^{\infty} \{A_n^2[\cos(m\gamma)] + A_n^2[\sin(m\gamma)]\} \lambda_n^{-1}/[1 + (\omega/\lambda_n)^2] + [1 - C_m(T)]4(mL)^{-2}[1 - \cos(mL)]\tau_k/[1 + (\omega\tau_k)^2] + [1 - C_m(T)] \sum_{n=1}^{\infty} \{A_n^2[\cos(m\gamma)] + A_n^2[\sin(m\gamma)]\} \tau_{kn}/[1 + (\omega\tau_{kn})^2] \Bigg), \tag{63a}$$

where

$$(\tau_{kn})^{-1} = (\tau_k)^{-1} + \lambda_n , \tag{63b}$$

$$\lambda_n = (n\pi/L)^2 D_r . \tag{63c}$$

For each correlation time τ_k the equations for carbon-13 T_1 [Eq. (6)] and $T_{1\rho}$ [Eq. (7)] may be written

$$1/T_{1k} = 27/256\, \gamma_I^2 \gamma_S^2 \hbar^2 r^{-6} \{3/4 \sin^4(\beta) j_{2k}(\omega_S - \omega_I) + \sin^2(2\beta) j_{1k}(\omega_S - \omega_I) + 3/2[1 - \cos^4(\beta)] j_{2k}(\omega_S) + 2[\cos^2(2\beta) + \cos^2(\beta)] j_{1k}(\omega_S) + 3/4[1 + 6\cos^2(\beta) + \cos^4(\beta)] j_{2k}(\omega_S + \omega_I) + 4[1 - \cos^4(\beta)] j_{1k}(\omega_S + \omega_I)\} \tag{64}$$

and

$$1/T_{1\rho k} = 27/256 \gamma_I^2 \gamma_S^2 \hbar^2 r^{-6} \{3/2 \sin^4(\beta) j_{2k}(\omega_e) + 2\sin^2(2\beta) j_{1k}(\omega_e) + 3/2[1 - \cos^4(\beta)] j_{2k}(\omega_I) + 2[\cos^2(2\beta)\cos^2(\beta)] j_{1k}(\omega_I) + 3/8 \sin^4(\beta) j_{2k}(\omega_S - \omega_I) + \tfrac{1}{2}\sin^2(2\beta) j_{1k}(\omega_S - \omega_I) + 3/4[1 - \cos^4(\beta)] j_{2k}(\omega_S) + [\cos^2(2\beta) + \cos^2(\beta)] j_{1k}(\omega_S) + 3/8[1 + 6\cos^2(\beta) + \cos^4(\beta)] j_{2k}(\omega_S + \omega_I) + 2[1 - \cos^4(\beta)] j_{1k}(\omega_S + \omega_I)\} . \tag{65}$$

Thus at each angle β, the lab frame relaxation rate is displayed in the form of the plot of $\log_e\{(A_\infty - A_\tau)/2A_\infty\}$ vs delay time τ. Thus we calculate

$$\log_e\{(A_\infty - A_\tau)/2A_\infty\} = \log_e\left\{\sum_{k=1}^{K} \exp[-\tau/T_{1k}(\beta)] P_k\right\} . \tag{66}$$

This equation will apply to the intensity of certain positions of the CSA line shape corresponding to specific values of β. From the CSA line shape and proton T_1 and $T_{1\rho}$ interpretations we can specify all model parameters needed for carbon-13 calculations. At 34 ppm $\beta = 0$, and we compare data and theory in Fig. 2. At each end of the tensor $\beta = 90$, and we combine this data to check the theory in Fig. 3.

The carbon-13 MASS data of Schaefer can be compared with the prediction based on the same correlation function. The MASS $T_{1\rho}$ dispersion is calculated by summing over all orientations and this result then is compared with the experimental data in Fig. 10. The prediction does not match the data, with the experimental data decaying more rapidly and with less evidence of a dispersion. A match can only be obtained by allowing for an additional relaxation pathway with a single exponential time constant, T_x. Adding this contribution to the relaxation caused by molecular motion yields the expression

$$A(\tau) = \tfrac{1}{2}A_0 \exp(-\tau/T_x) \times \int_0^{\pi} \sum_{k=1}^{K} \exp[-\tau/T_{1\rho k}(\beta)] P_k \times \sin(\beta)\, d\beta . \tag{67}$$

Allowing T_x to vary to produce a good fit yields a time constant of 21 ms for this pathway. This indicates that about 80% of the carbon-13 MASS $T_{1\rho}$ results from motions considered in the model and 20% arises from another source.

Natural abundance carbon-13 T_1 data on the phenylene carbons taken under MASS conditions was also measured at 62.9 MHz. The experimentally determined decay curve is

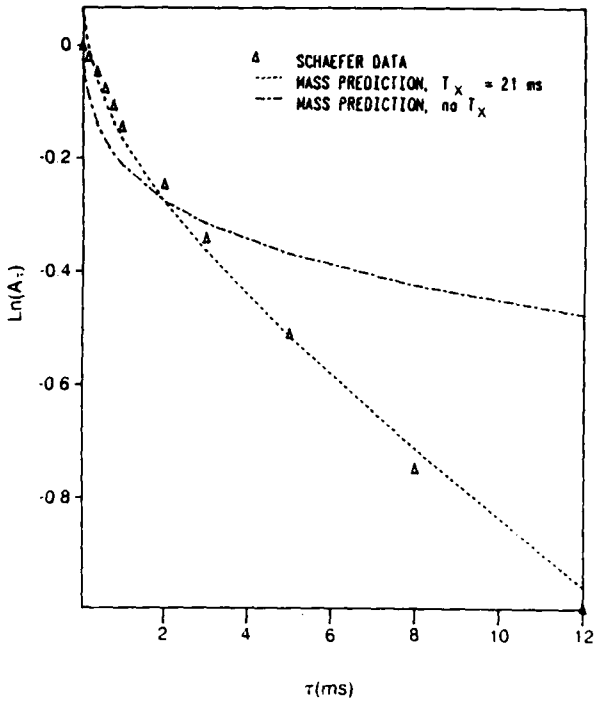

FIG. 10. The logarithm of the amplitude after spin lock time τ vs τ for carbon-13 spin–lattice relaxation in the rotating frame under MASS conditions (Ref. 8). Calculated curves show predictions with and without T_x.

compared with the theoretical curve in Fig. 4. Again as with the carbon-13 MASS $T_{1\rho}$ data this corresponds to a sum over all orientations. The predicted slope is approximately correct though the data indicates a greater dispersion than the correlation function. This difference and the additional relaxation pathway[8,20] will be considered further in the Discussion section.

DISCUSSION

The description of motion developed here in the form of a correlation function for polycarbonate provides a reasonably successful quantitative summary for a number of NMR experiments including proton T_1 and $T_{1\rho}$, carbon-13 T_1 and $T_{1\rho}$, and carbon-13 CSA line shapes. This same description also accounts for the breadth and temperature of the shear mechanical loss peak measured at 1 Hz.[7]

The geometry of motion was determined as π flips and libration based on line shape collapse.[1,6,39] The largely temporal description of π flips given here was determined from the carbon-13 line shape collapse[4,7] and the proton $T_{1\rho}$ data. The time scale of the librational motion was mostly determined by the proton T_1 data. The rotational diffusion constant falls in the range of 10^8 to 10^9 s^{-1} though this estimate is probably an order of magnitude estimate since the librational motion is a minor contribution even to the proton T_1 at 90 MHz. The librational contribution to the proton T_1 is shown relative to the observed relaxation times in Fig. 9 and it can be seen as a small contribution except at the highest temperatures.

The librational aspects can be checked by the carbon-13 T_1 data since it is also a fairly significant contributor to this data as well. For the carbon-13 T_1 data taken across the CSA tensor on the enriched sample there appears to be good agreement between the prediction based on the motional description and the experimental decay curve as shown in Figs. 2 and 3. There are deviations in the decay curves at long times, beyond 2 s, and the most likely cause is spin diffusion among the carbon-13 sites. Apparently spin diffusion from a slowly relaxing site to a rapidly relaxing site offers a new pathway in the enriched samples at delay times in the 3 to 4 s range. This would indicate the rapidly and slowly relaxing sites are only 5 to 10 Å apart which corresponds to heterogeneity in a very local scale,[40] i.e., rigid and mobile regions in very close proximity.

While the decay curve for T_1 data on the enriched samples shows less heterogeneity than the motional description, the decay for the MASS T_1 shows a greater heterogeneity than the motional description. A reduction in the estimate of D_{ir} by a factor of 2 or 3 would result in a decay curve closely matching the experimental curve in both rate and dispersion characteristics. The estimate of D_{ir} was developed primarily from the temperature dependence of the proton T_1 data assuming an amplitude of libration given by the carbon-13 line shape data. Actually the carbon-13 line shape data only determines the librational amplitude well for temperatures above 20 °C since below that temperature the rate of the π flip process primarily determines the line shape. The temperature dependence of the amplitude observed from 20 to + 120 is extrapolated to the region 0 to − 120 and this yields a successful line shape simulation. The point is that the amplitude in 0 to − 120 range is somewhat uncertain and the librational contribution to the proton T_1 is a secondary factor so the overall determination of D_{ir} is an order of magnitude estimate. Within this range of accuracy the carbon-13 T_1 MASS data agrees with the overall description of the dynamics though the data points to a somewhat slower librational motion than estimated from the proton data.

One of the new aspects to come out of this more complete interpretation is the diffusion constant for the librational motion, D_{ir} which takes on values in the range of 10^8 to 10^9 s^{-1}. These values are indicative of restricted rotation as opposed to oscillation since true torsional oscillation would be expected to fall at much higher frequencies. The time scale of this libration is too fast to be associated with mechanical processes such as the low temperature loss peak. However, the motion is very similar to restricted rotation observed in solution in polycarbonates where the rotational restriction arises from intramolecular steric factors. A comparison of the time scale and temperature dependence of libration in bulk polycarbonate with that observed in solution for substituted polycarbonates is contained in Table I. The similarity is surprising since the source of the interactions restricting rotations differs. In solution, unsubstituted polycarbonates undergo stochastic rotation about the twofold axis with a correlation time of a few nanoseconds, and barrier heights of 13 to 20 kJ which includes a contribution from solvent drag. In the substituted polycarbonates, complete rotation slows and restricted rotation becomes the primary process contributing to T_1.[41,42] The time scale for the restricted rotation remains on the nanosecond time scale so

TABLE I. Phenylene ring libration in several polycarbonates. Time scale and temperature dependence of libration in bulk BPA-PC vs dissolved and substituted polycarbonates.

	$D_{\perp} = AT - B, T(\mathrm{K})$		
Polymer	$A \times 10^{-6}$	$B \times 10^{-8}$	State
TMBPA-PC[a,b]	5.6	2.6	10 wt. % in $C_2D_2Cl_4$
NB-PC[a,b]	8.3	1.25	10 wt. % in $C_2D_2Cl_4$
BPA-PC	1.47	0.222	Bulk

[a] Structures for these polycarbonate analogs are shown in Fig. 1.
[b] From Refs. 41 and 42.

one might surmize that the potential is similar to a square well with rotational diffusion occuring in the bottom of the well but extending over a range less than complete anisotropic rotation because of a rapid rise in the potential when the steric hindrance of the substituents comes into play. Similarly, in bulk polycarbonate, restricted rotational diffusion occurs in the nanosecond region over a certain angular range. The angular range is now determined by intermolecular interactions which must enter the potential rather rapidly but do not greatly change the rotational environment inside the range over which the restricted rotation is observed. The fact that the amplitude of restricted rotation grows with $T^{1/2}$ dependence and does not go to zero amplitude at absolute zero remains as a point for further consideration.

The observed carbon-13 T_1's at different points across the CSA tensor are all near 1 s, though since there is a dispersion of relaxation times the decay rate cannot be characterized by a single time constant. The near total lack of an orientation dependence is reproduced by the correlation function developed to summarize the dynamics as shown in Figs. 2 and 3. If a single exponential correlation time for the π flip process characterized the dynamics, a reasonably strong dependence of relaxation on orientation would be expected as shown in Table II. It is clear that this orientational dependence is obscured by the distribution of correlation times arising from heterogeneity of the glass. This effect may be generally evident in systems exhibiting dynamic behavior of a distributional character.

As mentioned in the interpretation, it was necessary to introduce another relaxation pathway to produce agreement between the observed natural abundance carbon-13 MASS $T_{1\rho}$ and the dynamic description. The $T_{1\rho}$ dispersion in the natural abundance data is considerably reduced from the prediction based on the inhomogeneous distribution. This loss of inhomogeneous character which is specific to the carbon $T_{1\rho}$ data and not the carbon T_1 data must derive from a source which selectively influences the $T_{1\rho}$ behavior.

TABLE II. Prediction of the orientation dependence of a carbon-13 $T_{1\rho}$ at 28 kHz based on π flips with a single correlation time of 100 ns and no libration.

β	$T_{1\rho}$ (ms)
0	182.0
15	8.7
30	3.0
45	2.2
60	2.8
75	7.0
90	26.3

At least two possible sources of an additional relaxation pathway can be envisioned. In Schaefer's motional interpretation of glassy polycarbonate, main-chain wiggling is proposed[43] but such a motion has not been included in the motional description presented here. Main-chain wiggling is also suggested to occur in the kHz frequency regime so that it would contribute more to the carbon-13 $T_{1\rho}$ and less to carbon-13 T_1 thus providing the source of relaxation needed to reconcile the correlation and the carbon-13 $T_{1\rho}$ data. One would think that proton $T_{1\rho}$ data at the same temperature would be equally affected by main-chain wiggling but this data served as the primary temporal basis for our quantitative description and main-chain wiggling was not introduced.

An alternative explanation for the additional relaxation pathway is a spin-dynamics contribution.[20] In fairly rigid, tightly proton dipolar coupled polymeric systems, an additional spin–spin pathway through the proton reservoir has been identified. The time constant for this pathway is referred to as T_{CH}^{D} which would be identified with T_x of Eq. (67). This pathway would not contribute to carbon-13 T_1 nor to either proton $T_{1\rho}$ or T_1 relaxation. The radio field strength dependence of the carbon-13 $T_{1\rho}$ has been observed[8] and is not indicative of a single time constant spin–spin relaxation pathway. Schaefer[14] has placed an experimentally determined upper bound for the spin–spin transfer rate of 50 ms which is a little more than twice the 21 ms estimated here. An additional theoretical estimate can be made using equations presented by Schaefer[44] or by Cheung and Yaris[45] in combination with data given by Schaefer[46] and such an estimate is a factor of 50 greater than the 21 ms value.

The inability to cleanly interpret the carbon-13 $T_{1\rho}$ data with the same approach which accounts for other relaxation data is disconcerting though as mentioned about 80% of the carbon $T_{1\rho}$ relaxation is predicted by the model. Stated in a positive fashion, the correlation function presented here does account for the carbon-13 chemical shift anisotropy line shape collapse as a function of temperature,[7] proton T_1 and $T_{1\rho}$ over more than a 200 deg range, and carbon-13 T_1 data both across the chemical shift anisotropy pattern and under MASS conditions.

The correlation function developed for this interpretation includes π flips of the phenylene group and phenylene group libration about the same axis with a number of associated parameters. The geometry of the π flip process and the angular amplitude of the libration is determined from the line shape process. The temporal aspects of the π flip process at a given temperature requires assignment of a correlation time and a breadth parameter, the latter being the fractional exponent in the Williams–Watts function. At each temperature the assignment of actual numbers is made to match the state of the line shape collapse and the proton $T_{1\rho}$ value. The

temporal aspect of the libration is set primarily from the proton T_1 value, though this relaxation time is still dominated by the π flip process and thus must agree with the description of the π flip process. The carbon-13 T_1 data provides a check of the assignment of the π flip and librational parameters since these are interpreted without further adjustment. In this sense, the model parameters are overdetermined by the data base.

The same temporal description of the π flip process also predicts the position and breadth of the shear mechanical loss peak[7] which is a reassuring check of the model. Along this same line, the apparent activation energy of the correlation time in the fractional exponential matches that deduced from shear mechanical data.

ACKNOWLEDGMENTS

This research was carried out with the financial support of the National Science Foundation Grant No. DMR-790677, National Science Foundation Equipment Grant No. CHE 77-09059, National Science Foundation Grant No. DMR-8108679, and of the U. S. Army Research Office Grants DAAG 29-82-G-0001, and DAAG 29 85-K0126. We thank the Worcester Consortium NMR Facility for use of the WM250 spectrometer, and Mr. Frank Shea for his assistance.

[1]H. W. Spiess, Colloid Polym. Sci. **261**, 193 (1983).
[2]H. W. Spiess, in *Advances in Polymer Science*, edited by H. H. Kausch and H. G. Zachmann (Springer, Berlin, 1985), Vol. 66.
[3]J. F. O'Gara, Ph.D. thesis, Clark University, 1984.
[4]J. F. O'Gara, A. A. Jones, C.-C. Hung, and P. T. Inglefield, Macromolecules **8**, 1117 (1985).
[5]A. K. Roy, A. A. Jones, and P. T. Inglefield, J. Magn. Reson. **64**, 441 (1985).
[6]J. Schaefer, E. O. Stejskal, D. Perchak, J. Skolnick, and R. Yaris, Macromolecules **18**, 368 (1985).
[7]A. K. Roy, A. A. Jones, and P. T. Inglefield, Macromolecules **19**, 1356 (1986).
[8]J. R. Steger, J. Schaefer, E. O. Stejskal, and R. A. McKay, Macromolecules **13**, 1127 (1980).
[9]D. Wallach, J. Chem. Phys. **47**, 5258 (1967).
[10]D. A. Torchia, J. Magn. Reson. **30**, 613 (1978).
[11]O. Edholm and C. Bloemberg, Chem. Phys. **42**, 449 (1979).
[12]D. A. Torchia and A. Szabo, J. Magn. Reson. **49**, 107 (1982).
[13]D. A. Torchia and A. Szabo, J. Magn. Reson. **64**, 135 (1985).
[14]J. Schaefer, E. O. Stejskal, and R. Buchdahl, Macromolecules **10**, 384 (1977).
[15]A. Blumen, G. Jumofen, and J. Klafter, Phys. Rev. B **30**, 5379 (1984).
[16]M. F. Shlesinger, J. Stat. Phys. **36**, 639 (1984).
[17]M. E. Rose, in *Elementary Theory of Angular Momentum* (Wiley, New York, 1957), Chap. 4.
[18]W. Gronski and N. Murayama, Makromol. Chem. **179**, 1521 (1978).
[19]W. Gronski, Makromol. Chem. **180**, 1119 (1979).
[20]D. L. VanderHart and A. N. Garroway, J. Chem. Phys. **71**, 2773 (1979).
[21]S. Ganapathy, V. P. Chacko, and R. G. Bryant, Macromolecules **19**, 1021 (1986).
[22]J. Schaefer, E. O. Stejskal, T. R. Steger, M. D. Sefcik, and R. A. McKay, Macromolecules **13**, 1121 (1980).
[23]M. D. Sefcik, J. Schaefer, E. O. Stejskal, and R. A. McKay, Macromolecules **13**, 1132 (1980).
[24]G. Williams and D. C. Watts, Trans. Faraday Soc. **66**, 80 (1970).
[25]M. G. Gibby, Ph.D. thesis, M. I. T., 1972.
[26]D. C. Look and I. J. Lowe, J. Chem. Phys. **44**, 2995 (1966).
[27]M. Mehring, in *Principles of High Resolution NMR in Solids*, 2nd ed. (Springer, New York, 1983).
[28]A. Abragam, in *Principles of Nuclear Magnetism* (Oxford University, Oxford, 1961).
[29]N. Bloembergen, E. M. Purcell, and R. V. Pound, Phys. Rev. **73**, 679 (1948).
[30]I. Solomon, Phys. Rev. **99**, 559 (1955).
[31]N. Bloembergen, Phys. Rev. **104**, 1542 (1956).
[32]U. Haeberlen and J. S. Waugh, Phys. Rev. **185**, 420 (1969).
[33]J. S. Blicharski, Acta Phys. Pol. A **41**, 223 (1972).
[34]H. W. Spiess, in *NMR Basic Principles and Progress* (Springer, New York, 1978), Vol. 15.
[35]Slotfeldt-Ellingsen and H. A. Resing, J. Phys. Chem. **84**, 2204 (1980).
[36]A. A. Jones, J. Polym. Sci., Polym. Phys. Ed. **15**, 863 (1977).
[37]J. T. Bendler and M. F. Shlesinger, in *The Wonderful World of Stochastics*, edited by M. F. Shlesinger and G. H. Weiss (North-Holland, Amsterdam, 1985), Vol. 12.
[38]J. J. Kaplan and A. N. Garroway, J. Magn. Reson. **49**, 464 (1982).
[39]P. T. Inglefield, A. A. Jones, R. P. Lubianez, and J. F. O'Gara, Macromolecules **14**, 288 (1981).
[40]P. M. Henrichs and M. Linder, J. Magn. Reson. **58**, 458 (1984).
[41]J. J. Connolly and A. A. Jones, Macromolecules **18**, 906 (1985).
[42]A. K. Roy and A. A. Jones, J. Polym. Sci. Polym. Phys. Ed. **23**, 1793 (1985).
[43]J. Schaefer, E. O. Stejskal, R. A. McKay, and N. T. Dixon, Macromolecules **17**, 479 (1984).
[44]J. Schaefer, M. D. Sefcik, E. O. Stejskal, and R. A. McKay, Macromolecules **17**, 1118 (1984).
[45]T. T. P. Cheung and R. Yaris, J. Chem. Phys. **72**, 3604 (1980).
[46]J. Schaefer, M. D. Sefcik, E. O. Stejskal, and R. A. McKay, Macromolecules **14**, 280 (1981).

Reprinted from Macromolecules, 1987, *20*, 1434.

Local Intermolecular Structure in an Antiplasticized Glass by Solid-State NMR

An antiplasticized glass is a combination of a polymer with a low molecular weight diluent which results in a material with a higher modulus.[1,2] The increase in modulus is associated with a suppression of local chain motion,[3] and this suppression can sometimes be directly observed as the disappearance of a low-temperature mechanical loss peak[4,5] or as the slowing of a specific local reorientation in a solid-state NMR spectrum.[5,6]

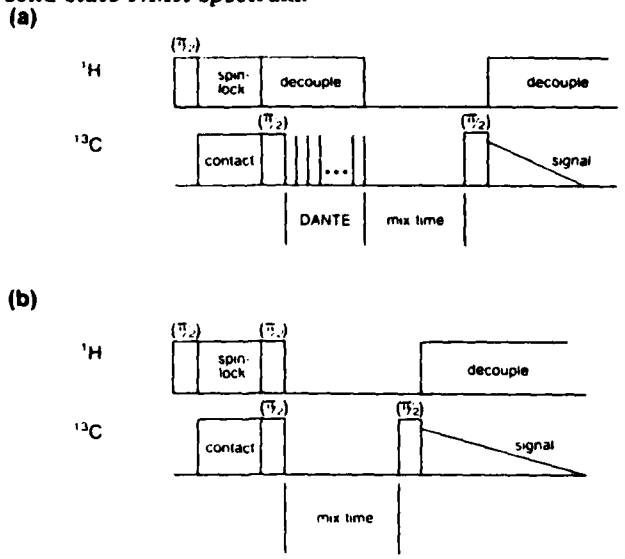

Figure 1. (a) Solid-state carbon-13 MASS pulse sequence for the measurement of spin diffusion. The pulse sequence begins with the normal cross polarization procedure. The first $\pi/2$ carbon pulse creates magnetization and the DANTE sequence selectively inverts the labeled magnetization. The mix time allows for spin diffusion between the inverted peak and the remaining resonances. The last $\pi/2$ carbon pulse just places magnetization in the xy plane for detection. (b) Solid-state carbon-13 MASS pulse sequence for the measurement of spin-lattice relaxation.[14]

Several mechanisms have been suggested for the increase in modulus and the associated suppression of sub-glass transition motion. A densification of the antiplasticized polymer is often noted[3,4] that is identified with a loss of free volume and thus a suppression of motion. At first glance, the addition of a low molecular weight diluent would be expected to increase free volume. Since just the opposite is observed for antiplasticizer, this type of diluent is supposed to go into the "holes" in the amorphous glass so as to alter the free volume distribution.[5]

To a certain extent, this explanation begs the question since it does not clearly identify the property that distinguishes a plasticizer from an antiplasticizer. Some investigators have proposed specific interactions between the polymer and the diluent as the key property of an antiplasticizer.[3,4,7] It is the purpose of this report to seek evidence for such a specific interaction by the presence of a preferred position of the antiplasticizer relative to the polymer repeat unit. The system to be examined is polycarbonate (BPA-PC) and di-*n*-butyl phthalate (DBP). The diluent, DBP, acts as an antiplasticizer at low concentrations and a plasticizer at high concentrations.[8]

The experimental approach for the determination of local structure will be carbon-13 spin diffusion between a labeled site on the DBP and various natural abundance sites in the BPA-PC repeat unit. Carbon-13 spin diffusion experiments have been developed[9,10] and have been used to demonstrate intimate mixing in blends.[11] However, no observation of spin diffusion has been made prior to this report which shows specificity at the level of chemical structure in an amorphous glass. Atomic site selectivity within a polymeric repeat unit has however been suggested as a desirable possibility in carbon-13 spin diffusion experiments.[11]

Carbon-13 labeled DBP enriched at one of the carbonyl sites was prepared from phthalic acid-α-^{13}C (99%) obtained from Merck, Inc. The phthalic acid was esterified with unlabeled 1-butanol. Diluent samples of 10 and 25 wt % were prepared by dissolving DBP and BPA-PC in

0024-9297/87/2220-1434$01.50/0

dichloromethane followed by evaporation. Unlabeled DBP was also combined with BPA-PC in the same manner.

The one-dimensional solid-state magic-angle sample spinning NMR pulse sequence used to detect spin diffusion is shown in Figure 1. The time course of the experiment is conveniently divided into four periods, analogous to two-dimensional NMR experiments.[12] In period 1, carbon-13 magnetization is prepared by using standard cross polarization techniques. The phase-alternated 90° pulse duration was typically 5.5 μs, and the spin-lock and contact pulses were 2 ms in duration. At the end of the cross polarization, the enhanced carbon magnetization is aligned along the x axis. A 90° pulse is then applied along the y axis, rotating the magnetization parallel to the z axis. At the beginning of the evolution period, a DANTE pulse train is used to selectively invert the peak corresponding to the labeled carbon.[9] This is accomplished by centering the radio-frequency field at the selected peak and applying 18 pulses of 0.8-μs width with a pulse interval spacing of 75 μs. Hence the total time duration of the pulse train is 1.3 ms. These parameters correspond in the frequency domain to a series of pulse sidebands with a spacing of 13.3 kHz, an excitation width of approximately 670 Hz, and a resulting flip angle of 180°. Since the spectrum width is 25 kHz, only the selected peak is maximally affected by the DANTE pulse train. In addition, protons are decoupled during this period in order to prevent spin diffusion from occurring.[13] During the mixing period, the proton decoupler is turned off, broadening the carbon line widths and causing the peaks to overlap. Carbon-13 magnetization relaxes by spin diffusion and spin–lattice relaxation during this period. A 90° pulse (phase alternated in parallel with the initial 90° pulse in the preparation period) then rotates the magnetization into the xy plane for detection. Any nonlinear effects of the DANTE sequence will be constant for different mixing periods and thus decay times will be essentially unaffected.

T_1 experiments are performed on unlabeled DBP–BPA-PC blends by using the same sequence as the spin diffusion experiment but without the DANTE pulse train. The pulse sequence is essentially identical with that described by Torchia[14] for measuring T_1 and is shown in Figure 1.

A Bruker WM-250 spectrometer with an IBM solids accessory module was used to perform carbon-13 magic-angle sample spinning experiments at 62.9 MHz. The magic-angle spinning rate was 3.5 kHz, and the measurements were made at ambient temperature (21 °C). In order to perform these experiments, two modifications of the IBM solids accessory were required. The noise-blanking circuitry was modified to allow the application of multiple pulses in the carbon-13 transmitter channel. Without this modification, the length of the DANTE pulse sequence and the mixing time are severely constrained. Furthermore, a safety feature limiting the total time span of any single experiment to approximately 1 s was altered to permit single experiments requiring up to 10 s. This is necessary to obtain data with mixing times greater than 1 s.

A spectrum for the antiplasticized polycarbonate is shown in Figure 2 along with peak assignments. The spectra generated by a typical one-dimensional spin diffusion experiment are shown in Figure 3 where the labeled peak is inverted and the intensities of the BPA-PC resonances are monitored as a function of mix time. Figure 4 displays several decay curves of signal amplitude vs. mix time for some of the resonances corresponding to single BPA-PC atomic sites. These data are compared with the

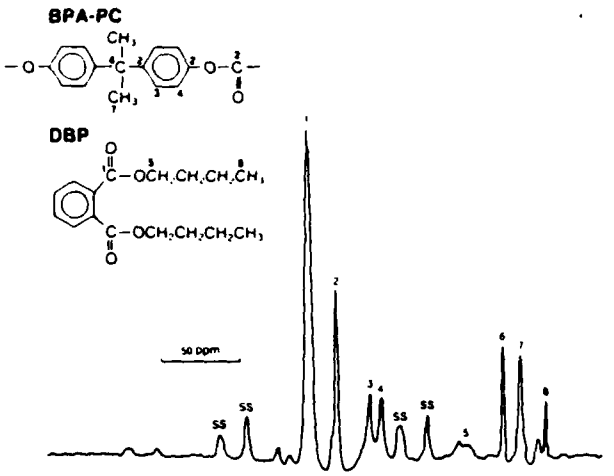

Figure 2. MASS spectrum of polycarbonate antiplasticized with di-n-butyl phthalate. Various resonances are identified with the molecular structure. (Chemical shifts: C_1, 167; C_2, 149; C_3, 127; C_4, 120; C_5, 62; C_6, 42; C_7, 31; C_8, 13 ppm). Note that peak 2 is a composite of three chemically distinct carbons that can be resolved in solution.

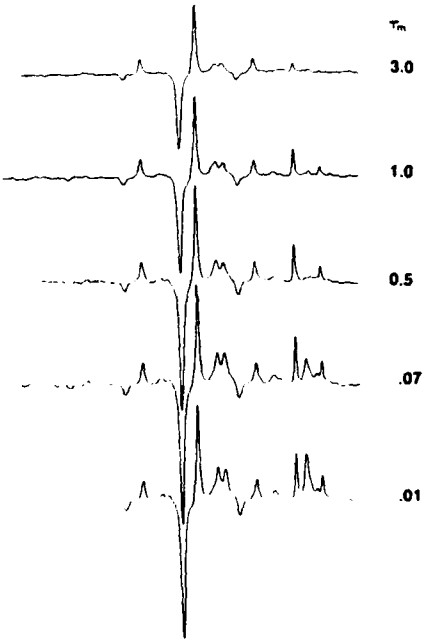

Figure 3. Typical spectra obtained during the spin diffusion experiment with inversion of the labeled carbon site.

decay of signal amplitude observed in the T_1 experiment on the same sites in the comparable unlabeled sample.

The presence of spin diffusion is indicated by an accelerated decay rate of the magnetizations of BPA-PC sites in the DANTE experiment relative to the decay rate observed in the simple T_1 experiment. This is clearly seen in Figure 4a where the quaternary aliphatic carbon in the 25 wt % sample decays more rapidly in the experiment with the inverted DBP carbonyl magnetization than in the simple T_1 experiment. The change in decay rate can be roughly quantified by fitting both types of decay curves to a single-exponential time constant over equivalent time regimes with the typical linear least-squares procedure. Since some of the decay curves are nonexponential, this procedure is only suitable for qualitative comparisons, and the resulting time constants are listed in Table I.

A perusal of the decay curves in Figure 4 and the decay rates in Table I shows a clear difference between the 10

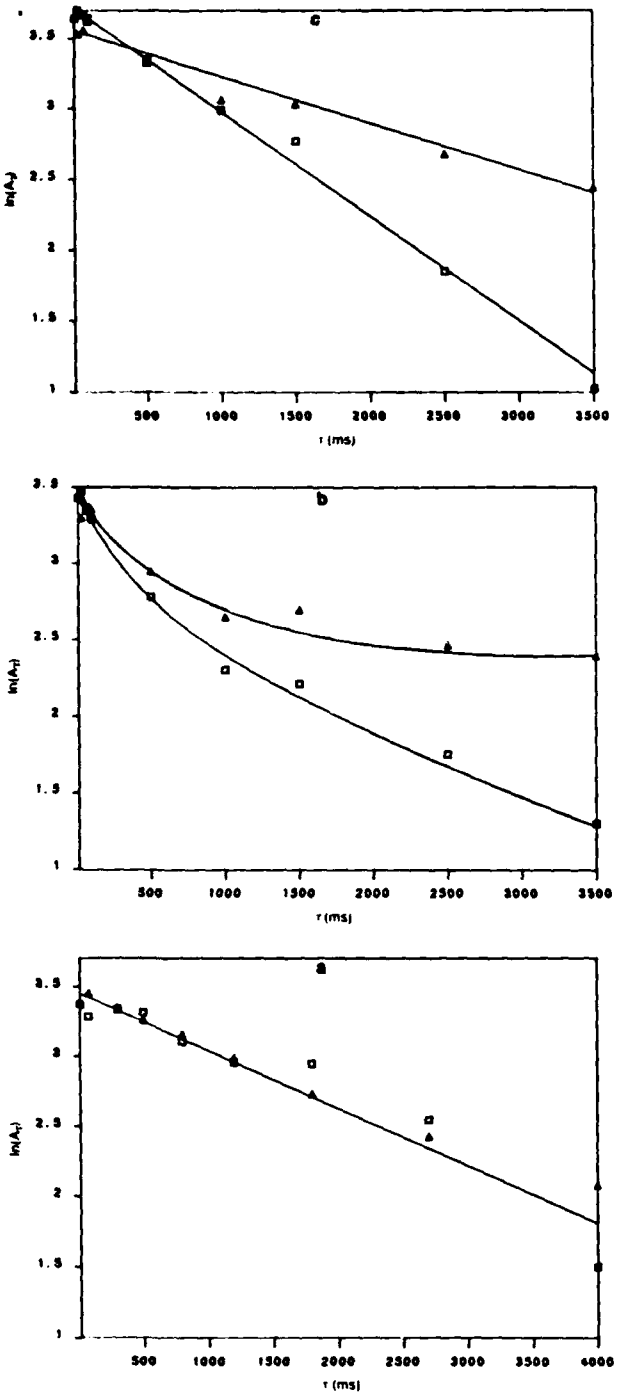

Figure 4. Decay curves observed in the spin diffusion experiment (□) with the labeled DBP and the spin-lattice relaxation experiment (△) with unlabeled DBP: (a) amplitude of the BPA-PC quaternary aliphatic carbon resonance at 25 wt % DBP; (b) amplitude of the BPA-PC protonated aromatic carbon (4) resonance at 25 wt % DBP; (c) amplitude of the BPA-PC quaternary aliphatic resonance at 10 wt % DBP.

wt % sample and 25 wt % sample. In the plasticized sample at 25 wt %, resolved lines corresponding to the two protonated aromatic peaks and the quaternary aliphatic peak all show significant spin diffusion in the form of an increased decay rate in the DANTE experiment on the labeled system relative to the T_1 experiment on the unlabeled system. This indicates molecular level mixing with spatial proximity on a distance scale of angstroms.[11] At the lower concentration of 10 wt %, corresponding to antiplasticization, the relative rate situation to the several BPA-PC sites is distinctly different. Significant spin diffusion is still seen for the two protonated aromatic sites, but little spin diffusion is noted at the quaternary aliphatic site. This distinction between the aromatic and the aliphatic sites is evident in Table I or the decay curves.

Table I
Decay Times (in s)

	25 wt % DBP		10 wt % DBP	
BPA-PC site	DANTE	T_1	DANTE	T_1
methyl	0.08	0.11	0.08	0.09
quaternary aliphatic	1.59	3.37	3.23	3.13
phenyl 3	1.77	4.99	1.83	5.05
phenyl 4	1.90	4.89	1.95	4.70

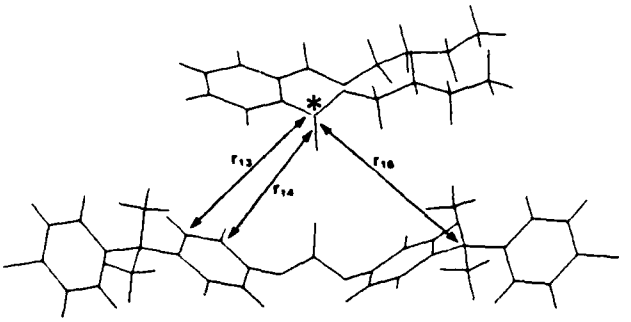

Figure 5. Pictorial representation of the relative location of DBP to the repeat unit of BPA-PC. The heavy lines indicate intermolecular distance from the labeled carbonyl: r_{13} is to the protonated aromatic carbon nearest the quaternary aliphatic carbon, r_{14} is to the protonated aromatic carbon nearest the carbonate group, and r_{16} is to the quaternary aliphatic carbon. The location of DBP is such that $r_{16} > r_{13} > r_{14}$, in agreement with the observed spin diffusion rates. The asterisk indicates the labeled carbonyl.

We believe the change in spin diffusion between the 10 wt % case and the 25 wt % case reflects a change in the level of structurally specific relative positions between an antiplasticized system and a plasticized system. Spin diffusion is determined by several factors including spatial proximity, relative orientation, and overlap of line shapes.[11] Since an amorphous glass is under study, a sum over all orientations is observed, removing this as a possible source of the difference. Changes in the overlap of line shapes are an unlikely source of the difference since the quaternary aliphatic line shape would be the same at 10 and 25 wt %, both of which are glasses at room temperature. If anything, the line width at 25 wt % should be reduced, assuming enhanced mobility in the plasticized regime, but this is where more spin diffusion is observed. This leaves spatial proximity as the remaining factor, and indeed spin diffusion depends on distance to the minus sixth power, which could certainly lead to pronounced effects.

If spatial proximity is the controlling factor, then the labeled carbonyl of DBP must be closer to the quaternary aliphatic carbon on the average in the 25 wt % case than in the 10 wt % case. Spin diffusion to the protonated aromatic carbons is still seen at 10 wt % just as it is at 25 wt %, so the spatial proximity to the phenylene groups must persist at 10 wt %. Thus the carbonyl ester of DBP must be near the phenylene groups but removed from the quaternary aliphatic site at 10 wt %. At 25 wt % this intermolecular structural specificity is lost and the labeled carbonyl is near both the phenylene and quaternary aliphatic sites.

Figure 5 depicts the position of the labeled DBP carbonyl at 10 wt % relative to the BPA-PC repeat units so that spatial proximity to the phenylene groups is maxim-

ized while spatial proximity to the quaternary aliphatic group is minimized. This picture is a greatly simplified representation and the proposed order is also localized. However, the spatial criteria for the placement of the DBP carbonyl derived from spin diffusion lead to a location of this functional group near the carbonate of BPA-PC. This is consistent with the presence of a specific interaction between the antiplasticizer and the polymer as postulated in some of the classic models of antiplasticization.[3,4,7]

At higher concentrations of DBP structurally selective spin diffusion is not observed and plasticization behavior commences. This indicates a loss of specific relative spatial positioning, and, in our view, this corresponds to the presence of DBP molecules near BPA-PC units that are not at a specific relative position and are not interacting with a particular functional group of the BPA-PC unit in question. The presence of nonspecifically interacting diluent is the cause of the onset of plasticization behavior, again in agreement with the premise of certain of the antiplasticizer–plasticizer models.[3,4,7]

In this report we have qualitatively connected structurally selective spin diffusion with preferential disposition of diluent molecules relative to the polymer chain in an antiplasticized glass. Currently a more quantitative approach involving numerical analysis of the decay curves based on coupled differential equations describing the concurrent contributions of spin–lattice relaxation and spin diffusion[11] in conjunction with a lattice model to count diluent–polymer contacts is under development. At this stage, carbon-13 spin diffusion appears to be at least capable of identifying local structure in multicomponent amorphous glasses. The method holds promise for the determination of intermolecular structure in other amorphous systems such as polymer blends where local interactions are presumed[15] but only identified in special cases such as hydrogen bonding.[16] More detailed models of intermolecular structure could result from a quantitative analysis of spin diffusion and from studies involving labeling several chemical positions of a given component.

Acknowledgment. This research was carried out with the financial support of National Science Foundation Grant No. DMR-8106234, National Science Foundation Equipment Grant No. DMR-8108679, and U.S. Army Research Office Grant DAAG 29 85-K0126.

Registry No. BPA-PC (SRU), 24936-68-3; BPA-PC (copolymer), 25037-45-0; DBP, 84-74-2.

References and Notes

(1) Jackson, W. J.; Caldwell, J. R. *J. Appl. Polym. Sci.* **1967**, *11*, 211.
(2) Jackson, W. J.; Caldwell, J. R. *J. Appl. Polym. Sci.* **1967**, *11*, 227.
(3) Petrie, S. E. B.; Moore, R. S.; Flick, J. R. *J. Appl. Phys.* **1972**, *43*, 4318.
(4) Robeson, L. M.; Faucher, J. A. *J. Polym. Sci., Polym. Lett. Ed.* **1969**, *7*, 35.
(5) Fischer, E. W.; Hellman, G. P.; Spiess, H. W.; Horth, F. S.; Carius, U. E.; Wehrle, M. *Makromol. Chem. Suppl.* **1985**, *12*, 189.
(6) Dumais, J. J.; Cholli, A. L.; Jelinski, L. W.; Hedrick, J. L.; McGrath, J. E. *Macromolecules* **1986**, *19*, 1884.
(7) Makaruk, L.; Polanska, H. *Polym. Bull. (Berlin)* **1981**, *4*, 127.
(8) Belfiore, L. A.; Henrichs, P. M.; Massa, D. J.; Zumbulyadis, N.; Ruthwell, W. P.; Cooper, S. L. *Macromolecules* **1983**, *16*, 1744.
(9) Caravatti, P.; Bodenhausen, G.; Ernst. R. R. *J. Magn. Reson.* **1983**, *55*, 88.
(10) Bronniman, C. E.; Szeverenyi, N. M.; Maciel, G. E. *J. Chem. Phys.* **1983**, *79*, 3694.
(11) Linder, M.; Henrichs, M.; Hewitt, J. M.; Massa, D. J. *J. Chem. Phys.* **1985**, *82*, 1585.
(12) Szeverenyi, N. M.; Sullivan, M. J.; Maciel, G. E. *J. Magn. Reson.* **1982**, *47*, 462.
(13) Suter, D.; Ernst, R. R. *Phys. Rev. B: Condens. Matter* **1985**, *32*, 5608.
(14) Torchia, D. A. *J. Magn. Reson.* **1978**, *30*, 613.
(15) Paul, D. R.; Newman, S., Eds. *Polymer Blends*; Academic: New York, 1978.
(16) Coleman, M. M.; Painter, P. C. *Appl. Spectrosc. Rev.* **1984**, *20*, 255.

A. K. Roy, P. T. Inglefield, J. H. Shibata, and A. A. Jones*

Jeppson Laboratory
Department of Chemistry
Clark University
Worcester, Massachusetts 01610

Received January 20, 1987

DYNAMICS OF SORBED $^{13}CO_2$ IN POLYCARBONATE BY NMR

by

Wen-Yang Wen, Edward Cain, Paul T. Inglefield and Alan A. Jones

Department of Chemistry, Clark University
Worcester, MA 10610

INTRODUCTION

The mobility of sorbed gases in polymers is an interesting scientific problem with important technological implications. Considerable effort has been invested in understanding the sorption, diffusion, permeability and permselectivity of gases in polymers. The impetus for the work comes from application of polymers in *gas separation*[1] *and in* packaging.[2]

At present there is disagreement about the description of the state of sorbed gas in glassy polymers. Two models embody the current controversy: the dual-mode model[3-7] and the matrix model.[8,9] Various techniques have been employed to investigate the interaction between the sorbed gas and glassy polymers.[1,10,11] NMR experiments have been performed by Assink[12] on NH_3 sorbed in polystyrene but interpretation of his results became a subject of heated controversy.[7,8] Recently Safcik and Schaefer and their coworkers[13,14] have performed carbon-13 NMR investigations on a CO_2-poly(vinyl chloride) system and obtained some interesting results.

We have carried out a NMR study of *carbon dioxide* sorbed in bisphenol-A polycarbonate (BPAPC). The CO_2-BPAPC system has been widely studied by classical sorption and permeability techniques. As a polymer, BPAPC is one of the best characterized amorphous glasses with considerable attention paid to molecular dynamics.[15-19] The mobility of the CO_2 was monitored by spin lattice relaxation experiments on carbon-13 labelled CO_2.

EXPERIMENTAL

Sample Preparations: Lexan polycarbonate obtained from General Electric Co. were used in one of the following two forms: (i) cylindrical block (7 mm in diameter and 30 mm in length); (ii) rectangular strips (0.127 mm x 0.5 mm x 40 mm). The block or strips were placed in a NMR pressure-valve glass tube (manufactured by Wilmad Glass Co.) and evacuated to remove the sorbed air. Measured amounts of enriched $^{13}CO_2$ (99.8%, Merck & Co.) were introduced into the NMR tube and the CO_2 pressure changes were monitored with a transducer-electrometer system as a function of time. Approximate diffusion coefficients calculated from the rate of sorption were in general agreement with the published values.[5,6,7] Flame sealed glass tubes were also used for NMR measurements at different temperatures.

NMR Measurements: Carbon-13 spin-lattice relaxation times were measured at Larmor frequencies of 22.6, 62.9 and 126 MHz on Bruker SXP 20-100, WM-250 and WM-500 FT NMR spectrometers, respectively. Proton spin-lattice relaxation times in the rotating frame were measured at a radio-frequency field strength of 1.0 mT using a standard $\pi/2$-phase-shifted locking pulse sequence. Temperature control was maintained to within ±1 K with Bruker temperature controllers.

RESULTS

Values of carbon-13 T_1's are obtained for $^{13}CO_2$ sorbed in BPAPC polymer at three Larmor frequencies and as a function of temperature and CO_2 pressure. The experimental results are shown in Figures 1 and 2. ^{13}C spectra at the higher frequencies clearly reveal increased shielding for the sorbed CO_2 with respect to the free gas and an increase in line width for the sorbed species relative to the free gas. (Separate resonances are clearly discernible in samples containing both sorbed and free gas with a chemical shift of 3.7 ppm indicative of a chemical association.) At room temperature the line is still relatively narrow (~60 Hz) but it broadens to nearly 4000 Hz at −60°C.

The Nuclear Overhauser Enhancement (NOE) of $^{13}CO_2$ was measured at 300 K and 5 atm CO_2 pressure for the three Larmor frequencies and the results are shown in Table I. The values obtained are indicative of a relatively small dipole-dipole contribution to the relaxation even at the lowest frequency where it can be estimated to be 13%.

INTERPRETATION

We proceed to analyze the T_1 data assuming three relaxation mechanisms: spin rotation (SR), chemical shift anisotropy (CSA), and dipole-dipole (DD). The pertinent equations are:

$$1/T_1 = (1/T_1)_{SR} + (1/T_1)_{CSA} + (1/T_1)_{DD} \quad (1)$$

$$(1/T_1)_{SR} = (4IkT/3h^2)C_k^2\tau_{SR} \quad (2)$$

$$(1/T_1)_{CSA} = (2/15)\omega^2(\Delta\sigma)^2\tau_{CSA} \quad (3)$$

$$(1/T_1)_{DD} = (3/4)(32\pi/405)\gamma_C^2\gamma_H^2\hbar^2(N_A/1000)([H]/bD)$$
$$(J_o + 3J_1 + 6J_2) \quad (4)$$

$$J_o = J_o(\omega_H - \omega_C);\ J_1 = J_1(\omega_C);\ J_2 = J_2(\omega_H + \omega_C) \quad (5)$$

$$J(\omega) = (1 + 5z/8 + z^2/8)/(1 + z + z^2/2 + z^3/6 +$$
$$4z^4/81 + z^5/81 + z^6/648) \quad (6)$$

$$z = 2\omega\tau_t)^{1/2};\ \tau_t = b^2/D_t \quad (7)$$

$$(NOE)_{DD} - 1 = (\gamma_C/\gamma_H)(6J_2 - J_o)/(J_o + 3J_1 + 6J_2) \quad (8)$$

Equations 4 through 7 are those given by Polnaszek and Bryant[20] based on Freed's theory[21] and the main quantities of interest to us are three correlation times τ_{SR}, τ_{CSA}, and τ_t, as well as the translational diffusion constant D_t. The procedure for obtaining these quantities are illustrated below.

At 300 K and 22.6 MHz we have two experimental quantities: T_1 = 6.0 s and NOE = 1.25. The percent of the *dipole-dipole mechanism*, %DD, operating under these conditions is given by

$$\%DD = 100\ ((NOE) - 1)/((NOE)_{DD} - 1) = 100\ T_1/(T_1)_{DD} \quad (9)$$

Since the functional relations for $(NOE)_{DD}$ vs. τ_t and $(T_1)_{DD}$ vs. τ_t are known from Equation 8 and Equation 4, respectively, one can solve for τ_t and then for %DD. Using this τ_t value one obtains the values of $(T_1)_{DD}$ at 22.6 MHz and at 126 MHz. Now one has two equations of the type,

$$(1/T_1)_{SR} + (1/T_1)_{CSA} = 1/T_1 - (1/T_1)_{DD}, \text{ or}$$

$$(1/T_1)_{SR} + 3.025 \times 10^8\ \tau_{CSA} = 0.189 \text{ (at 22.6 MHz)} \quad (10)$$

and

$$(1/T_1)_{SR} + 9.332 \times 10^9\ \tau_{CSA} = 0.453 \text{ (at 126 MHz)} \quad (11)$$

From Equations 2, 10, and 11, two correlation times τ_{SR} and τ_{CSA} are obtained. Using these values of τ_t, τ_{SR} and τ_{CSA} we then test the consistency with the data at 62.9 MHz, specifically the value of τ_{SR}. The results at 300 K and 5 atm are summarized in Tables I and II.

CONCLUSIONS

At high field the dominant source of relaxation is the chemical shift anisotropy mechanism yielding a correlation time for rotation of 2.9×10^{-11} s. At all frequencies, spin rotation is important and leads to a collision correlation time of 3.9×10^{-13} s. At the lowest frequency, a dipole-dipole contribution is observed which leads to a correlation time for translational diffusion of 1.2×10^{-10} s. This can be converted to a translational diffusion constant D_t if the distance of closest approach b is known. If we assume the value of b to fall in the range of 0.2 to 0.3 nm, then the value of D_t should fall in the range of $(3 \sim 8) \times 10^{-6}$ cm^2/s. In terms of both rotational and translational motions, these NMR results are indicative of very mobile CO_2. In fact the values of D_t estimated from the NMR data are about two orders of magnitude greater than those obtained by macroscopic measurements, e.g., by measurement of CO_2 permeation through polymer membranes.[22] While the NMR estimate of D_t is not precise, it would appear that local translation may be more rapid than macroscopic translation. Locally fast translation could be reduced by barrier regions in the heterogeneous glass leading to the observation of slower macroscopic diffusion.

ACKNOWLEDGEMENT

We gratefully acknowledge the assistance of the staff at Yale University Chemistry Department Instrumentation Center for use of their Bruker WM-500 NMR spectrometer. This research was carried out with a partial support of the NSF Grant DMR-8108679 and of the U.S. Army Research Office Grant DAAG 29-85-K0126.

REFERENCES

(1) See, for example, "Industrial Gas Separations," ed. T.E. Whyte, Jr., C.M. Yon and E.H. Wagener, ACS Symp. Ser. 223 (1983).
(2) P. Masi and D.R. Paul, J. Membrane Sci. 12, 137 (1982).
(3) P. Meares, J. Am. Chem. Soc. 76, 3415 (1954).
(4) R.M. Barrer, J.A. Barrie and J. Slater, J. Polym. Sci. 27, 177 (1958).
(5) D.R. Paul and W.J. Koros, J. Polym. Sci. Polym. Phys. Ed. 14, 675 (1976).
(6) D.R. Paul, Ber. Bunsenges. Phys. Chem. 83, 294 (1979).
(7) R.T. Chern, W.J. Koros, E.S. Sanders, S.H. Chen and H.B. Hopfenberg, in "Industrial Gas Separation" (see ref. 1), pp. 47-73 and the references cited therein.
(8) D. Raucher and M.D Sefcik, in "Industrial Gas Separations" (see ref. 1), p. 111.
(9) R.J. Pace and A. Datyner, J. Polym. Sci. Polym. Phys. Ed. 17, 437, 453, and 465 (1970).
(10) J.H. Wendorff and E.W. Fischer, Kollois-Z. Z. Polym. 251, 876 (1973).
(11) J.J. Curro and R.-J. Roe, J. Polym. Sci. Polym. Phys. Ed. 21, 1785 (1983).
(12) R.A. Assink, J. Polym. Sci. Polym. Phys. Ed. 13, 1665 (1975).
(13) M.D. Sefcik, J. Schaefer, F.L. May, D. Raucher and S.M. Dub, J. Polym. Sci. Polym. Phys. Ed. 21, 1041 (1983).
(14) M.D. Sefcik and J. Schaefer, J. Polym. Sci. Polym. Phys. Ed. 21, 1055 (1983).
(15) A.K. Roy, A.A. Jones and P.T. Inglefield, Macromolecules 19, 1356 (1986).
(16) A.A. Jones, Macromolecules 18, 902 (1985).
(17) J.J. Connolly, E. Gordon and A.A. Jones, Macromolecules 17, 722 (1984).
(18) J.J. Connolly and A.A. Jones, Macromolecules 18, 906 (1985).
(19) P.T. Inglefield, R.M. Amici, J.F. O'Gara, C.-C. Hung, and A.A. Jones, Macromolecules 16, 1552 (1983).
(20) C.F. Polnaszek and R.G. Bryant, J. Chem. Phys. 81, 4038 (1984).
(21) J.H. Freed, J. Chem. Phys. 68, 4043 (1978).
(22) W.J. Koros, Ph.D. Thesis, University of Texas at Austin, 1977.
(23) J.F. O'Gara, A.A. Jones, C.-C. Hung and P.T. Inglefield, Macromolecules 18, 1117 (1985).

Table I: Contributions of Different Mechanisms to the Spin-Lattice Relaxation of $^{13}CO_2$ in BPAPC Polymer at 300 K and 5 atm

MHz	T_1/(s)	NOE	$(T_1)_{SR}$(s)	$(T_1)_{CSA}$(s)	$(T_1)_{DD}$/s
22.6	4.6	1.25	5.6	113	35
62.9	3.5	1.08	5.2*	15	39
126	2.1	1.00	5.6	3.7	44

*This value should be 5.6 s instead of 5.2 s with a fitting error of about 6%.

Table II: Correlation Times for Spin-Rotation, CSA, and Translational Motion as well as Estimated Diffusion Constants for $^{13}CO_2$ in BPAPC Polymer at 300 K and 5 atm

$\tau_{SR} = 3.9 \times 10^{-13}$ s; $\tau_{CSA} = 2.9 \times 10^{-11}$ s

$\tau_t = 1.2 \times 10^{-10}$ s

$$D_t = \begin{cases} 3.3 \times 10^{-6} \text{ cm}^2/\text{s if } b = 2.0 \text{ nm} \\ 7.5 \times 10^{-6} \text{ cm}^2/\text{s if } b = 0.3 \text{ nm} \end{cases}$$

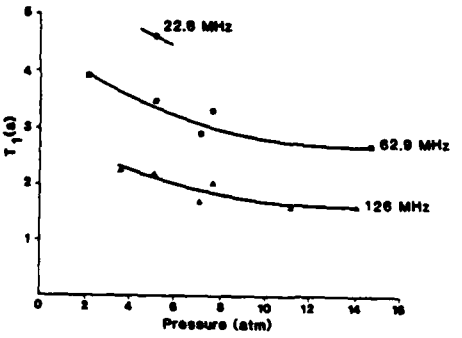

Figure 1: Experimental T_1 Data for $^{13}CO_2$ Sorbed in BPAPC Polymer at 300 K as a Function of Pressure.

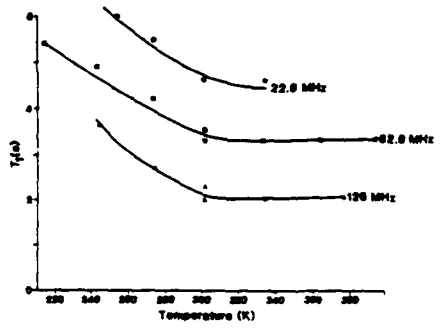

Figure 2: Experimental T_1 Data for $^{13}CO_2$ Sorbed in BPAPC Polymer as a Function of Temperature.

Zeitschrift für Physikalische Chemie Neue Folge, Bd. 155, S. 181 – 197 (1987)
 – 0044-3336/87 $3.00 + 0.00

Dynamics of Sorbed $^{13}CO_2$ in Polycarbonate Probed by Nuclear Magnetic Resonance

By Wen-Yang Wen, Edward J. Cain, Paul T. Inglefield and Alan A. Jones

Department of Chemistry, Clark University, Worcester, Massachusetts 01610, USA

Dedicated to Hermann Gerhard Hertz on the occasion of his 65th birthday

(Received April 6, 1987)

NMR* / $^{13}CO_2$ / *Dynamics* / *Polycarbonate

The mobility of carbon dioxide sorbed in bisphenol-A polycarbonate polymer was monitored by spin-lattice relaxation experiments on carbon-13 labelled CO_2. In addition the line widths and nuclear Overhauser effect of sorbed $^{13}CO_2$ were measured as a function of temperature. To interpret the temperature and magnetic field dependence of our data, we are presenting a two-site model. It is a model containing many parameters, but it seems to be consistent with most of our experimental data.

Die Beweglichkeit von Kohlendioxid, gelöst in polymerem Bisphenol-A-polykarbonat, wurde durch Messungen der Spin-Gitter-Relaxation an ^{13}C-markiertem CO_2 ermittelt. Zusätzlich wurden die Linienbreiten und der Overhauser-Effekt des gelösten $^{13}CO_2$ als Funktion der Temperatur gemessen. Zur Interpretation der Temperatur- und Feldabhängigkeit unserer Ergebnisse stellen wir ein Zwei-Zustands-Modell vor. Das Modell enthält zahlreiche Parameter, doch scheint es mit den meisten unserer experimentellen Daten vereinbar zu sein.

Introduction

The mobility of sorbed gases in polymers is an interesting scientific problem with important technological implications. Considerable effort has been invested in understanding the sorption, diffusion, permeability and permselectivity of gases in polymers. The impetus for the work comes from application of polymers in gas separation [1] and in packaging including softdrink bottling [2].

At present there is disagreement about the description of the state of sorbed gas in glassy polymers. Two models embody the current controversy: the dual-mode model [3 – 7] and the matrix model [8, 9]. Various

techniques have been employed to investigate the interaction between the sorbed gas and glassy polymers [1, 10, 11]. NMR experiments have been performed by Assink [12] on NH_3 sorbed in polystyrene but interpretation of his results became a subject of heated controversy [7, 8]. Recently Sefcik and Schaefer and their coworkers [13, 14] have performed carbon-13 NMR investigations on a CO_2-poly(vinyl chloride) system and obtained some interesting results.

We have carried out a NMR study of carbon dioxide sorbed in bisphenol-A polycarbonate (BPAPC). The CO_2-BPAPC system has been widely studied by classical sorption and permeability techniques. As a polymer, BPAPC is one of the best characterized amorphous glasses with considerable attention paid to molecular dynamics [15 – 19]. Several types of NMR experiments have been performed. First the mobility of the CO_2 was monitored by spin-lattice relaxation experiments on carbon-13 labelled CO_2. Secondly, the line widths, and thirdly the nuclear Overhauser effect (NOE) of $^{13}CO_2$ sorbed in BPAPC were measured as a function of temperature. (Some line widths in deuterated BPAPC were also measured.)

We are presenting a two-site model to interpret the temperature and magnetic field dependence of our data (T_1, NOE, and line widths of sorbed $^{13}CO_2$ in BPAPC). It is a model containing many parameters, but it seems to be consistent with most of our experimental data. Using the parameters determined we can characterize the molecular dynamics of sorbed CO_2 in the glassy polycarbonate.

Experimental

Sample Preparation: Lexan polycarbonate obtained from General Electric Co. were used in one of the following two forms: (i) cylindrical block (7 mm in diameter and 30 mm in length); (ii) rectangular strips (0.127 mm × 0.5 mm × 40 mm). The block or strips were placed in a NMR pressure-valve glass tube (manufactured by Wilmad Glass Co.) and evacuated to remove the sorbed air. Measured amounts of enriched $^{13}CO_2$ (99.8%, Merck & Co.) were introduced into the NMR tube and the CO_2 pressure changes were monitored with a transducer-electrometer system as a function of time. Approximate diffusion coefficients calculated from the rate of sorption were in general agreement with the published values [5 – 7]. Flame sealed glass tubes were also used for NMR measurements at different temperatures.

NMR Measurements: Carbon-13 spin-lattice relaxation times were measured at Larmor frequencies of 22.6, 62.9 and 126 MHz on Bruker SXP 20-100, WM-250 and WM-500 FT NMR spectrometers, respectively. NOE data were obtained by using a gated decoupling technique [20]. A decoupler power of 6 or 12 W was applied for the NOE measurements at 22.6 MHz. Resonance line widths were obtained directly from the spectra and the value of T_2 were calculated from the formula, $T_2 = (\pi \times \text{line width})^{-1}$.

Results

Experimental values of the spin-lattice relaxation time, T_1, for $^{13}CO_2$ sorbed in BPAPC polymer at various pressure, temperature, and Larmor

Table 1. Experimental T_1 data for $^{13}CO_2$ sorbed in BPAPC polymer.

P/atm	Temperature/K	T_1/s
22.6 MHz		
5–6 (block)	233	6.33
5–6 (block)	253	6.0
5–6 (block)	273	5.5
5–6 (block)	300	4.6
5–6 (block)	333	4.6
62.9 MHz		
5–6 (block)	213	5.4
5–6 (block)	242	4.9
5–6 (block)	272	4.16
5–6 (block)	300	3.5
7.5 (strips)	300	3.3
7.5 (strips)	333	3.3
7.5 (strips)	363	3.3
7.5 (strips)	393	3.3
14.6 (strips)	300	2.7
126 MHz		
5–6 (block)	213	5.7
5–6 (block)	243	3.6
5–6 (block)	300	2.2
7.5 (strips)	300	2.0
7.5 (strips)	333	2.0
5–6 (block)	373	2.7
7.5 (strips)	375	2.0
14 (strips)	300	1.6

frequencies are presented in Table 1 and plotted in Figs. 1 and 2. While T_1 seems to decrease slightly with the increase of carbon dioxide concentration in the polymer, T_1 diminishes considerably with the increase of the magnetic field strength (from 22.6 MHz to 126 MHz). The effect of temperature is noteworthy: At 233 K, T_1 is 5 to 6 s and it shortens significantly with the increase of temperature up to 300 K, but then T_1 becomes constant and remains unchanged when the temperature is increased above 300 K up to around 380 K.

The nuclear Overhauser effect factor (NOEF) of the sorbed $^{13}CO_2$ in BPAPC at 6 atm was found to be 1.00 at 126 MHz and 1.08 at 62.9 MHz both at 300 K. These data seem to indicate the absence of the dipole-dipole (DD) relaxation mechanism at the highest field (126 MHz) and a marginal presence of DD mechanism at the intermediate field (62.9 MHz). In contrast, at the lowest field (22.6 MHz), we found the values of NOEF to be substantially greater than one and to increase considerably with the decrease of temperature. These data are summarized and shown in Table 2.

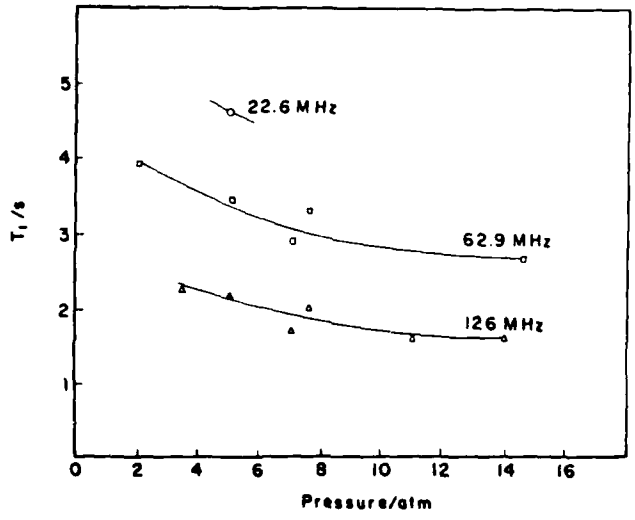

Fig. 1. Experimental T_1 data for $^{13}CO_2$ sorbed in BPAPC polymer at 300 K as a function of pressure.

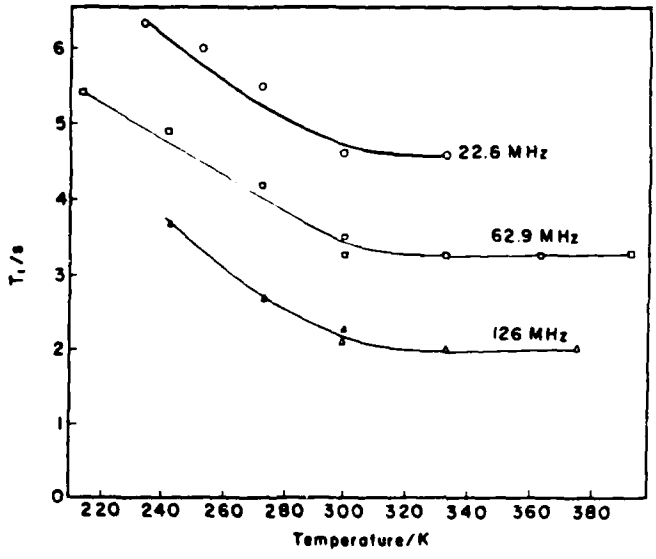

Fig. 2. Experimental T_1 data for $^{13}CO_2$ (5–7.5 atm) sorbed in BPAPC polymer as a function of temperature.

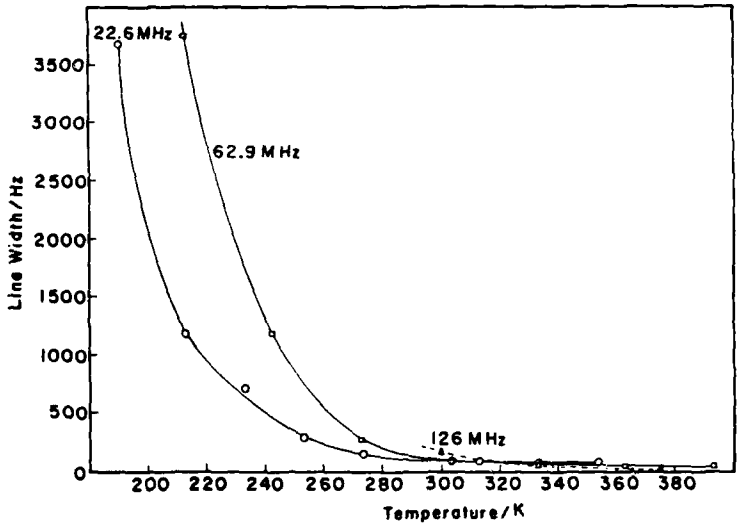

Fig. 3. Carbon-13 line widths of $^{13}CO_2$ sorbed in BPAPC polymer as a function of temperature.

Table 2. Nuclear Overhauser effect factors (NOEF) of sorbed $^{13}CO_2$ (6 atm) in BPAPC polymer block.

Larmor frequency	T/K	NOEF	Uncertainty in NOEF
22.6 MHz	213	1.55	0.07
	233	1.40	0.04
	253	1.33	0.03
	273	1.28	0.03
	300	1.25	0.03
	313	1.28	0.03
	333	1.28	0.03
	353	1.28	0.03
62.9 MHz	300	1.08	0.03
126 MHz	300	1.00	0.03

The observed carbon-13 line widths of $^{13}CO_2$ sorbed in BPAPC are plotted as a function of temperature in Fig. 3. As can be seen from Fig. 3, the line width broadens greatly when the temperature is lowered below 273 K. The striking line broadening indicates the presence of immobilized CO_2 molecules in the polymer at low temperatures. Approximate values of

Table 3. T_2 values calculated from the C-13 line widths of sorbed $^{13}CO_2$ (5 – 6 atm) in BPAPC polymer.

T/K	T_2 in s		
	22.6 MHz	62.9 MHz	126 MHz
190	1.08×10^{-4}		
213	3.13×10^{-4}	8.44×10^{-5}	
233	6.06×10^{-4}		
243		2.67×10^{-4}	
253	1.28×10^{-3}		
273	3.1×10^{-3}	1.27×10^{-3}	
300	4.5×10^{-3}		2.23×10^{-3}
313	4.9×10^{-3}	4.82×10^{-3}	
333	5.1×10^{-3}		8.6×10^{-3}
353	5.6×10^{-3}	1.22×10^{-2}	
363			
375		1.27×10^{-2}	1.77×10^{-2}

Table 4. Carbon-13 line widths and T_2 of sorbed $^{13}CO_2$ (6 atm) in deuterated BPAPC polymer strips at 22.6 MHz. (Deuterated BPAPC is 85% d_{14} and 15% d_6) (C-13 peak consists of three components: $^{13}CO_2$ gas peak, $^{13}CO_2$ sorbed-in-polymer peak, and a gap of about 66 Hz separating these two peaks).

T/K	Line width/Hz	T_2/s
188	870	3.66×10^{-4}
233	163	1.95×10^{-3}
253	123	2.59×10^{-3}
273	115	2.77×10^{-3}
313	96	3.32×10^{-3}

the spin-spin relaxation time T_2 are calculated from the line widths and shown in Table 3.

Measured carbon-13 line widths and calculated T_2 of sorbed $^{13}CO_2$ (6 atm) in deuterated BPAPC polymer strips at 22.6 MHz are listed in Table 4. The deuterated polymer contains about 90% ^2H and 10% ^1H for the hydrogens. At the Larmor frequency of 22.6 MHz, the C-13 peak consists of three components: $^{13}CO_2$ gas peak, $^{13}CO_2$ sorbed-in-polymer peak, and a gap of about 66 Hz between these two peaks. At temperatures of 188 and 233 K, the line widths of $^{13}CO_2$ in deuterated polymer are narrower than the corresponding line width of $^{13}CO_2$ in protonated polymer by a factor of about four. The observed NOEF of $^{13}CO_2$ in deuterated polymer is 1.00 in agreement with the expectation of greatly diminished dipole-dipole interaction.

Interpretation of data at 300 K

Our first step is to interpret the T_1 and NOE data at 300 K assuming the presence of only one type of CO_2 molecules in the glassy polymer. In the next section we shall present a "two-site model" for the purpose of interpreting the experimental data (T_1, NOE, and T_2) covering a wide temperature range.

We proceed to analyze the T_1 data assuming three relaxation mechanisms: spin rotation (SR), chemical shift anisotropy (CSA), and dipole-dipole (DD). The pertinent equations are:

$$1/T_1 = (1/T_1)_{SR} + (1/T_1)_{CSA} + (1/T_1)_{DD} \tag{1}$$

$$(1/T_1)_{SR} = (4IkT/3h^2)C_k^2\tau_{SR} \tag{2}$$

$$(1/T_1)_{CSR} = (2/15)^2(\omega)^2\tau_{CSA} \tag{3}$$

$$(1/T_1)_{DD} = (96\,\pi/1620)\gamma_C^2\gamma_H^2\,h^2(N_A/1000)([H]/bD_t)(J_0 + 3J_1 + 6J_2) \tag{4}$$

$$J_0 = J_0(\omega_H - \omega_C);\ J_1 = J_1(\omega);\ J_2 = J_2(\omega_H + \omega_C) \tag{5}$$

$$J(\omega) = (1 + 5z/8 + z^2/8)/(1 + z + z^2/2 + z^3/6 + 4z^4/81 + z^5/81 + z^6/648) \tag{6}$$

$$z = (2\,\omega\tau_t)^{1/2};\ \tau_t = h^2/D_t \tag{7}$$

$$(\mathrm{NOEF})_{DD} - 1 = (\gamma_C/\gamma_H)(6J_2 - J_0)/(J_0 + 3J_1 + 6J_2) \tag{8}$$

where the meanings of the symbols used are given in a glossary at the end of this paper. Eqs. (4) through (7) are those given by Polnaszek and Bryant [21] based on Freed's theory [22] and the main quantities of interest to us are three correlation times τ_{SR}, τ_{CSA}, and τ_t, as well as the translational diffusion constant D_t. The procedure for obtaining these quantities is illustrated below.

At 300 K and 22.6 MHz we have two experimental quantities: T_1 = 6.0 s and NOEF = 1.25. The percent of the dipole-dipole mechanism, %DD, operating under these conditions is given by

$$\%\mathrm{DD} = 100((\mathrm{NOEF}) - 1)/((\mathrm{NOEF})_{DD} - 1) = 100\ T_1/(T_1)_{DD}\,. \tag{9}$$

Since the functional relations for $(\mathrm{NOEF})_{DD}$ vs. τ_t and $(T_1)_{DD}$ vs. τ_t are known from Eqs. (8) and (4), respectively, one can solve for τ_t and then for %DD. Using this τ_t value one obtains the values of $(T_1)_{DD}$ at 22.6 MHz and at 126 MHz. Now one has two equations of the type,

$$(1/T_1)_{SR} + (1/T_1)_{CSA} = 1/T_1 - (1/T_1)_{DD}$$

or

$$(1/T_1)_{SR} + 3.025 \times 10^8\ \tau_{CSA} = 0.189 \text{ (at 22.6 MHz)} \tag{10}$$

and

$$(1/T_1)_{SR} + 9.332 \times 10^9\ \tau_{CSA} = 0.453 \text{ (at 126 MHz)}\,. \tag{11}$$

Table 5. Contributions of different mechanisms to the spin-lattice relaxation of $^{13}CO_2$ in BPAPC polymer at 300 K and 5 atm.

MHz	T_1/s	NOE	$(T_1)_{SR}$/s	$(T_1)_{CSA}$/s	$(T_1)_{DD}$/s	%DD	%CSA	%SR
22.6	4.6	1.25	5.6	113	35	13	4	83
62.9	3.5	1.08	5.2[a]	15	39	9	24	67
126	2.1	1.00	5.6	3.7	44	5	57	38

[a] This value should be 5.6 s instead of 5.2 s with a fitting error of about 6%.

Table 6. Correlation times for spin-rotation, CSA, and translational motion as well as estimated diffusion constants for $^{13}CO_2$ in BPAPC polymer at 300 K and 5 atm.

$$\tau_{SR} = 3.9 \times 10^{-13}\ \text{s} \qquad \tau_{CSA} = 2.9 \times 10^{-11}\ \text{s}$$
$$\tau_t = 1.2 \times 10^{-10}\ \text{s}$$
$$D_t = \begin{cases} 3.3 \times 10^{-6}\ \text{cm}^2/\text{s if } b = 0.2\ \text{nm} \\ 7.5 \times 10^{-6}\ \text{cm}^2/\text{s if } b = 0.3\ \text{nm} \end{cases}$$

From Eqs. (2), (10) and (11), two correlation times τ_{SR} and τ_{CSA} are obtained. Using these values of τ_t, τ_{SR} and τ_{CSA} we then test the consistency with the data at 62.9 MHz, specifically the value of τ_{SR}. The results at 300 K and 5–6 atm are summarized in Tables 5 and 6.

At high field the dominant source of relaxation is the chemical shift anisotropy mechanism yielding a correlation time of 2.9×10^{-11} s. At all frequencies, spin rotation is important and leads to a collision correlation time of 3.9×10^{-13} s. At the lowest frequency, a dipole-dipole contribution is observed which leads to a correlation time for translational diffusion of 1.2×10^{-10} s. This can be converted to a translational diffusion constant D_t if the distance of closest approach b is known. If we assume the value of b to fall in the range of 0.2 to 0.3 nm, then the value of D_t should fall in the range of $(3 \sim 8) \times 10^{-6}$ cm^2/s. In terms of both rotational and translational motions, these NMR results are indicative of very mobile CO_2.

Two-site model

The method of treatment outlined above to interpret the T_1 and NOE data seems to work fairly well at 300 K with a fitting error of about 5%. However, when the same method of treatment is applied to T_1 and NOE data obtained at low temperatures, it leads to large fitting errors. Moreover, the line widths or T_2 data are not included in the above treatment.

The probable presence of more than one type of CO_2 molecules sorbed in the polymer at low temperatures (273 – 190 K) is indicated by the observations that (i) T_1 values are still short (several seconds), but (ii) the line

widths increase greatly with the decrease of temperature (100 Hz to 3600 Hz at Larmor frequency of 22.6 MHz). The observation (i) points to a liquid like environment, while the observation (ii) points to a solid like environment of CO_2 molecules. Therefore, a two-site model will be developed to describe the temperature and field dependence of the observed data (T_1, NOE, and line widths).

As before we consider three relaxation mechanisms: SR relaxation, CSA relaxation, and intermolecular DD relaxation. The correlation time τ_{SR} in Eq. (2) and CSA correlation time τ_{CSA} in Eq. (3) are assumed to be given by Eqs. (12) and (13), respectively.

$$\tau_{SR} = I/f' \tag{12}$$

$$\tau_{CSA} = f'/6kT \tag{13}$$

where f' is the viscous retarding torque. These two equations will lead to the Hubbard relation [24]. In the non-extreme-narrowing limit Eq. (3) is generalized to

$$(1/T_1)_{CSA} = (2/15)\omega^2(\Delta\sigma)^2\tau_{CSA}/(1+\omega^2\tau_{CSA}^2). \tag{14}$$

The translational diffusion constant D_t in Eq. (7) may be written as:

$$D_t = kT/f \tag{15}$$

where f is the translational friction coefficient. We will assume that $f = f'$ and f has an Arrhenius temperature dependence:

$$f = f_0 \exp(\Delta H/RT) \tag{16}$$

where ΔH is the enthalpy of activation for the translational motion. Applying this relation to the SR correlation time, we can calculate its value at temperature T from its value at 300 K, designated as our reference temperature:

$$\tau_{SR}(T) = \tau_{SR}(300\text{ K})\exp(-(\Delta H/R)(300-T)/300\,T). \tag{17}$$

Similar equations can be written for the CSA correlation time and for the translational diffusion constant:

$$\tau_{CSA}(T) = \tau_{CSA}(300\text{ K})(300/T)\exp((\Delta H/R)(300-T)/300\,T) \tag{18}$$

$$D_t(T) = D_t(300\text{ K})(T/300)\exp(-(\Delta H/R)(300-T)/300\,T). \tag{19}$$

Our attempts to describe the temperature dependence of T_1, NOE, and line widths based on these equations have not been successful. We assume, therefore, that there are two types of CO_2 molecules with rapid interchange of the two types. There may actually be continuous distribution of CO_2 mobilities but, as a first approximation, we will treat the distribution as bimodal (i.e., two components).

If rapid exchange occurs the relevant expressions for T_1 and T_2 are

$$1/T_1 = P_A/T_{1A} + P_B/T_{1B} \quad \text{and} \quad 1/T_2 = P_A/T_{2A} + P_B/T_{2B} \tag{20}$$

where P_A and P_B are population fractions of the type A molecules and type B molecules, respectively. Each of the three relaxation mechanisms could contribute in the two environments. Let us consider the mobile environment to be A so that

$$1/T_{1A} = (1/T_{1A})_{SR} + (1/T_{1A})_{CSA} + (1/T_{1A})_{DD} . \tag{21}$$

Each of the equations developed before is applied to the three contributions. For the immobile environment, the comparable expression is

$$1/T_{1B} = (1/T_{1B})_{SR} + (1/T_{1B})_{CSA} + (1/T_{1B})_{DD} . \tag{22}$$

However, since the slowly moving molecules do not have significant SR relaxation contributions, the term $(1/T_{1B})_{SR}$ can be omitted.

$$1/T_{1B} = (1/T_{1B})_{CSA} + (1/T_{1B})_{DD} . \tag{22'}$$

Now let us turn to the T_2 expression of Eq. (20). At high temperatures (313−393 K), the observed T_2 is less than 100 Hz and is dominated by static field inhomogeneity arising from the complex nature of the sample (gas sorbed in strips of polymer). The key experimental effect to account for is the broadening from 100 Hz at 273 K to 3600 Hz at 190 K. If the correlation times developed at 300 K to interpret T_1 and the NOE are indicative of the liquid like environment, then they contribute essentially nothing to the low temperature line widths even if they slow by an order of magnitude. The low temperature line widths must be dominated by the immobile species. We have, therefore,

$$1/T_2 \approx P_B/T_{2B} \quad \text{and} \quad 1/T_{2B} = (1/T_{2B})_{CSA} + (1/T_{2B})_{DD} . \tag{23}$$

The relevant T_2 expressions for the two relaxation mechanisms are

$$(1/T_2)_{CSA} = (1/45)\omega^2(\Delta\sigma)^2(3\,\tau_{CSA}/(1 + \omega^2\tau_{CSA}^2) + 4\,\tau_{CSA}) \tag{24}$$

and

$$(1/T_2)_{DD} = \gamma_I^2\gamma_S^2\hbar^2 S(S+1)(32\,\pi/405)(N_A/1000)[H]\,\{2J_0(O) + 0.5J_0\,(\omega_I - \omega_S) + 1.5\,J_1(\omega_I) + 3J_1(\omega_S) + 3J_2(\omega_I + \omega_S)\} . \tag{25}$$

With regard to the translational diffusion relaxation, careful considerations are required, since the translational diffusion is a mechanism for exchange between CO_2 in an immobile environment (B) and CO_2 in the more mobile environment (A). For conceptual convenience we identify A as "dissolved" (D) environment and B as "Langmuir" (L) environment of the dual-mode model [5, 23]. If we assume these environments to have a distance scale of Angstroms, then there should be four possible types of translational diffusions:

(1) Translation from a dissolved environment to another dissolved environment with a correlation time $\tau_{DD} = b^2/D_{DD}$.

(2) Translation from a Langmuir environment to another Langmuir environment with a correlation time $\tau_{LL} = b^2/D_{LL}$.

(3) Translation from a Langmuir environment to a dissolved environment with a correlation time $\tau_{LD} = b^2/D_{LD}$.

(4) Translation from a dissolved environment to a Langmuir environment with a correlation time $\tau_{DL} = b^2/D_{DL}$.

The principle of microscopic reversibility requires that

$$P_D/\tau_{DL} = P_L/\tau_{LD} \quad \text{or} \quad P_D/P_L = \tau_{DL}/\tau_{LD} . \tag{26}$$

We need, therefore, three correlation times, say, τ_{DD}, τ_{LL}, and τ_{LD}. The Arrhenius factor for translational friction coefficient ΔH which appeared in Eq. (19) also requires further specifications: ΔH_{DD}, ΔH_{LL}, and ΔH_{LD}. We assume that ΔH_{LD}, the Arrhenius factor for the Langmuir to dissolved process, is given by the mean:

$$\Delta H_{LD} = (\Delta H_{LL} + \Delta H_{DD})/2. \tag{27}$$

Thus, only two Arrhenius factors, ΔH_{LL} and ΔH_{DD} are needed.

The translational relaxation produced by each process should be weighted by a population factor: the population of the site left multiplied by the population of the site entered. Therefore, the τ_{LL} term should be weighted by P_L^2, the τ_{DD} term by P_D^2, and the τ_{LD} term by $P_L P_D$. The dipolar relaxation associated with exchange between the dissolved and Langmuir environments requires new term to be added to the expressions for T_1, T_2, and NOE, because the exchange term is associated with neither of the two environments.

$$1/T_{1D} = P_D/(T_{1CSA})_D + P_D/(T_{1SR})_D + P_D^2/(T_{1DD})_D \tag{28}$$

$$1/T_{1L} = P_L/(T_{1CSA})_L + P_L^2/(T_{1DD})_L \tag{29}$$

$$1/T_{1ex} = P_D(1 - P_D)/(T_{1DD})_{DL} + (1 - P_D)P_D/(T_{1DD})_{LD} \tag{30}$$

$$1/T_1 = 1/T_{1D} + 1/T_{1L} + 1/T_{1ex}. \tag{31}$$

The equations for T_2 are quite analogous to the equations for T_1 given above. To calculate the NOE we will use the following general formula:

$$\text{NOEF} - 1 = (\gamma_H/\gamma_C)\,(\text{Dipolar rate})\,/\,(\text{Total rate})\,((6J_2 - J_0)\,/\,(J_0 + 3J_1 + 6J_2)) \tag{32}$$

where

$$\text{Dipolar rate} = P_D^2/(T_{1DD})_D + P_L^2/(T_{1DD})_L + P_D(1 - P_D)((1/T_{1DD})_{LD} + (1/T_{1DD})_{DL}) \tag{33}$$

Table 7. Population distribution according to the dual-model model (obtained by an extrapolation of the temperature dependence reported by Chan and Paul [25] and on the assumption that the dependence is parallel to that of PET given by Koros [23]).

T/K	P_D	P_L
173	0.15	0.85
193	0.16	0.84
213	0.18	0.82
233	0.23	0.77
253	0.30	0.70
273	0.38	0.62
293	0.47	0.53
313	0.65	0.35
333	0.80	0.20
353	0.88	0.12
373	0.94	0.06
393	0.96	0.04

Table 8. Parameters at 300 K used for the two-site model calculations.

τ_{SR}(dissolved)	$= 1.7 \times 10^{-13}$ s	
τ_{CSA}(dissolved)	$= 5 \times 10^{-11}$ s	τ_{CSA}(Langmuir) $= 5 \times 10^{-8}$ s
$D_t(D-D) = D_{DD}$	$= 7 \times 10^{-7}$ cm^2/s	$\Delta H_{DD} = 6000$ J/mol
$D_t(D-L) = D_{DL}$	$= 4.5 \times 10^{-7}$/s	$\Delta H_{LL} = 12000$ J/mol
$D_t(L-L) = D_{LL}$	$= 3 \times 10^{-11}$ cm^2/s	$b = 3.2 \times 10^{-8}$ cm

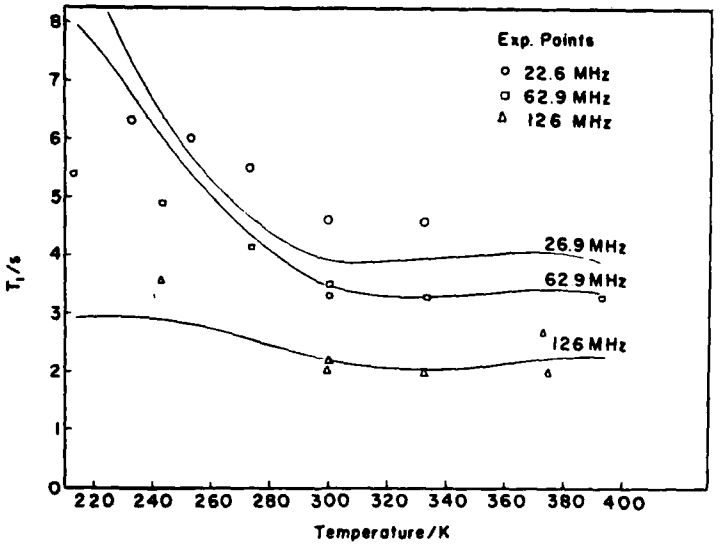

Fig. 4. Temperature dependence of T_1. Comparison of calculated results based on the two-site model and experimental values.

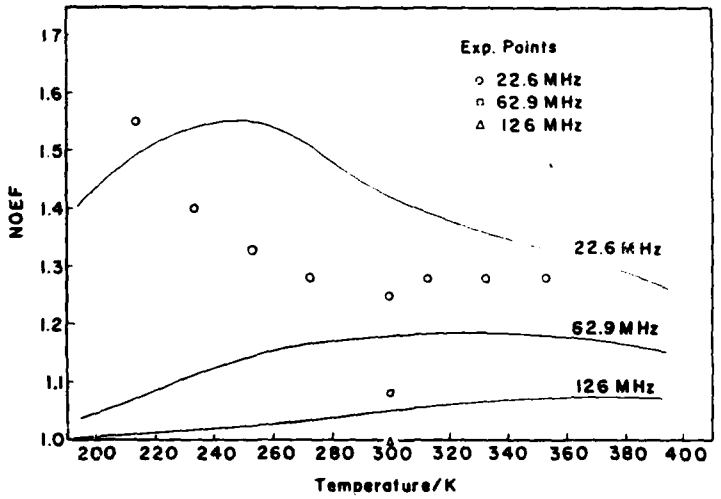

Fig. 5. Temperature dependence on NOE. Comparison of calculated results based on the two-site model and experimental values.

and "Total rate" is given by Eq. (31). To calculate the values of J's in Eq. (32) we define $JT(i)$ such that

$$JT(i) = P_D^2 J_D^2(i) + P_L^2 J_L^2(i) + P_D P_L (J_{DL}(i) + J_{LD}(i)) \tag{34}$$

in which

$$J_2 = JT(2),\ J_1 = JT(1),\ \text{and}\ J_0 = JT(0)\ .$$

We now report the results of our calculations using the two-site model. The population distribution between the Langmuir and the dissolved species is obtained by extrapolating the data of Chan and Paul [25] based on the dual-mode model and is tabulated in Table 7. Nine parameters at 300 K are employed to fit the experimental data; these parameters are listed in Table 8. The results of our computer calculations are presented and compared with the experimental data in Figs. 4–6. As can be seen from the figures, the agreement of the calculated results and experimental data is good for NOE (with fitting errors of 10% or less), good for T_1 (with fitting errors of 20% or less), and fair for T_2 (off by a factor of between 2 and 10). It should be remembered that our T_2 data are derived from the line widths and not determined directly from the CPMG method. We believe that the parameters can be chosen more carefully to improve the fit. In conclusion, the model seems to be able to describe the temperature and field dependence of the observed T_1, NOE, and T_2 data semi-quantitatively.

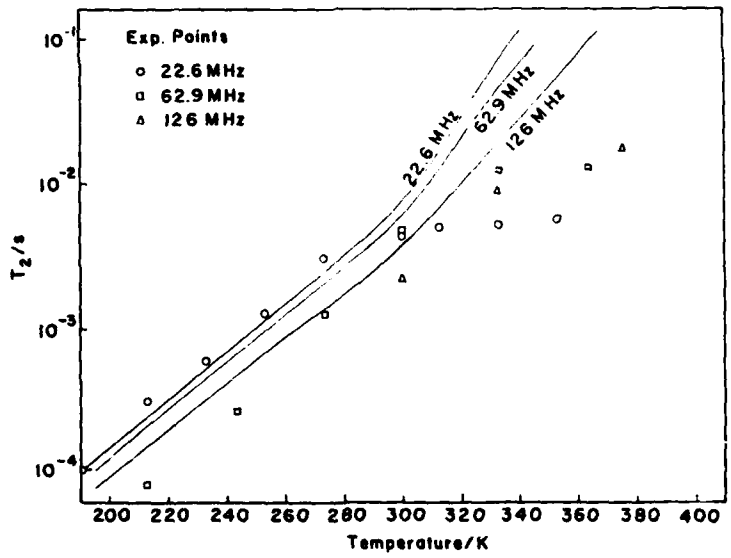

Fig. 6. Temperature dependence of T_2. Comparison of calculated results based on the two-site model and experimental values derived from line widths.

Discussion

The parameters generated by the two-site model are of interest, since they characterize the molecular dynamics of CO_2 sorbed in BPAPC polymer. The values of parameters (τ_{SR}, τ_{CSA}, and D_t) determined earlier and given in Table 6 are not greatly different from those listed in Table 8 and specified as "Dissolved" and "Dissolved – Dissolved" ("D – D") of the two-site model. At 300 K the population of CO_2 molecules in the mobile environment consists only about 53% of the total, but this 53% population dominates and determines the experimental T_1, T_2, and NOE data. The CSA correlation time of CO_2 in the immobile environment is 5×10^{-8} s, which is about 1000 times larger than the corresponding quantity (5.0×10^{-11} s) in the mobile environment.

The translational diffusion constant D_t in different environments are of particular interest. The value of D_t in the mobile environment (7×10^{-7} cm^2/s) is about 2.3×10^4 times greater than the corresponding value in the immobile environment (3×10^{-11} cm^2/s). For the process of transfering sorbed CO_2 from a mobile environment to an immobile environment, the value of D_{DL} is 4.5×10^{-7} cm^2/s which is greater than the geometric mean of the other two diffusion constants. In their well-known treatment Koros and Paul [5, 23] considered two diffusion constants (corresponding to our D_{DD} and D_{LL}), but did not include the third diffusion

constant D_{LD}. Their values of diffusion constants for CO_2 in BPAPC seem to change slightly from one publication to another, and one of the recent papers gives $D_{DD} = 5.15 \times 10^{-8}$ and $D_{LL} = 5.07 \times 10^{-9}$ cm^2/s at 35 C [26].

If we evaluate the mean diffusion constant D by the expression,

$$D = P_D^2 D_{DD} + P_D P_L D_{DL} + P_L P_D D_{LD} + P_L^2 D_{LL},$$

we obtain $D = 4.38 \times 10^{-7}$ cm^2/s. This value is not too far from the reported diffusion constant ($D_{eff} = 3 \times 10^{-8}$ cm^2/s at 35 C) obtained by macroscopic measurements, e.g., by measurement of CO_2 permeation through polymer membranes [1, 5, 23].

Concerning the chemical nature of the mobile and immobile environments for the sorbed CO_2 in BPAPC polymer, we would like to make the following suggestions. When a sorbed CO_2 molecule is surrounded by carbonate groups of the polymer and engages in intermolecular interaction of carbon-to-oxygen bonds, it may be in an immobile environment. When a sorbed CO_2 molecule is surrounded by methyl or phenylene groups and engages in weaker intermolecular interaction, it may be in a mobile environment.

The two-site (or two-environment) model is an over-simplified approach and more elaborate multi-site model may be necessary to describe the detailed molecular dynamics of sorbed gas in the glassy polymer.

In this paper we have focused our attention on the temperature and field dependence of the NMR data of sorbed $^{13}CO_2$ under 5–6 atm in BPAPC. We have not treated the pressure or concentration dependence of the NMR data in this system. That will be a subject of our future investigations. We assume that, with a larger data base and more sophisticated simulation procedures, the model parameters can be determined with a greater level of confidence and precision.

Acknowledgement

We gratefully acknowledge the assistance of the staff at Yale University Chemistry Department Instrumentation Center for use of their Bruker WM-500 NMR spectrometer. This research was carried out with a partial support of the NSF Grant DMR-8108679 and of the U.S. Army Research Office Grant DAAG 29-85-K0126.

Glossary of symbols

T_1:	Experimental value of the spin-lattice relaxation time
$(1/T_1)_{SR}$:	Relaxation rate by spin rotation mechanism
$(1/T_1)_{CSA}$:	Relaxation rate by chemical shift anisotropy mechanism
$(1/T_1)_{DD}$:	Relaxation rate by dipole-dipole interaction mechanism
I:	Moment of inertia of CO_2
k:	Boltzmann constant

T:	Temperature on Kelvin
h:	Planck constant divided by 2π
C_k:	Spin-rotation coupling constant (-3.605×10^4 Hz)[*1] for CO_2
ω:	Larmor angular frequencies
$\Delta\sigma = \sigma_\parallel - \sigma_\perp$:	Difference in shielding (or chemical shift) along and perpendicular to the symmetry axis of CO_2 (-3.35×10^{-4}) (ref.)[a]
τ_{SR}:	Spin-rotation (or angular momentum) correlation time
τ_{CSA}:	Chemical shift-anisotropy (or rotational) correlation time
τ_t:	Correlation time for translational motion
γ_C:	Gyromagnetic ratio for carbon-13 nucleus
γ_H:	Gyromagnetic ratio for proton
N_A:	Avogadro's number
[H]:	Concentration of protons in the polymer
b:	Distance of the closest approach between ^{13}C and protons
D_t:	Diffusion constant for the translational motion of $^{13}CO_2$
$J(\omega)$:	Spectral density function
$(NOE)_{DD}$:	Nuclear Overhauser effect when the relaxation mechanism is 100% dipole-dipole
NOE:	experimental value of the nuclear Overhauser effect

[a] Ref.: Beeler, Orendt, Grant, Cutts, Michl, Zilm, Downing, Facelli, Schindler and Kutzelnigg, J. Am. Chem. Soc. **106** (1984) 7672.

References

1. See, for example, *Industrial Gas Separations*, ed. T. E. Whyte, Jr., C. M. Yon and E. H. Wagener, Acta Chem. Scand. Symp. Ser. **223** (1983).
2. P. Masi and D. R. Paul, J. Membrane Sci. **12** (1982) 137.
3. P. Meares, J. Am. Chem. Soc. **76** (1954) 3415.
4. R. M. Barrer, J. A. Barrie and J. Slater, J. Polym. Sci. **27** (1958) 177.
5. D. R. Paul and W. J. Koros, J. Polym. Sci. Polym. Phys. Ed. **14** (1976) 675.
6. D. R. Paul, Ber. Bunsenges. Phys. Chem. **83** (1979) 294.
7. R. T. Chern, W. J. Koros, E. S. Sanders, S. H. Chen and H. B. Hopfenberg, in: *Industrial Gas Separation* (see ref. 1), pp. 47–73 and the references cited therein.
8. D. Raucher and M. D. Sefcik, in: *Industrial Gas Separations* (see ref. 1), p. 111.
9. R. J. Pace and A. Datyner, J. Polym. Sci. Polym. Phys. Ed. **17** (1979) 437, 453 and 465.
10. J. H. Wendorff and E. W. Fischer, Kolloid-Z. Z. Polym. **251** (1973) 876.
11. J. J. Curro and R. J. Roe, J. Polym. Phys. Ed. **21** (1983) 1785.
12. R. A. Assink, J. Polym. Sci. Polym. Phys. Ed. **13** (1975) 1665.
13. M. D. Sefcik, J. Schaefer, F. L. May, D. Raucher and S. M. Dub, J. Polym. Sci. Polym. Phys. Ed. **21** (1983) 1041.
14. M. D. Sefcik and J. Schaefer, J. Polym. Sci. Polym. Phys. Ed. **21** (1983) 1055.
15. A. K. Roy, A. A. Jones and P. T. Inglefield, Macromolecules **19** (1986) 1356.
16. A. A. Jones, Macromolecules **18** (1985) 902.
17. J. J. Connolly, E. Gordon and A. A. Jones, Macromolecules **17** (1984) 722.
18. J. J. Connolly and A. A. Jones, Macromolecules **18** (1985) 906.

19. P. T. Inglefield, R. M. Amici, J. F. O'Gara, C.-C. Hung and A. A. Jones, Macromolecules **16** (1983) 1552.
20. R. A. Komoroski, J. Maxfield and L. Mandelkern, Macromolecules **10** (1977) 545.
21. C. F. Polnaszek and R. G. Bryant, J. Chem. Phys. **81** (1984) 4038.
22. J. H. Freed, J. Chem. Phys. **68** (1978) 4043.
23. W. J. Koros, Ph.D. Thesis, University of Texas at Austin, 1977.
24. P. S. Hubbard, Phys. Rev. **131** (1963) 1155; W. T. Huntress, J. Chem. Phys. **48** (1968) 3524.
25. Chan and Paul, Polym. Eng. Sci. **20** (1980) 87.
26. S. M. Jordan, W. J. Koros and G. K. Fleming, "The effects of CO_2 exposure on pure and mixed gas permeation behavior: Comparison of glassy polycarbonate and silicone rubber", submitted for publication in 1986.

TWO-SITE MODEL FOR THE RELAXATION OF $^{13}CO_2$ SORBED IN GLASSY POLYCARBONATE

Edward J. Cain, Alan A. Jones, Paul T. Inglefield
and Wen-Yang Wen
Department of Chemistry
Worcester, Massachusetts 01610

Introduction:

There are few spectroscopic investigations of the mobility of gases sorbed in polymers though there is a great deal of interest in the permeation properties of polymeric films.[1-2] The solubility and permeability of gases in polymers has been studied and has led to the widely accepted dual mode model.[3-7] This model assumes the presence of two types of sorbed gas in glassy polymers: a Langmuir sorbed, immobile species and a Henrys Law, mobile species. The purpose of this study is to seek molecular level evidence from NMR spectroscopy for the presence of two types of CO_2 in glassy polycarbonate.

Experimental:

Carbon-13 labeled CO_2 is sorbed into a pellet of glassy polycarbonate at a fixed pressure contained in a 10 mm NMR tube. The gas pressure is maintained in the NMR tube either by sealing the tube or by closing a stopcock. Spin-lattice relaxation times (T_1), nuclear Overhauser enhancements (NOE) and line widths of the $^{13}CO_2$ are determined as a function of temperature and Larmor frequency. The results are presented in Figures 1-3.

Interpretation:

Three relaxation mechanisms contribute to carbon-13 relaxation of the sorbed CO_2. At low Larmor frequency (22 MHz), the primary mechanisms are spin-rotation relaxation and intermolecular dipole-dipole relaxation between the carbon-13 of the gas and the protons of the polymer. At higher frequencies (62 and 126 MHz) an additional mechanism comes into play, relaxation by chemical shift anisotropy.

If only a single type of CO_2 is assumed to be present, it is not possible to interpret the T_1, NOE, and line width data as a function of temperature and Larmor frequency. In particular, the line widths are too broad to be consistent with the T_1's under the assumption of a single dynamical species. The second step in the interpretation is to parallel the dual mode model and assume the presence of two sorbed species of differing mobility. Since only a single NMR resonance is observed even in the T_1 experiment at various delay times, it is further assumed that the two species are undergoing rapid exchange on the NMR time scale. The mechanism of exchange is translational diffusion since the immobile Langmuir species is imagined to involve certain sites in the glassy polymer matrix while the mobile Henry's Law species is imagined to involve other sites. The two types of sites are spatially separated and the gas molecules are exchanged between the sites by translational diffusion. Since there are two types of sites, there are four possible diffusion constants, though the four are interrelated through the populations of the two sites and the concept of microreversibility.

The relaxation data was fit by a non-linear least squares procedure and the fits are shown in Figures 1-3. The parameters of the fit are listed below.

τ_{SR} (dissolved) = dissolved spin-rotation correlation time = 2.7×10^{-13}s

τ_{CSA} (dissolved) = dissolved rotational correlation time = 4.5×10^{-11}s

τ_{CSA} (Langmuir) = Langmuir rotational correlation time = 5.7×10^{-8}

D_{HH} = Henry's to Henry's diffusion = 4.1×10^{-6}cm^2/s

D_{HL} = Henry's to Langmuir diffusion = 4.7×10^{-6}cm^2/s

D_{LH} = Langmuir to Henry's diffusion = 7.0×10^{-6}cm^2/s

D_{LL} = Langmuir to Langmuir diffusion = 4.5×10^{-11}cm^2/s

ΔH_{HH} = 1.3 kJ/mol $\quad$ ΔH_{HL} = 3.2 kJ/mol

ΔH_{LH} = 3.3 kJ/mol $\quad$ ΔH_{LL} = 5.2 kJ/mol

b = distance of closest approach = 1.7×10^{-8}cm

Discussion:

The correlation times for rotational motion and collisions for CO_2 in the Henry's sites is comparable to that of low molecular weight liquid[8] such as CS_2. The correlation time for collisions in the Langmuir site is too short to be determined from NMR data but the correlation time for rotation is much longer than a low molecular weight liquid and is in fact comparable to that of a polymer rubber.

The diffusion constants cover a very wide range with the value associated with Henry's sites comparable to a low molecular weight liquid while the time associated with Langmuir sites is typical of a solid. The diffusion constants determined here from NMR data span a greater range than those determined from permeability data though the range includes the permeability values. The diffusion constants are derived from the intermolecular dipole-dipole contributions to relaxation and reflect diffusion over very short distances. This microscopic view of the NMR experiment may well influence the determination of diffusion constants as may the two-site model with the inclusion of rapid exchange by diffusion.

A more reasonable view of diffusion in a polymeric glass might well allow for a wide range of mobilities as is observed in other experiments on molecular dynamics in these systems.[9-10] A two-site model is frequently the simplest approach to initially approximate a distribution but only a large data base will allow for a sound determination of the character of the distribution.

Acknowledgements:

Acknowledgement is made to the donors of the Petroleum Research Fund, administered by the American Chemical Society, for support of this research.

References:

1. R.A. Assink, J. Polym. Sci. Polym. Phys. Ed. (1975) 13, 1665.

2. M.D. Sefcik, J. Schaefer, J.A.E. Desa and W.B. Yelon, Polym. Prepr., Div. Poly. Chem., Am. Chem. Soc. (1983) 24(1), 85.

3. P. Meares, J. Am. Chem. Soc. (1954) 76, 3415.

4. R.M. Barrer, J.A. Barrie and J. Slater, J. Polym. Sci. (1958) 27, 177.

5. D.R. Paul and W.J. Koros, J. Polym. Sci. Polym. Phys. Ed. (1976) 14, 675.

6. D.R. Paul, Ber. Bunsenges, Phys. Chem. (1979) 83, 294.

7. R.T. Chern, W.J. Koros, E.S. Sanders, S.H. Chen and H.B. Hopfenberg, "Industrial Gas Separations," ed. T.E. Whyte, Jr., C.M. Yon and E.H. Wagener, ACS Symp. Ser. (1983) 223, 47.

8. H.W. Spiess, D. Schweitzer, U. Haeberlin and K.H. Hausser, J. Magn. Res. (1971) 5, 101.

9. H.W. Spiess, Colloid and Polymer Sci. (1983) 261, 193.

10. A.K. Roy, A.A. Jones and P.T. Inglefield, Macromolecules (1986) 19, 1356.

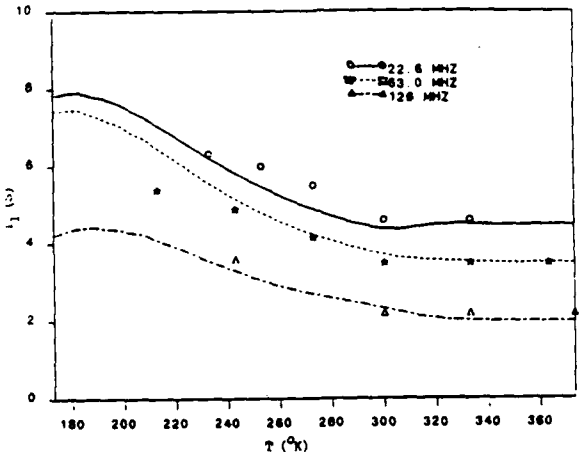

Figure 1: Temperature Dependence of T_1. Experimental values are compared with the fit based on the two-site model.

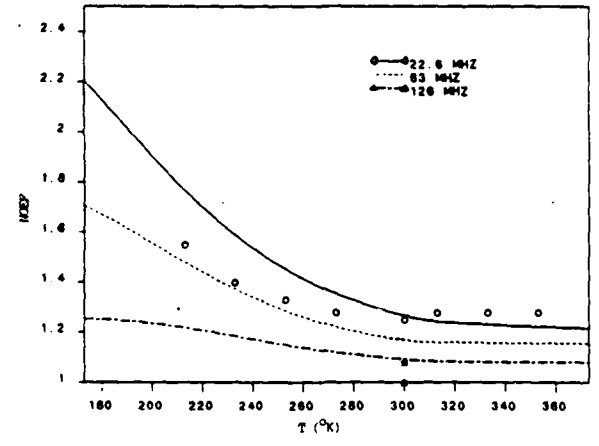

Figure 2: Temperature Dependence of NOE. Comparison of experimental values are compared with the fit based on the two-site model.

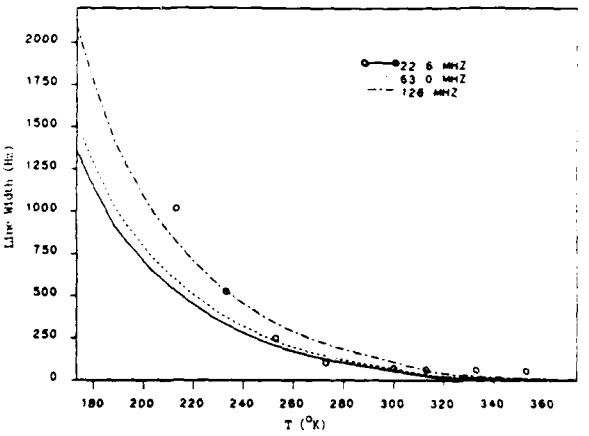

Figure 3: Temperature Dependence with the Line Width. Experimental values are compared with the fit based on the two-site model.

MOTION OF TRIOCTYL PHOSPHATE IN A PPO POLYSTYRENE BLEND BY ^{31}P LINE SHAPE

Paul T. Inglefield, Alan A. Jones and Bonnie J. Cauley
Department of Chemistry
Clark University
Worcester, Massachusetts 01610

Roger P. Kambour
Polymer Physics and Engineering
General Electric Company
Research and Development Center
Schnectady, New York 12301

Introduction:

The glass transition and modulus of a glassy, amorphous polymer can often be lowered by the addition of a low molecular weight diluent.[1-4] The commonly proposed mode by which this process of plasticization occurs is an increase in the rate or amplitude of molecular level motion. The presence of motion at the level of the chemical structure of the constituents of a glass can be followed by solid state NMR.[5-7] In particular, solid state line shape collapse can often be used to determine the rate, amplitude and geometry of particular motions defined with respect to the chemical structure. In this report, the motion of the diluent itself will be monitored for consideration relative to the mechanical and thermal properties[8] of the modified polymeric glass.

The polymer system selected here is a blend of polystyrene (PS) and poly(phenylene oxide) (PPO) where each component is present in equal amounts by weight. To this polymer blend, two diluents will be added at the level of 20% by weight. The first is trioctyl phosphate (TOP) and the second is triphenyl phosphate (TPP). The mobility of these diluents will be followed by phosphorus-31 chemical shift anisotropy line shape collapse. The glass transition, Young's Modulus, and dynamic mechanical spectrum have been determined in a separate study.[8] Of special interest in the dynamic mechanical spectrum is the observation that no subglass transition loss peak is present[9] until the diluent TOP is added.

Experimental:

Preparation of the ternary blends and the associated mechanical and thermal properties are reported elsewhere.[8] The ^{31}P line shapes were measured on a Bruker WM-250 at a frequency of 101 MHz and a sweep width of 100 kHz. The spectra are shown in Figures 1 and 2 as a function of temperature.

Interpretation:

At low temperatures, both the phosphorus line shapes are those observed for rigid polycrystalline systems which is indicative of little motion. As temperature is raised in the TOP system, line narrowing is apparent at temperatures beginning at -40 to -20°C. By the time the temperature approaches the glass transition of the ternary blend near 70°C, the line shape is primarily a fairly narrow Lorentzian line indicative of nearly isotropic motion. Thus as the temperature is swept over a 100 degree range from -40 to +60°C the diluent goes from no motion to rapid, isotropic motion on the NMR time scale.

Several other features of the line shape collapse and diluent mobility can also be deduced. Line shape collapse occurs over a very broad temperature range in this system. At temperatures in the midst of the collapse process, the observed line shape consists of a broad component plus a narrow component. The broad component is close to the rigid line shape observed at low temperatures and the narrow component is close to the Lorentzian line shape observed at high temperatures. This is an indication of motional heterogeneity.[5-7] The broad component is associated with rather immobile phosphate ester molecules located in spatial regions of the glass where intermolecular interactions restrict motion. The narrow component is associated with rather mobile phosphate ester molecules located in spatial regions of the glass where intermolecular interactions are weak and motion is facile. This spatial heterogeneity of the glass which leads to a dynamic heterogeneity exists on a molecular distance scale.

This description of motion and the spectra themselves are apparently bimodal. However, the bimodal characteristic is probably superficial and the more correct description involves a broad distribution of mobilities associated with a broad distribution of intermolecular environments. The distribution of mobilities can be more directly observed in the dynamic mechanical response of the material which shows a broad loss peak centered at -60°C. It is a reasonable assumption to link this mechanical loss peak to the rotation[10-13] of the diluent determined by NMR since this loss peak is only present upon addition of the diluent. However, a quantitative link through a simultaneous interpretation of the line shape collapse and the position and breadth of the mechanical loss peak with a single correlation function would support the assertion of a relationship.[7,14] A fractional exponential correlation function will be used to try to develop the common interpretational base.

Although the motion of the diluent is isotropic, there is still two possible modes of rotation. They are jump diffusion and Brownian diffusion and they lead to different line shape collapse patterns.[15] These patterns have been predicted for the case of motion characterized by a single correlation time and we are now trying to extend the predictions for the case of a distribution of correlation times for comparison with the observed spectra. It remains to be seen whether the distinction between jump diffusion and Brownian diffusion can still be observed in the presence of a broad distribution of correlation times.

The blends produced by the two different diluents, TOP and TPP, have very nearly the same glass transition temperature. However, the temperature at which rotation of the diluent commences is quite different as can be determined by comparing Figures 1 and 2. The rotational motion of TPP is substantially slower and a temperature increase of about 40° is required to produce about the same level of line shape collapse as is observed for TOP. As was mentioned, there is no correlation of this shift in rate of motion with the glass transition temperature of the ternary blends However, a correlation between the glass transition temperature of the pure diluent and the onset of rotation was noted in the mechanical and thermal studies[8] of these materials and that view is decisively reinforced by the NMR data.

Acknowledgement:

This research was carried out in part with support from the U.S. Army Research Office Grant DAAG2985-K0126 and National Science Foundation Grant DMR-8619380.

References:

1. W.J. Jackson, Jr. and J.R. Caldwell, Adv. Chem. Ser. (1965) 48, 185.

2. W.J. Jackson and J.R. Caldwell, J. Polym. Sci. (1967) 11, 211 and 227.

3. R.E. Robertson and C.W. Joynson, J. Appl. Polym. Sci. (1972) 16, 733.

4. L.M. Robeson and J.A. Faucher, J. Polym. Sci. B (1969) 7, 35.

6. H.W. Spiess, Colloid Polym. Sci. (1983) 261, 193.

7. H.W. Spiess, in Advances in Polymer Science, Vol. 66, H.H. Kausch and H.G. Zachmann, eds., Springer-Verlag, Berlin (1985).

8. A.K. Roy, A.A. Jones and P.T. Inglefield, Macromolecules (1986) 19, 1356.

9. R.P. Kambour, J.M. Kelly and B.J. McKinley, J. Polym. Sci. Polym. Phys. Ed., submitted.

10. A.F. Yee, Polym. Eng. and Sci. (1977) 17, 213.

11. S.E.B. Petrie, R.S. Moore and J.R. Flick, J. Appl. Phys. (1972) 43, 4318.

12. P.J. Haina and G. Williams, Polymer (1975) 16, 725.

13. E.W. Fischer, G.P. Hellman, H.W. Spiess, F.J. Horth, U. Ecarius and M. Wehrle, Makrom. Chem. Suppl. (1985) 12, 189.

14. K. Adachi, M. Hattori and Y. Ishida, J. Polym. Sci. Polym. Phys. Ed. (1977) 15, 693.

15. A.A. Jones, J.F. O'Gara, P.T. Inglefield, J.T. Bendler, A.F. Yee and K. Ngai, Macromolecules (1983) 16, 658.

16. H. Sillescu, J. Chem. Phys. (1971) 54, 2110.

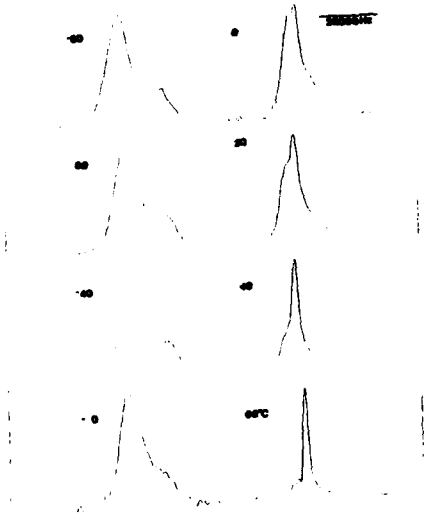

Figure 1: ^{31}P line shapes of the three component system: PPO/PS/TOP as a function of temperature.

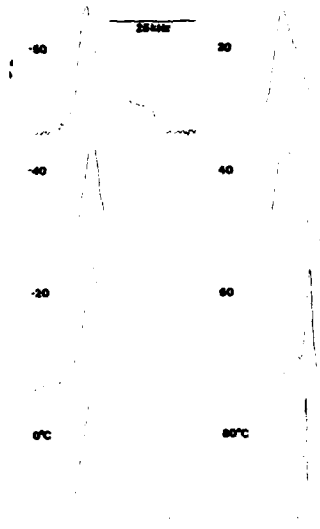

Figure 2: ^{31}P line shapes of the three component system: PPO/PS/TPP as function of temperature.

Spectroscopic Studies of Diluent Motion in Glassy Plasticized Blends

Roger P. Kambour, John M. Kelly and Barbara J. McKinley
Polymer Physics and Engineering
General Electric Corporate Research and Development Center
Schenectady, New York 12301

Bonnie J. Cauley, Paul T. Inglefield and **Alan Anthony Jones**
Jeppson Laboratory
Department of Chemistry
Clark University
Worcester, Massachusetts 01610

ABSTRACT

No sub-glass transition mechanical loss peaks are observed in 50-50 blends of poly(2,6-dimethyl-1,4-phenylene oxide) and polystyrene. However, if trioctyl phosphate is added to the blend the modulus lowers and a broad low temperature loss peak appears. Non-spinning phosphorous line shapes were observed to determine if the diluent itself were moving in the glassy matrix which is clearly the case. At low temperatures a typical axially symmetric line shape is observed which evolves to a narrow line just below the glass transition of the three component system. The pattern of the collapse appears to take the form of a shift in population from nearly immobile diluent to fairly mobile diluent. This pattern of collapse can be associated with broad distribution of correlation times. The geometric character of the motion of the mobile diluent is apparently isotropic rotation.

The mechanical properties of bulk amorphous polymers depend on the local chain motions present and in turn the local motions reflect the chemical structure of the repeat unit of the polymer chain. The motions are also influenced strongly by intermolecular interactions between chains so that in the glassy state the apparent activation energy of a given motion may be much higher than that expected for the same motion in an isolated polymer chain[1]. Two general strategies can be followed to control properties of amorphous polymers without changing the morphology. First, the local motions present can be changed by modifications of the chemical structure of the repeat unit; and second, intermolecular interactions can be modified by the addition of a second type of molecule to the bulk polymer. In the latter case, the second component could either be a small molecule diluent or another polymer. The addition of a second type of polymer not only modifies the intermolecular interactions but also introduces a new repeat unit structure which may have its own set of local motions distinct from the host polymer.

A recent survey[2] of the mechanical properties of a set of plasticized blends has revealed a strong dependence of these properties on the T_g of the diluent, independent of its effect on the polymer T_g. In this communication we report the mechanical data for a particular diluent and a nuclear magnetic resonance study of the microscopic mobility of the diluent in the blend.

The general behavior of low molecular weight diluents in glassy polymers is often categorized as either plasticization or anticplasticization[3-6]. Plasticizers are diluents which lower the glass

transition and lower the modulus. Antiplasticizers also lower the glass transition but not necessarily the modulus. One mechanism for antiplasticization is suppression of local motions and by contrast a mechanism for plasticization would be by increase in either the rate or the amplitude of local chain motion. An increase in the rate or amplitude of motion could be produced through a reduction in intermolecular interactions. That is, the diluent molecule may act as a lubricant, reducing interchain interactions and allowing for more chain motion[7]. The results presented below indicate that the behavior of diluents is more complex and includes possibilities not contained in this brief summary.

The polymer system reported here is a combination of polystyrene (PS) and poly(2,6-dimethyl-1,4-phenylene ether) (PPE) where each component is present in equal amounts by weight. These two polymers are miscible over the whole composition range[8] though only the one composition mentioned will be used as the basic polymeric component. Moreover neither resin exhibits substantial secondary motions at low temperatures[9]. The diluent blended with the two polymers is trioctyl phosphate which is particularly convenient for NMR studies since the phosphorous chemical shift anisotropy line shape can be used to monitor the motion of the diluent. No magic angle spinning or isotopic labeling is required to follow the motion of the diluent since it is the only component containing phosphorous. Furthermore phosphorous 31 is a 100% spin one-half isotope which simplifies data acquisition and interpretation. The NMR data are used to supplement determinations of shear dynamic mechanical response, compressive yield stress, Young's modulus and the glass transition temperature. The combination of traditional materials science techniques with NMR spectroscopy provides new insights into the

action of diluents in polymer blends.

The PPE used was General Electric PPO^R resin powder with intrinsic viscosity of 0.05dl/gm with M_n = 17000 and M_w = 34000. The polystrene (PS) was Shell Chemical Company general purpose polystyrene 203 with M_n = 84000 and M_w = 250000. The diluent is a tri-2-ethylhexylphosphate (TOP). By differential scanning calorimetry its T_g was found to be -134°C.

The PPO/PS/TOP blend was compounded on a twin screw extruder under conditions that produced clear homogeneous extrudates. Compression molded sheets approximately 2.3 mm thick were formed from chopped extrudates under time-temperature conditions designed to minimize molecular orientation. Cylinders about 1 cm in diameter and 2.5 cm in length were compression molded from these blends.

The elastic modulus of the blend was determined on specimens cut from sheets compression molded one month before testing. Measurements were made at 0.02 inches/min in an Instron servohydraulic tester using an extensometer. Modulus was calculated from the slope of the force-strain curve between 0.02% and 0.4% strain. Viscoelastic characterization of selected blends from -150 to 25 ° C was effected at 1Hz in rectangular torsion in a Rheometrics Dynamic Spectrometer. Yield stress was determined under compressive loading at a crosshead rate of 0.002 inches/min on an Instron Universal tester. Glass transition temperatures, T_g, of all blends were determined with a Perkin Elmer DSC II differential scanning calorimeter at a heating rate of 20°/min.

Mechanical and thermal data are summarized in Table I and dynamic mechanical data are presented in Figure 1.

For observation of the ^{31}P line shape, pellets of the ternary system were sealed in a 10 mm NMR tube under vacuum. The spectra were taken on a Bruker WM-250 at a frequency of 101 MHz and a sweep width of 100 kHz. Temperature was maintained within two degrees and the probe temperature was calibrated with the usual chemical standards. The resulting spectra are shown in Figure 2.

Young's modulus and the glass transition temperature drop continuously as the TOP concentration is raised indicative of plasticization behaviour. More interestingly, a distinct though broad loss peak appears in the shear dynamic mechanical response and is centered near -60^0C at a frequency of 1 Hz. There is no comparable sub-glass transition loss peak in the polymer blend without the diluent present.

A well defined loss peak is usually associated with the presence of a motion which can be characterized in terms of some aspect of the chemical structure of the polymeric glass. Since the polymeric blend without diluent shows no loss peak, it is particularly intriguing to attempt to identify molecular motions present in this system. Some earlier spectroscopy (mechanical, dielectric and NMR) studies have pointed to motion of the diluent as a cause of relaxations below the polymer T_g[10-13]. The possibility of rotational motion of the diluent can be explored through the ^{31}P spectra as a function of temperature. The solid state ^{31}P line shape of trioctyl phosphate is dominated by chemical shift anisotropy which arises from the magnetic shielding of the electronic environment surrounding the phosphorous nucleus. The lowest temperature spectra shown in Figure 2 are classic examples of the "polycrystalline" line shape expected for an axially symmetric chemical shift anisotropy which is consistent with the local electronic environment of a phosphorous nucleus

in a trialkyl phosphate. The term "polycrystalline" refers to the presence of a sum over all orientations in the sample and an absence of molecular motion. Both of these characteristics are reasonable for a low temperature spectrum of an amorphous glass.

As temperature is raised, the ^{31}P line shape narrrows which is conclusive evidence for motion of the TOP. The nature of the line shape collapse allows for the identification of several important features of the motion. The geometry of the motion can be determined from the line shape pattern which appears at the higher temperatures. All spectra displayed in Figure 2 are below the glass transition but the 60°C spectrum is largely composed of a single sharp line. This result indicates that the TOP is rotating isotropically with a correlation time shorter than tenths of milliseconds at the highest temperature observed.

A second feature of the motion of the TOP can be determined by a consideration of the intermediate spectra which are only partially collapsed. The line shape at -80°C is indicative of no motion on the NMR time scale which is of the order of milliseconds for these phophorous line shapes. The line shape at 60°C is indicative of nearly isotropic motion on a time scale which is fast relative to the NMR time scale. The intermediate spectra, especially those at 0, 20 and 40°C can be approximated as a superposition of the low temperature spectrum and the high temperature spectrum with an increasing proportion of the high temperature spectrum as temperature is raised.

This superficially bimodal character of the intermediate spectra is evidence for heterogeneous motion which is a characteristic of local motion in glassy polymers demonstrated in earlier line shape studies[14-16]. Previous line shape studies have focussed on the local motion of the polymer chain and the result obtained here shows that heterogeneity of

motion is a general feature of glassy dynamics which is not a chain property. Rather it is to be identified as a property of a glass which is structurally heterogeneous on the size scale of chemical groups. Local motions on this same size scale show the heterogeneity dynamically because the local intermolecular environment differs at various spatial distributions in the glass. Intermolecular interactions are the major source of the apparent activation energies so that it is easy to imagine a distribution of intermolecular interactions leading to a distribution of barrier heights and thus a distribution of rates of motion.

The superficially bimodal appearance of the line shapes can be explained through examination of Figure 3. For numerical discussions of NMR line shape collapse, the correlation time, τ, is used which is the inverse of the rate constant for collapse. If the motion is heterogenous there is a broad distribution of rates and this situation is depicted in Figure 3. As explained there are three general rates of motion which can be classified relative to line shape collapse. Those labeled rigid in Figure 3 are too slow to produce collapse, those labeled intermediate produce partial collapse and those labeled fast are so fast collapse has already occurred and little further line shape narrowing is produced by faster rates. If the distribution of rates or times is broad, the rigid and fast parts of the distribution account for the majority of rates and lead to the superficially bimodal spectra. The intermediate rates which yield intermediate stages of collapse are a smaller fraction of the observed line and therefore less obvious. Although the motion is identified as isotropic and heterogeneous further details remain to be considered. The rotation can occur by jump diffusion or Brownian diffusion and a distribution of amplitudes may be present. The ability to distinguish these subtle

differences from the NMR data is uncertain.

NMR spectroscopy has clearly identified the diluent as a mobile species in the ternary system of interest. It is our proposal that the mechanical loss peak arises from the liquid-like motion of the diluent, a conclusion that reinforces the results of a survey of mechnical properties of a large number of plasticized PPE/PS blends[2]. Further quantitative work will be carried out to link the collapse of the NMR line shape to the breadth and temperature of the mechanical loss peak as has been done in an earlier study[1] of polymer motion in glasses.

With this proposal in mind, two distinct mechanisms of plasticization can be imagined. First a diluent may expedite a local motion of the polymer and thereby lower the modulus of the glass. Secondly the diluent itself may undergo local motion changing the modulus of the glass. Of course both or neither of these mechanisms may be operative when a diluent is added to a glassy polymer. In addition we have not yet introduced modes for antiplasticization behaviour. However a focus on identifying local motions via solid state NMR and relating these motions to bulk mechanical behaviour is a powerful approach for understanding plasticization and antiplasticization.

Acknowledgement

This research was carried out in part with support from the U.S. Army Research Office Grant DAAG 29 85-K0126 and National Science Foundation Grant DMR-8619380.

References

1. A. A. Jones, J. F. O'Gara, P. T. Inglefield, J. T. Bendler, A. F. Yee and K. Ngai, Macromolecules (1983) 16, 658.
2. R. P. Kambour, J. M. Kelly and B. J. McKinley, J. Polym. Sci., Polym. Phys. Ed.; submitted.
3. W. J. Jackson, Jr. and J. R. Caldwell, Adv. Chem. Ser. (1965) 48, 185.
4. W. J. Jackson, and J. R. Caldwell, J. Polym. Sci. (1967) 11, 211 and 227.
5. R. E. Robertson and C. W. Joynson, J. Appl. Polym. Sci. (1972) 16, 733.
6. L. M. Robeson and J. A. Faucher, J. Polym. Sci. B (1969) 7, 35.
7. L. A. Belfiore, P. M. Henrichs, D. J. Massa, N. Zumbulyadis, W. P. Rothwell and S. L. Cooper, Macromolecules (1983) 16, 1744.
8. N. E. Weeks, F. E. Karasz and W. J. MacKnight, J. Appl. Phys. (1977) 48, 4068.
9. A. F. Yee, Polym. Eng. and Sci. (1977) 17, 213.
10. S. E. B. Petrie, R. S. Moore and J. R. Flick, J. Appl. Phys. (1972) 43, 4318.
11. P. J. Hains and G. Williams, Polymer (1975) 16, 725.
12. E. W. Fischer, G. P. Hellman, H. W. Spiess, F. J. Horth, U. Ecarius, and M. Wehrle, Makrom. Chem. Suppl. (1985) 12, 189.
13. K. Adachi, M. Hattori and Y. Ishida, J. Polym. Sci., Polym. Phys. Ed. (1977) 15, 693.
14. H. W. Spiess, Colloid Polym. Sci. (1983) 261, 193.
15. H. W. Spiess, In Advances in Polymer Science, Vol. 66, H. H. Kausch and H. G. Zachmann, Eds., Springer-Verlag, Berlin (1985).
16. A. K. Roy, A. A. Jones and P. T. Inglefield, Macromolecules (1986) 19, 1356.

TABLE I

MECHANICAL AND THERMAL PROPERTIES

Wt. % TOP	Tensile E (MN/m2)	Compressive Yield Stress (MN/m2)	Tg (deg. C.)
0	3006	107.5	150
5	2980	99.3	112
10	2888	92.4	104
15	2520	84.8	96
20	2580	64.8	72
25	2020	51.0	60

Legend to Legends

Figure 1: Temperature dependence of storage and loss shear moduli G' and G" for the neat blend (PPO and PS, 50:50)(squares) and a blend containing 20% trioctyl phosphate (circles).

Figure 2: ^{31}P line shapes of the three component system: PPO/PS/TOP as a function of temperature.

Figure 3: Weighting factor for a given correlation time as a function of correlation time for a typical distribution of correlation times. Rigid, intermediate and fast refer to characteristics of the NMR line shape.

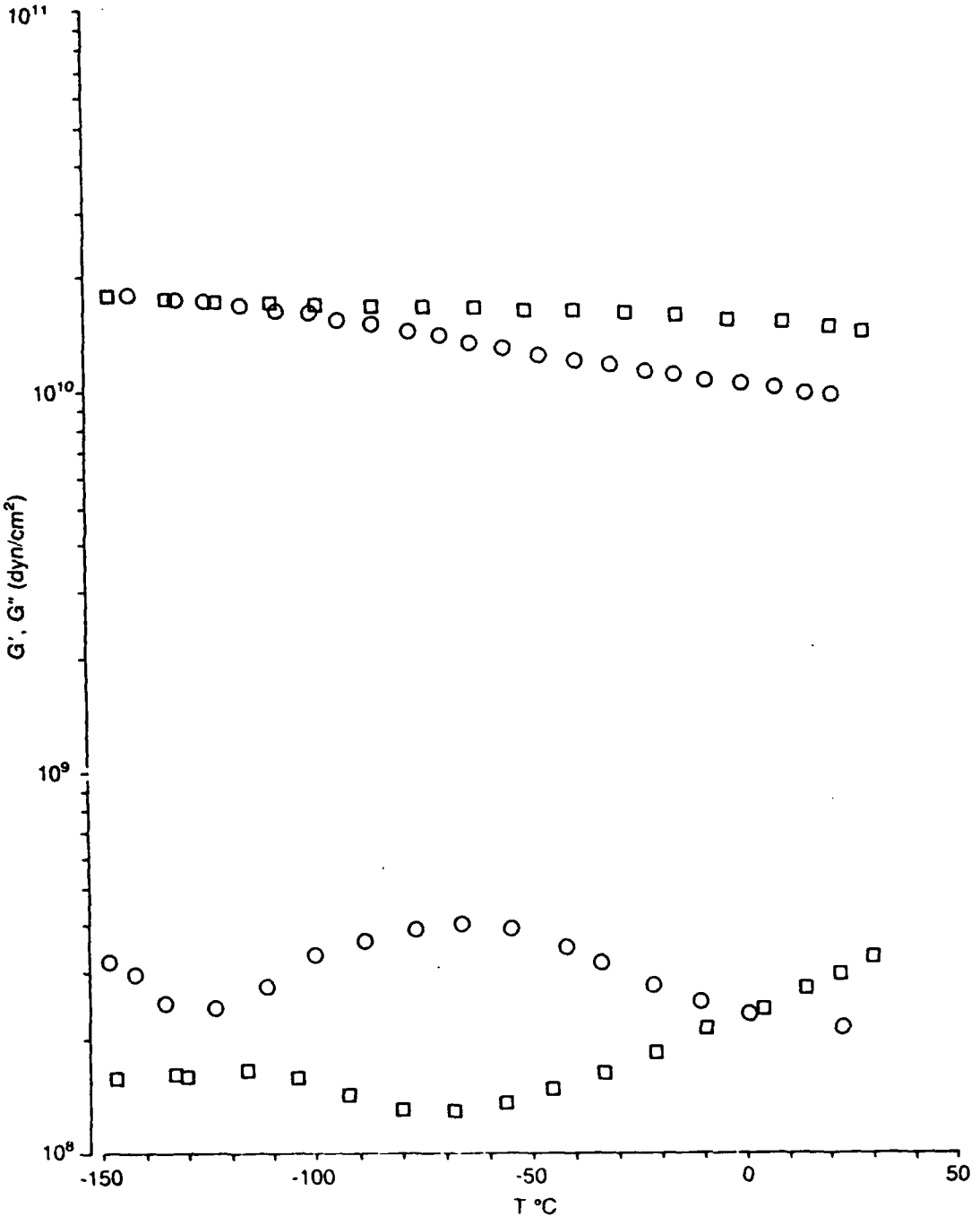
10^{11}
10^{10}
10^{9}
10^{8}
G', G" (dyn/cm^2)
-150
-100
-50
0
50
T °C

Fig 2

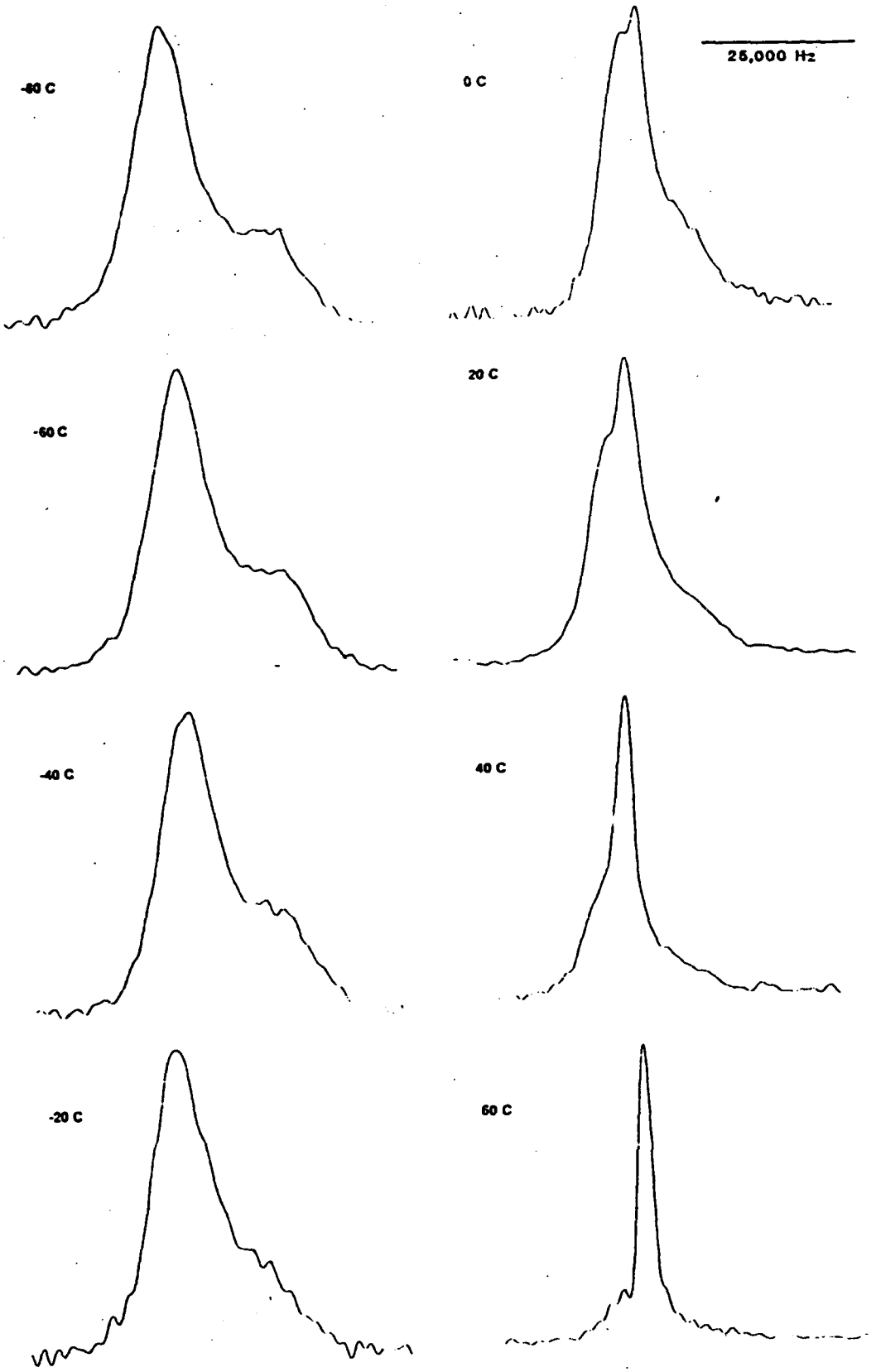

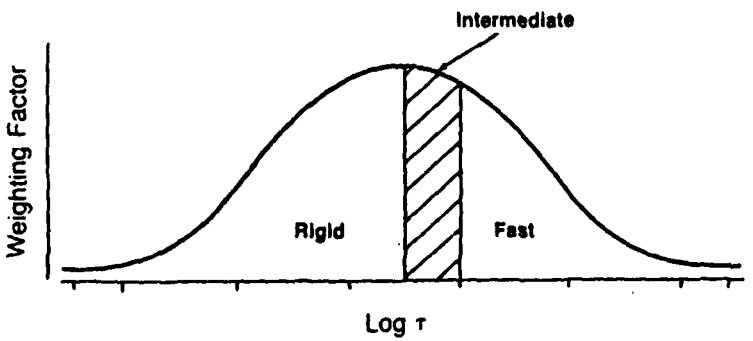
Intermediate
Weighting Factor
Rigid
Fast
Log τ